SUBSTITUTION REACTIONS BETWEEN AQUATETRACYANONITRIDORHENATE(V) IONS AND DIFFERENT BIDENTATE LIGANDS CONTAINING N, O-DONOR ATOMS

A thesis submitted to meet the requirements for the degree of

Philosophiae Doctor

in the

Department of Chemistry

Faculty of Natural and Agricultural Sciences

at the

University of the Free State

by

Thato Nicholas Mtshali

Promoter

Prof. W. Purcell

Co-promoter

Prof. S.S. Basson

May 2006

“Chemistry is the science of molecules and their transformations. It is the science not so much of the one hundred elements, but of the infinite variety of molecules that may be built from them”

Roald Hoffman

ACKNOWLEDGEMENTS

I wish to express my gratitude to the Almighty Father from whom we receive all grace.

I express gratitude and appreciation to:

- Prof. W. Purcell (my promoter) and Prof. S.S Basson (my co-promoter), for their excellent guidance, professional support and encouragement throughout this study. I could not wish for better supervisors.

- The Faculty of Natural and Agricultural Sciences, Department of Chemistry for showing confidence in me, and giving me the opportunity to study with them.

- The Mellon Foundation Scholarship for making it possible for me to complete my studies through their financial support.

- Sigma Aldrich for supplying me with the materials.

- My family for the support they have given me in my academic journey. I salute my late parents (Christina Thandi and Samuel Thomas Mtshali), my three sisters and brother, my son (Wandisile Mtshali), and to many other people who motivated me throughout my studies.

- Finally, to my girlfriend (Historina Maletsatsi Mofokeng), friends and my colleagues (Phillip and Michael) for giving me confidence: you met me at a critical stage of this study, and encouraged me to go on. This work is a token of my commitment to you for life.

Thato Nicholas Mtshali

TABLE OF CONTENTS

CHAPTER 3

CHELATE FORMATION IN TRANSITION METAL COMPLEXES 29

CHAPTER 4

SYNTHESIS AND CHARACTERIZATION OF COMPLEXES 53

ABSTRACT

The aim of this study was to determine the products as well as the mechanism for the reaction between $[ReN(H_2O)(CN)_4]^{2-}$ complex and different bidentate ligands (pyridine-2-carboxylate (pic^-), quinoline-2-carboxylate ($quin^-$) and pyridine-2,3-dicarboxylate ($2,3\text{-}dipic^-$)). Solid state and solution studies, which investigate different aspects of these systems, were performed. Elucidation of the mechanism was achieved by utilizing X-ray crystallography and reaction kinetics.

X-ray crystallographic structure determinations show that all the complexes studied crystallize in the triclinic space group Pī. The different bond distances and angles of all the complexes studied were determined, as well as the significant mode of distortion of the coordinated octahedron in these complexes. The large *trans*-influence of the nitrido ligand was also evidenced in the bond distances of the *trans* bonded ligands. For bidentate substituted complexes, the carboxylato oxygen of pic^- and $quin^-$ anions are bonded *trans* to the nitrido ligand while the cyano ligand is bonded *trans* to one of the cyano ligands. Small bite angles for chelation were also detected. A cyano-bridged binuclear rhenium(V) complex was isolated for the first time.

Kinetic studies of all the ligands studied show the same tendency towards substitution reactions. A two-step reaction process was spectrophotometrically observed and kinetically investigated. The first fast reaction was regarded as the aqua substitution (reaction **C**, in **Scheme A**) while the second slow reaction resulted in the cyano substitution during the ring-closure step (reaction **E**, in **Scheme A**). A reaction mechanism (**Scheme A**) was proposed for all the reactions that were possible with the conditions that prevailed during the study. The acid dissociation constants were determined spectrophotometrically and kinetically. Negative entropy of activation was determined for the second step of the reactions and points to an associative mechanism.

Abstract

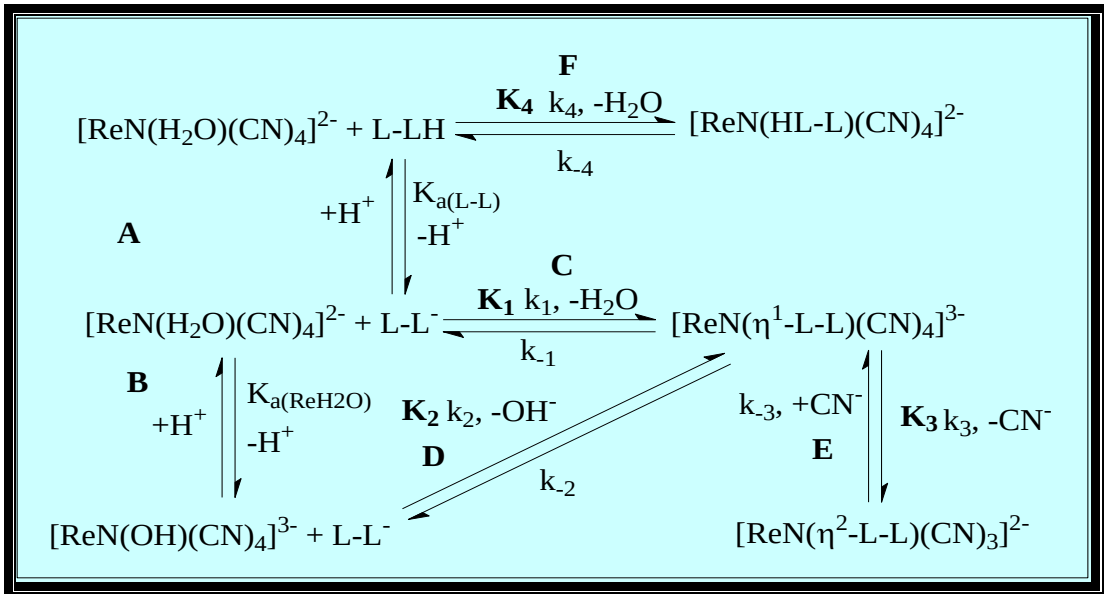

Scheme A: Protonation reactions and bidentate substitution behaviour of the $[ReN(H_2O)(CN)_4]^{2-}$ complex (L-L = bidentate ligand).

The above-mentioned crystallographic and kinetic results were compared to other known results from studies involving the groups 6 and 7 metal complexes containing oxo and nitrido ligands. The obtained results showed good correlations with known systems.

Keywords:

Kinetics, crystallography, chelation, bidentate ligands, acid dissociation constant, stability constant, entropy and enthalpy of activation, cyano complexes.

OPSOMMING

Hierdie studie het die identifikasie van produkte, asook die meganisme waarvolgens die reaksie tussen die $[ReN(H_2O)(CN)_4]^{2-}$ kompleks en verskillende bidentate ligande (piridien-2-karboksilaat- (pic^-), kinolien-2-karboksilaat- ($quin^-$) en piridien-2,3-dikarboksilaat anione ($2,3\text{-dipic}^-$) plaasvind, ten doel. Navorsing is op die vaste toestand en verskeie oplossingseienskappe van die verskillende produkte uitgevoer. Die suksesvolle daarstelling van die meganisme vir hierdie substitusiereaksies is met behulp van X-straalkristallografie en reaksiekinetika uitgevoer.

Die kristalstruktuurbepalings wat tydens hierdie studie onderneem is, het aangetoon dat al die produkte in die trikliniese Pī ruimtegroep kristalliseer. Belangrike bindingsafstande en –hoeke, asook die mate van oktaëdriese verwringing wat in hierdie verbindings teenwoordig is, is bepaal. Die relatiewe groot *trans*-invloed van die nitridoligand is duidelik sigbaar in die verskillende groepe en ligande wat *trans* ten opsigte van die nitridoligand teenwoordig is. Die karboksilatosuurstofatoom vir beide pic^- en $quin^-$ is *trans* ten opsigte van die nitridogroep in die verskillende komplekse gebind terwyl die piridienstikstof *trans* ten opsigte van 'n sianiedgroep gebind is. Relatiewe klein bythoeke is vir die gecheleerde ligande waargeneem. Tydens hierdie studie is die eerste sianiedgebrugde bikernige renium(V) kompleks geïsoleer.

Die kinetiese studies wat tydens hierdie studie onderneem is het almal dieselfde substitusiegedrag openbaar. 'n Tweestap-substitusieproses is spektrofotometries asook kineties waargeneem. Die eerste reaksie word as die akwasubstitusiestap beskou (reaksie **C**, in **Skema A**), terwyl die stadiger tweede stap die substitusie van 'n sianiedgroep met die gepaardgaande ringsluiting van die bidentate ligand behels (reaksie **E**, in **Skema A**). **Skema A** word vir al die moontlike reaksies wat onder die gegewe reaksiekondisies kan plaasvind, voorgestel. Die suurdissosiasiekonstantes vir die metaalkompleks asook die verskillende ligande is spektrofotometries asook kineties bepaal. 'n Negatiewe aktiveringsentropie dui op assosiatiewe aktivering tydens die finale stappe van die substitusieproses.

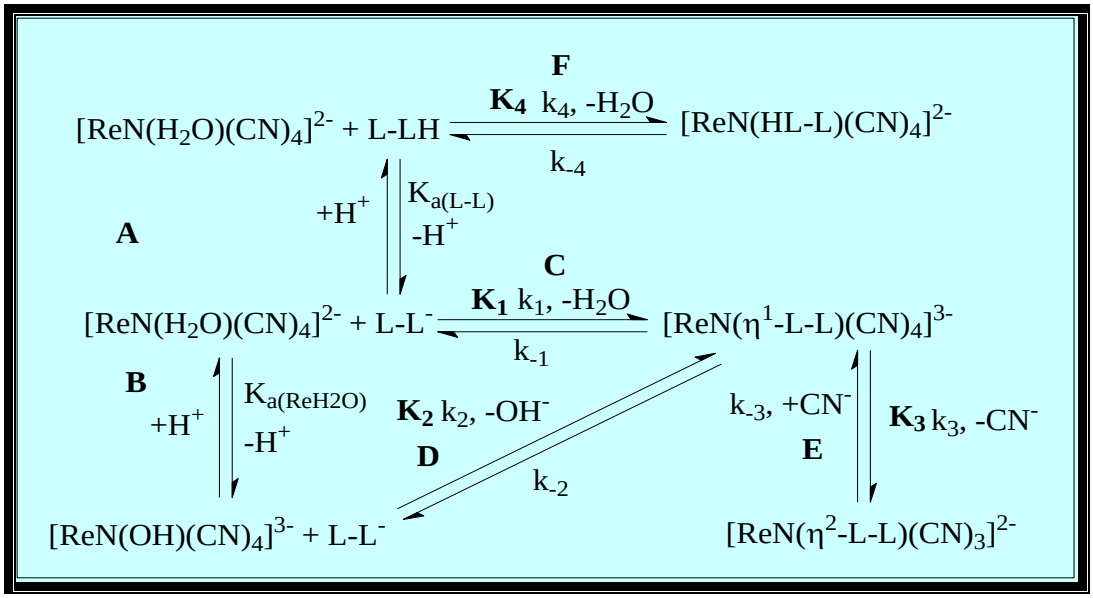

Skema A: Protoneringsreaksies en bidentate substitusiegedrag van die $[ReN(H_2O)(CN)_4]^{2-}$ kompleks (L-L = bidentate ligand).

Hierdie strukturele en kinetiese data is dan ook met dié van ander isolektroniese groep 6 en 7 metaalkomplekse vergelyk en goeie ooreenkomste is tussen die verskillende okso- en nitridokomplekse verkry.

Sleutelwoorde:

Kinetika, kristallografie, chelering, bidentate ligand, suurdissosiasiekonstante, stabiliteitskonstante, entropie en entalpie van aktivering, sianokomplkse.

LIST OF PUBLICATIONS FROM THIS STUDY

MTSHALI, T.N., PURCELL, W., VISSER, H.G. & BASSON, S.S. 2006**.** A crystallographic and kinetic study of the formation of the tricyanonitrido (pyridine-2-carboxylato-κN,κO)rhenate(V) ion, $[ReN(\eta^2\text{-pic})(CN)_3]^{2-}$. *Polyhedron*: (in press).

ABBREVIATIONS

$\Delta H^{\neq}$	Enthalpy change of activation
$\Delta S^{\neq}$	Entropy change of activation
ΔG^{o}	Standard free energy change
$\Delta H°$	Standard enthalpy change
$\Delta S°$	Standard entropy change
ε	Molar extinction coefficient
μ	Ionic strength
$t_{1/2}$	Half-life
UV/VIS	Ultraviolet/visible
IR	Infrared
pK_a	Acid dissociation constant
LFER	Linear free energy relationship
$AsPh_4^+$	Tetraphenylarsonium cation
PPh_4^+	Tetraphenylphosphonium cation
PPh_3	Triphenylphosphine
HCN	Hydrogen cyanide
$KReO_4$	Potassium perrhenate
N_3^-	Azide ion
py	Pyridine
en	Ethylenediamine
TU	Thiourea
NNDMTU	N,N-dimethylthiourea
NMTU	N-methylthiourea

1 INTRODUCTION AND AIM

1.1 INTRODUCTION

Coordination chemistry is, quite simply, the chemistry of coordination compounds or metal complexes. These compounds contain a central atom or ion, usually a metal, surrounded by several coordinated anions or molecules, called ligands (Wilkinson, *et al*., 1987:2). Coordination compounds play an essential role in the chemical industry and in life itself (natural complexes). The importance of metal complexes becomes clear when one realizes that chlorophyll, which is vital to photosynthesis in plants, is a magnesium complex ($[C_{55}H_{72}O_5N_4Mg]$) and that haemoglobin ($[C_{34}H_{32}FeN_4O_4]$), which carries oxygen to animal and human cells, is an iron complex (Basolo & Johnson, 1986:2, a).

The nature and properties of metal complexes have been the subject of important research for many years and continue to intrigue some of the world's best chemists. Different historians ascribe different dates to the discovery of the first coordination compound. Perhaps the earliest one on record was Prussian Blue, potassium iron(II) hexacyanoferrate(II), a complex with a chemical formula $K_2Fe[Fe(CN)_6]$, which was obtained accidentally in 1704 by Diesbach, an artist's colour maker from Berlin (Basolo & Johnson, 1986:3, b). This material was prepared by heating equal parts of cream of tartar ($KHC_4H_4O_6$) and saltpetre (KNO_3) with oxblood (or animal flesh). The product was then dissolved in water, treated with green vitriol $[FeSO_4]\cdot 7H_2O$, and alum $K[Al(SO_4)_2]\cdot 12H_2O$, and, finally, hydrochloric acid to obtain the desired blue pigment (Martell, 1978:2, a). Initially it was described as a nontoxic pigment suitable for oil colours.

In 1798, Tassaert, a Parisian chemist, discovered the first hexaammine-cobalt(III) chloride complex, $[Co(NH_3)_6]Cl_3$, and this marked the real beginning of coordination chemistry, because of the unique properties of these complexes which stimulated considerable interest and research in similar systems (Basolo & Johnson, 1986:3, b).

Chapter 1

In 1913, Alfred Werner received a Nobel Prize for his coordination theory of transition metal-ammine complexes. At the start of the 20th century, inorganic chemistry was not a prominent field until Werner studied the metal-ammine complexes such as $[Co(NH_3)_6]Cl_3$. He recognized the existence of several forms of cobalt-ammonia chloride compounds (**Table 1.1**). These compounds showed properties that seemed puzzling in light of the bonding theories at that time. **Table 1.1** lists a series of these compounds which all have strikingly different colours that resulted from the reaction of cobalt(II) chloride with ammonia.

Table 1.1: Cobalt compounds according to their colour.

Original Formulation	Colour	Name	Morden Formulation
$CoCl_3 \cdot 6NH_3$	Yellow	Luteocobaltic chloride	$[Co(NH_3)_6]Cl_3$
$CoCl_3 \cdot 5NH_3$	Purple	Purpereocobaltic chloride	$[CoCl(NH_3)_5]Cl_2$
$CoCl_3 \cdot 4NH_3$	Green	Praseocobaltic chloride	*trans*-$[Co(NH_3)_4Cl_2]Cl$
$CoCl_3 \cdot 4NH_3$	Violet	Violeocobaltic chloride	*cis*-$[Co(NH_3)_4Cl_2]Cl$
$CoCl_3 \cdot 5NH_3 \cdot H_2O$	Red	Raseocobaltic chloride	$[Co(NH_3)_5H_2O]Cl_3$

From this, Werner proposed a theory that successfully explained the observations in **Table 1.1**, and it became the basis for understanding coordination chemistry. He proposed that the metal ions exhibit both *primary* and *secondary* valences. The primary valence is the oxidation state of the metal, while the secondary valence is the number of atoms directly bonded to the metal ion, which is also called coordination number. For these cobalt complexes, Werner deduced a coordination number of 6 with the ligands in an octahedral arrangement around the Co^{3+} ion for these complexes (Basolo & Johnson, 1986:7, c) (**Figure 1.1**).

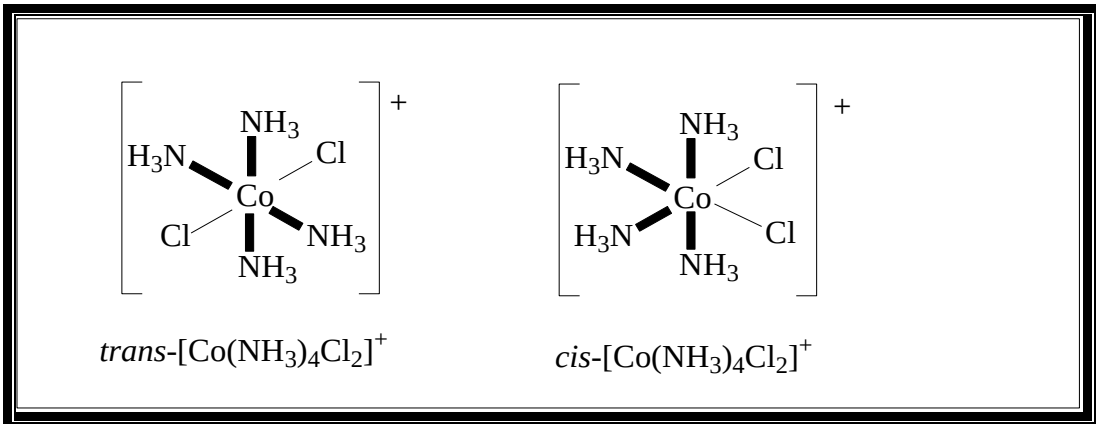

trans-$[Co(NH_3)_4Cl_2]^+$ *cis*-$[Co(NH_3)_4Cl_2]^+$

Figure 1.1: Cobalt complexes.

After this, a large amount of effort was expended on studies of the complexes of chromium, technetium, nickel, iron and platinum metals (Jones, 1964:1, a).

Although metal complexes containing transition metal ions have been known for a long time, the coordination chemistry of rhenium (the last of the stable elements to be discovered in 1925) has undergone tremendous growth in the last 25 years. This element occupies an important place in contemporary inorganic chemistry. Entry into its chemistry is usually afforded by access to commercially available (but relatively expensive) perrhenate salts, NH_4ReO_4 or $KReO_4$, although rhenium metal is sometimes used as the starting material. The salts of perrhenate ions (including perrhenic acid) are not only the single most important group of starting material for the synthesis of other rhenium compounds, but are also of importance as reagents, catalysts in industrial processes and other commercial processes. The heptavalent oxide, Re_2O_7, on dissolving in water, forms perrhenic acid, $HReO_4$, from which many other compounds can be prepared. A large number of rhenium compounds are now well established, among them cyanides, halides, oxides, and sulfides.

Nowadays, an interest in coordination chemistry of rhenium is partly due to the recent use of the ^{186}Re (β^- = 1.07 MeV, γ = 137 keV, $t_{1/2}$ = 90 h) and ^{188}Re (β^- = 2.12 MeV, γ = 155 keV, $t_{1/2}$ = 17 h) as suitable candidates for therapeutic applications in nuclear medicine. ^{186}Re is especially attractive because of its half-life (90 hrs) and the fact that it emits γ-rays at essentially the same energy as the γ-emission of ^{99m}Tc (Mathieu *et al*., 1979:725; Eisenhut, 1982:99). On the other hand, ^{188}Re, because of its

higher intensity β-irradiation (2.12 MeV) is, in principle, even more suitable for therapy than the ^{186}Re. This dual emission property of $^{186/188}$Re allows the biodistributions of $^{186/188}$Re radiophamaceuticals to be monitored using the same gamma-camera instrumentation employed for ^{99m}Tc. Thus, the development of therapeutic $^{186/188}$Re agents based on diagnostic ^{99m}Tc agent has highlighted the synergic relationship between inorganic chemistry and nuclear medicine. Metal complexes are usually studied to gain more insight into the reactivity of these complexes towards biosystems. These studies normally highlight similarities and differences between metal complexes containing metal centres such as Tc and Re which are usually employed in the design of new therapeutical agents (Gerber *et al*., 1995:2189).

Periodically, rhenium and technetium show considerable chemical similarity which differs significantly from that of manganese. These elements have a great tendency to form low-spin diamagnetic complexes, i.e. having a paired d^2 configuration. Rhenium and technetium have a large number of oxidation states (ranging from -1 to +7), and the most important one is the +5 oxidation state. The most characteristic feature of Re(V) and Tc(V) is the existence of a large number of diamagnetic octahedral complexes in which the metal forms multiple bonds with oxygen complexes containing the $[MO]^{3+}$, $[MO_2]^{+}$ and $[M_2O_3]^{+}$ and with nitrogen complexes containing $[MN]^{2+}$ and $[MNR]^{3+}$ units (Botha, 1995:20, a). Although the tendency to form multiple bonds with nitrogen is shared with adjacent elements in their higher oxidation state, e.g., molybdenum(IV) $[MoO_3N]^{3-}$ (trioxonitridomolybdates) (Watt & Davies, 1948:2041), and osmium(VI) $[OsO_3N]^{-}$ (trioxonitrido-osmiates) (Fritsche & Struve, 1847:97), it appears to be more pronounced for rhenium(V) than for any other transition metal (Perils, 1995:5).

It was previously shown that tetracyanometalate complexes of the type $[MX(H_2O)(CN)_4]^{n-}$ (M = Mo(IV), W(IV), Re(V), Tc(V), and Os(VI) and X = O^{2-} and N^{3-}) behave very similarly towards protonation, substitution etc. (Leipoldt *et al*., 1993:289). In the past 15 years, Leipoldt and co-workers (1992:2277) reported a series of complexes containing molybdenum(IV), tungsten(IV), rhenium(V), technetium(V) and osmium(VI) which were obtained from the replacement of one ligand (H_2O) in $[MX(H_2O)(CN)_4]^{n-}$ with various monodentate nucleophiles (such as N_3^-, F^-, NCS^-, and py).

One of the major differences observed between the substitution behaviour of different $[MO(H_2O)(CN)_4]^{n-}$ complexes was the ability of molybdenum(IV) and tungsten(IV) complexes to react with bidentate ligands such as 1,10-phenanthroline, pyridine-2-carboxylic acid and 2,2'-bipyridyl (with aqua and cyanide substitution from the parent complex) to form the corresponding $[MO(L\text{-}L)(CN)_3]^{n-}$ (L-L = bidentate ligand) complexes (Samotus *et al*., 1990:129; Leipoldt *et al*., 1986:323; 1987:57; Roodt *et al*., 1994:599; Basson *et al*., 1984:71; Szklarzewicz *et al*., 2005:1749).

The initial observation that $[MO(H_2O)(CN)_4]^{2-}$ complexes (M = Mo(IV) and W(IV)) react with bidentate ligands was, however, not limited to the oxo-aqua complexes. It was also reported that nitridotetracyano complexes of the type $[MnN(H_2O)(CN)_4]^{2-}$ reacted in the same manner with bidentate ligands (Van der Westhuizen, 2004:90, a). These reactions may, therefore, constitute an alternative route to the synthesis of *trans*-nitrodotetracyanorhenate(V) complexes with bidentate ligands.

1.2 AIM

To date, research on the reactions between nitridotetracyanorhenate(V) complexes of the type $[ReN(H_2O)(CN)_4]^{2-}$ with bidentate ligands has remained relatively unexplored. As part of this study, the main objective was the investigation of the reaction between the $[ReN(H_2O)(CN)_4]^{2-}$ complex and different bidentate ligands containing N,O-donor atoms and to isolate and characterize the final products of the form $[ReN(L\text{-}L)(CN)_3]^{2-}$ with different physical techniques such as crystal structure determinations. This, however, necessitated the gathering of all the information regarding the substitution and formation of $[ReN(L\text{-}L)(CN)_3]^{2-}$ complexes.

With above-mentioned in mind, the main objectives were the following:

1. Synthesis of a rhenium(V) complex containing the $[ReN(H_2O)(CN)_4]^{2-}$ anion as starting material.

2. Characterization of the starting $[ReN(H_2O)(CN)_4]^{2-}$ complex as well as all the different products $[ReN(L\text{-}L)(CN)_3]^{n-}$ obtained from substitution reactions

using different physical and chemical techniques such as infrared and UV/VIS spectrophotometry.

3. X-ray structure and stereochemical determinations of these substitution products.

4. A detailed kinetic study of the substitution reactions of the $[ReN(H_2O)(CN)_4]^{2-}$ complex and different bidentate ligands.

5. Determination of the acid-base behaviour (acid dissociation constant pK_a) of these complexes as well as the investigation of the steric and electronic impact of the different ligands on these reactions.

6. Determination of the mechanism of the substitution reaction of $[ReN(H_2O)(CN)_4]^{2-}$ with different bidentate ligands.

2 GENERAL OVERVIEW: TETRACYANO COMPLEXES OF TRANSITION METALS

2.1 INTRODUCTION

In order to develop and use any new complexes, whether they have catalytic, biological or other useful properties, it is crucial that sufficient knowledge exists regarding the fundamental physical and chemical properties of the complexes involved.

The dioxo complexes $[MO_2(CN)_4]^{n-}$ (M = Mo(IV), W(IV), Tc(V), Re(V) and Os(VI)) as well as the nitrido complexes $([MN(H_2O)(CN)_4]^{n-}$ (except for Mo(IV) and W(IV)) are relatively well characterized (Leipoldt *et al*., 1993:241). All these metal complexes are not only d^2 species, but are also isoelectronic and exhibit the same intrinsic physical characteristic properties and chemical behaviour. The nitrido complexes compared to the dioxo complexes are not that well researched and some outstanding issues need to be addressed. In this chapter, a general overview of the oxo and nitridotetracyano complexes of groups 6 and 7 transition metals will be discussed.

2.2 LITERATURE REVIEW

2.2.1 Synthesis

Tetracyano complexes $[M(X)(H_2O)(CN)_4]^{m-}$ (X = O^{2-} or N^{3-}) have been described for many transition metals and have given rise to a bulk of knowledge, particularly in the case of the dioxotetracyano complexes of Mo(IV), W(IV), Re(V), and Os(VI). The dioxo complexes were prepared in the early half of the 20th century (Bucknall & Wardlow, 1927:2981; Collenberg, 1924:246; Morgan & Davies, 1938:1858; Dudek *et al.*, 1980:1710; Kraus & Schrader, 1928:36), but the dioxotetracyanotechnetate(V) ion was only reported in 1980 by Trop *et al*. (1980:1993).

The preparation of the above-mentioned complexes has been described by many authors. According to a number of different authors, the dioxotetracyano complexes of Mo(IV) and W(IV) can be prepared in two ways, namely, photochemically or thermally (Dudek & Samotus, 1985:271; Keissling *et al*., 1980:843; Lippard & Russ, 1967:1943; Nagorsik *et al*., 1974:353; Samotus *et al*., 1979:1129; Smit *et al*., 1996:1389; 1995:1795).

Photochemical preparation involves the photolysis of a basic solution of the $[M(CN)_8]^{4-}$ complexes, which produce the corresponding dioxotetracyanometalate(IV) complexes with a yield greater than 90%. In the absence of a high-intensity photochemical source, sunlight has been found to be more than adequate. A disadvantage of this method is that it involves the preparation of the octacyanometalate ions in the first step. Procedures for the effective preparation of these $[M(CN)_8]^{4-}$ ions, involving the reduction of the $[MO_4]^{2-}$ ion by H^+/BH_4^- in the presence of an excess of cyanide ion, have been developed. This made the photochemical preparation route less viable (Leipoldt *et al*., 1974:350; 1974:343).

The thermal preparation of the $[MO_2(CN)_4]^{n-}$ complexes for Mo(IV) and W(IV) has been described and involves the same procedure for the synthesis of the octacyanometalate but at a much lower cyanide concentration (Smit *et al*., 1995:1795). With this method, care needs to be taken to limit further substitution reaction towards higher cyanide coordination once the dioxotetracyano complex has been formed, in order to reduce the formation of cyano complexes higher than the $[M(CN)_5]^{3-}$ ion. The reason is that the latter can still be hydrolyzed to the dioxotetracyano complexes by the manipulation of solution basicity. Higher cyanide concentrations result in the formation of octacyano complexes (*via* third-order kinetics, in terms of $[CN^-]$) which cannot be converted thermally to the corresponding dioxo complexes. Since higher coordination of the cyanide ion to tungsten(IV) and molybdenum(IV) centres proceeds *via* $[MO(H_2O)(CN)_4]^{2-}$, limitations of the concentration of this aqua species, therefore, also provide an easy way of limiting higher cyanide coordination by pH manipulation.Yields of more than 50% of the dioxotetracyanometalate of molybdenum(IV) and tungsten(IV) are obtained in a short period of time (less than 2 hrs).

A series of procedures for the preparation of dioxotetracyano complexes of Re(V) that involve cyanide ion substitution of more labile ligands such as pyridine and PPh_3 have been described by Chakravorti (1972:893), Johnson (1969:1843) as well as Lock and Wilkinson (1964:2281). A similar procedure (as in the case of the Mo(IV) and W(IV) systems) that produces acceptable yields of $[ReO_2(CN)_4]^{3-}$ directly from the ReO_4^- ion, has been described by Leipoldt *et al*. (1987:209). Once again, the process is based on the H^+/BH_4^- reduction of ReO_4^-, followed by careful temperature and pH manipulation.

The preparation of the nitridotetracyano complexes of Re(V), Tc(V) and Os(VI), $[MN(H_2O)(CN)_4]^{n-}$, is achieved by first introducing the nitrido ligand to the central metal by reflux with acidic sodium azide, with the formation of tetrahalometalate, $[MNX_4]^{n-}$. Ligation of the halide ions by a cyanide ion produced the tetracyanonitridometalate complexes. A yield of greater than 80% was reported for some of these preparations (Purcell *et al*., 1992:387; Lock & Wilkinson, 1964:2281; Johnson, 1969:1843; Baldas *et al*., 1990:233; Griffith & Pawson, 1973:1315; Che *et al*., 1989:1529).

These complexes were found to be excellent models for theoretical studies (Leipoldt *et al.*, 1993:241). The oxo- and nitrido complexes of Mo(IV), W(IV), Tc(V), Re(V) and Os(VI) demonstrated a large variation in reactivity which made them excellent for kinetic studies with regard to the substitution of the aqua ligand from the coordinated sphere with monodentate ligands and both aqua and one cyanide ligand with bidentate ligands.

2.2.2 Protonation Reaction

In-depth studies have shown that the *trans*-tetracyanodioxo complexes of the type $[MO_2(CN)_4]^{n-}$ (M = Mo(IV), W(IV), Tc(V) and Re(V)), with the exception of Os(VI), can undergo stepwise protonation reactions to form the corresponding oxohydroxo $[MO(OH)(CN)_4]^{(n-1)-}$ and oxoaqua $[MO(H_2O)(CN)_4]^{(n-2)-}$ complexes as shown in **Figure 2.1** (Lippard & Russ, 1967:1943; Roodt *et al*., 1992:1080, Hemjo *et al*., 1973:311; Van der Poel & Neumann, 1968:2086; Chakravorti, 1972:893; Toppen & Murmann, 1970:139).

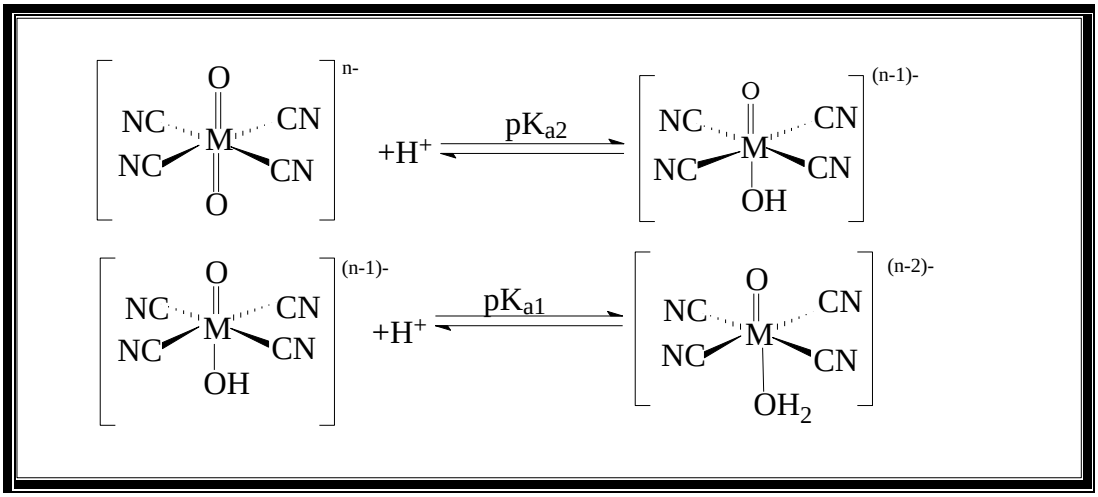

Figure 2.1: Protonation reactions of $[MO_2(CN)_4]^{n-}$ complexes.

Similarly, it has been reported that nitridotetracyano complexes $[MN(H_2O)(CN)_4]^{2-}$ can also undergo protonation reactions according to the following reaction (**Figure 2.2**) (Purcell *et al*., 1992:387; Damoense *et al*., 1994:619; Van der Westhuizen *et al*., 1994:717).

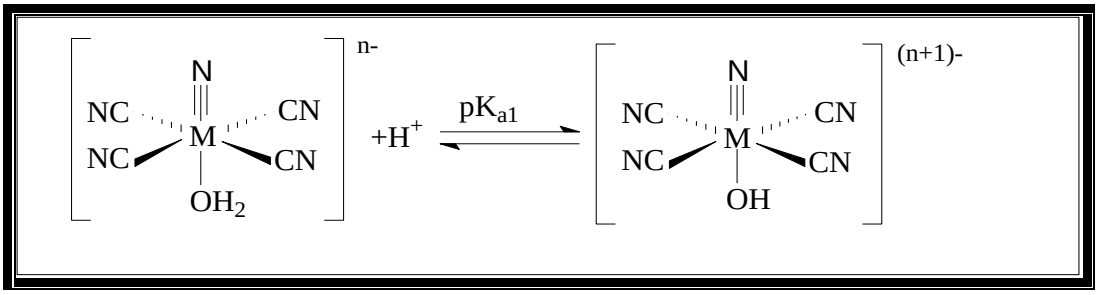

Figure 2.2: Protonation reactions of $[MN(H_2O)(CN)_4]^{n-}$ complexes.

The kinetic studies as well as the crystal structure determination of $(AsPh_4)_2[OsN(OH)(CN)_4]$ showed that the nitrido-hydroxo complexes, $[MN(HO)(CN)_4]^{(n+1)-}$, cannot be deprotonated any further to form the $[MN(O)(CN)_4]^{(n+2)-}$ type of complexes and, to date, the existence of this type of complex has not been proven in literature (Van der Westhuizen *et al*., 1994:717). The determined pK_a values of the $[MX(H_2O)(CN)_4]^{n-}$ complexes (M = Mo(IV), W(IV), Re(V), Tc(V) and Os(VI), X = N^{3-} or O^{2-} and n = 1 or 4) are reported in **Table 2.1**.

Table 2.1: Acid dissociation constants of $[MX(H_2O)(CN)_4]^{n-}$ complexes ($X = N^{3-}$ or O^{2-}).

M	X	pK_{a1}	pK_{a2}	Ref.
Mo^{IV}	O	9.88	12.5	**1**
W^{IV}	O	7.89	14.5	**2**
Tc^{V}	O	2.90	5.0	**3**
Re^{V}	O	1.31	3.72	**4**
Re^{V}	N	11.6	--	**5**
Os^{VI}	O	-3.0	≤1.0	**6**
Os^{VI}	N	7.49	--	**7**

1 Leipoldt *et al*., (1987:57); **2, 3, 6** Roodt *et al*., (1988:336; 1992:1080; 1995:350); **4, 7** Purcell *et al*., (1989:224; 1994:717); **5** Damoense *et al*., (1994:619).

The pK_{a1} values for all the complexes were determined fairly accurately, but there is doubt about the pK_{a2} values of the W(IV), and especially the Mo(IV), complexes. Chakravorti, (1972:893) determined the pK_a values of the $[ReO(H_2O)(CN)_4]^-$ complex potentiometrically, but these values as well as the existence of the $[ReO(H_2O)(CN)_4]^-$ and $[ReO(OH)(CN)_4]^{2-}$ anions were questioned by Toppen and Murmann (1970:139). This was due to a dimerization reaction which takes place after acidifying the $[ReO_2(CN)_4]^{3-}$ complex which resulted in the isolation of a purple dimer, $[Re_2O_3(CN)_8]^{4-}$ from the reaction mixture as the final product (Shandless *et al*., 1971:2785; Lumme *et al*., 1991:501).

Leipoldt *et al*., however, succeeded in obtaining the crystalline salts of $[ReO(H_2O)(CN)_4]^-$ and $[ReO(OH)(CN)_4]^{2-}$, suitable for X-ray analysis, by adding $(PPh_4)Cl$ and $N(C_2H_5)_4Cl$ to a solution of $[ReO_2(CN)_4]^{3-}$ at pH 3.5 and pH 1.0, respectively (Purcell *et al*., 1990:239; 1989:5). The concentrations of the different salts were such that crystals of $(PPh_4)_2[ReO(OH)(CN)_4]\cdot 5H_2O$ (brown) and $(N(C_2H_5)_4)[ReO(H_2O)(CN)_4]\cdot 2H_2O$ (blue) were obtained within half an hour after adjusting the pH values from about 7 (at this pH the main product is $[ReO_2(CN)_4]^{3-}$, which is very stable in solution) to the appropriate pH. Since the dimerization of the $[TcO(OH)(CN)_4]^{2-}$ is a much faster reaction than for the corresponding Re(V) system, it would be more difficult to isolate salts of the oxo-aqua

and oxo-hydroxo complexes of technetium (Roodt *et al*., 1992:1080). To date, only the $[TcO(H_2O)(CN)_4]^-$ complex has been isolated in a crystalline form and crystallographically characterized.

The pK_a values of $[TcO(H_2O)(CN)_4]^-$ and $[ReO(H_2O)(CN)_4]^-$ were also determined kinetically during the kinetic studies of the substitution reactions of these oxo-aqua complexes with thiocyanate ions (see **Table 2.1**) (Roodt *et al*., 1992:1080; Purcell *et al*., 1989:224). The acid dissociation constants decrease significantly upon going from a second- to a third-row metal complex (from 10 to 7.8 for the group VI metal ions and from 2.9 to 1.4 for the group VII metal ions), indicating the increase in metal-aqua bond strength (see **Table 2.1**). The same tendency was also observed in the relative reactivity of these complexes toward substitution reaction: the substitution reactions of the oxo-aqua complexes of the third-row metal ions are order of magnitude slower than the substitution reactions of the second-row metal ions.

The charge of the metal centre also has a large influence on the pK_{a1} value of the dioxo-aqua complexes: pK_a value decreases by more than five pK_a units from a metal ion with a formal charge of +4 (molybdenum(IV) and tungsten(IV)) to a metal ion with a formal charge of +5 (techenetium(V) and rhenium(V)) (**Table 2.1**). This reduction of the charge on the metal ion is an indication of the weakening of the metal-aqua bond, and can also have a very large effect on the reactivity of the aqua complex towards substitution reactions (as will be pointed out in **Paragraph 2.2.3**). Increasing the charge on the metal ion to +6 (osmium(VI) in group VIII) resulted in a complex that cannot be protonated ($[OsO_2(CN)_4]^{2-}$), even at high hydrogen ion concentrations. This is an indication that $[OsO(H_2O)(CN)_4]$ is a very strong acid (as a result of high charge on the metal ion) and cannot exist in the protonated form (Purcell *et al*., 1991:60).

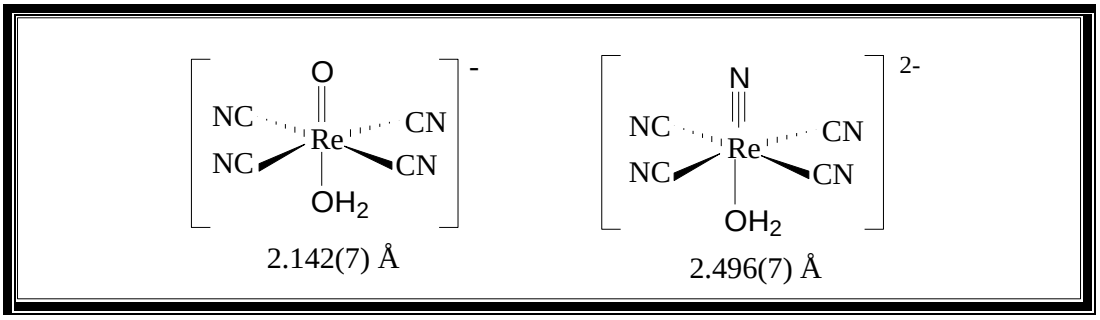

Figure 2.3: ***trans*** **effect of the O^{2-} and N^{3-} ligands in Re(V) complexes.**

An interesting result obtained from the protonation reactions of these types of complexes (oxo and nitridotetracyano) is that, replacing the oxo ligand with a nitrido ligand results in an increase in pK_a values: the pK_a values of $[ReN(H_2O)(CN)_4]^{2-}$ and $[ReO(H_2O)(CN)_4]^{-}$ are 11.6 and 1.4, respectively (Purcell *et al*., 1992:387; Chakravorti, 1972:893) (**Table 2.1**). This increase is an indication of the weakening of the metal-aqua bond as a result of a large *trans*-influence of the nitrido ligand in comparison with the *trans*-influence of the oxo ligand (**Figure 2.3**). This is in agreement with the fact that the nitrido ligand is one of the strongest π-bonding ligands known.

The products of the protonation reactions, as well as the dioxotetracyano complexes of molybdenum(IV) and rhenium(V) were isolated and crystallographically characterized (Purcell *et al*., 1989:5; 1990:239; Day & Hoard, 1968:3374; Murmann & Schlemper, 1971:2352). The results obtained from the crystal structure determinations of the dioxotetracyano complexes of the above-mentioned metals showed that they are highly symmetrical and that the metal ion is in the centre of the plane formed by four carbon atoms of the cyano ligands.

The bond between the metal centre and the progressively more protonated oxygen atom is weakened (longer bond distances) during each protonation step. Simultaneously this leads to a shortening of the bond distance between the metal centre and un-protonated oxygen bond (see **Table 2.2**).

Table 2.2: Bond data for isoelectronic tetracyano complexes of Mo(IV), W(IV), Re(V), Tc(V) and Os(VI) containing oxo or nitrido ligands.

Complex	M=O, M≡N (Å)	M-L[a] (Å)	D (Å)	υ(M=O), υ(M≡N) (cm^{-1})	Ref.
$[MoO_2(CN)_4]^{4-}$	1.834(9)	1.834(9)	0	747	**8**
$[MoO(OH)(CN)_4]^{3-}$	1.698(7)	2.077(7)	0.19	915	**9**
$[MoO(H_2O)(CN)_4]^{2-}$	1.668(5)	2.271(4)	0.34	990	**10**
$[WO_2(CN)_4]^{4-}$	1.842(4)	1.842(4)	0	728	**11**
$[WO(OH)(CN)_4]^{3-}$	--	2.11(1)	--	915	**12**
$[WO(H_2O)(CN)_4]^{2-}$	--	2.16(1)	--	980	**13**
$[ReO_2(CN)_4]^{3-}$	1.781(3)	1.781(3)	0	785	**14**
$[ReO(OH)(CN)_4]^{2-}$	1.70(1)	1.90(1)	0.08	952	**15**
$[ReO(H_2O)(CN)_4]^{-}$	1.67(1)	2.142(7)	0.30	1038	**16**
$[ReN(H_2O)(CN)_4]^{2-}$	1.64(1)	2.496(7)	0.35	1060	**17**
$[OsO_2(CN)_4]^{2-}$	1.75(1)	1.75(1)	0	840	**18**
$[OsN(OH)(CN)_4]^{2-}$	1.80(1)	1.98(2)	0.04	1050	**19**

[a] Ligand *trans* to M≡N or $M=O^-$; [8, 15] Day & Hoard, (1968:3374); [9] Lippard & Russ, (1967:1943); [10, 13] Wieghardt *et al*., (1983:44); [11] Abou-Hamdan *et al*., (1998:1278); [12] Robinson *et al*., (1995:2035); [14, 16, 17, 18] Purcell *et al*., (1989:5; 1990:239; 1992:387; 1991:60); [19] Van der Westhuizen *et al*., (1994:582).

It has been observed that the Mo=O bond distance decreases from 1.834(9)Å in $[MoO_2(CN)_4]^{4-}$ to 1.698(7)Å in $[MoO(OH)(CN)_4]^{3-}$ and finally to 1.668(5) Å in $[MoO(H_2O)(CN)_4]^{2-}$ (Day & Hoard, 1968:3374; Lippard & Russ, 1967:1943; Wieghardt *et al*., 1983:44), whereas the Re=O bond distance decreases from 1.781(3)Å in $[ReO_2(CN)_4]^{3-}$ to 1.70(1)Å in $[ReO(OH)(CN)_4]^{2-}$ and 1.67(1)Å in $[ReO(H_2O)(CN)_4]^{-}$ (Murmann & Schlemper, 1971:2352; Purcell *et al*., 1989:5; 1990:239) (**Figure 2.4**). This decrease in metal-oxo bond distance is accompanied by two factors:

(i) there is a large and significant increase in the metal-oxygen bond *trans* to the oxo ligand: from 1.834(9)Å in $[MO_2(CN)_4]^{4-}$ to 2.077(7)Å in $[MoO(OH)(CN)_4]^{3-}$ and 2.271(4)Å in $[MoO(H_2O)(CN)_4]^{2-}$ (**Table 2.2)** and

from 1.781(3)Å in $[ReO_2(CN)_4]^{3-}$ to 1.90(1)Å in $[ReO(OH)(CN)_4]^{2-}$ and 2.142(7)Å in $[ReO(H_2O)(CN)_4]^-$ (**Figure 2.4**);

(ii) the distortion of the octahedral geometry of the coordination polyhedron during protonation: the central metal ion is pulled out of the plane formed by the carbon atoms of the four cyano ligands towards the oxo ligand by 0.19 and 0.34Å for $[MoO(OH)(CN)_4]^{3-}$ and $[MoO(H_2O)(CN)_4]^-$, respectively, and by 0.08 and 0.30Å for $[ReO(OH)(CN)_4]^{2-}$ and $[ReO(H_2O)(CN)_4]^-$, respectively (Lippard & Russ, 1967:1943; Purcell *et al*., 1990:239) (**Table 2.2**).

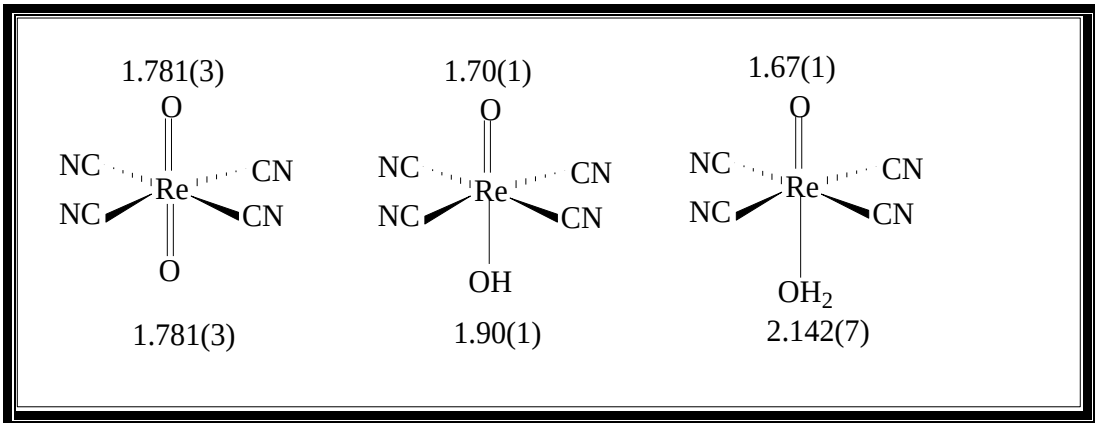

Figure 2.4: Increase in metal-oxygen bond *trans* to oxo ligand and decrease in Re=O bond upon protonation reaction of $[ReO_2(CN)_4]^{3-}$.

There is, however, a significant difference in the metal-oxygen bond distances: 1.834(9)Å in molybdenum, 1.781(3)Å in the rhenium and 1.75(1)Å in the osmium complex (see **Table 2.2**). This behaviour can be explained in terms of the charge of the metal ions; a high positive charge makes the metal ion a good π-acceptor, which increases the metal-oxygen bond strength and thus shortens the bond.

The results were also correlated by IR data of the metal-oxygen stretching frequencies of the different rhenium(V) complexes (**Table 2.2**). The increase in the M=O stretching frequency from $[ReO_2(CN)_4]^{3-}$ (758 cm^{-1}) to $[ReO(H_2O)(CN)_4]^-$ (1038 cm^{-1}) can be attributed to a shortening of the M=O bond distance (Leipoldt *et al*., 1987:209).

2.2.3 Substitution Reactions

2.2.3.1 Monodentate Ligands

The investigation into substitution behaviour of the oxo and nitridotetracyano complexes of Mo(IV), W(IV), Re(V), and Tc(V) was initiated after it has been realized that the weakening of one of the metal-oxygen bonds during the protonation reaction might lead to the substitution of the hydroxo and especially the aqua ligand by strong σ-donating nucleophiles. As a result of a large difference between the metal-hydroxo and the metal-aqua bond distances, it is expected that the aqua complex will be much more reactive towards substitution than the hydroxo complex, as was indeed observed (Basson *et al*., 1985:121; 1987:82; Wieghardt *et al*., 1983:44; Arzoumaniann *et al*., 1991:422; Leipoldt *et al*., 1986:179; Roodt *et al*., 1990:439; Purcell *et al*., 1989:369). The dioxo complex with two relatively strong metal-oxygen bonds, in comparison with the hydroxo and aqua complexes, is, as may be expected from the short metal-oxygen bonds, totally inert towards substitution reactions.

A large number of detailed kinetic studies of the substitution reactions of the protonated form of the dioxo and nitrido complexes of these metal ions showed that the relative reactivity of these complexes towards substitution with a number of σ-donating monodentate ligands is what one would expect from the bond distances (and thus the bond strengths) in these complexes.

The preparation of the products of substitution reactions between the aqua complexes of Mo(IV), W(IV), Re(V) and Tc(V) and various incoming monodentate ligands such as NC^-, NCS^-, N_3^- and F^- and the subsequent crystal structure determinations of some of these substitution products were isolated and crystallographically characterized: [2,2'-H_2bipy][TcO(NCS)$(CN)_4$] (Purcell *et al*., 1989:369), $(PPh_4)_2$[MoO(MeCN)$(CN)_4$] (Arzoumaniann *et al*., 1991:422), K_3[WO(F)$(CN)_4$] (Leipoldt *et al*., 1986:179), (Cs_2Na)[MoO$(N_3)(CN)_4$] (Basson *et al*., 1985:121), [4,4'-H_2bipy][ReO(NCS)$(CN)_4$] and $[N(CH_3)_4]_3$[WO(NCS)$(CN)_4$]·NaNCS (Purcell *et al.*, 1989:369; Roodt *et al.*, 1990:439), $(PPh_4)_3$[ReN$(CN)_5$]·$7H_2O$, (Cs_2Na)[ReN$(N_3)(CN)_4$] and $(PPh_4)_3$[[MoO$(CN)_5$]·$7H_2O$ (Purcell *et al*., 1992:217; 1991:473; Wieghardt *et al*., 1983:44). These crystal structure

determinations showed that only the aqua ligand is substituted by monodentate ligands even in the presence of a large excess of the incoming ligand. The cyano ligands are thus not substituted by monodentate ligands. This is not surprising in view of the strong metal-cyano bonds in the equatorial plane of the complex (**Figure 2.5**).

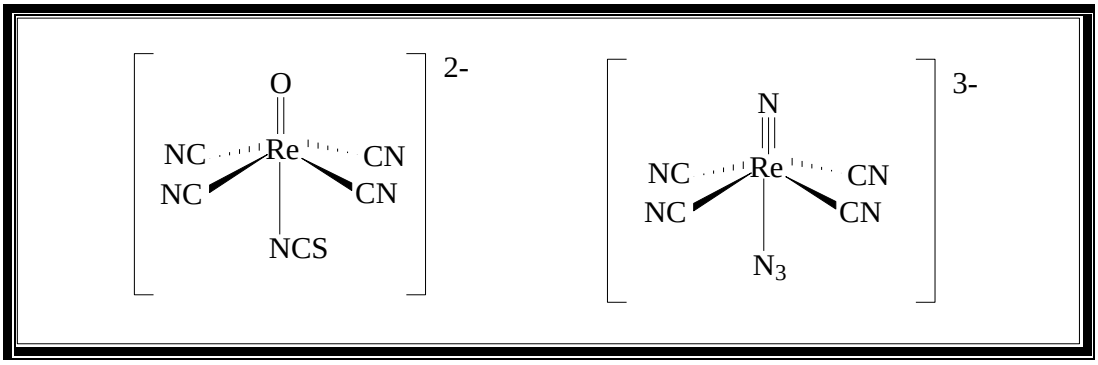

Figure 2.5: Monodentate ligands (NCS^- and N_3^-) substitution in $[ReX(H_2O)(CN)_4]^{n-}$ complexes ($X = O^{2-}$ or N^{3-}).

The structural results obtained on these substitution products also showed that the oxo and nitrido ligands have about the same effects on the structure (bond length and especially the mode of distortion of the coordinated polyhedron) of these substitution products as on the structure of the hydroxo and especially the aqua complex (see **Table 2.2**). The amount of displacement of the heavy atom out of the square plane of the four cyano ligands, as well as the Re=O and Re≡N bond length, is sensitive to the nature of the incoming ligand and may be used as an indication of the bond strength and *trans*-influence of the incoming ligand (**Figure 2.5**).

The most important bond lengths and other structural features of the oxo and nitridotetracyano complexes of Mo(IV), W(IV), Re(V), Tc(V) and Os(VI) are summarized in **Table 2.3**.

Table 2.3: Bond data in isoelectronic tetracyano complexes of Mo(IV), W(IV), Re(V), and Tc(V) and Os(VI) containing oxo or nitrido ligands.

Complex	M≡N or M=O (Å)	M-L[a] (Å)	M-C[b] (Å)	D[c] (Å)	Ref.
$[MoO(N_3)(CN)_4]^{3-}$	1.70(1)	2.29(2)	2.17(1)	0.28	**20**
$[MoO(CN)_5]^{3-}$	1.705(4)	2.373(6)	2.18(1)	0.38	**21**
$[MoO(CH_3CN)(CN)_4]^{2-}$	1.658(7)	2.500(7)	2.159	0.46	**22**
$[WO(F)(CN)_4]^{3-}$	1.77(1)	2.017(8)	2.14(2)	0.18	**23**
$[WO(NCS)(CN)_4]^{3-}$	1.61(2)	2.23(2)	2.14(3)	0.35	**24**
$[Re_2O_3(CN)_8]^{4-}$	1.69(1)	1.92(1)	2.12(1)	0.11	**25**
$[ReO(NCS)(CN)_4]^{2-}$	1.67(1)	2.12(1)	2.11(1)	0.30	**26**
$[ReN(N_3)(CN)_4]^{2-}$	1.65(2)	2.36(2)	2.11(1)	0.34	**27**
$[ReN(CN)_5]^{3-}$	1.68(1)	2.16(1)	2.12(1)	0.31	**28**
$[TcO(NCS)(CN)_4]^{2-}$	1.61(1)	2.16(1)	2.11(1)	0.33	**29**
$[OsN(CN)_5]^{2-}$	1.647(7)	2.353(8)	2.082(8)	0.35	**30**

[a] Ligand *trans* to M≡N or M=O; [b] Equitorial M-CN bonds; [c] Displacement of the central metal atom from the plane formed by four cyano ligands. [20] Basson *et al*., (1985:121); [21] Wieghardt *et al*., (1983:44); [22] Arzoumaniann *et al*., (1991:422); [23] Leipoldt *et al*., (1986:179); [24] Roodt *et al*., (1990:439); [25] Basson *et al*., (1987:82); [26, 27, 28] Purcell *et al*., (1989:369; 1992:217; 1991:473); [29] Roodt *et al*., (1992:1080). [30,] Che *et al*., (1989:1529).

A very interesting result obtained from these crystal structure determinations was that the coordination polyhedra are significantly distorted when two ligands, with different bonding capacity, are bonded *trans* with respect to another (see **Table 2.3**). The rhenium atom is, for example, extracted from the plane formed by four carbon atoms of the cyanide ligands towards the oxo and nitrido ligands in $[ReO(NCS)(CN)_4]^{2-}$ and $[ReN(N_3)(CN)_4]^{3-}$ complexes, respectively (**Figures 2.5**). This type of distortion is a frequent phenomenon for octahedrally-coordinated transition metals containing a strongly π-bonded ligand (like oxo and nitrido group) and a weakly bonded *trans* ligand.

The above-mentioned displacement of the central metal atom towards the oxo and nitrido ligands results in a carbon-metal-aqua bond angle which is significantly smaller than 90° for an ideal octahedron: for example, an angle of 81.6° was found for the

$[ReO(H_2O)(CN)_4]^-$ and 80.4° for the $[ReN(H_2O)(CN)_4]^{2-}$ anion (Purcell *et al*., 1990:239; 1992:387) (see **Table 2.3**). This mode of distortion will cause the aqua complex (reactant) to be crowded in the region of the square plane of the four cyano ligands containing the metal-aqua bond which is the most probable region of attack for incoming ligands in an associative mechanism. An associative mechanism will, however, be less likely, since a dissociative mechanism will actually be promoted as a result of the repulsion between the four cyano ligands and the weakly bonded aqua ligand.

A number of detailed kinetic studies of the substitution reactions of these metal complexes showed that the relative reactivity of these complexes towards substitution by monodentate nucleophiles is in agreement with bond distances and thus the bond strengths of the dioxo, hydroxo and aqua ligands (Leipoldt *et al*., 1986:179; 1986:323; Roodt *et al.*, 1992:1080; 1988:336; Potgieter *et al.,* 1988:209; Purcell *et al*., 1989:224; 1991:339). The dioxo complexes with strong metal-oxygen bonds observed in the crystal structure determinations of $K_3Na[MoO_2(CN)_4]\cdot 6H_2O$ (Day & Hoard, 1968:3374), $K_3[ReO_2(CN)_4]$ (Murmann & Schlemper, 1971:2352) and $Cs_2[OsO_2(CN)_4]$ (Purcell *et al*., 1991:60) are completely inert to oxo substitution reactions. The oxo-hydroxo complexes with relatively short (strong) metal-hydroxo bonds, observed in crystal structure determinations of $(Cr(en)_3][MoO(OH)(CN)_4]\cdot H_2O$ (Romeo *et al*., 1992:4383) and $(PPh_4)_2[ReO(OH)(CN)_4]$ (Purcell *et al*., 1989:5), are also inert, whereas aqua complexes with relatively weak (long) metal-aqua bonds, observed in $[MoO(H_2O)(CN)_4]^{2-}$ (Wieghardt *et al*., 1983:44) and $[ReO(H_2O)(CN)_4]^-$ (Purcell *et al*., 1990:239) are relatively reactive towards monodentate substitution.

Based on the fact that only the aqua (or hydroxo) ligand is substituted by monodentate nucleophiles, the reaction scheme for the substitution reactions of these complexes with monodentate nucleophiles (L) may be represented by **Scheme 2.1.**

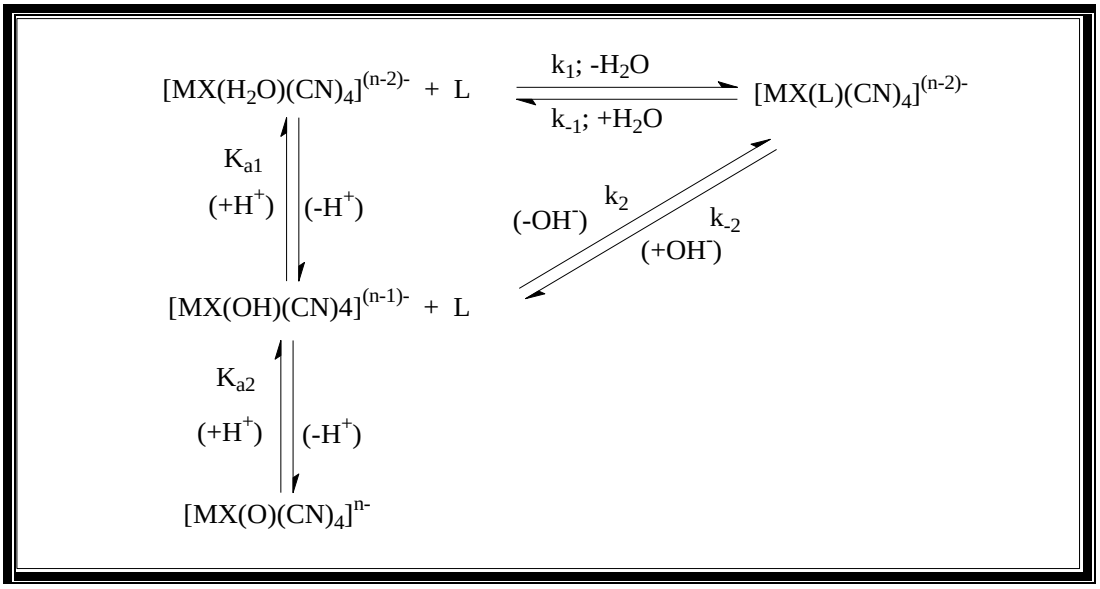

Scheme 2.1: Reaction scheme for the substitution reaction of the protonated forms of nitrido- and dioxotetracyano complexes with monodentate ligands. X in this scheme is N or O.

In accordance with **Scheme 2.1**, the rate law, on condition that [L] >> [{MO/N(H_2O)$(CN)_4$}$^{n-}$], is given by **Eq. 2.1**.

$$k_{obs} = \frac{k_1 + k_2 \dfrac{K_a}{[H^+]}}{1 + \dfrac{K_a}{[H^+]}} [L] + k_{-1} + k_{-2}[OH^-] \qquad \textbf{(2.1)}$$

The kinetic results for all the monodentate reactions studied could be fitted to **Eq. 2.1** (Potgieter *et al.*, 1988:209). The rate constant for the substitution reactions of the hydroxo complexes (k_2) were found to be zero within the margin of experimental error.

The effect of bond strength on the relative reactivity of these complexes is identified by comparing the values of k_1 for the reactions of the oxo and nitrido complexes of rhenium(V) with only NCS^- ligand (**Table 2.4**). A factor of 50–200 decrease in the reaction rate is observed for the group 6 metals and a decrease of a factor of 6300 was found upon going from second- to third-row elements. This suggests that the metal-aqua

bonds are significantly stronger for the third-row elements compared to second-row elements, as would be expected.

Another significant feature of the results obtained from the kinetic studies, is the decrease in the reaction rate upon going from a group VIB metal centre with formal charge of +4 to a group VIIB metal ion with a formal charge of +5. There is a decrease in the reaction rate of a factor 10 from molybdenum(IV) to technetium(V) and an 820 times decrease in the reaction rate from tungsten(IV) to rhenium(V). This indicates that the aqua ligand is more strongly bonded to a metal centre with a higher formal charge, probably as a result of the metal centre with high positive charge being a better π-acceptor, which increases the metal-ligand bond strength (**Table 2.2**). This is again manifested in the pK_a values of these complexes (see **Table 2.1**).

The following detailed kinetic results, including pH profiles, of the substitution reactions of the oxo and nitrido complexes of Mo(IV), W(IV), Re(V), Tc(V) and Os(VI) with various incoming ligands were performed (**Table 2.4**).

The nitrido complexes with the weak metal-aqua bond ($Re\text{-}OH_2$ = 2.496(7) Å) reacts about 10^6 times faster than the oxo complexes with a much stronger metal-aqua bond ($Re\text{-}OH_2$ = 2.142(7) Å). The effect of the rhenium-aqua bond strength in the oxo and nitrido complexes is also evidenced by the very large increase in the pK_{a1} values of 1.4 for oxo complex to 11.6 for the nitrido complexes. The large dependency of the rate of substitution on the rhenium-aqua bond distances, as observed in comparing the oxo and nitrido complexes, suggests a dissociative mechanism, and this also explains the high reactivity of the nitrido complex.

Table 2.4: Kinetic data for the reaction of $[MX(H_2O)(CN)_4]^{(n-2)-}$ ($X = N^{3-}$ or O^{2-}, M = Mo(IV), W(IV), Tc(V), Re(V), and Os(VI)) with different nucleophiles at 25°C[a].

MX	L	k_1 ($M^{-1}s^{-1}$)	k_{-1} (s^{-1})	K_1 (M^{-1})	$\Delta H^{\neq}$ ($kJmol^{-1}$)	$\Delta S^{\neq}$ ($Jmol^{-1}K^{-1}$)	Ref
MoO	F^{-}[b]	18.7(6)	1.6(4)	12.1(9)	49(3)	-59(13)	**31**
	CN^{-}[c]	116(2)	1.20(5)	95(5)	51(4)	-53(14)	**32**
	HCN[a]	$4.8(2)\times10^{2}$	$1.4(3)\times10^{3}$	3(1)	35(1)	-80(4)	**33**
WO	F^{-}[c]	$1.06(3)\times10^{-1}$	$1.0(1)\times10^{-3}$	$1.4(2)\times10^{2}$	70(3)	-28(10)	**34**
	CN^{-}	1.15(3)	$8(2)\times10^{-3}$	$1.1(1)\times10^{3}$	90(5)	12(20)	**35**
	HCN	9(1)	8(2)	1.0(2)	69(3)	-5(10)	**36**
	N_3^{-}	4.2(1)	0.20(6)	4.8(11)	67(3)	-10(8)	**37**
	NCS^{-}	2.88(11)	2.129(5)	2.0(1)	73(3)	8(9)	**38**
	Py	6.9(4)	14.0(2)	0.5(1)	98(2)	101(6)	**39**
TcO	NCS^{-}	22.2(3)	0.43(4)	54(2)	62(4)	-9(12)	**40**
ReO	NCS^{-}	$3.48(4)\times10^{-3}$	$4.8(4)\times10^{-5}$	87(7)	73(8)	-46(20)	**41**
	TU	$3.99(9)\times10^{-2}$	$7.3(2)\times10^{-3}$	7.0(4)	52(1)	-95(3)	**42**
	NMTU	$6.7(2)\times10^{-2}$	$2.6(5)\times10^{-3}$	16.0(4)	42(3)	-125(10)	**43**
	NDMTU	$5.9(2)\times10^{-2}$	$2.5(3)\times10^{-3}$	31(2)	45(11)	-119(4)	**44**
	HN_3	$6.4(2)\times10^{-2}$	$6.9(6)\times10^{-4}$	3.2(3)	60(2)	-87(6)	**45**
ReN	CN^{-}[b]	$7.2(4)\times10^{3}$	12(2)	600(100)	39(2)	-40(6)	**46**
	HCN[b]	66	78	0.9			**47**
OsN	N_3^{-}	1.89(7)	$9.5(5)\times10^{-3}$	189(8)	58(2)	-45(3)	**48**

[a] See Scheme 2.1; [b]15°C; [c]20°C; [c] First-order rate constant; [31] Potgieter *et al*., (1988:209); [32, 33] Smit *et al*., (1993:2271); [34., 37]Leipoldt *et al*., (1986:179; 1986:4639); [35, 36] Smit, (1995:71); [38, 39, 40] Roodt *et al*., (1988:336; 1992:1080); [41, 42, 43, 44, 45] Purcell *et al*., (1989:224; 1991:339); [46, 47] Damoense *et al*., (1994:619); [48] Van der Westhuizen *et al*., (1994:717).

The large effect of the metal-aqua bond strength on the reaction rate of these complexes is also illustrated by the plot of log k_1 *vs*. pK_{a1} values of the $[MX(H_2O)(CN)_4]^{n-}$ (see **Figure 2.6**).

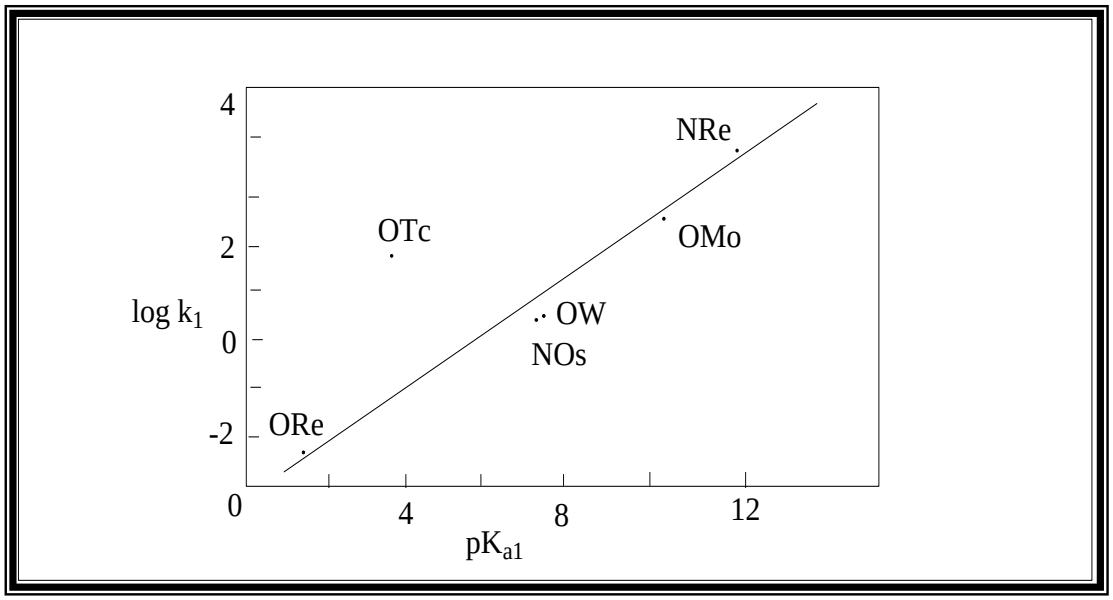

Figure 2.6: Linear free energy relationship for the reaction between various $[MX(H_2O)(CN)_4]^{n-}$ complexes and NCS, ORe = $[ReO(H_2O)(CN)_4]^-$; OTc = $[TcO(H_2O)(CN)_4]^-$; OW = $[WO(H_2O)(CN)_4]^{2-}$; OMo = $[MoO(H_2O)(CN)_4]^{2-}$; NOs = $[OsN(H_2O)(CN)_4]^{2-}$ and NRe = $[ReN(H_2O)(CN)_4]^{2-}$.

The observed LFER also points to a dissociative mechanism. The large deviation for the Tc(V) complex is difficult to explain (Roodt *et al*., 1992:1080). The pressure dependence of the pseudo first-order rate constant for the reaction between $WO(H_2O)(CN)_4]^{2-}$ with azide indicated a significant decrease in k_{obs} with increase in pressure, and the corresponding volume of (+10.6(5) $cm^3.mol^{-1}$) was obtained. Thus, a large positive volume of activation is, however, convincing evidence for a dissociative mechanism (Leipoldt *et al*., 1986:4639).

2.2.3.2 Bidentate ligands

It was also reported that the protonated complexes of $[MO_2(CN)_4]^{4-}$ (M = molybdenum(IV) and tungsten(IV)) are reactive towards bidentate ligand substitutions. The reaction between 1,10-phenanthroline (phen) and $[MoO(H_2O)(CN)_4]^{4-}$ was the first substitution reaction of these complexes that was studied by Basson *et al*. (1984:71; 1984:57) and Leipoldt *et al.* (1987:57). The crystal structure determination of the above-mentioned reaction product clearly showed the substitution of the aqua and one

cyano ligand by phen ligand (**A** in **Figure 2.7**). Two other phen molecules which were bonded to the sodium ion were also part of the crystal structure composition. The very large *trans*-influence of the oxo ligand was also observed in the structure of $[MoO(\eta^2\text{-phen})(CN)_3]^-$. The Mo-N bond *trans* to the oxo ligand was found to be about 0.19Å longer than the Mo-N bond *trans* to one of the cyano ligands. Similar results were obtained for the crystal structure determination of the $[WO(\eta^2\text{-bipy})(CN)_3]^-$ complex (where η indicates hapticity of the bidentate ligand) (Samotus *et al*., 1990:129; Szklarzewicz *et al*., 1990:2959).

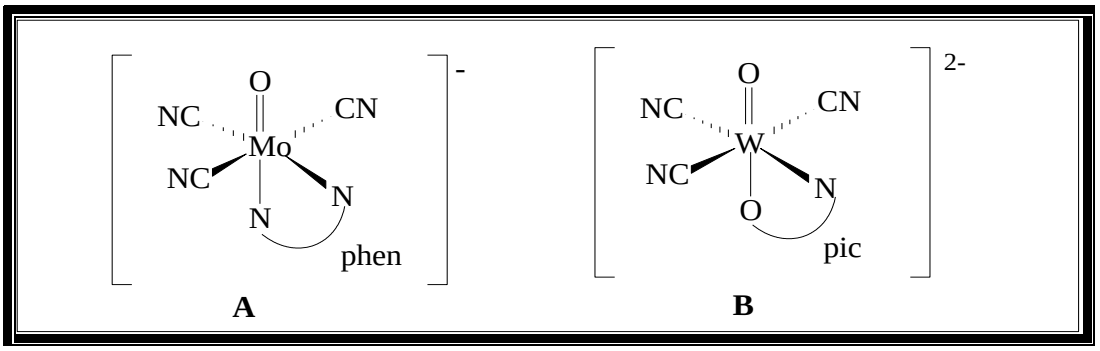

Figure 2.7: Bidentate ligands (1,10-phenanthroline (phen) and pyridine-2-carboxylate (pic)) substitution in $[MO(H_2O)(CN)_4]^{n-}$ complexes (M = Mo(IV) and W(IV)).

The question of which ligand (aqua or cyano) was substituted during the first step of this two-step process immediately arose. For this reason, Leipoldt *et al*. (1986:323) determined the crystal structure of the product of the reaction between $[WO(H_2O)(CN)_4]^{2-}$ and the unsymmetrical pyridine-2-carboxylate (pic). The results obtained from this study indicated that the carboxylato oxygen atom was bonded *trans* to the oxo ligand and that the pyridine nitrogen atom was bonded *cis* with respect to the oxo group (**B** in **Figure 2.7**). Kinetic results of the reactions between these two species showed a two-step reaction process. Since a metal-aqua bond is usually much weaker than a metal-cyano bond (due to the large *trans*-influence of the oxo ligand), one would expect that the aqua ligand would be substituted first during this two-step process.

According to the above-mentioned structural and kinetic results, the following reaction scheme (**Scheme 2.2**) was predicted for the reaction of $[MO(H_2O)(CN)_4]^{n-}$ (M = Mo(IV) and W(IV)) with κ^2-N,N and κ^2-N,O bidentate ligands:

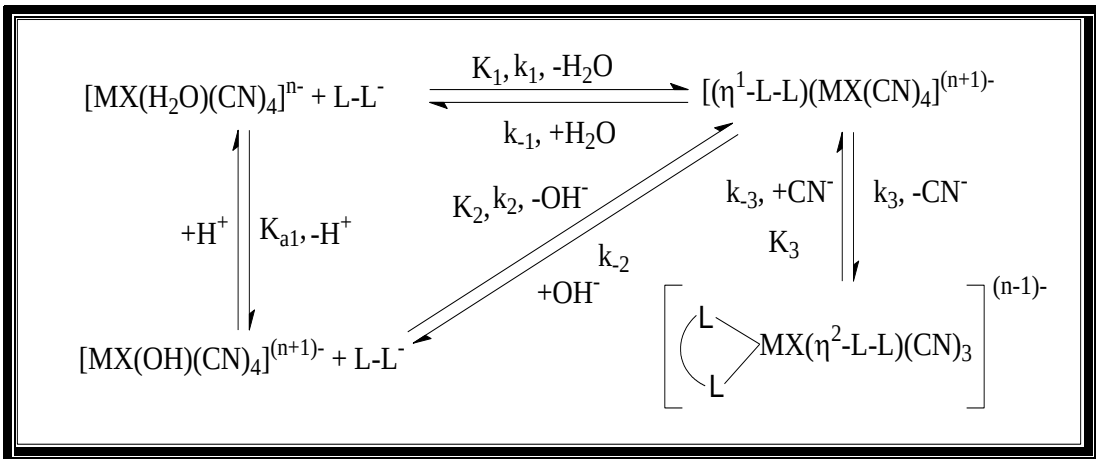

Scheme 2.2: The proposed reaction scheme for the reaction of the protonated nitrido and oxo complexes with bidentate ligands (X = N^{3-} or O^{2-}).

Recently, it has also been observed that the nitridotetracyano complex of Mn(V) is also reactive towards picolinate type ligands (such as pyridine-2-carboxylate, quinoline-2-carboxylate, pyridine-2,3-dicarboxylate, pyridine-2.4-dicarboxylic acid and pyridine-2,5-dicarboxylate) (Van der Westhuizen, 2004:109, b). The crystal structure determinations of $[MnN(\eta^2\text{-pic})(CN)_3]^{2-}$ and $[MnN(\eta^2\text{-quin})(CN)_3]^{2-}$ complexes were isolated and showed similar substitution behaviour to those of $[WO(\eta^2\text{-pic})(CN)_3]^{2-}$ and $[MoO(\eta^2\text{-pic})(CN)_3]^{2-}$ complexes (Leipoldt *et al.*, 1986:323; Szklarzewicz *et al.*, 2005:1749).

2.2.4 Formation of Octacyano Complexes

Although the octacyano complexes of molybdenum(IV) and tungsten(IV) have been known for many years and more convenient methods for synthesizing these complexes were more recently published by Leipoldt *et al.* (1974:350; 1974:343), little is known about the mechanism of the formation of these complexes. The reactions of the molybdenum(IV) and tungsten(IV) complexes with cyanide ions proceed *via* the same scheme as those of other monodentate ligands, with the formation of the pentacyano

complex. This very fast reaction is followed by a much slower reaction with the production of the octacyano complex in the presence of an excess of cyanide ions. A recent kinetic study of the formation of these complexes showed that the overall reaction may be presented as follows (**Scheme 2.3**):

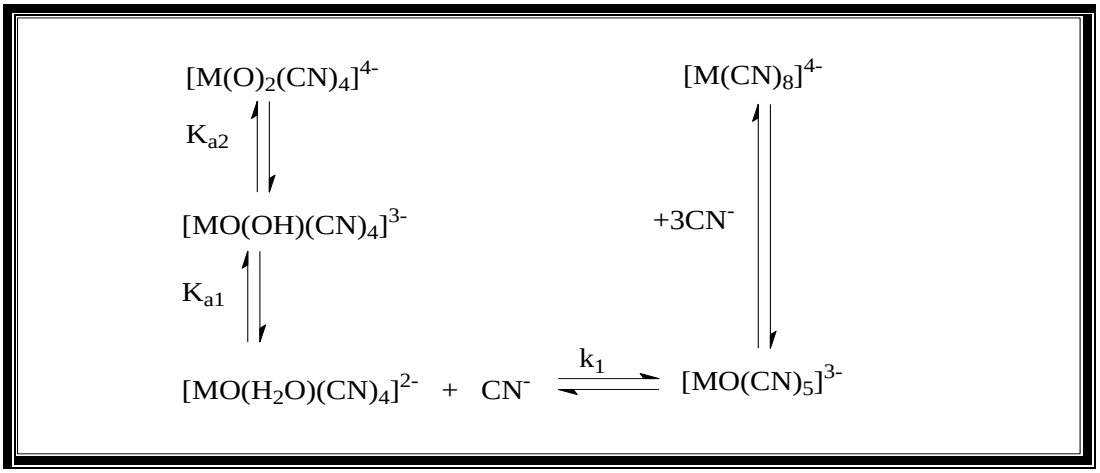

Scheme 2.3: Reaction scheme for the formation of octacyano complexes (M = Mo(IV) and W(IV).

The substitution of the aqua ligand (the formation of the pentacyano complex) was found to be a relatively fast reaction with rate constants of about 116 and 2.9 $M^{-1}s^{-1}$ for molybdenum (20°C) and tungsten (25°C) complexes respectively, while the formation of the octacyano complex from the pentacyano complex is a relatively slow reaction with a half-life of *ca*. 20 minutes (at $[CN^-]$ = 1.0M) for tungsten and 10^3 minutes for molybdenum complexes (Leipoldt *et al*., 1986:323; 1986:4639; Potgieter *et al*., 1988:209). The formation of $[M(CN)_8]^{4-}$ from $[MO(CN)_5]^{3-}$ was found to be third-order in cyanide ion concentration. The kinetic results indicated that the final rate-determining step probably involved the substitution of the aqua ligand in $[M(H_2O)(CN)_7]^{3-}$ with cyanide ions (Roodt *et al*., 1992:2864).

Scheme 2.3 makes it possible to explain for the first time why the octacyano complex of rhenium(V) (also a d^2 species) is still unknown, in spite of several attempts by different groups to synthesize this complex in the past. It was reported by Purcell *et al*. (1989:224) and Chakravorti (1972:893) that the reactive $[ReO(H_2O)(CN)_4]^-$ complex with pK_a of 4.2 and $[ReO(OH)(CN)_4]^{2-}$ with pK_a of 1.4, does not exist at pH > 8 where there are enough

free cyanide ions. The formation of the intermediate $[ReO(CN)_5]^{2-}$ (see **Scheme 2.3**) is thus impossible, preventing the formation of high cyanide complexes for rhenium(V) *via* this method.

2.2.5 Photochemical Reaction

The photosensitivity of aqueous and non-aqueous solutions of $[M(CN)_8]^{3-}$ where M = molybdenum(IV) and tungsten(IV), is well known and has been thoroughly investigated (Dudek & Samotus, 1985:271). Results from these studies have shown that photolysis reduces the octacyano d^1 species of the above-mentioned complexes to yield $[M(CN)_8]^{4-}$ as the main photoproduct. It was also shown that the primary product is also photosensitive and produces $[MO_2(CN)_4]^{4-}$ and the mono ($[MO(OH)(CN)_4]^{3-}$) as well as diprotonated ($[MO(H_2O)(CN)_4]^{2-}$) complexes (depending on pH) during photolysis. The following **Scheme 2.4** was proposed for these reactions.

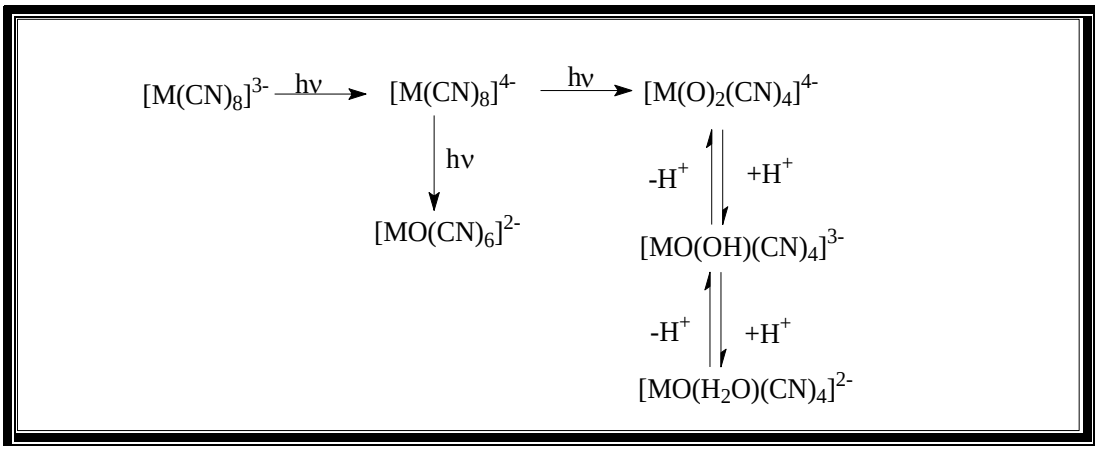

Scheme 2.4: Reaction scheme showing important photolytic reaction product of the octacyano complexes of Mo(V) and W(V).

Van der Westhuizen *et al*. (2002:506) investigated the first photolytic reaction between $[ReN(H_2O)(CN)_4]^{2-}$ and ethylenediamine in an attempt to synthesise a bidentate substitution reaction complex $[ReN(en)(CN)_3]^{2-}$. The reaction product, which was isolated as yellow crystals indicated that, in the final product, 1,2-ethanediamine acts as a bridge ligand between the two rhenium atoms and the final product was reported to be $[\{ReN(CN)_4\}_2(\mu\text{-en})]^{2-}$ (**Figure 2.7**).

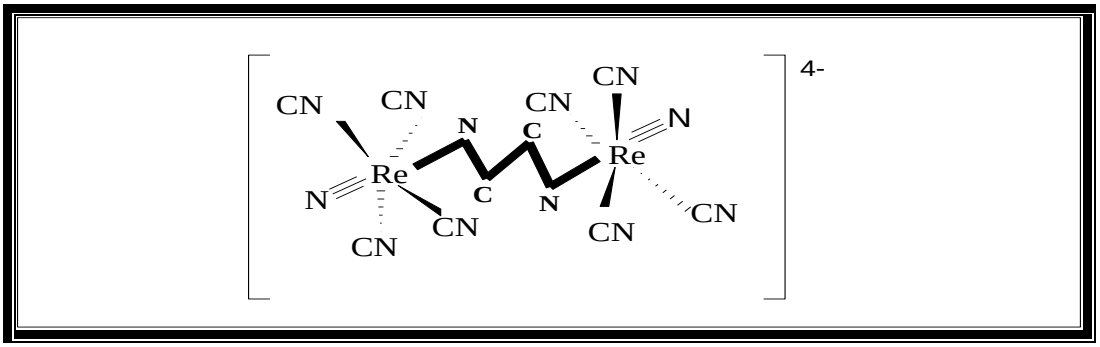

Figure 2.7: Structure of the $[\{ReN(CN)_4\}_2(\mu\text{-en})]^{4-}$ complex.

The crystal structure determination pointed to the following possible reaction for the formation of the final product:

$$2[ReN(H_2O)(CN)_4]^{2-} + en \rightleftharpoons^{h\nu} [\{ReN(CN)_4\}_2(\mu{-}en)]^{4-} + 2H_2O \qquad \textbf{(2.2)}$$

3 CHELATE FORMATION IN TRANSITION METAL COMPLEXES

3.1 INTRODUCTION

In the early development of coordination chemistry, the existence of a chelate containing organic moiety linked to a metal atom through more than one donor atom was discovered by Alfred Werner in 1893. Werner's insight into molecular structures of complexes led him unerringly to the concept of ring formations which he exemplified by discussing the structure of the compound $[Pt(NH_2C_2H_4NH_2)_2)]Cl_2$. It was clear to him that, in this compound, two molecules of ethylenediamine had replaced the four molecules of ammonia in $[Pt(NH_3)_4]Cl_2$. He concluded that each molecule of ethylenediamine occupied two of the four coordination positions and that, in so doing, it formed a five-membered heterocyclic ring. This idea of a ring structure in ethylenediamine complexes was the first to be discovered and published by Diehl (1937:39). In his classical paper of 1893, Werner was quite explicit about the structure of this ethylenediamine compound of platinum representing it as shown in **Figure 3.1**.

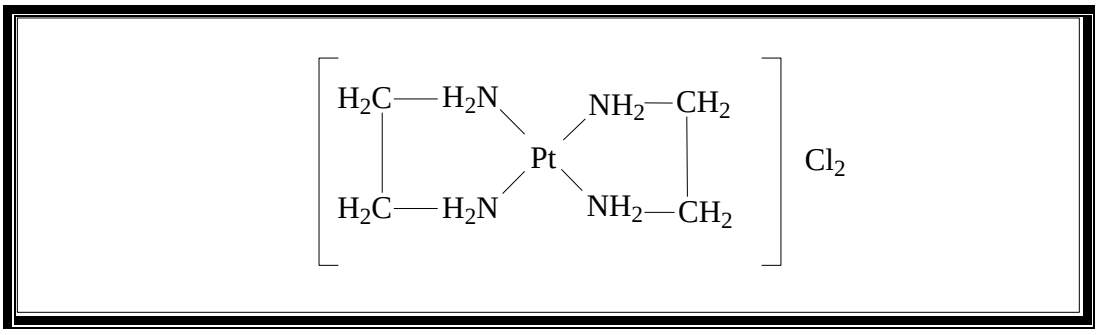

Figure 3.1: Structure of $[Pt(NH_2C_2H_4NH_2)_2)]Cl_2$.

After the discovery of chelation of ethylenediamine, the number and variety of molecules recognized as having the ability to chelate grew very rapidly. Oxalic acid was probably the next molecule to be recognized as a chelating agent in 1899 when Werner and Vilmos described the compound $[Co(en)_2(C_2O_4)]Cl$ which they had prepared by treating $[Co(en)_2Cl_2]Cl$ with an alkali oxalate. They regarded the oxalate group as occupying the two (*cis*) coordination positions previously occupied by the chlorine atoms. Ever since

their chelating properties were first discovered, ethylenediamine and oxalic acid have been widely used in studying the structures of metal complexes. They are amongst the simplest of all the chelating molecules and the literature abounds with references to many hundreds of metal chelates derived from them (Dwyer & Mellor, 1964:7, a).

3.2 CHELATION

In 1920, after Werner's discovery, Morgan and Drew (1920:1456) proposed the term "chelate" to designate the type of ring formations or acyclic structures which arise from the interactions of metallic atoms with organic or inorganic molecules or ions. To gain a common understanding of what a chelate is, it is necessary to establish first a definition. The word "chelate" was derived from the Greek word *chéle* (lobster or other crustaceans), is suggested for the caliperlike groups which function as two associating units and fasten to the central atom so as to produce heterocyclic rings. This type of ring formation was named chelation by Morgan and Drew, and the term has been used to cover all types of ring systems with metals and with hydrogen, without regarding the nature of the chemical bond involved (Jones, 1964:19, b).

There are, however, many molecules that have more than two points of attachment to the metal atom and form interlocking or fused chelate rings. According to the number of donor atoms capable of combining with a metal atom, the terms bidentate, tridentate, quinquedentate, sexadentate and octadentate chelating molecules were also proposed by the same authors to denote complexes formed with molecules or ions containing two, three, five, six and eight donor groups, respectively (Bailar & Busch, 1956:115, a). For example, unidentate ligand such as NH_3 cannot form a ring, but a bidentate ligand containing N,O- or N,N-donor atoms can form a chelate structure with the metal atom (see **Figure 3.2**).

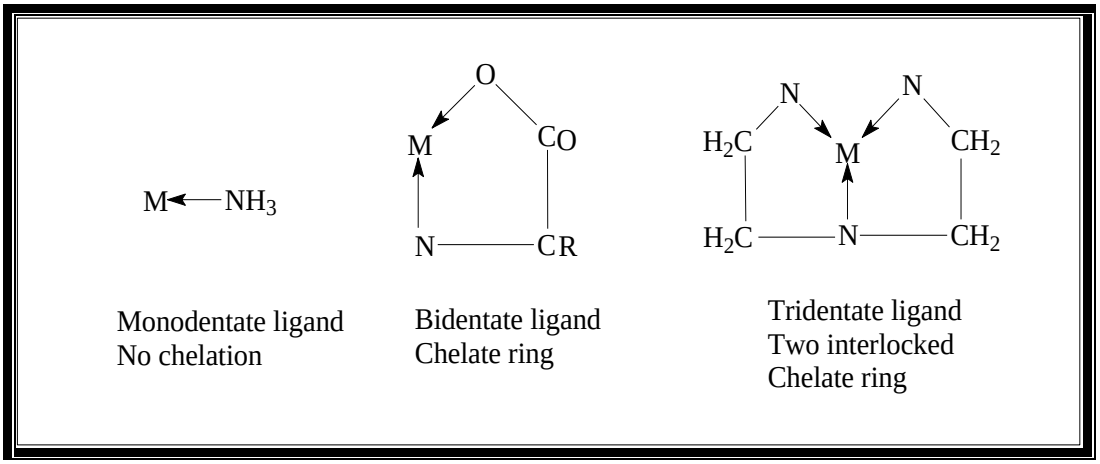

Figure 3.2: Chelates or ring formation by multidentate ligands.

The best known and the most studied chelating agents are undoubtedly the bidentate ligands. Thus, cyclic compounds in which a metal is jointed to two or more donor groups of a single molecule or ion, are particularly important since they have exceptionally high stability and, in many cases, have remarkable and valuable properties. The usefulness of metal chelates in various branches of theoretical and applied chemistry and allied fields is now generally recognized. The reagents which form metal chelates are used extensively in both qualitative and quantitative analysis. Dimethylglyoxime, pyridine-2-carboxylic acid, 8-hydroxyquinoline, cupferron, Fehling solutions and *o*-phenanthroline are example of substances which are indispensable to analytical separations and precipitations.

In the past 50 years, research on multidentate chelating agents has been stimulated by a number of factors such as their interesting and very often unique stereochemical properties, their widespread occurrence in living matters, and many practical applications in nuclear medicine. This interest has led to the recent synthesis and study (kinetics and crystallography) of wide variety of new chelate compounds containing N,O- and N,N-donor atoms (**Figure 3.3**) in tetracyanometalates complexes ($[MX(H_2O)(CN)_4]^{n-}$ (M = transition metal, X = O^{2-} or N^{3-}) of groups 6 and 7 elements (Roodt *et al*., 1994:599; Leipoldt *et al*., 1987:57; Samotus *et al*., 1991:614). Much work has been done on these types of complexes, but there are still uncertainties and questions regarding the reaction steps leading to the formation of the final product as well as the reaction mechanism involved. As part of this study, an investigation on these types of complexes with chelate agents containing heterocyclic N,O-donor atoms was undertaken. Some examples of the chelate agents are listed in **Figure 3.3**.

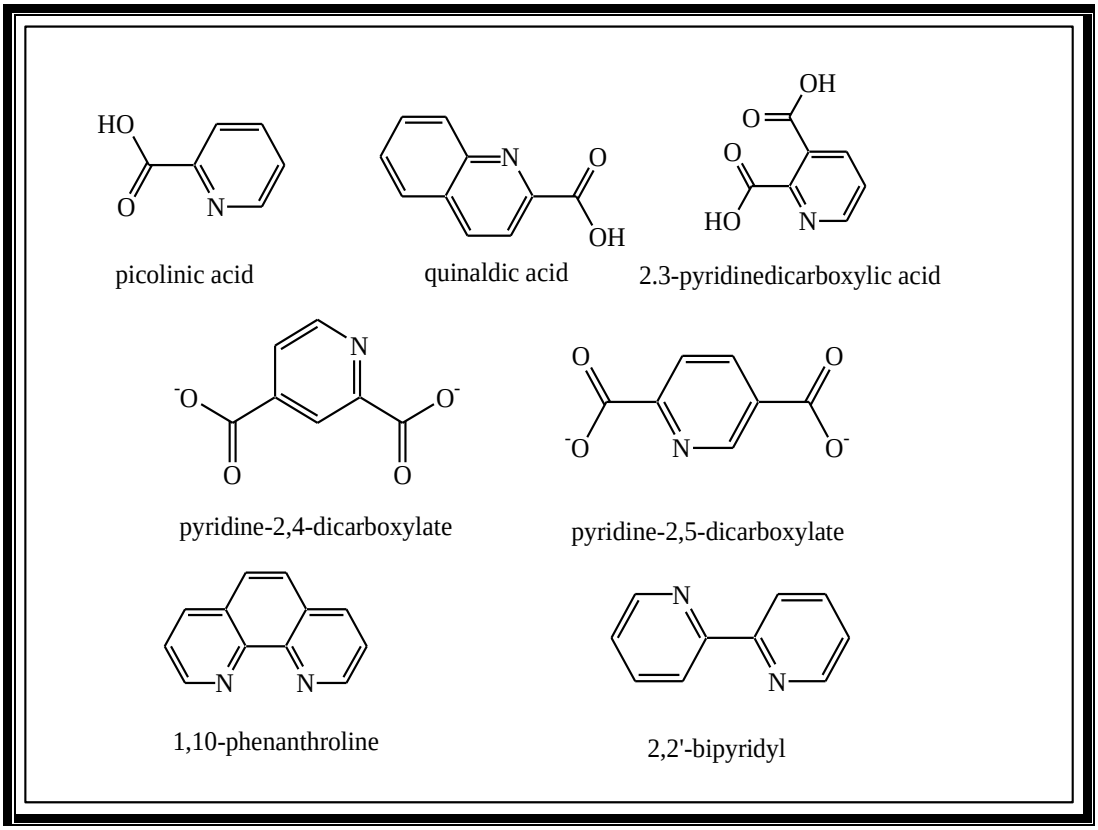

Figure 3.3: Different chelating agents.

In the following sections, some important factors contributing to the chelate formation in metal complexes will be discussed.

3.3 CONDITIONS NECESSARY FOR CHELATION

If a molecule is to function as a chelating agent, it must fulfill at least two conditions. Firstly, it must possess at least two appropriate functional groups, the donor atoms of which are capable of combining with the metal atom by donating a pair of electrons. These electrons may be contributed by a basic coordinating group such as NH_2 or acidic groups that have lost a proton.

Some acidic groups that combine with metal atoms by replacement of hydrogen are:

-COOH, -OH (enol and phenolic), -N-H, $-P(O)(OH)_2$, -SH, $-SO_3H$, -SH, R, and

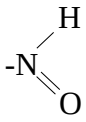

Coordinating groups include:

=O, $-NH_2$, -NH, -N=, -O-R, =NOH, -OH (alcoholic), –S- (thioether), $-AsR_2$ and $-PR_2$.

Secondly, these functional groups must be orientated in such a way in the molecule that they permit the formation of a ring with a metal atom as the closing member. These two conditions are necessary in chelate formation, but they are not always sufficient for the formation of a chelate ring (Dwyer & Mellor, 1964:17, b).

3.4 CHELATE EFFECT

The chelate effect refers to the advantage (stability) that a double-ended ligand such as ethylenediamine has when compared to the stability of the separate ligands (such as ammonia or methylamine) when bonded to the metal centre. There are two aspects that contribute to the chelate effect:

(i) in one, the standard free energy change (ΔG^o) for a bidentate coordination by a double-ended ligand can simply be twice compared to that of monodentate binding of one of the separate analogs. This is due to the fact that the double-ended ligand has two binding interactions compared with one interaction for a simple monodentate ligand.

(ii) the other aspect is that, in bidentate ligands, the second interaction can have a substantial entropy advantage. That is, once the one end of the bidentate ligand is attached to the metal centre, the second end is in the vicinity of the metal centre and can coordinate without paying the translational and rotational entropy cost of the first binding interaction. In this case, chelate coordination

> by a bidentate ligand can have a free-energy contribution more than twice that of the monodentate ligand (Breslow *et al*., 2000:333).

In the past decade, there has been a good deal of argument about the origin of the chelate effect, and there is no doubt that a number of factors are involved. A partial explanation may be given in terms of translational entropy (as discussed above) (Dwyer & Mellor, 1964:43, d). In other words, when two or more donor groups tied together to form an additional chelate ring without materially altering the donor groups, the increased stability of the chelate, as reflected in an increase in the formation constants, is due to an entropy increase (entropy difference) (Martell & Calvin, 1952:150, a). A difference in the heat of reaction between the ion and the donor molecule would also be reflected in a difference in the formation constants, but this would not be considered unless the donors differ appreciably, or unless the steriochemical structure of the chelate is greatly affected by the tying together of the organic groups (Bailar & Busch., 1956:244, b).

The chelate effect (as indicated above) can be seen by comparing the reaction of a chelating ligand and a metal ion with the corresponding reaction involving comparable monodentate ligands. For example, the comparison of the binding of ethylenediamine (en) and ammonia bindings to the metal centre. Calvin and Bailes (1946:949) as well as Spike and Parry (1953:2726 and 3770) have studied several complexes of Cd^{2+} and Ni^{2+} in order to illustrate the entropy-based chelate effect with these two ligands respectively. The results obtained are summarized in **Tables 3.1** and **3.2**. It has been known for many years that a comparison of this type always shows that the complex resulting from coordination with the chelating ligand is much more thermodynamically stable. This can be seen by comparing the values of the addition of two monodentate ligand with the values of the addition of one bidentate ligands; or comparing the addition of four monodentate ligands with two bidentate ligands; or comparing the addition of six monodentate ligands with three bidentate ligands (**Tables 3.1** and **3.2)**.

Table 3.1: Reactions of ammonia and ethylenediamine with Cd^{2+}.

Complex	log K	ΔH^o (kJmol^{-1})	ΔS^o (JK^{-1}mol^{-1})	ΔG^o (kJmol^{-1})
$[Cd(NH_3)_2]^{2+}$	4.950	-29.79	-5.19	-28.24
$[Cd(en)]^{2+}$	5.836	-29.41	+13.05	-33.30
$[Cd(NH_3)_4]^{2+}$	7.44	-53.14	-35.50	-42.51
$[Cd(en)_2]^{2+}$	10.62	-56.48	+13.75	-60.67

Table 3.2: Reaction of ammonia and ethylenediamine with Ni^{2+}.

# of ligands	ΔG^o (kJmol^{-1})	log K
1 NH_3	-16.0	2.8
2 NH_3 (1 en)	-28.5 (-42.8)	5.0 (7.51)
3 NH_3	-37.7	6.6
4 NH_3 (2 en)	-44.9 (-79.1)	7.87 (13.86)
5NH_3	-49.1	8.6
6 NH_3 (3 en)	-49.2 (-104.4)	8.61 (18.28)

A number of interesting observations can be made from the results in **Tables 3.1** and **3.2**. The stability of the metal chelate in each case is greater than that of the corresponding non-chelate complex. The ΔH^o values of the formation steps are almost identical: that is, heat is evolved to about the same extent, whether forming a complex involving monodentate or bidentate ligands. The difference in the obtained stability constant can be attributed to the significant change in the ΔS^o term which changes from negative (monodentate coordination) to positive (bidentate coordination) (see **Table 3.1**). There is also an increase in the size of the ΔS^o term for adding two monodentate ligand (NH_3) compared to adding four monodentate ligands (-5.19 to -35.50 JK^{-1}mol^{-1}, see **Table 3.1**). In case of the complex formation of Ni^{2+} with ammonia or ethylelediamine, by rewriting the equilibria, the following equations are produced:

$$[Ni(H_2O)_6]^{2+} + 6NH_3(aq) = [Ni(NH_3)_6]^{2+} + 6H_2O \quad (\mathbf{3.1})$$

$$[Ni(H_2O)_6]^{2+} + 3\ en(aq) = [Ni(en)_3]^{2+} + 6H_2O \quad (\mathbf{3.2})$$

By combining these two reactions a direct comparison was possible:

$$[Ni(NH_3)_6]^{2+} + 3\ en\ (aq) = [Ni(en)_3]^{2+} + 6NH_3\ (aq) \quad (\mathbf{3.3})$$

From the **Eq. 3.3**, the ΔG^o, ΔH^o and $-T\Delta S^o$ components were found to be -54, -29, and -25 $kJmol^{-1}$ respectively, and at 25ºC (298 K) $\Delta S^o = +88\ JK^{-1}mol^{-1}$. Considering the close similarities of the Ni-N bonds in both complexes, it is not surprising that the enthalpy of both the reactions will be the same ($\Delta H^o = -29\ kJmol^{-1}$). As indicated above, the entropy term found for these complexes is larger for the reactions involving a chelate (bidentate ligand) compared to the non-chelate (monodentate ligands). Thus, the increase in entropy by the displacement of ammonia or aqua with ethylenediamine can be explained by the number of moles of the reactants on the left-hand side compared to the number of moles of the products on the right-hand side. In the first reaction (**Eq. 3.1**) the number of moles on the left and right-hand side does not change. In the second and third reactions (**Eqs. 3.2** and **3.3**), there are four moles of reactants on the left-hand side, whereas on the right-hand side there are seven moles of products: i.e. there is a net gain of three moles as the reaction proceeds when six monodentate ligands are substituted by three bidentate ligands (**Eqs. 3.2** and **3.3**). Therefore, a disorder of the reaction increases with the resultant entropy increases (Cotton *et al*., 1995:186).

An alternative explanation comes from trying to understand how the reaction might proceed. Thus, to form a complex with six monodentate ligands requires six separate favourable interactions between the metal ion and the ligand molecules. The formation of the *tris*-bidentate metal complex requires three initial interactions for the ligand to attach itself by one end to the metal centre and the other end is always nearby and only requires a rotation of the end to enable the ligand to complete the chelate ring formation (Cotton *et al*., 1995:186).

The chelate effect also suggests that multiple ring formation should result in enhanced chelate stability. It has been reported that the chelate effect in a bidentate ligand is about half of that in a tridentate ligand which can form two interlocking rings and is about one third of that in a tetradentate ligand which can form three rings to the metal centre (Bailar & Busch, 1956:251, c).

3.5 IMPORTANCE OF THE STABILITY CONSTANT

The driving force towards the formation of metal chelates lies in the thermodynamic properties of the products. It has been found that complexes containing chelating ligands are generally more stable thermodynamically than those with an equivalent number of monodentate ligands (Purcell & Kotz, 1977:739, a). Since the stability constant (K) refers to a system in equilibrium, it may be used to calculate the free energy change (ΔG^o) and other thermodynamic parameters of the reaction involved. In order to understand the chelate effect, the following well-known thermodynamic relationship was introduced (**Eqs. 3.4, 3.5** and **3.6**):

$$\Delta G^o = -RT \ln K \qquad (\mathbf{3.4})$$

$$\Delta G^o = \Delta H^o - T\Delta S^o \qquad (\mathbf{3.5})$$

$$\Delta G^o = -2.303\ RT \log K \qquad (\mathbf{3.6})$$

where ΔG^o = the standard free energy change, R = gas constant, K = equilibrium constant, ΔH^o = standard heat-constant change (enthalpy change) and ΔS^o = standard entropy change.

These are important parameters in a kinetic study of any reaction. If accurate values of equilibrium constant (K) at two controlled temperatures are known, the quantities ΔG^o, ΔH^o and ΔS^o may be calculated from these relationships (Dwyer & Mellor, 1964:42, c). Unfortunately, very little information is available about chelate stability constants, and even less is known about the effect of temperature. The amount of work being done in this field, however, is steadily increasing, and further advances in this type of research

will probably make the important contributions to our knowledge of chelation for some years to come.

3.6 STABILITY OF THE CHELATE STRUCTURES

The conditions required for the maximal or complete formation of a complex may be predicted on the basis of its stability constant. The determination of equilibrium constants is of primary importance in the study of chelate compounds, since it is the most promising approach to obtain valuable data which should lead to a more comprehensive understanding of chelates and the relationship which governs their formation and structure (Dwyer & Mellor, 1964:42; c).

The stability constant for a metal ion and its ligand is related to the free energy for the reaction. From the definition of the ΔG^o (see **Paragraph 3.5** above), the next obvious question is which of the two thermodynamic functions, ΔH^o or ΔS^o, is the controlling factor which determines the extent of the stability of the product produced (Purcell & Kotz, 1977:736, b). The results in **Figure 3.4** give some indication of the factors that play an important role in complex stability**.** For the two ligands, having an amino donor group such as ethylenediamine and glycine, the plot of ΔH^o against the metal ion shows the same trend as the Irving-Williams series Therefore, at least for ligands having the amino donor group, the reaction is enthalpically controlled (**Figure 3.4**).

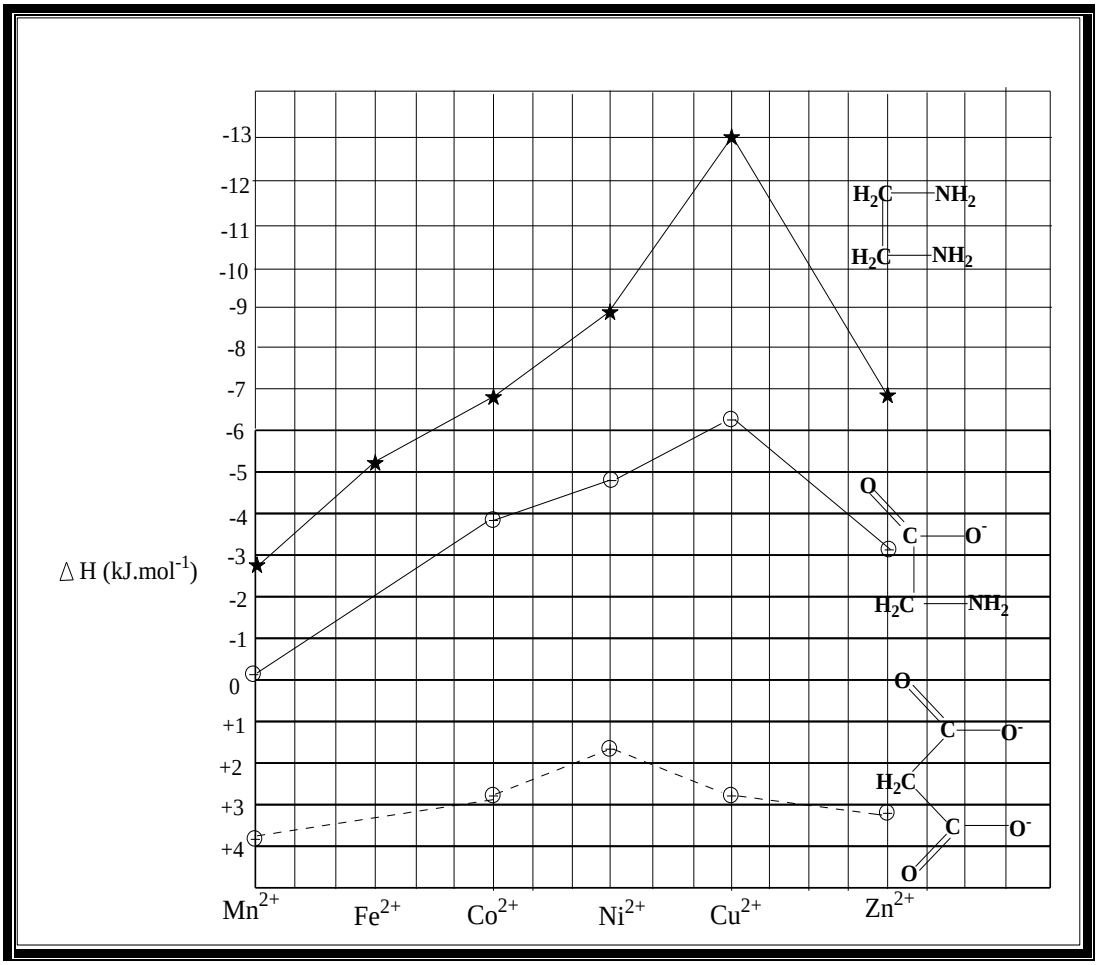

Figure 3.4: The trend in ΔHº values (for the reaction M^{2+} + L = ML^{n+}) as a function of M^{2+}.

On the other hand, the malonate ion reactions are all endothermic, so the stability of its complexes must arise from a large, positive ΔSº of reaction (data in **Table 3.3** support this conclusion). The positive ΔSº apparently arises from the extensive desolvation of the carboxylate group upon complexation of that group with the metal ion; an anion in aqueous solution is a good "organizer" of solvent, and this organization is lost when the carboxylate binds to the metal ion. The positive ΔHº for the carboxylate ion complexation reaction also has its origin in the ligand dissolvation. The reason for this is the fact that water is normally bound more strongly to the anionic carboxylate than to the dipolar amine group. Therefore, more energy is necessary to dissolve the carboxylate than the amine (Purcell & Kotz, 1977:736, b).

Table 3.3: Enthalpy and entropy change for the reaction $M^{2+} + L = ML^{n+}$ (where M = Mn^{2+}, Fe^{2+}, Co^{2+}, Ni^{2+}, Cu^{2+} and Zn^{2+}, L = ethylenediamine, glycinate or malonate[a]).

Chelate agent	ΔH° and ΔS°	Mn^{2+}	Fe^{2+}	Co^{2+}	Ni^{2+}	Cu^{2+}	Zn^{2+}
$NH_2{\cdot}CH_2{\cdot}CH_2{\cdot}NH_2$	ΔH°	-2.8	-5.1	-6.9	-8.9	-13.0	-6.7
	ΔS°	3.0	3.0	4.0	5.5	5.4	4.0
$NH_2{\cdot}CH_2{\cdot}COO^-$	ΔH°	-0.3	-	-2.8	-4.9	-6.2	-3.3
	ΔS°	13.5	-	13.7	11.9	18.4	12.7
$^-OOC{\cdot}CH_2{\cdot}COO^-$	ΔH°	3.68	-	2.9	1.88	2.85	3.13
	ΔS°	27.4	-	27.0	25.0	35.4	28.0

[a] Aschcroft & Mortimer, (1970:445).

3.7 FACTORS INFLUENCING THE STABILITY OF THE METAL CHELATES

Two general approaches have been made to the problem of discovering the factors which influence the stability of metal complexes. The first involves the investigation of the stability of the complexes formed by a particular metal with a series of different, but usually related, chelating molecules. The second, which is essentially complementary to the first, involves the investigation of the stability of complexes formed by a series of metal ions with a given chelating molecule (Dwyer & Mellor, 1964:44, e).

In the first approach, the following factors are considered:

(i) Size of the chelate ring
(ii) Number of rings (fused rings in multidentate chelating molecules)
(iii) Basic strength of the chelating molecule

3.7.1 Size of the Chelating Ring

Generally it was found that five- and six-membered rings are by far the most common among metal chelates. Structures have been proposed for compounds in which the existence of larger chelate rings has been postulated, but very few have been studied by X-ray crystal analysis. Seven- and eight-membered rings are formed by higher homologue of some sexadentate molecules (e.g., the higher homologue of ethylenediaminetetraacetic acid). It has also been reported that five-membered chelate rings are more stable than six-membered rings which are, in turn, more stable than seven-membered rings (Bailar & Busch, 1956:227, d).

The ring size effects are also evident in **Table 3.4** when comparing the log K for metal ions in the +2 oxidation state which was introduced by Irving-Williams (1948:746). That is, for most metal ions, five-membered ring chelates formed by ethylenediamine, oxalate, and glycinate are more stable than the six-membered ring chelates of the malonate ion.

Table 3.4: The Irving-Williams series and the trend in log K_1 values as M^{2+} is changed.

Ligand	**log K_1**					
	Mn^{2+}	**Fe^{2+}**	**Co^{2+}**	**Ni^{2+}**	**Cu^{2+}**	**Zn^{2+}**
Ethyldiamine	2.84	4.21	5.91	7.76	10.20	5.92
Glycine	3.15	-	4.67	6.21	8.51	5.23
Oxalate	3.85	-	4.83	5.22	6.32	-
Malonate	3.52	-	3.81	4.06	5.62	3.85

The data in **Table 3.4** shows that for chelating rings of the same size with the same metal ion, the log K values will usually be in the order $(O\text{-}O)^{2-} < (O\text{-}N)^{-} <$ N-N. Thus, in general, diamine complexes will be more stable than amino acids complexes which will, in turn, be more stable than dicarboxylate complexes. This can be observed, at least, for the first row 2+ transition metal ions from Co^{2+} to Zn^{2+} (**Tables 3.3** and **3.4**, **Paragraph 3.6)** (Purcell & Kotz, 1977:740, c).

The stability of five-membered rings is not restricted to the coordination of amines. In 1947, Dey (1947:6169) compared the efficacy of dicarboxylic acids in the formation of coordination compounds with the metal(II) ions (Irving-Williams series). **Figure 3.5** illustrates the importance of ring size for a series of dicarboxylate ligands (Purcell & Kotz, 1977:740, c).

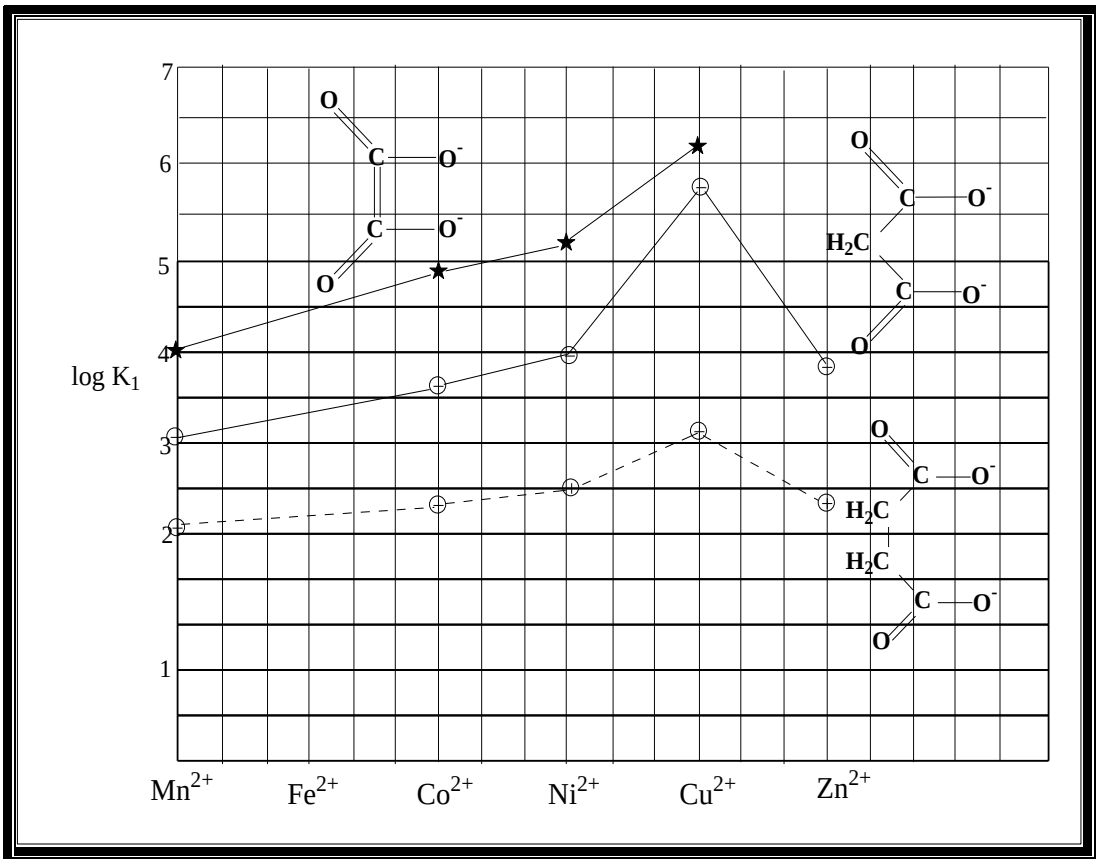

Figure 3.5: Complex stability (log K_1) as a function of ring size.

The log K_1 decreases from oxalic, malonic and succinic acids. This corresponds to a decrease in chelate stability as one goes from a five- to seven-membered ring.

3.7.2 Number of Chelate Rings

An increase in the number of rings within a particular chelate structure also affects complex stability. This is illustrated in **Table 3.5** by comparing log K_1 for the copper complexes with different amine chelates. On going from ethylenediamine to diethylenetriamine to triethylenetetramine complexes, the stability of the product

increases because the entropy of the reaction increases (more water molecules are released per metal ion upon complexation) and because the enthalpy change becomes marginally larger (see **Table.3.5**). These also illustrate the increase in stability which is associated with the chelate effect (Bailar & Busch, 1956:237, e).

Table 3.5: Stability constants of copper chelates as a function of the number of rings[a].

Chelate agent	Number of Donor groups	log K				ΔH^o	ΔS^o
		K_1	K_2	K_3	K_4		
NH_3	1	4.2	3.5	2.9	2.1	-	-
$NH_2 \cdot CH_2 \cdot CH_2 \cdot NH_2$	2	10.8	-	9.3	-	-24.6	+7
$NH_2(CH_2 \cdot CH_2 \cdot NH_2)_2$	3	16.0	-	-	5.4	-23.0	+8
$N(CH_2 \cdot CH_2 \cdot NH_2)_3$	4	18.8	-	-	-	-17.5	+21

[a] Basolo & Murmann, (1952:5243; 1954:211).

3.7.3 Basic Strength of the Chelating Molecule

The basicity (free energy change or equilibrium constant for $H^+ + L = HL^+$) of a ligand will most certainly be related to the complex stability, but this effect is not always as predictable as one might wish. At first it will seem reasonable to assume that complex stability should be directly related to ligand basicity, that is, more stable complexes are formed with more basic ligands. There are reasonable correlations between ligand basicity (as measured by the pK_a of the ligand conjugate acid) and log K, but good correlations only exist for series of closely related ligands (Purcell & Kotz, 1977:738, d). When a series of complexes do show a correlation between log K and pK_a, several very interesting observations may be made. The correlation between log K and pK_a is normally illustrated by a straight line ($\log K = \mathbf{a}pK_a + \mathbf{b}$). The constant **a**, is the slope of the line and is usually positive for the formation of more stable complexes with more basic ligands (Martell & Calvin, 1952:151, b).

The relationship between the chelate basic strength and stability was first pointed out by Calvin and Wilson (1945:2003) when they studied the stabilities of cupric chelates for a number of enolic substances. The complex stability constants and the hydrogen ion dissociation constants are listed in **Table 3.6** for some of the compounds investigated (Martell & Calvin, 1952:151, b).

Table 3.6: Stability constants and acid strength of different chelate ligands.

Chelate agent	**Log K**	**pK_a**
Salicylaldehyde	13.0	9.5
3-nitro-salicylaldehyde	8.2	6.0
5-nitro-salicylaldehyde	8.8	5.9
Acetylacetone	17.4	9.7
Trifloroacetylacetone	12.2	6.7
Benzoylacetone	18.0	9.8
c-methylacetylacetone	14.6	11.8
Ethylacetoacetate	14.2	11.2
2-hydroxyl-1-naphthaldehyde	14.0	8.4
3-ethoxy-salicylaldehyde	14.2	9.4

On plotting log K against pK_a, Calvin and Wilson obtained a number of roughly parallel straight lines, each line corresponding to a particular series of chelating agents. This showed that, for a series of closely related chelating agents, the greater the basic strength (pK_a) the greater the stability of the metal chelate (Dwyer & Mellor, 1964:45, f).

3.8 MECHANISM OF CHELATE SUBSTITUTION REACTIONS

The rate of substitution reactions of the aqua metal ions with multidentate ligands as entering groups varies much more than the corresponding reactions with monodentate ligands. The rate-determining step can change from the first coordination step to the later ring-closing step, depending on the type of the multi-dentate ligand. Steric effect may become important in ring-closure reactions (chelation) as well as in the initial

coordination step. Electrostatic repulsion due to a partially protonated multi-dentate ligand can influence the formation of the outer sphere complex and thus the total rate of the reaction. In certain cases, proton-shifting reactions of a partially-coordinated ligand can limit the overall reaction rate. All these factors tend to decrease the rate of formation reaction, but there are other factors which can make multi-dentate ligand reactions faster than monodentate ligands complex reactions. Electrostatic attraction between the metal ions and strongly negatively charged multi-dentate ligands is an obvious factor leading to rapid reaction rates. In addition, significant enhancement in the final reaction rate can result from the outer-sphere interaction of the multidentate ligand with coordinated water molecules (Martell, 1978:26, b).

3.8.1 Kinetics of Chelate Formation

It is constructive to consider first a general mechanism for a flexible bidentate substitution reaction or chelate formation from a kinetic analysis of the individual step involved.

Previous investigations of transition metal ion-chelating reactions have shown that the chelate coordination to the metal centre requires at least two steps (Kurstin *et al*., 1966:4610):

(i) First, there is a diffusion-limited ion-pair formation between the aquated metal ion and the incoming ligand.

(ii) Secondly, and rate determining, is the substitution of the aqua ligand out of the inner coordination shell. This process is normally controlled by the rate of release of a water molecule from the inner coordination sphere and is, therefore, a characteristic of the metal ion.

In 1967, Kowal *et al*. (1967:3126) reported that there is also a kinetic chelate effect. **Eqs. 3.7**, **3.8** and **3.9** illustrate the possible substitution reaction between octahedral metal complex and a bidentate ligand L-L as entering ligand.

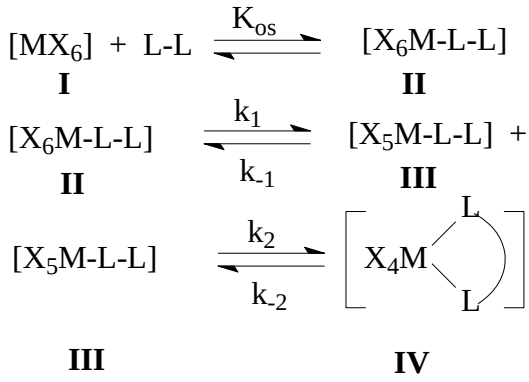

(**3.7**)

(**3.8**)

(**3.9**)

The species **II** in **Eq. 3.7** is an outer-sphere complex (fast reaction) with the stability constant $K_{os} = k_{os}/k_{-os}$. In scenarios where species **III** is formed under flow-equilibrium conditions and k_{-2} can be neglected, the forward rate constant of the formation of the final complex is given by **Eq. 3.10**:

$$\text{Rate} = \frac{k_{os}\, k_2 k_1}{k_{-1} + k_2} \qquad (\mathbf{3.10})$$

When the ring closure is much faster than the departure of the first monodentate ligand, **Eq. 3.10** simplifies and the forward rate constant is given by **Eq. 3.11**:

$$\text{Rate} = k_{os} k_1 \qquad (\mathbf{3.11})$$

The observed rate for the reaction is, therefore, the same as that for the monodentate substitution. As the rate-limiting step shifts to the ring-closure step, the forward rate constant will decrease with the proportion $[k_2/(k_{-1} + k_2)]$ and the reverse rate tends towards the limiting value of k_2 ($k_{-1} > k_2$). This means that the rate of the reaction will be slower than expected by monodentate substitution or water exchange rate constants and that the rate-determining step becomes the ring-closure step. For the bidentate ligand reactions, this decrease in reaction rate is sometimes the only proof of the first bond formation (k_1) being faster with ring closure (k_2) the rate-determining step (Wilkins, 1974:196; Margerum *et al*., 1978:42).

The rate of displacement of aqua and one cyano ligand in $[MX(H_2O)(CN)_4]^{n-}$ complexes with κ^2-N,O and κ^2-N,N ligands has been measured for a variety of metal ions (**Table 3.7**).

Table 3.7: Rate constants for the formation of $[MX(L\text{-}L)(CN)_3]^{n-}$ complexes (M = Mo(IV), W(IV) and Mn(V), X = O^{2-} or N^{3-}, L-L = bidentate ligands).

Metal	L-L	X	k_1 / $(M^{-1}s^{-1})^a$	k_2 / $(M^{-1}s^{-1})^a$	Ref.
W(IV)	Pyridine-2-carboxylate	O	0.80(7)	$1.70(8)\times10^{-3}$	**1**
Mn(V)	Pyridine-2-carboxylate	N	$1.15(4)\times10^{-3}$	0.02(2)	**2**
	pyridine-2,3-dicarboxylate	N	$1.1(1)\times10^{-3}$	0.12(4)	**2**
	pyridine-2,4-dicarboxylate	N	$8.5(5)\times10^{-3}$	-	**2**
	pyridine-2,5-dicarboxylate	N	$1.08(4)\times10^{-3}$	-	**2**
Mo(IV)	1,10-phenanthroline	O	$2.68(2)\times10^{-1}$	1.04(4)	**3**

[a] 25°C, [1] Roodt *et al*., (1994:599); [2] Van der Westhuizen, (2004:109, b); [3] Leipoldt *et al*., (1987:57).

It is believed that the mechanism for many of these complexes involves the very rapid dissociative activation in the first step (k_1) of the aqua substitution with an entering ligand to form a monodentate coordinated species (**Scheme 3.1**).

For a variety of metal ions it has been found that the rate of the reaction for a fast reaction is similar to those of monodentate substitution reactions (k_1 step). It was found, for example, that during the reaction between pyridine-2-carboxylate anion with tungsten(IV) system, the fast reaction observed involves the substitution of the aqua ligand and the forward rate constant of 0.80(8) $M^{-1}s^{-1}$ obtained for this step corresponds very well with the values obtained for aqua substitution by CN^-, N_3^-, NCS^-, and py (k_1 = 1.15(3), 4.2(1), 2.9(1) and 6.9(4) $M^{-1}s^{-1}$ respectively) (Smit, 1995:71; Roodt *et al*., 1988:336; Leipoldt *et al*., 1986:179; 1986:4639). The following reaction mechanism was proposed for these bidentate chelates with $[MX(H_2O)(CN)_4]^{n-}$ complexes (**Scheme 3.1**).

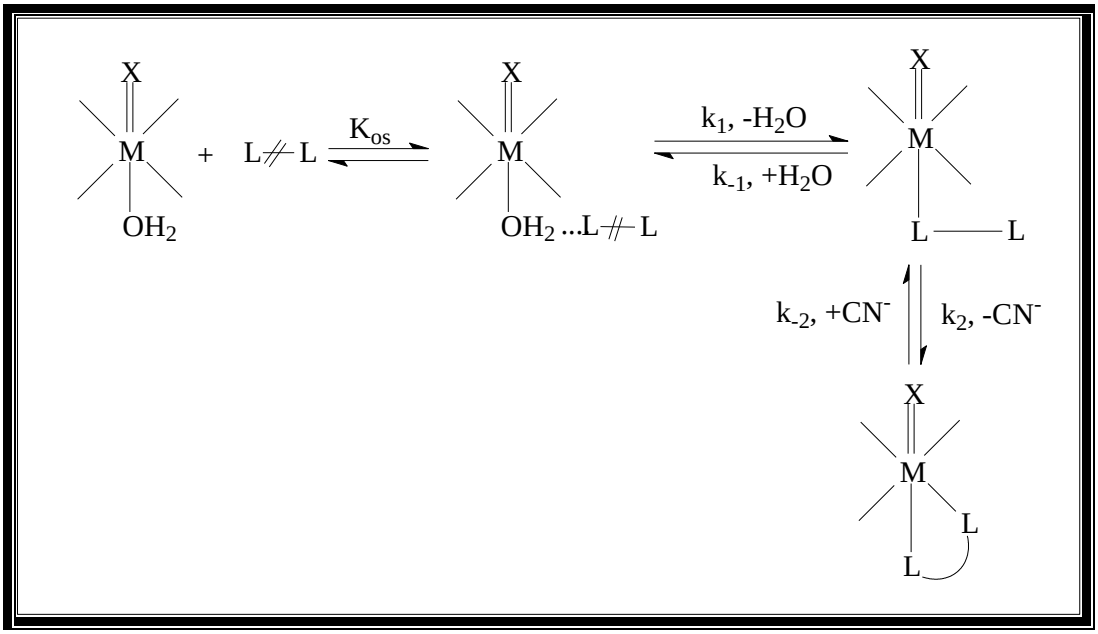

Scheme 3.1: Reaction mechanisms between $[MX(H_2O)(CN)_4]^{n-}$ complexes.

In the formation rate constants of the reactions of ammonia and the polyamines with metal aqua complexes of nickel(II) and Cu(II), it was found that ethylenediamine reacts 20 to 80 times faster than ammonia with $[Cu(H_2O)_6]^{2+}$ and $[Ni(H_2O)_6]^{2+}$, and 50 times faster than ethylamine with $[Ni(H_2O)_6]^{2+}$. This was reported by Rorabacher (1966:1891) with the use of the internal conjugate base mechanism (ICB) (see **Table 3.8** and **Scheme 3.2**).

Table 3.8: Comparative logarithmic rate constants for formation reactions showing the ICB effect for ethylenediamine[a].

Ligands	log K_1	
	Ni(II)	**Cu(II)**
NH_3	3.7	8.3
CH_2NH_2	3.1	-
$C_2H_5NH_2$	2.9	-
en	5.5	9.6

[a] Rorabacher & Melendez-cepeda, (1971:6071); Rorabacher, (1966:1891); Diebler & Rosen, (1972:1031); Kirschenbaum & Kurstin, (1970:684); Taylor *et al*., (1974:1282).

The ICB mechanism is outlined in **Scheme 3.2** for ethylenediamine ligand. **Scheme 3.2** is a combination of the conjugate base effect as elucidated by Basolo and

Pearson (1967:225) and the internal hydrolysis of the metal-ligand-inner sphere complex proposed by Eigen (1963:97).

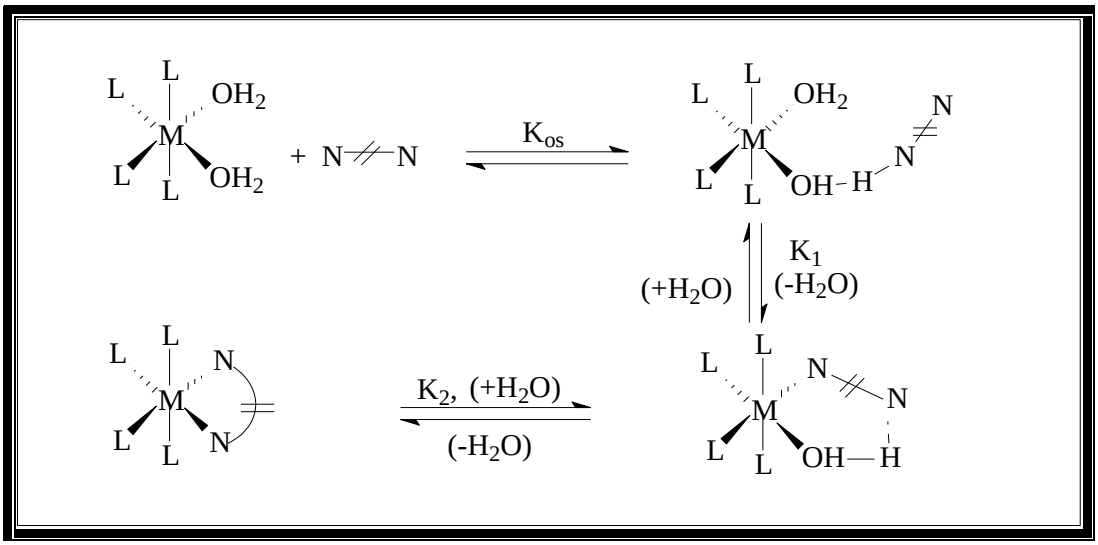

Scheme 3.2: Schematic representation of the conjugate base effect in the coordination of ethylenediamine.

The general prediction of the ICB mechanism is that the multidentate ligand must have one strongly basic donor atom which can form a strong hydrogen bond with a coordinated water molecule to give a stronger outer-sphere complex (large k_{os}) and to labilize the subsequent water exchange from an adjacent position on the metal ion so that the other donor atoms from the ligand can rotate freely enough to readily occupy an inner-sphere coordination position. Hence, the ICB effect might be expected for ligands with one amine group and one basic group such as the amino acids.

The primary criteria which are used to identify the ICB mechanism are the reaction rates of bidentate substitution reactions. They are faster than expected according to the monodentate substitution or water exchange rate constants. In a way, this turns out to be a self-limiting criterion because the ICB effect can contribute to a shift in the location of the rate-determining step in amino acids and in other similar ligands. This shift, in turn, often leads to smaller chelation rate constants and, therefore, hides any effect which ICB formation may have in the initial coordination step. Steric effects could, however, cause a very small ring closure equilibrium constant and could, therefore, overshadow any ICB effect (Martell, 1978:32, c).

The substitution kinetics of various transition metals complexes with amino acid as entering bidentate ligands were first studied by Kurstin, Pasternack and co-workers (1966:4610; 1967:3126; 1968:2295; 1968:2805; 1969:3814; 1972:2329). It was found that the amino acids react much slower than expected. Wilkins (1970:408) proposed that the amino group bind first, but Lin and Rorabacher (1973:2402) were in favour of the carboxylate group coordination in the first step. Based on the experimental data, it can be argued that the amino group cannot bind first if the ring closure is rate-determining. It is, however, expected that the carboxylate group of the amino acids would bind first, for the following reasons:

(i) There is a strong electrostatic attraction between the carboxylate group and the positive metal ion.

(ii) The carboxylate group forms a stronger hydrogen bond with the coordinated aqua-ligand which orientates the bidentate ligand with respect to the metal complex during the formation of the outer-sphere complex.

(iii) The ICB effect, where the outer-sphere association of the coordinated water molecule with the amino group accelerating the displacement of the other coordinated water molecules.

(iv) A pre-condition for ring-closure as a rate-determining step is that $(k_2/k_{-1}) < 1$. This would happen when the $-COO^-$ group binds first seeing that k_{-1} is larger for metal-carboxylate than for metal-amino complex due to weaker bonding and probable ICB effects. A proportion of $(k_2/k_{-1}) < 1$ is more probable seeing that k_2 will be smaller for amino group ring-closure due to weaker electrostatic attraction, and also due to a coordinated $-COO^-$ group that will labilise the other water molecule in a smaller way as a NH_3 group.

Amino carboxylate ligands as entering groups are not the only ligands for which proof of ring-closure as a rate-determining step is found. The k_2/k_{-1} proportion for the reaction of $[Ni(H_2O)_6]^{2+}$ ions with 2,2'bypiridine as bidentate ligands was determined as 0.5 which shows that the ring-closure contributes to the total rate of the reaction. The reaction of $[Cu(H_2O)_6]^{2+}$ with 2,2'-bipyridyl is also approximately a factor of 10 slower than the reaction with HN_3 and imidazole was predicted. This shows that the ring-closure often contributes to the rate-determining step (Martell, 1978:32, c).

The considerable variation in the rate-determining step of the substitution reactions of various metal ions with multidentate ligands, shows that the formation rate constants are frequently dependent on the character of the entering ligands. This can be explained by a dissociative mechanism when all the factors contributing to the reaction rate are being considered. It has been shown that, especially with aminocarboxylic acid ligands, the ring-closure becomes the rate-determining step (Roodt *et al*., 1994:599). Steric effects can also influence the formation rate constants by changing the value of K_{os}. Steric hindrance can, therefore, also be responsible for the rate-determining step shifting to ring-closure.

3.9 CRYSTAL STRUCTURE ANALYSIS OF METAL CHELATES

Although chemical methods of investigation (kinetics) left no doubt about the existence of the chelate ring formation and about the general features of the structure of the metal chelates of the type $[MX(L\text{-}L)(CN)_3]^{n-}$ (M = Mo(IV), W(IV) and Mn(V), X = O^{2-} or N^{3-}), confirmation of the correctness of these and other structures by X-ray crystal analysis can greatly strengthen our knowledge of chelation (Leipoldt *et al*., 1986:323; Szklarzewicz *et al*., 2005:1749; Samotus *et al*., 1991:614). X-ray structure analysis introduces a metrical element into the understanding of chelate rings by revealing the length and angles of chemical bonds and other structural details that could not be gained by the purely chemical method. The precise allocation of all the atoms within a unit cell of a crystal by X-ray analysis provides the strongest and most detailed evidence available for the existence of the chelate ring (Dwyer & Mellor, 1978:31, g).

Many properties of the chelation are determined by the nature of the organic chelating agent which combines with the metal ion. As indicated earlier (**Paragraph 3.7**), the size of the ring and the number of rings formed with a given metal ion are governed by the structure of the chelating agent. These factors, for the most part, are the characteristics of the chelate alone, not of the complex in general, and provide some justification for the study of metal chelates as a special class of chemical compounds. The most important effect is that of tying together donor groups (making a ring to the metal ion and corresponding entropy effect). This, in fact, provides the best means of understanding the special nature of the chelate compounds (Martell, 1978:2, a).

In the process of chelation, there may be some modification of the natural bond angles of the metal and the chelating agent to permit ring formation. The natural angle, 90º, of the octahedral and square-coordinated metal complexes, is not the angle of regular or nearly regular five- and six-membered rings. Generally, the deviation from 90º is not great, though in extreme cases (for example, in four-membered rings), it may be as large as 20º. Not only does chelation sometimes result in a modification of the bond angles of the chelating agent but it may also modify bond lengths and the chemical reactivity of the agent (Dwyer & Mellor, 1964:19, h).

Some of the crystal structure determinations of different chelating agents in transition metal complexes of groups 6 and 7 will be discussed in **Chapter 5**.

4 SYNTHESIS AND CHARACTERIZATION OF COMPLEXES

4.1 INTRODUCTION

The syntheses of all complexes and relevant synthetic reagents used in this study are described in this chapter, and the relevance of these complexes is illustrated in **Scheme 6.1** (**Chapter 6**). Several of the complexes described were characterized by means of X-ray crystallography and will be discussed in more details in **Chapters 5**. Correlations between UV/VIS, IR data and X-ray crystal structure determinations will also be discussed.

Syntheses of nitrido complexes of rhenium(V) have been described in literature during past decades. The first nitrido complex of rhenium, the nitridotrioxorhenate(VII) ion ($[ReO_3N]^{2-}$), was synthesized by Clifford and Olsen (1960:167). In 1962 other nitrido-complexes of rhenium(V) of the type $[ReNX_2(PPh_3)_2]$ and $[ReNX_2(PR_3)_3]$ (where X = Cl, Br or I, R = alkyl or aryl groups) were isolated by Chatt and Rowe (1962:4019), and then, in 1964, Chatt *et al*. (1964:1012) formulated the previously described $[ReX_2(PPh_3)_2]$ as $[ReNX_2(PPh_3)_2]$ because the nitrogen was not originally suspected to be part of the coordination sphere.

The above-mentioned stable complexes are perfect starting materials for synthesis of aquanitridotetracyano complexes of rhenium(V) ($[ReN(H_2O)(CN)_4]^{2-}$). Lock and Wilkinson (1964:2281) isolated two different products from the reaction between perrhenic acid with potassium cyanide and hydrazine sulphate. The yellow $K_3[ReN(CN)_5]$ product was obtained by the reaction of $[ReNX_2(PPh_3)_2]$ with a solution of an excess potassium cyanide in methanol, but when potassium cyanide was not in excess, a pink $K_2[ReN(CN)_4]\cdot H_2O$ was obtained. These two products do not dissolve in water at the same rate and, through this characteristic, these products were separated and identified by IR-data analysis.

The IR-data showed that the most soluble product had a strong cyanide frequency at 2100 cm^{-1} and a strong peak at 780 cm^{-1}. These results indicated that this product was the $[ReN(CN)_4]^{3-}$ ion, since the cyanide stretching frequency agreed well with that obtained previously for the $[ReO_2(CN)_4]^{3-}$ complex (Davies & Morgan, 1938:1858). The IR spectra of a less soluble pink product showed a strong peak that splits into two at 974 and 997 cm^{-1} and a single strong peak at 2160 cm^{-1}. Lock and Wilkinson (1964:2281) attributed these two peaks at 974 and 997 cm^{-1} to the Re≡N stretching frequency, because of the previous results of nitrido-complexes of rhenium. The strong peak at 2160 cm^{-1} was attributed to the Re-C≡N stretching frequency in a planar $[Re(CN)_4]^-$ configuration. A strong peak at 1609 cm^{-1} was observed for the first time by Lock and Wilkinson for the pink product. He assigned this characteristic peak to the coordinated water molecule and from these results the anion of the pink product was then proposed as the *trans*-$[ReN(CN)_4(H_2O)]^{2-}$ ion.

The existence of the *trans*-$[ReN(CN)_4(H_2O)]^{2-}$ complex was further confirmed by Johnson (1969:1843). In his study he found that the Re≡N entity of the $[ReN(CN)_4]^{2-}$ ion has a stretching frequency at 988 and 959 cm^{-1} in solid state and 1087 cm^{-1} in aqueous solution. With these results, he proposed that $[ReN(CN)_4]^{2-}$ exists in solution as the *trans*-$[ReN(CN)_4(H_2O)]^{2-}$ ion, and this ion showed two strong peaks at 994 and 965 cm^{-1}, a single strong peak at 2120 cm^{-1} and a medium peak at 1609 cm^{-1}. These peaks were attributed to Re≡N, C≡N, and H-O-H stretching frequencies, respectively.

The structural analysis of $K_2[ReN(CN)_4]$ was first reported by Davies *et al*. (1969:736). The X-ray structural results indicated that the $K_2[ReN(CN)_4]\cdot H_2O$ consists of infinite chains of alternating nitrogen and rhenium atoms, with four cyanide groups around each rhenium atom. Furthermore, the nitrido-nitrogen atoms interact with two rhenium atoms in the solid, but with only one in solution. According to these results the anion $[ReN(CN)_4]^{2-}$ exists in the solid state, but in aqueous solution probably exists as *trans*-$[ReN(CN)_4(H_2O)]^{2-}$.

Previous reports have shown that the $[ReN(H_2O)(CN)_4]^{2-}$ complex can undergo monodentate ligands substitution reaction with the replacement of the aqua ligand in the *trans* position to the nitrido ligand and this resulted in the formation of the

$[ReN(L)(CN)_4]^{2-}$ complex (L = monodentate ligands). These substitutions were made possible by the very stable $Re{\equiv}N^{2+}$ unit, which is the result of a nitrido ligand being one of the strongest π-donor atoms known (Purcell *et al*., 1991:473; 1992:387; 1992:217).

Research into nitridotetracyano complexes of rhenium(V) with bidentate ligands has not received much attention up to date, whereas the corresponding analogues of molybdenum(IV), tungsten(IV) and manganese(V) are known. Thus $[MoO(\eta^2\text{-phen})(CN)_3]^-$ (Basson *et al*., 1984:71), $[WO(\eta^2\text{-pic})(CN)_3]^{2-}$ (Leipoldt *et al*., 1986:323), $[MnN(\eta^2\text{-pic})(CN)_3]^{2-}$, $[MnN(\eta^2\text{-quin})(CN)_3]^{2-}$, $[MnN(\eta^2\text{-dipic})(CN)_3]^{2-}$, $[MnN(\eta^2\text{-phen})(CN)_3]^-$, $[MnN(\eta^2\text{-bipy})(CN)_3]^-$ and $[MnN(\eta^2\text{-en})(CN)_3]^-$ (Van der Westhuizen, 2004:90, a) complexes have been synthesized and the tetraphenylphosphonium or tetraphenylarsonium salts of these anions have been characterized crystallographically.

In this study the preparation of the tetraphenylphosphonium and tetraphenylarsonium salts of the different isolated complexes of the type $[ReN(L\text{-}L)(CN)_3]^{2-}$ containing a variety of bidentate ligands such as pyridine-2-carboxylate (pic^-) and quinoline-2-carboxylate ($quin^-$) will be attempted. These products will be characterized by means of IR and UV/VIS spectrophotometry and discussed in detail. As indicated in **Chapter 2** (**pharagraph 2.2.3.2**) it is expected that all the complexes investigated under study will also show similar behaviour towards substitution reactions.

4.2 CHEMICALS AND INSTRUMENTATION

Caution! Cyanide compounds are extremely toxic and HCN can be generated under certain conditions while working with these compounds. Therefore, the appropriate care was taken as far as possible and all manipulations of the complexes were done in a fume hood.

Chemicals and instruments: All chemicals used during the syntheses of the complexes were obtained from Merck and Sigma-Aldrich Chemical Company and used without further purification. Double distilled water was used in the syntheses and all the

syntheses were performed in a fume hood. The UV/VIS spectra were recorded on Varian Cary (model 50Conc) and Hitachi (model 150–20) spectrophotometers using 1.000±0.001 cm quartz cells at 80°C. All the infrared spectra of the complexes were recorded on a Digilab Merlim FT-IR spectrometer with a total of 32 scans and a resolution of 8.

4.3 SYNTHESIS OF COMPLEXES

The starting material $[ReNCl_2(PPh_3)_2]$ used for the synthesis of $K_2[ReN(H_2O)(CN)_4]$ was prepared according to the methods described by Johnson (1969:1843) and Damoense *et al*. (1994:619) and will be discussed in this section. The intensity of the IR stretching frequencies are presented as: **s** = strong, **m** = medium, **w** = weak

4.3.1 Synthesis of $[ReOCl_3(PPh_3)_2]$

$[ReOCl_3(PPh_3)_2]$ was prepared by a slight variation of the method reported by Johnson (1969:1843).

$KReO_4$ (1.0g, 3.46mmol) was dissolved in warm water (100ml, 50°C) and to this, a solution of tetrabutylammonium chloride hydrate (1g, 4.51mmol) in water (100ml, 50°C) was added. The solution was allowed to cool at room temperature, after which the solid was filtered and washed with water (3 × 5ml) (quantitative yield). The white solid was re-dissolved in concentrated hydrochloric acid (7ml) and slowly added to a suspension of triphenylphosphine (25g, 95mmol) in (250ml) glacial acetic acid. This solution was stirred for 30 minutes, and the green precipitate was removed by vacuum filtration and washed with glacial acetic acid (2 × 20ml) and diethyl ether (3 × 50ml) to give the desired product. Yield: 1.61g (56%), Mr = 833.14 g mol^{-1}.

There are other methods of preparation of $[ReOCl_3(PPh_3)_2]$ that will give a better yield (up to 95%) (Botha, 1995:35, b). The IR spectrum of this material is identical to that reported by Johnson (1969:1843).

Spectral data:

IR (powder): ν(Re=O), 996; other peaks; 1478(**m**), 1435(s), 1145(**w**), 1095(**w**), 741(**s**), 691(**s**), 608(**s**) cm^{-1}.

4.3.2 Synthesis of $[ReNCl_2(PPh_3)_2]$ (**Method A:** Johnson (1969:1843))

$[ReOCl_3(PPh_3)_2]$ (5.0g, 6.3mmol), triphenylphosphine (2.23g, 8.5mmol) and hydrazine sulphate (2.45g, 18.8mmol) were dissolved in ethanol and refluxed for three days under nitrogen atmosphere. The formed product was filtered and washed well with ethanol, warm water, ethanol and diethyl ether as brown microcrystals was obtained. Yield: 1.723g (36%), Mr = 795.7 g mol^{-1}.

The IR spectrum of this material correspond very well to that reported by Chatt *et al*., (1969:2288) with exception of the ν(Re≡N) stretching frequency.

Spectral data:

IR (powder): ν(Re≡N), 1094 cm^{-1}; other peaks; 1478(**w**), 1435(**m**), 744(**m**) and 691(**s**) cm^{-1}.

4.3.3 Synthesis of $[ReNCl_2(PPh_3)_2]$ (**Method B**: Damoense *et al.*, 1994:619)

Concentrated hydrochloric acid (10ml) was added to $KReO_4$ (0.5g, 1.7mmol), and the mixture was heated under reflux in a stream of nitrogen atmosphere for 30 minutes. Sodium azide (2.0g, 30.8mmol) dissolved in water (4ml) was added to the reaction mixture and further heated for 30 minutes. Triphenylphosphine (15.0g, 57.2mmol) dissolved in acetone (50ml) was then added and the reaction mixture was heated under reflux for 1.5 hrs. The sparingly soluble brown product was washed successively with hot water, ethanol and acetone to give brown microcrystals. Yield: 1.06g (77%), Mr = 795.7 g mol^{-1}.

Spectral Data:

IR (powder): ν(Re≡N), 1097 cm^{-1}; other stretching frequencies; 1466(**w**), 1435(**m**), 743(**m**) and 692(**s**) cm^{-1}.

$[ReNCl_2(PPh_3)_2]$ was also prepared by a slight modification of the method reported by Damoense *et al*. (1994:619).

Concentrated hydrochloric acid (10ml) was added to $KReO_4$ (0.5g, 1.7mmol), and the mixture was heated under reflux in a stream of nitrogen atmosphere for 30 minutes. Triphenylphosphine (15g, 57.2mmol) was dissolved in acetone (50ml) and the reaction mixture was further heated under reflux for 1.5 hrs. The solution turned green. Sodium azide (2g, 30.8mmol) dissolved in water (4ml) was then added (dropwise) to a reaction mixture and further heated for 30 minutes. The sparingly soluble brown product was washed successively with hot water, ethanol and acetone to give brown microcrystals. Yield: 1.13g (82%), Mr = 795.7 g mol^{-1}.

Spectral Data:

IR (powder): ν(Re≡N), 1096 cm^{-1}; other stretching frequencies; 1468(**w**), 1435(**m**), 744(**m**) and 693(**s**) cm^{-1}.

4.3.4 Synthesis of $K_2[ReN(H_2O)(CN)_4]$

A suspension of $[ReNCl_2(PPh_3)_2]$ (2.0g, 10.7mmol) and potassium cyanide (1.25g, 19.2mmol) in methanol (125ml) was heated under reflux in a stream of nitrogen atmosphere for 1.5 hrs. The resultant solid was filtered and dissolved in a solution of potassium cyanide (1g, 15.4mmol) in water (10ml) and then precipitated with methanol (50ml). The yellow solid was dissolved in water (9ml) and precipitated with methanol (45ml) as salmon pink microcrystals. Yield: 0.59g (58%), Mr = 400.5 g mol^{-1}.

The IR spectrum of this complex correspond very well to that reported by Johnson (1969:1843)

Spectral data:

IR (powder): ν(Re≡N), 966 and 993 cm^{-1}; ν(C≡N), 2117 cm^{-1}; ν(HOH), 1608 cm^{-1}

UV/VIS: λ_{max} = 284 nm, ε_{284} = 163 $M^{-1}cm^{-1}$;

λ_{max} = 385 nm, ε_{385} = 215 $M^{-1}cm^{-1}$.

4.3.5 Synthesis of $(AsPh_4)_2[ReN(H_2O)(CN)_4]\cdot 5H_2O$

$K_2[ReN(H_2O)(CN)_4$ (0.04g, 0.1mmol) was dissolved in H_2O (3ml). $(AsPh_4)Cl$ (0.04g, 0.1mmol) was dissolved in H_2O (3ml). The two solutions were mixed and left at ambient temperature to evaporate. Orange crystals, suitable for X-ray analysis, were obtained after 24 hrs: Mr = 1179.03 g mol^{-1}.

Spectral data:

IR (crystal): ν(Re≡N), 1107 and 1084 cm^{-1}; ν(C≡N), 2104 cm^{-1}.

UV/VIS: λ_{max} = 285 nm, ε_{285} = 96 $M^{-1}cm^{-1}$

λ_{max} = 388 nm, ε_{388} = 190 $M^{-1}cm^{-1}$.

4.3.6 Synthesis of $(PPh_4)_2[ReN(H_2O)(CN)_4]\cdot 5H_2O$

The synthesis of $(PPh_4)_2[ReN(H_2O)(CN)_4]\cdot 5H_2O$ was prepared according to the method described in the previous paragraph (**Paragraph 4.3.4**). The tetraphenylphosphonium was used instead of tetraphenylarsonium salts. Yellow crystals, suitable for X-ray analysis, were obtained after 24 hrs: Mr = 1091.29 g mol^{-1}.

Spectral data:

IR (crystal): ν(Re≡N), 1106 and 1089 cm^{-1}; ν(C≡N), 2105 cm^{-1}.

UV/VIS: λ_{max} = 323 nm, ε_{232} = 88 $M^{-1}cm^{-1}$

λ_{max} = 385 nm, ε_{385} = 180 $M^{-1}cm^{-1}$.

4.3.7 Synthesis of $(PPh_4)_4[ReN(H_2O)(CN)_3\text{-}\mu\text{-}CN\text{-}ReN(CN)_4]\cdot 5H_2O$

Pyridine-2,3-dicarboxylic acid (0.285g, 1.7mmol) was added to a solution of $K_2[ReN(H_2O)(CN)_4]$ (0.0285g, 0.07mmol) in water (8ml). The pH of the solution was adjusted to about 6.5 using acetic acid (5M). The reaction mixture was heated at 60°C for 3 hrs. The volume of the solution was kept constant (at 8ml) by adding distilled water. Tetraphenylphosphonium chloride hydrate (0.042g, 0.1mmol) in water (2ml) was added to a cooled reaction mixture and then allowed to evaporate at room temperature. Yellow

crystals, suitable for X-ray analysis, were obtained after 24 hrs: Mr = 2074.18 g mol^{-1} (see further discussion on page 70).

Spectral data:

IR (crystal): ν(Re≡N), 1080 cm^{-1}; ν(C≡N), 2102 cm^{-1}.

UV/VIS: λ_{max} = 410 nm, ε_{410} 199 $M^{-1}cm^{-1}$

λ_{max} = 360 nm, ε_{360} = 256 $M^{-1}cm^{-1}$

4.3.8 Synthesis of $(AsPh_4)_2[ReN(\eta^2\text{-pic})(CN)_3]\cdot 4H_2O$

$K_2[ReN(H_2O)(CN)_4]$ (0.50g, 1.25mmol) was dissolved in water (1ml). Pyridine-2-carboxylic acid (0.75g, 6.1mmol) and sodium carbonate (0.33g, 3.1mmol) were dissolved in water (10ml) and added to the first solution after effervescence had ceased. The reaction mixture was heated at 60°C for 6 hrs. The volume of the solution was kept constant at (12ml) by adding distilled water. The reaction mixture was allowed to cool at room temperature and tetraphenylarsonium chloride (0.82g, 0.19mmol) dissolved in water (2ml) was then added. Orange crystals, suitable for X-ray analysis, were obtained after 8 hrs: Mr = 1239.08 g mol^{-1}.

Spectral data:

IR (crystal): ν(Re≡N), 1061 cm^{-1}; ν(C≡N), 2106 cm^{-1}.

UV/VIS: λ_{max} = 355 nm, ε_{355} = 2300 $M^{-1}cm^{-1}$

λ_{max} = 400 nm, ε_{400} = 2000 $M^{-1}cm^{-1}$

4.3.9 Synthesis of $(AsPh_4)_2[ReN(\eta^2\text{-quin})(CN)_3]\cdot 2H_2O$

Quinaldic acid (quinoline-2-carboxylic acid) (0.025g, 1.4mmol) was added to a solution of $K_2[ReN(H_2O)(CN)_4]$ (0.057g, 0.14mmol) in water (6 ml). The pH of the solution was adjusted to about 6.5 using acetic acid (5M). Tetraphenylarsonium chloride (0.042g, 0.1mmol) in water (2ml) was added dropwise to a reaction mixture and allowed to evaporate at room temperature. Reddish crystals, suitable for X-ray analysis were obtained after 24 hrs: Mr = 1253.10 g mol^{-1}.

Spectral data:

IR(crystal): ν(Re≡N), 1080 cm^{-1}; ν(C≡N), 2106 cm^{-1}.

UV/VIS: λ_{max} = 450 nm, ε_{450} = 166 $M^{-1}cm^{-1}$.

4.3.10 Attempted Preparation of $[ReN(CN)_3(\eta^2\text{-phen})]^{n-}$ and $[ReN(CN)_3(\eta^2\text{-bipy})]^{n-}$ Complexes

The preparation of complexes formed between $[ReN(H_2O)(CN)_4]^{2-}$ and different bidentate ligands such as 1,10-phenanthroline and 2,2'-bipyridine was also attempted in this study. The same method as that described in **Paragraph 4.3.7** above, was used. Due to the slow reactions and weak solubility of these ligands in aqueous solution (at pH ~ 8.0), no crystals were isolated.

4.4 RESULTS AND DISCUSSION

The starting material, $[ReNCl_2(PPh_3)_2]$, was prepared by using two different methods described by Johnson (1969:1843) and Damoense *et al*. (1994:169) and these preparation routes towards the formation of $[ReN(H_2O)(CN)_4]^{2-}$ complex can be presented according to **Schemes 4.1** and **4.2**, respectively.

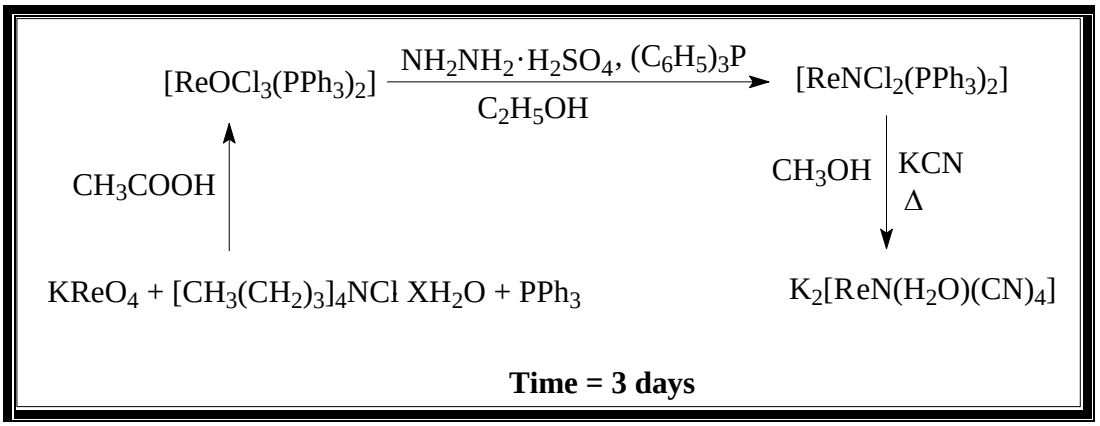

Scheme 4.1: Synthetic route for $K_2[ReN(H_2O)CN)_4]$ described by Johnson (1969:1843).

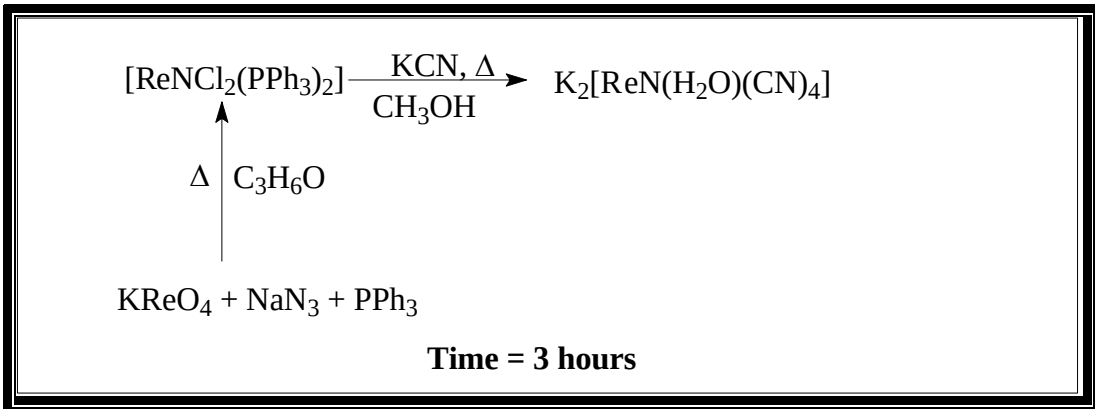

Scheme 4.2: Synthetic route of $K_2[ReN(H_2O)CN)_4]$ described by Damoense *et al.* (1994:169).

It has to be mentioned that during the preparation of $[ReNCl_2(PPh_3)_2]$ (**Scheme 4.1**), it is very important that this compound should be free from the oxo-compounds $[ReOX_3(PPh_3)_2]$ or $[ReO(OEt)X_2(PPh_3)]$ since these compounds can react with methanolic cyanide to give the $[ReO_2(CN)_4]^{3-}$ ion which is difficult to separate from the nitride-ion and results in low yield. When **Schemes 4.1** and **4.2** are compared, the

synthesis of $K_2[ReN(H_2O)(CN)_4]$ can be obtained in a much shorter period (3 hrs instead of 3 days) by using the method described in **Scheme 4.2**. One of the characteristic features of the pink $[ReN(H_2O)(CN)_4]^{2-}$ ion is that, upon dissolving in water, the colour of the solution changes from pink to yellow (**Eq. 4.1**). This pink product is slightly soluble and, therefore, no UV/VIS spectra are obtained.

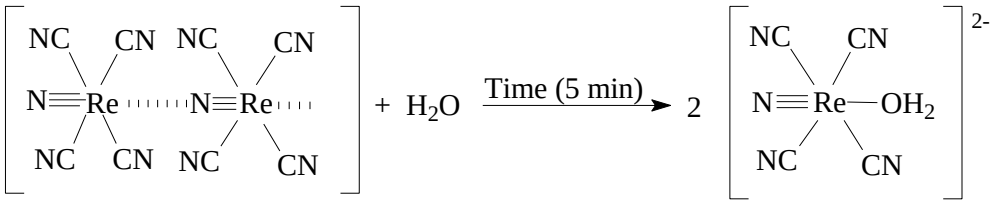

Salmon pink
Slightly soluble

Yellow
Highly soluble

(**4.1**)

The UV/VIS spectrum of $[ReN(H_2O)(CN)_4]^{2-}$ in aqueous solution scanned between 600 and 250 nm is shown in **Figure 4.1**. The $[ReN(H_2O)(CN)_4]^{2-}$ complex exhibits two absorption maxima at 385 nm (ε = 215 $M^{-1}cm^{-1}$) and 284 nm (ε = 162 $M^{-1}cm^{-1}$). These two characteristic bands correspond very well with other rhenium-nitrido complexes (386 and 292 nm in $[ReN(H_2O)(CN)_4]^{2-}$ and 422 and 287 nm in $[ReN(CN)_5]^{3-}$) (Purcell *et al*., 1992:387; 1991:473).

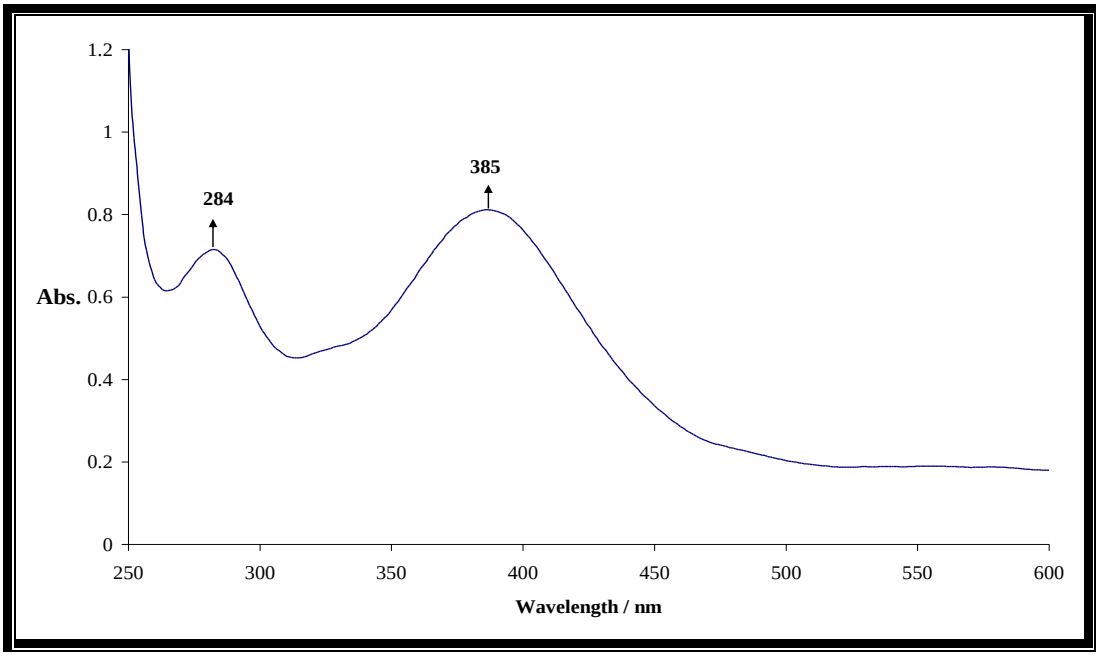

Figure 4.1: UV/VIS spectrum of the $[ReN(H_2O)(CN)_4]^{2-}$ complex in aqueous solution, $c_{ReN} = 1.0\times10^{-3}$M.

The reaction of $[ReN(H_2O)(CN)_4]^{2-}$ with different bidentate ligands (pyridine-2-carboxylate (pic), quinoline-2-carboxylate (quin) and pyridine-2,3-dicarboxylate (2,3-dipic) was initially performed at lower temperatures (below 30°C). During the reaction, there was no colour change of the reaction mixture, and a small absorbance change was observed. Upon heating the mixture (at temperatures above 60°C), a continuous change in absorbance, accompanied by a colour change of the reaction mixture, was observed with all the ligands studied. It was, therefore, decided to perform these reactions at a high temperature in order to get the desired products.

The UV/VIS spectral changes observed during the course of the reactions between $[ReN(H_2O)(CN)_4]^{2-}$ (which is the predominant ion under synthetic conditions) and different bidentate ligands are shown in **Figures 4.2, 4.3** and **4.4**, respectively.

The UV/VIS spectra observed during the reaction between $[ReN(H_2O)(CN)_4]^{2-}$ complex and pyridine-2-carboxylate at pH *ca*. 8.05 are shown in **Figure 4.2**.

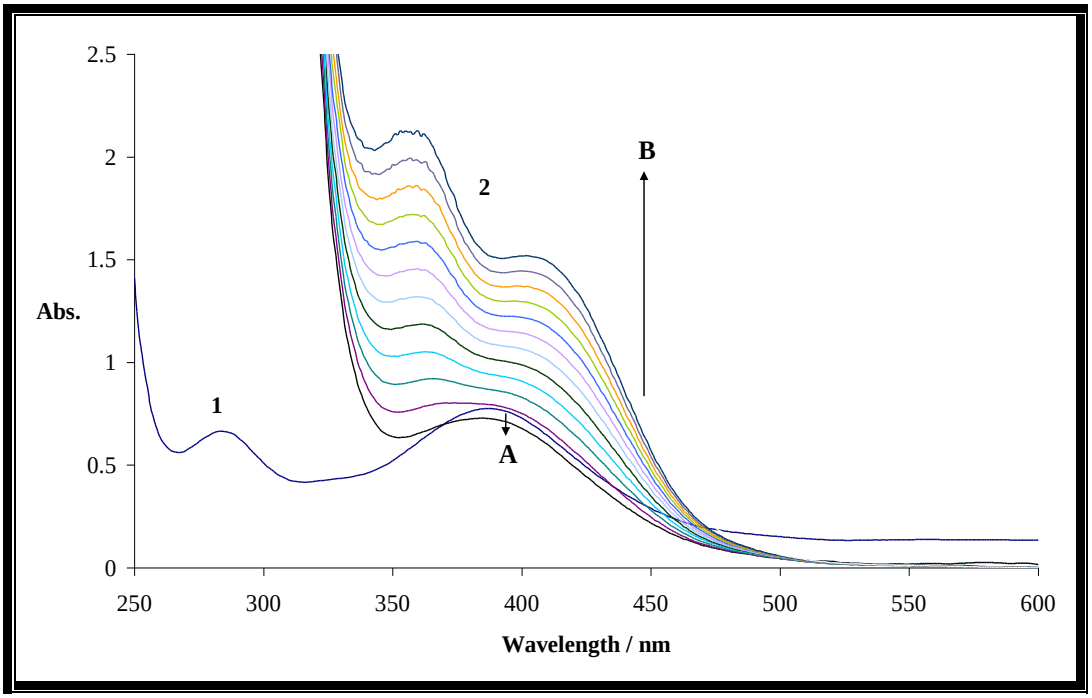

Figure 4.2: **The change in spectrum induced by addition of pic to the solution of $[ReN(H_2O)(CN)_4]^{2-}$; c_{ReN} = 1.0×10^{-3}M, c_{pic} = 1.0M, pH 8.05, T = 80.4°C. Time intervals: 1 minute; (1) Solution of $[ReN(H_2O)(CN)_4]^{2-}$ at pH 8.04; (2) Reaction mixture of $[ReN(H_2O)(CN)_4]^{2-}$ and [pic] at pH 8.04; (A) and (B) indicate the direction of absorbance changes.**

A continuous increase in absorbance resulted in the formation of two new absorption maxima at 355 and 400 nm (ε = 2300 and 2000 $M^{-1}cm^{-1}$, respectively), accompanied by the appearance of the yellow-orange colour. The formation of these maxima corresponds very well with the formation of the final complex $[ReN(\eta^2\text{-pic})(CN)_3]^{2-}$ according to the following reaction:

$$[ReN(CN)_4(H_2O)]^{2-} + pic^- \longrightarrow [ReN(\eta^2\text{-pic})(CN)_3]^{2-} + H_2O + CN^- \qquad (\mathbf{4.2})$$

On completion of the reaction, the addition of $(AsPh_4)Cl$ to the solution resulted in the isolation of orange crystals of $(AsPh_4)_2[ReN(\eta^2\text{-pic})(CN)_3]\cdot 4H_2O$ complex, which was confirmed by X-ray analysis (see crystal structure determination, **Chapter 5**).

The results in **Figure 4.3** show the UV/VIS spectra of the reaction between $[ReN(H_2O)(CN)_4]^{2-}$ and quinoline-2-carboxylate taken at pH *ca*. 8.02.

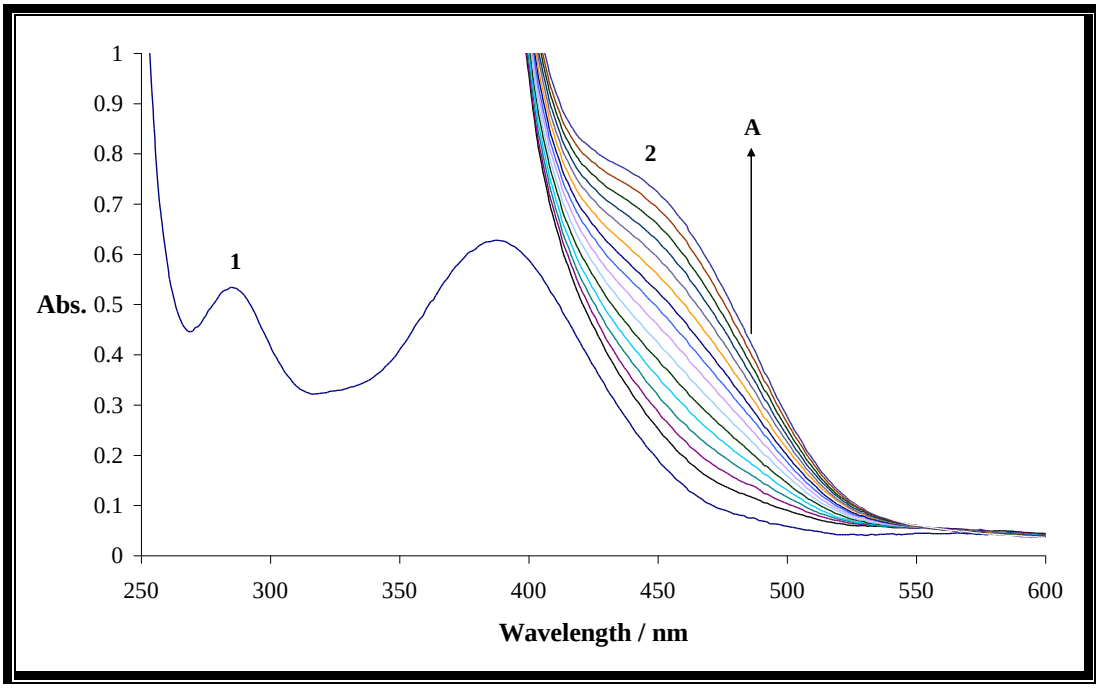

Figure 4.3: The change in spectrum induced by addition of quin to the solution of $[ReN(H_2O)(CN)_4]^{2-}$; c_{ReN} = 1.0×10^{-3}M, c_{quin} = 1.0M, pH 8.05, T = 80.4°C. Time intervals: 1 minute; arrows indicate the direction of the changes; (1) Solution of $[ReN(H_2O)(CN)_4]^{2-}$ at pH 8.03; (2) Reaction mixture of $[ReN(H_2O)(CN)_4]^{2-}$ and [quin] at pH 8.03; (A) indicate the direction of absorbance changes.

A continuous change in absorbance with the formation of a new band at 450 nm (ε = 199 $M^{-1}cm^{-1}$) and the appearance of a reddish colour was observed. This band can be ascribed to the formation of $[ReN(\eta^2\text{-quin})(CN)_3]^{2-}$ complex according to the following reaction:

$$[ReN(CN)_4(H_2O)]^{2-} + quin^- \longrightarrow [ReN(\eta^2\text{-quin})(CN)_3]^{2-} + H_2O + CN^- \qquad \textbf{(4.3)}$$

The isolation of the red crystals of $(AsPh_4)_2[ReN(\eta^2\text{-quin})(CN)_3]\cdot 2H_2O$ was obtained by adding $(AsPh_4)Cl$ to the solution at this stage and confirmed by X-ray analysis

(see crystal structure determination, **Chapter 5**). The mixture was left for a longer period of time, and there was no new band formation.

The UV/VIS spectra of the reaction between $[ReN(H_2O)(CN)_4]^{2-}$ and pyridine-2,3-dicarboxylate are shown in **Figure 4.4**.

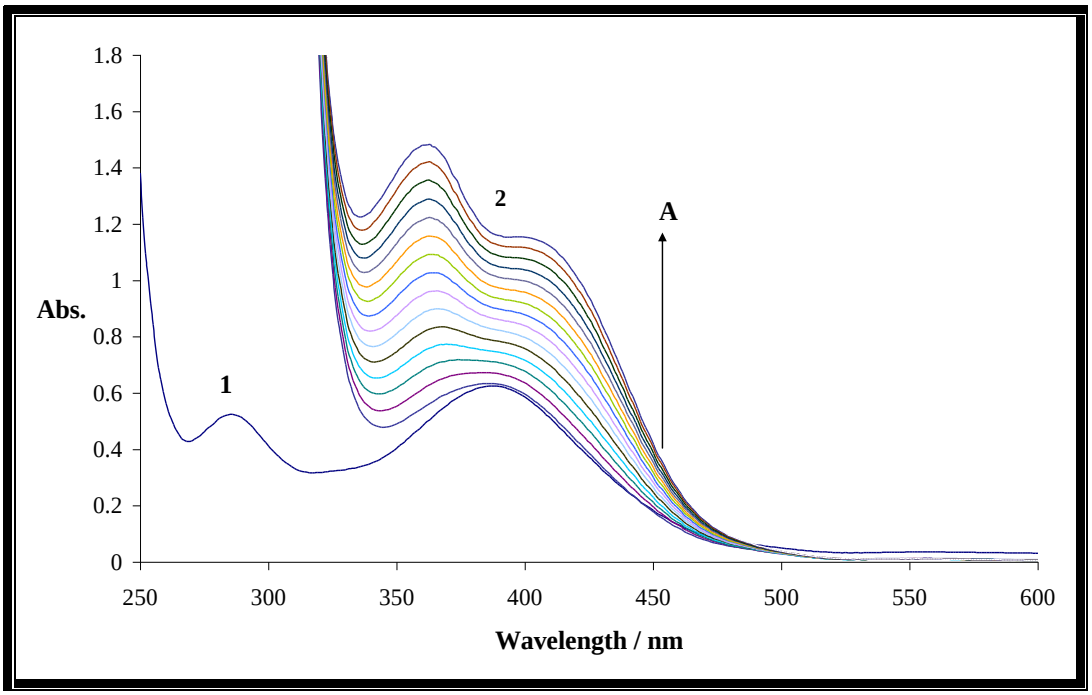

Figure 4.4: **The change in spectrum induced by addition of 2,3-dipic to the solution of $[ReN(H_2O)(CN)_4]^{2-}$; c_{ReN} = 1.0×10^{-3}M, $c_{2,3\text{-dipic}}$ = 1.0M, pH 8.05, T = 80.4°C. Time intervals: 1 minute; arrows indicate the direction of the changes; (1) Solution of $[ReN(H_2O)(CN)_4]^{2-}$ at pH 8.03; (2) Reaction mixture of $[ReN(H_2O)(CN)_4]^{2-}$ and [2,3-dipic] at pH 8.03.**

A continuous absorbance change with the formation of two new bands, one at 360 and 410 nm (ε = 256 and 199M^{-1}cm^{-1}, respectively), accompanied by an appearance of a yellowish colour was observed. These characteristic bands correspond to the formation of the $[ReN(H_2O)(CN)_3\text{-}\mu\text{-}CN\text{-}ReN(CN)_4]^{4-}$ anion according to the following reaction.

$$2[ReN(H_2O)(CN)_4]^{2-} \xrightarrow[\text{Acetic acid}\ (pH\ 6.5)]{\text{2,3-dipic, -}H_2O} [ReN(H_2O)(CN)_3\text{-}\mu\text{–}CN\text{-}ReN(CN)_4]^{4-} \quad (\mathbf{4.4})$$

The addition of (PPh_4)Cl to the solution (after the reaction was complete) resulted in the isolation of yellow crystals of $(PPh_4)_4[ReN(H_2O)(CN)_3$-μ-CN-$ReN(CN)_4]\cdot 5H_2O$ and confirmed by X-ray analysis (see crystal structure, **Chapter 5**). The isolated product showed that the bidentate ligand (2,3-dicarboxylate) obviously did not substitute the aqua and cyano ligands as was expected. However, through further work it becomes clear that, in order to bond bidentate ligands through substitution of aqua/cyano ligands, the solution has to be heated for several hours at 60°C or higher to enhance the reaction rate for the ring closure (*v. fra*).

During the reaction between $[ReN(H_2O)(CN)_4]^{2-}$ complex and pyridine-2,3-dicarboxylate (reaction **4.3**) there were uncertainties about the formation of the final product. The novel product ($[ReN(H_2O)(CN)_3$-μ-CN-$ReN(CN)_4]^{4-}$) obtained when 2,3-dipic$^-$ was used as bidentate ligand will be discussed in more detail with its structure determination in **Chapter 5**.

The infrared spectra have been employed to distinguish the coordination modes of these ligands to the metal centre. Selected IR data for $K_2[ReN(H_2O)(CN)_4]$, $(AsPh_4)_2[ReN(CN)_4]\cdot 5H_2O$, $(PPh_4)_2[ReN(CN)_4]\cdot 5H_2O$, $(PPh_4)_4[ReN(H_2O)(CN)_3$-μ-CN-$ReN(CN)_4]\cdot 5H_2O$ and $(AsPh_4)_2[ReN(\eta^2$-(pic)$(CN)_3]\cdot 4H_2O$ as well as $(AsPh_4)_2[ReN(\eta^2$-quin$)(CN)_3]\cdot 2H_2O$ are presented in **Table 4.3**, while the spectra are shown in **Figures 4.5, 4.6, 4.7, 4.8, 4.9** and **4.10**.

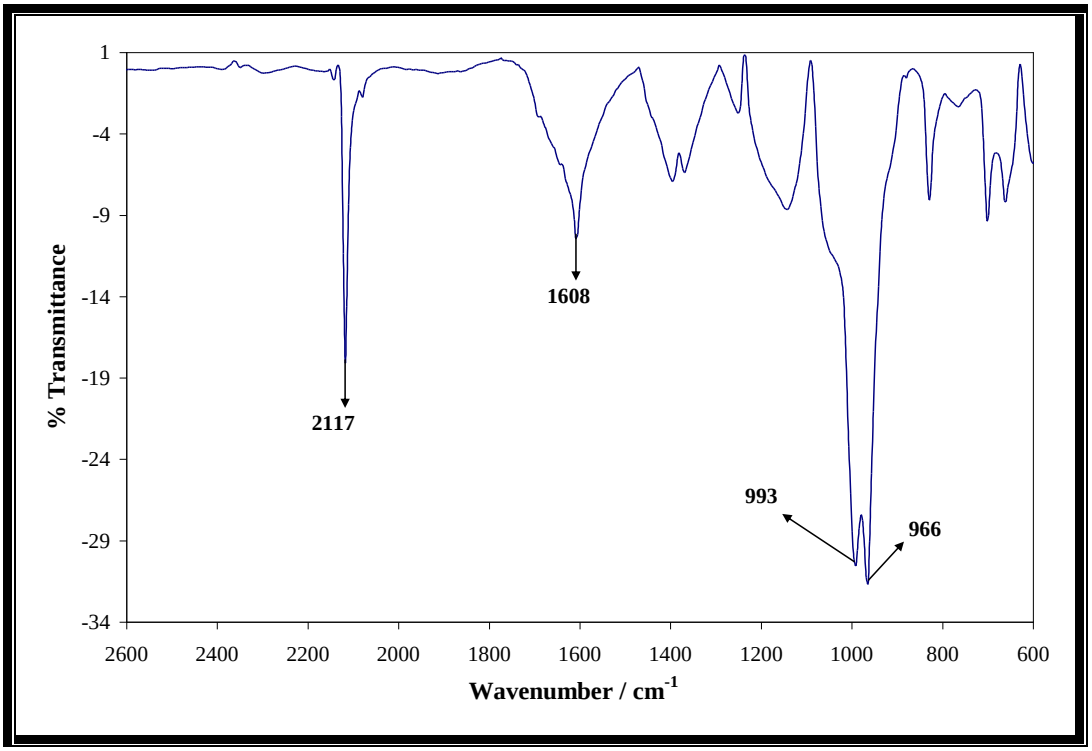

Figure 4.5: The IR spectrum of $K_2[ReN(H_2O)(CN)_4]$ complex as a powder.

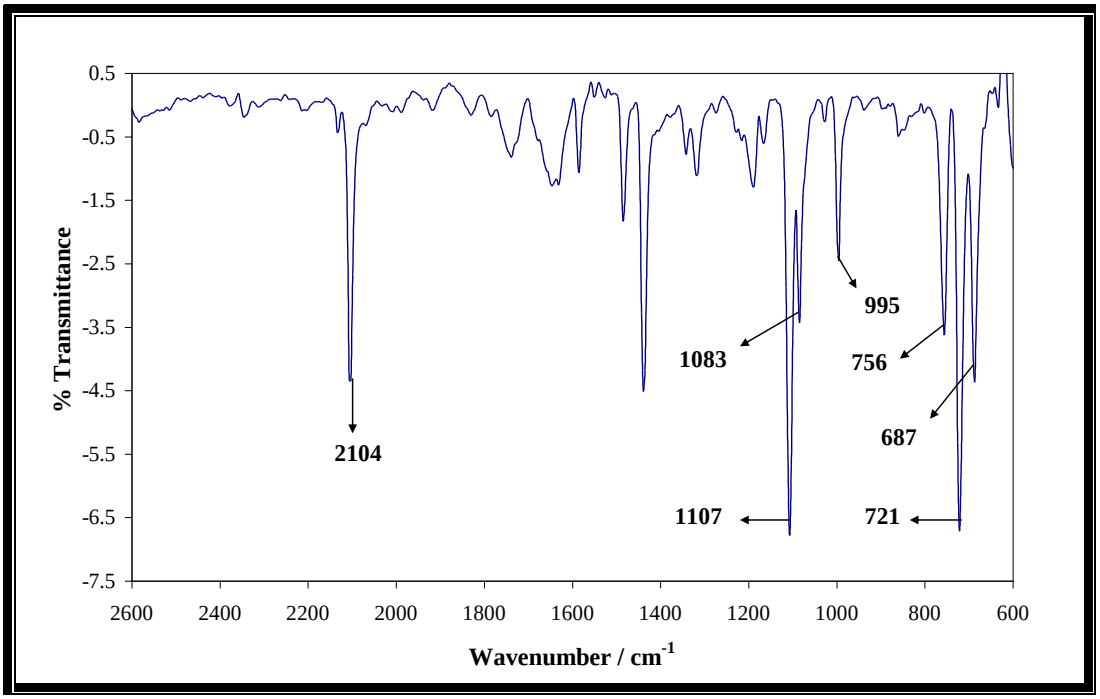

Figure 4.6: The IR spectrum of $(AsPh_4)_2[ReN(H_2O)(CN)_4]\cdot 5H_2O$ crystals.

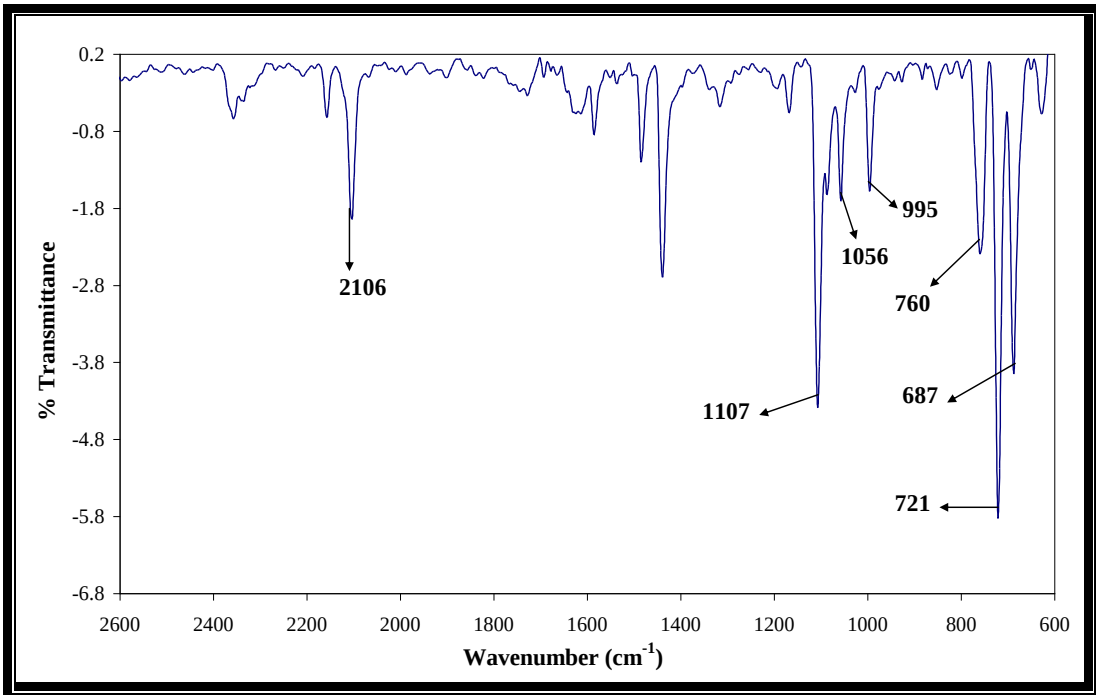

Figure 4.7: IR spectrum of $(PPh_4)_2[ReN(H_2O)(CN)_4]\cdot 5H_2O$ crystals.

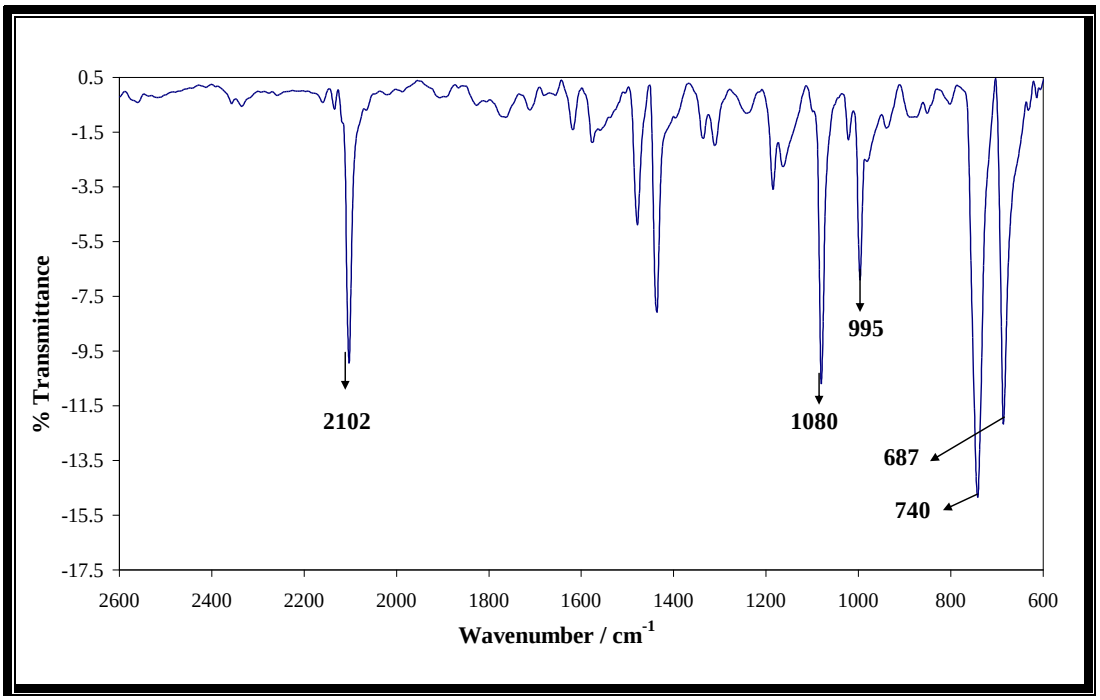

Figure 4.8: The IR spectrum of $(PPh_4)_4[ReN(H_2O)(CN)_3\text{-}\mu\text{-}CN\text{-}ReN(CN)_4]\cdot 5H_2O$ crystals.

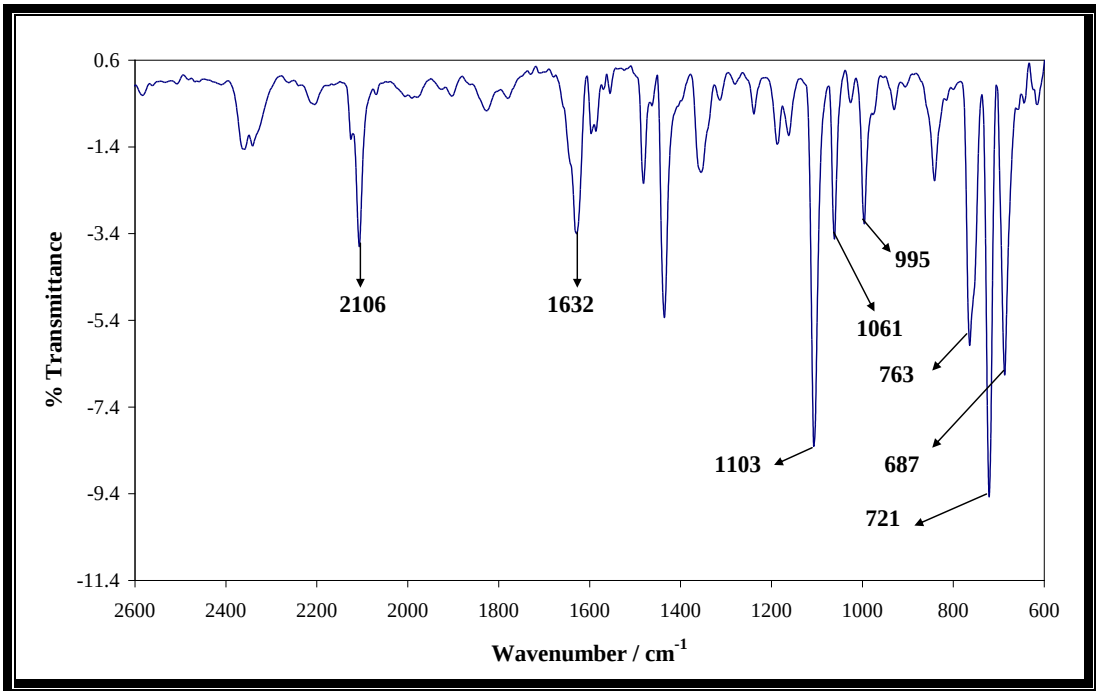

Figure 4.9: The IR spectrum of $(AsPh_4)_2[ReN(\eta^2\text{-pic})(CN)_3]\cdot 4H_2O$ crystals.

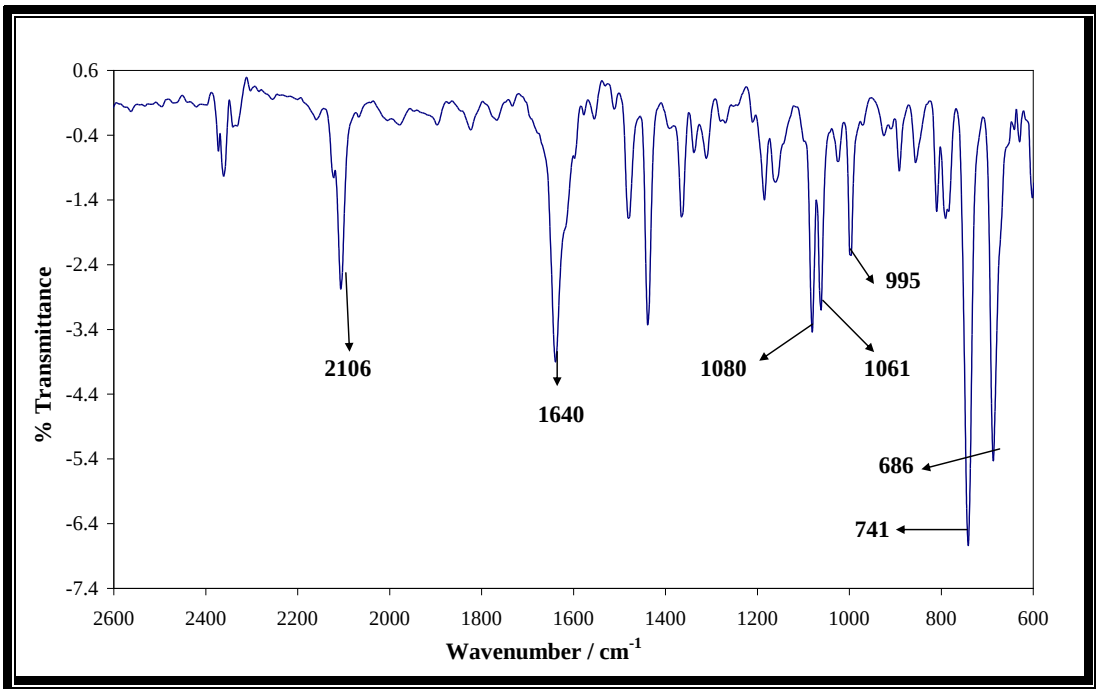

Figure 4.10: The IR spectrum of $(AsPh_4)_2[ReN(\eta^2\text{-quin})(CN)_3]\cdot 2H_2O$ crystals.

The typical IR spectrum for the pink $K_2[ReN(H_2O)(CN)_4]$ shows a broad $\nu(Re{\equiv}N)$ stretching frequency that splits into two peaks at 993 and 966 cm^{-1}, a single strong $\nu(C{\equiv}N)$ stretching frequency at 2117 cm^{-1} which is keeping with a planar $Re(CN)_4$ and

trans-N≡Re-OH_2 group. A strong absorption consistent with the presence of a coordinated water molecule, ν(H-O-H), was observed at 1608 cm^{-1} (**Figure 4.5**). Similar splitting of the ν(Re≡N) stretching frequency into two peaks, and a strong ν(C≡N) stretching frequency were observed by Johnson (1969:1843). He also found that the aqueous solution spectrum of $K_2[ReN(H_2O)(CN)_4]$ shows only one ν(Re≡N) stretching frequency at 1087 cm^{-1} and that this has been shown to be due to the interaction of the nitrogen with the neighbouring rhenium in the solid state and that the anion in aqueous solution is probably *trans*-$[ReN(H_2O)(CN)_4]^{2-}$ (see **Paragraph 4.1**)

The IR spectra of $(AsPh_4)_2[ReN(H_2O)(CN)_4]\cdot 5H_2O$ and $(PPh_4)_2[ReN(H_2O)(CN)_4]\cdot 5H_2O$ salts shown in **Figures 4.6** and **4.7**, exhibit ν(Re≡N) stretching frequencies at 1083 and 1056 cm^{-1} and a single ν(C≡N) stretching frequency at 2104 or 2106 cm^{-1}, respectively. These characteristic peaks are in agreement with those of the same complexes reported by Purcell *et al*. (1992:387; 1991:473; 1992:217) and other nitridotetracyano complexes (Van der Westhuizen *et al*., 2002:506; 1994:717) (see **Table 4.1**).

The IR spectra of $[ReN(H_2O)(CN)_3\text{-}\mu\text{-}CN\text{-}ReN(CN)_4]^{4-}$ (**Figure 4.8**) show only one ν(Re≡N) stretching frequency at 1080 cm^{-1} and a strong ν(C≡N) stretching frequency at 2102 cm^{-1}. This characteristic peak is in agreement with those of the other nitridocyano complexes reported in **Table 4.1**.

Table 4.1: Selected infrared data for nitridotetracyano complexes of Re(V), Tc(V) and Os(VI).

Complex	ν(M≡N) / cm^{-1}	ν(C≡N) / cm^{-1}	Ref.
$K_2[ReN(H_2O)(CN)_4]$	994 and 965	2120	**1**
$K_2[ReN(H_2O)(CN)_4]$	993 and 966	2117	**This work**
$(AsPh_4)_2[ReN(H_2O)(CN)_4]\cdot 5H_2O$	1107 and 1084	2104	**This work**
$(PPh_4)_2[ReN(H_2O)(CN)_4]\cdot 5H_2O$	1106 and 1089	2106	**This work**
$(PPh_4)_4[ReN(H_2O)(CN)_3\text{-}\mu\text{-}CN\text{-}ReN(CN)_4]\cdot 5H_2O$	1080	2102	**This work**
$(AsPh_4)_2[ReN(H_2O)(CN)_4]\cdot 5H_2O$	1060	2124	**2**
$K[OsN(H_2O)(CN)_4]$	1085	2160	**3**
$(AsPh_4)_2[OsN(OH)(CN)_4]$	1050	2148	**4**
$(AsPh_4)_2[TcN(H_2O)(CN)_4]$	1074	2152	**5**

[1] Johnson, (1969:1843); **[2]** Purcell *et al*., (1992:387); **[3, 4]** Van der Westhuizen *et al.*, (1994:717; 1994:582); **[5]** Baldas *et al.*, (1990:233).

The Re≡N stretching frequency in the six coordinated complex of the type $[ReN(L\text{-}L)(CN)_3]^{2-}$, with oxygen atom in the *trans* position, appears in the region 1150 – 1000 cm^{-1}. The IR spectra show Re≡N stretching frequency at 1061cm^{-1} for $[ReN(\eta^2\text{-pic})(CN)_3]^{2-}$ (**Figure 4.9**), and a split into two peaks at 1080 and 1061 cm^{-1} for $[ReN(\eta^2\text{-quin})(CN)_3]^{2-}$ (**Figure 4.10**). In the characteristic C≡N stretching region, one strong band was observed in all the complexes, at 2106 cm^{-1} for $[ReN(\eta^2\text{-pic})(CN)_3]^{2-}$ and $[ReN(\eta^2\text{-quin})(CN)_3]^{2-}$ (**Figure 4.9** and **4.10**). These characteristic stretching frequencies (ν(Re≡N) and ν(C≡N)) correspond very well with those of $[MN(X)(CN)_n]^{m-}$ complexes (M = Re(V), Tc(V), Mn(V) and Os(VI), X = mono- or bidentate ligands) which were prepared and identified previously (**Table 4.2**). The same strong octahedral deformation of $[ReN(L\text{-}L)(CN)_3]^{2-}$ type anions which was also confirmed by X-ray structural analysis (see **Chapter 5**).

Table 4.2: Selected infrared data for different nitridotetracyano complexes of Re(V), Os(VI), and Mn(V).

Complex	ν(M≡N) / cm^{-1}	ν(C≡N) / cm^{-1}	Ref.
$(AsPh_4)_2[ReN(\eta^2\text{-pic})(CN)_3]\cdot 4H_2O$	1103, 1061	2106	**This work**
$(AsPh_4)_2[ReN(\eta^2\text{-quin})(CN)_3]\cdot 2H_2O$	1080, 1061	2106	**This work**
$(PPh_4)_2[ReN(CN)_5]\cdot 7H_2O$	1040	2120	**4**
$(CsNa)[ReN(N_3)(CN)_4]$	1074	2124	**5**
$(PPh_4)_4[\{ReN(CN)_4\}_2(\mu\text{-en})]\cdot 4H_2O$	1070	2021	**6**
$(AsPh_4)_2[OsN(CN)_5]$	1050	2148	**7**
$(AsPh_4)_2[OsN(N_3)(CN)_4]$	1080	2152	**8**
$(AsPh_4)_2[MnN(CN)_4]\cdot 2H_2O$	1105	2114	**9**
$(AsPh_4)_2[MnN(\eta^2\text{-pic})(CN)_4]\cdot 2H_2O$	1032	2124	**10**

[4, 5] Purcell *et al*., (1991:473; 1992:217); **[6, 7, 9, 10]** Van der Westhuizen *et al*., (2002:506; 1994:582; 1994:717; 2004:90, a); **[8]** Che *et al*., (1989:1529).

Other spectral regions in the IR spectrum for these complexes are dominated by the stretching frequencies of tetraphenylarsonium and tetraphenylphosphonium salts, or either picolinic, quinaldic and pyridine-2,3-dicarboxylic acids and are reported in **Table 4.3**.

The identification of coordinated -COO^- groups in these complexes was assigned according to Nakamoto (1963:222). He proposed that uncoordinated –COO^- stretching frequencies occur at 1750 – 1700 cm^{-1}, whereas the ionized and coordinated –COO^- stretching frequencies occur at 1650 – 1590 cm^{-1}. The –COO^- stretching frequency is affected by coordination as well as the intermolecular interaction. As the M-O bond becomes stronger, an increase in this bond leads to a more symmetrical carbonyl group and results in an increase in the frequency separation of the two –COO^- stretching bands. Thus, in order to examine the effect of coordination on the –COO^- stretching frequency, it is important to interpret the results based on the structure obtained by X-ray analysis.

According to the structural data of the complexes, it was observed that the oxygen atom of the carboxylate group coordinates with the metal centre (in *trans* position to the nitrido ligand) with the substitution of an equatorial cyanide ligand.

The IR spectra of $[ReN(\eta^2\text{-pic})(CN)_3]^{2-}$ and $[ReN(\eta^2\text{-quin})(CN)_3]^{2-}$ complexes show strong bands at 1632 cm^{-1} and at 1640 cm^{-1}, respectively (see **Figures 4.9** and **4.10, Table 4.3**). These bands correspond to the previously-mentioned cyano complexes containing κ^2-N,O ligands which were reported by Szklarzewicz *et al*. (2005:1749) and Van der Westhuizen (2004:90, a).

Table 4.3: Selected bands in the IR spectra for isolated complexes.

Salt	ν(Re≡N) / cm^{-1}	ν(CN) / cm^{-1}	Others in 600-2600 cm^{-1}
$K_2[ReN(H_2O)(CN)_4]$	993 and 966	2117s	1606m, 1393m, 1368m, 1145m, 831s, 699m, 662m
$(AsPh_4)_2[ReN(H_2O)(CN)_4]\cdot 5H_2O$	1107s and 1084m	2104s	1635w, 1585w, 1484w, 1438s, 1055m, 996m, 758m, 721s, 687s
$(PPh_4)_2[ReN(H_2O)(CN)_4]\cdot 5H_2O$	1107s and 1056m	2106m	1641w, 1601m, 1478m, 1440m, 1080w, 995m, 760m, 721s, 687m.
$(PPh_4)_4[ReN(H_2O)(CN)_3\text{-}\mu\text{-}CN\text{-}ReN(CN)_4]\cdot 5H_2O$	1080s	2102s	1670m, 1635m, 1585m, 1481m, 1435s, 1319s, 1187s, 1106s, 996s, 850w, 744s, 688s.
$(AsPh_4)_2[ReN(\eta^2\text{-pic})(CN)_3]\cdot 4H_2O$	1103s and 1061m	2106s	1826w, 1740m, 1632m, 1629s, 1596w, 1481w, 1435s, 1361w, 995s, 840w, 763s, 721s, 686s
$(AsPh_4)_2[ReN(\eta^2\text{-quin})(CN)_3]\cdot 2H_2O$	1080s and 1061m	2106s	1740m, 1640s, 1635s, 1481m, 1435m, 1361w 995m, 1089w, 810w, 790w, 741s, 686s.

s = strong; **m** = medium; **w** = weak.

The stretching frequencies of the coordinated ligands are considerably shifted in all the complexes studied, with respect to that of the free acid. The strongest shift was observed for bands of the carboxylate groups of both pic^- and $quin^-$ complexes (that usually appears at 1721 cm^{-1} in picolinic acid, 1692 cm^{-1} in quinaldic acid and 1712 cm^{-1} in pyridine-2,3-dicarboxylic acid). Another shift in stretching frequency was observed on the ν(C≡N) peak (that usually appears at 2120 cm^{-1}). A shift in ν(C≡N) stretching frequency (of about a 10 cm^{-1}) was observed when bidentate ligands coordinate to the metal centre (see **Tables 4.1** and **4.2**). This probably indicates a direct bonding of both carboxyl group and pyridine nitrogen atom to the metal centre.

Crystal structure determination of the isolated complexes will be discussed in more details in **Chapter 5**.

5 CRYSTAL STRUCTURE DETERMINATIONS OF THE N,O-SUBSTITUTED NITRIDOCYANO COMPLEXES OF RHENIUM(V)

5.1 INTRODUCTION

The characterization of the reactants and products by means of X-ray structural determination is very important, since vital information concerning the geometry and bonding modes of the ligands, as well as correlation between the parameters observed in the solid state (X-ray crystallography) and in solution (kinetics) can be obtained. This knowledge will also provide additional evidence for the determination of a reaction mechanism.

In the past, numerous crystal structure determinations, as well as the kinetic studies of the substitution reactions between the oxo- and nitridotetracyano complexes of Mo(IV), W(IV), Tc(V) and Re(V) with monodentate ligands, have been investigated (Leipoldt *et al*., 1992:2277; 1986:179; 1993:241; Van der Westhuizen, 2004:90, a; 1994:717; Basson *et al.*, 1985:121; Purcell *et al*., 1989:369; 1991:473; 1992:217; Damoense *et al*., 1994:619). However, only a few crystal structure determinations and kinetic studies were reported for the reaction between the oxotetracyano complexes of Mo(IV) and W(IV) and nitridotetracyano complexes of Mn(V) with different bidentate ligands (Basson *et al*., 1984:71; Szklarzewicz *et al*., 1990:2959; Leipoldt *et al.*, 1986:323; 1987:57; Samotus *et al*., 1991:614; Roodt *et al*., 1994:599).

To date, none of the substitution reactions of nitridotetracyano complexes of rhenium(V) with bidentate ligands have been reported in literature. As one of the aims of this study, an investigation into the substitution reaction between nitridotetracyano complexes of rhenium(V) and different bidentate ligands was undertaken. Suitable pyridine- and quinoline-2-carboxylate ligands with N,O-donor atoms were chosen for this purpose.

The preparation and structural determinations of the title complexes fit into the broader context of this research which focuses on substitution, geometry and coordination mode of different κ^2-N,O ligands to form $[ReN(L\text{-}L)(CN)_3]^{2-}$ types of complexes. It was observed that the $[ReN(H_2O)(CN)_4]^{2-}$ complex reacts with pyridine-2-carboxylate and quinoline-2-carboxylate anions, respectively, resulting in the formation of the $(AsPh_4)_2[ReN(\eta^2\text{-pic})(CN)_3]\cdot 4H_2O$ and $(AsPh_4)_2[ReN(\eta^2\text{-quin})(CN)_3]\cdot 2H_2O$ complexes, (**Chapter 4)**. It is also anticipated that the introduction of these ligands will have a marked influence on the physical and chemical properties of Re(V) complexes (geometry and rate of reaction).

In order to investigate the influence of these ligands, the complexes $(AsPh_4)_2[ReN(\eta^2\text{-pic})(CN)_3]\cdot 4H_2O$ and $(AsPh_4)_2[ReN(\eta^2\text{-quin})(CN)_3]\cdot 2H_2O$ were isolated and structurally characterized. In this chapter, a crystal modification of $(AsPh_4)_2[ReN(H_2O)(CN)_4]\cdot 5H_2O$ will be characterized and an interesting cyano-bridged complex $(PPh_4)_4[ReN(H_2O)(CN)_3\text{-}\mu\text{-}CN\text{-}ReN(CN)_4]\cdot 5H_2O$ will be investigated by means of X-ray crystallography.

5.2 EXPERIMENTAL WORK

Preparation and characterization of complexes: All the above-mentioned complexes were prepared and characterized by means of UV/VIS and IR spectrophotometry as previously described in **Chapter 4**. The IR and UV/VIS measurements confirmed the existence of a rhenium-nitrido multiple bond and proved that the incoming bidentate ligands are coordinated to the metal centre. This was shown by the shift in the stretching frequencies and absorption of the complex in comparison with those of the free ligands and starting material. The spectophotometric analyses of these complexes established the formulation of all the products.

Data collection and other measurements: The intensity data collection for the X-ray structure determinations of all the Re(V) complexes was done on a Bruker SMART 1K CCD area detector diffractometer with graphite monochromated Mo K_α radiation (50 kV, 30 mA) (University of Witwatersrand). The collection method involved

ω-scan of width 0.3°. Data reduction was carried out using the program SAINT+ (Bruker, 1999: Vers. 6.02) and the absorbtion corrections were made using the program SADABS (Bruker, 1999: Vers. 5.1). The crystal structures were solved by direct methods using SHELXTL. Non-hydrogen atoms were first refined isotropically followed by anisotropic refinement by full matrix least-square calculations based on F^2 using SHELXTL. With exception of the H-atoms attached to the water molecule, all H-atoms were first located in the different maps then positioned geometrically and allowed to ride on their respective parent atoms. All crystals belonged to the triclinic system, space group Pī. The anion was placed on the inversion centre (Pī, 2 anions $cell^{-1}$). The density of the crystal was determined experimentally by floatation in benzene/diiodomethane. The program Diamond (Brandenburg & Putz, 2005: Vers. 3.0) was used to produce molecular diagrams of each of the respective complexes.

A summary of the crystal data and refinement parameters for all the nitridotetracyano complexes of Re(V) studied is provided in **Table 5.1**.

Table 5.1: Crystallographic data for different nitridocyano complexes of Re(V) determined in this study.

Crystal data	**$ReN(H_2O)$[a]**	**$(ReN)_2(CN)_7$[b]**	**Re-pic[c]**	**Re-quin[d]**
Empirical Formula	$C_{52}H_{52}As_2N_5O_6Re$	$C_{104}H_{92}N_{10}O_6P_4Re_2$	$C_{57}H_{52}As_2N_5O_6Re$	$C_{61}H_{50}As_2N_5O_4Re$
Formular weight	1179.03	2074.18	1239.08	1253.10
Crystal system	Triclinic	Triclinic	Triclinic	Triclinic
Space group	Pī	Pī	Pī	Pī
a (Å)	13.5549(6)	14.1366(7)	13.586(2)	13.367(4)
b (Å)	13.8823(6)	14.1754(7)	13.726(2)	13.370(4)
c (Å)	16.4004(8)	25.0990(12)	17.100(3)	17.083(5)
α (°)	68.961(3)	102.8260(10)	87.972(3)	72.831(5)
β (°)	88.619(3)	104.1660(10)	69.659(3)	88.917(5)
γ (°)	61.493(3)	92.9350(10)	62.209(3)	65.473(5)
Volume ($Å^3$)	2490.0(2)	4725.3(4)	2614.1(7)	2634.7(14)
Z	2	2	2	2
ρ $(g.cm^{-3})_{calc}$	1.573	1.458	1.574	1.580
ρ $(g.cm^{-3})_{exp}$	1.515	1.502	1.528	1.552
Crystal size (nm^3)	0.36×0.31×0.24	0.40×0.34×0.25	0.40×0.23×0.13	0.26×0.07×0.06
Absorption coefficient (mm^{-1})	3.812	2.687	3.636	3.606
F(000)	1176	2088	1236	1248
θ range for data collection	1.35 to 28.00	0.86 to 28.00	1.29 to 25.00	1.26 to 28.00
Index range	-17≤h≤17, -18≤k≤18, -21≤l≤21	-18≤h≤18, -18≤k≤18, -32≤l≤32	-16≤h≤16, -16≤k≤10, -19≤l≤20	-17≤h≤17, -17≤k≤17, -22≤l20
Reflections collected / unique	32214 / 12013	74366 / 22798	14322 / 9129	23415 / 12658
R(int)	0.0734	0.1064	0.0188	0.0398
Completeness to 2θ ,(%)	28.00, 99.9	20.00, 99.9	2500, 99.2	28.00, 99.4
Data / restraints / parameters	12013 / 82 / 613	22798 / 42 / 1168	9129 / 0 / 630	12658 / 5 / 659
Goodness-of-fit on F^2	1.039	1.040	1.005	1.006
Final R indices [I>2σ(I)]	R_1 = 0.0291, wR_2 = 0.0778	R_1 = 0.0418, wR_2 = 0.1035	R_1 = 0.0286, wR_2 = 0.0742	R_1=0.0361, wR_2=0.0771
R indices (all data)	R_1 = 0.0339, wR_2 = 0.0800	R_1 = 0.0528, wR_2 = 0.1088	R_1 = 0.0362, wR_2 = 0.0770	R_1=0.0608, wR_2=0.0894
Largest diff. peak and hole ($e.Å^{-3}$)	1.707 and -1.910	4.124 and -2.447	1.731 and -0.801	3.402 and -1.287

[a] $ReN(H_2O)$ = $(AsPh_4)_2[ReN(H_2O)(CN)_4]\cdot 5H_2O$, [b] $(ReN)_2(CN)_7$ = $(PPh_4)_4[ReN(H_2O)(CN)_3$-μ-CN-$ReN(CN)_4]\cdot 5H_2O$. [c] Re-pic = $(AsPh_4)_2[ReN(\eta^2$-pic$)(CN)_3]\cdot 4H_2O$, [d] Re-quin = $(AsPh_4)_2[ReN(\eta^2$-quin$)(CN)_3]\cdot 2H_2O$.

5.3 CRYSTAL STRUCTURES OF $(AsPh_4)_2[ReN(H_2O)(CN)_4]\cdot 5H_2O$ AND $(PPh_4)_4[ReN(H_2O)(CN)_3\text{-}\mu\text{-}CN\text{-}ReN(CN)_4]\cdot 5H_2O$

5.3.1 Crystal Structure Data of $(AsPh_4)_2[ReN(H_2O)(CN)_4]\cdot 5H_2O$

5.3.1.1 Introduction

The preparation of the $(AsPh_4)_2[ReN(H_2O)(CN)_4]\cdot 5H_2O$ complex and the growth of the yellow-orange crystals used for collection of the intensity data were reported in **Chapter 4**.

A partial projection of $(AsPh_4)_2[ReN(H_2O)(CN)_4]\cdot 5H_2O$ complex is shown in **Figure 5.1**, while the molecular diagram showing the numbering scheme of the anion is presented in **Figure 5.2**. Selected bond distances and angles are given in **Table 5.2**, with a discussion highlighting some of the important aspects of the $[ReN(H_2O)(CN)_4]^{2-}$ anion presented thereafter. Supplementary data containing complete lists of atomic coordinates, anisotropic displacement parameters, bond distances and angles as well as hydrogen bonds are given in **A1** (**Appendix A**).

5.3.1.2 Packing and Lattice Stabilization

The $(AsPh_4)_2[ReN(H_2O)(CN)_4]\cdot 5H_2O$ complex crystallizes in a triclinic space group, Pī, with two molecules per unit cell. The structure consists of discrete $AsPh_4^+$ cations and $[ReN(H_2O)(CN)_4]^{2-}$ anions. The As atoms are tetrahedrally surrounded by four phenyl rings with the average As-C bond distance of 1.915(3)Å, while the C-As-C bond angles range from 105.74(12) to 112.78(12)°. These results as well as the geometry of the phenyl rings are in agreement with those found in other structures containing $AsPh_4^+$ cations (1.912(11)Å and 107.3(4)° to 111.6(4)° in $(AsPh_4)_2[ReN(H_2O)(CN)_4]$) (Purcell *et al*., 1992:387). A drawing of the packing within the unit cell also shows that the cations and anions form a separate layer and water molecules are between them in a plane perpendicular to the *c*-axis (**Figure 5.1**).

There are two kinds of hydrogen bonds in the structure:

(i) the nitrogen atoms of the cyano ligands form hydrogen bonds with the oxygen atoms of water molecules, (O(**2**)-H(**2**)....N(**2**) = 2.921(4)Å, O(3)-H(**3**)….N(**1**) = 2.843(4) Å, O(**5**)-H(**5**)….N(**2**) = 2.870(4)Å and O(**6**)-H(**6**)….N(**4**) =2.784(4) Å

(ii) between water molecules only, (O(**1**)-H(**1**)….O(**4**) = 2.744(5), O(**1**)-H(**1**)….O(**6**) = 2.790(4), O(**2**)-H(**2**)….O(**3**) = 2.811(4)Å, O(**3**)-H(**3**)….O(**2**) = 2.797(4) and O(**4**)-H(**4**)….O(**5**) = 2.810(5).

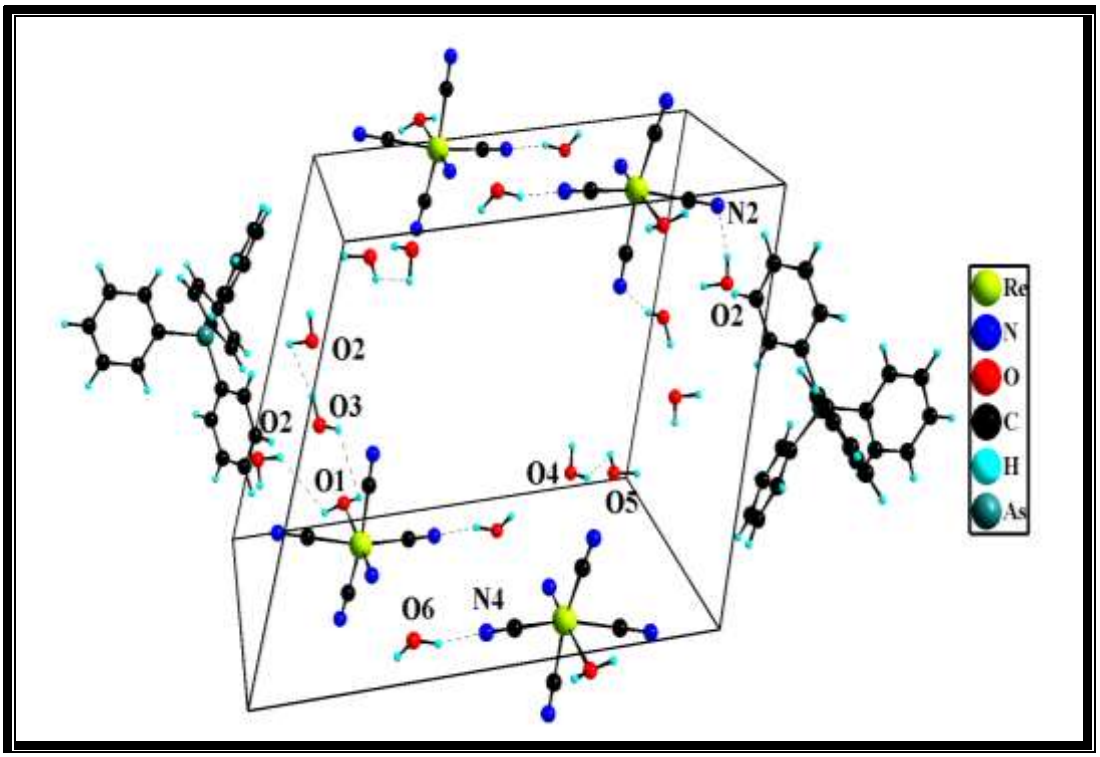

Figure 5.1: The partial projection of $[ReN(H_2O)(CN)_4]^{2-}$ (hydrogen bonding is shown).

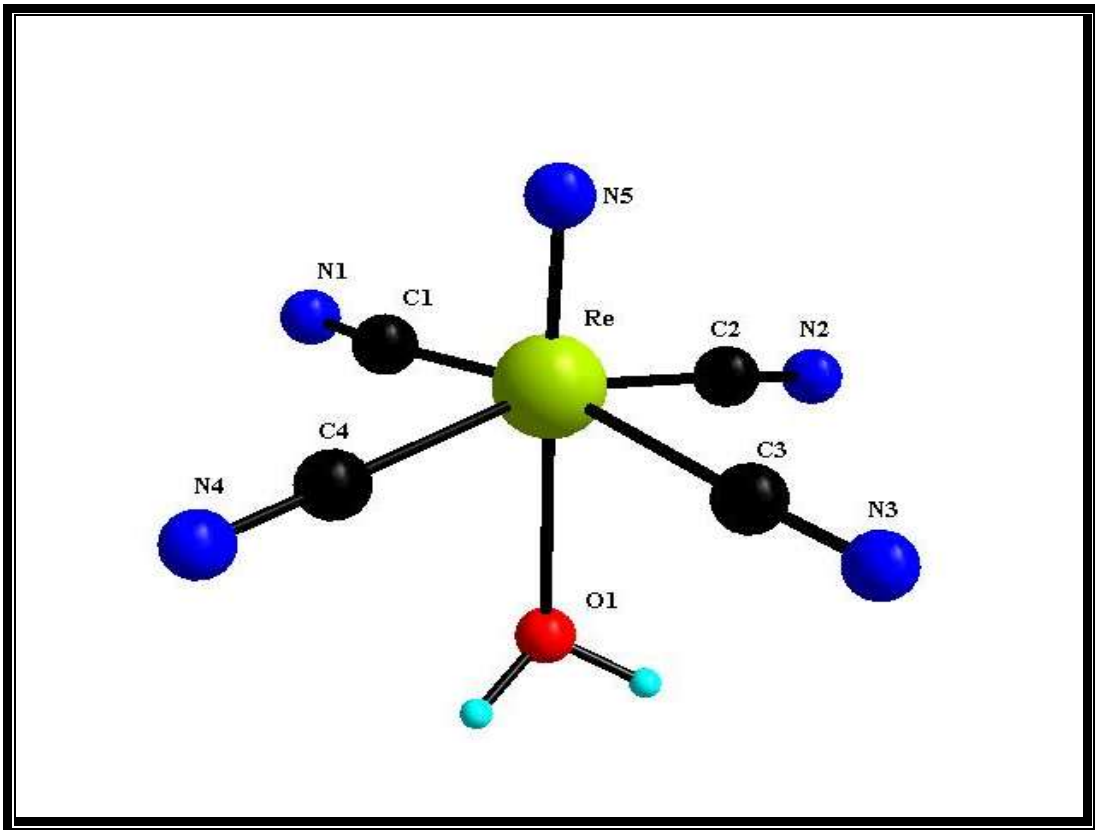

Figure 5.2: Molecular diagram showing the numbering scheme and displacement ellipsoids (50% probability) of the $[ReN(H_2O)(CN)_4]^{2-}$ anion. The cations are omitted for clarity.

Table 5.2: Selected bond distances (Å) and angles (°) for the $[ReN(H_2O)(CN)_4]^{2-}$ anion.

Bond distances (Å)			
Re-N(5)	1.663(2)	As(1)-C(31)	1.193(3)
Re-C(2)	2.104(3)	As(1)-C(41)	1.915(3)
Re-C(1)	2.118(3)	As(1)-C(11)	1.916(3)
Re-C(3)	2.117(3)	As(1)-C(21)	1.916(3)
Re-C(4)	2.108(3)	As(2)-C(51)	1.913(3)
N(1)-C(1)	1.147(4)	As(2)-C(81)	1.917(3)
N(2)-C(2)	1.163(4)	As(2)-C(71)	1.917(3)
N(3)-C(3)	1.155(4)	As(2)-C(61)	1.919(3)
N(4)-C(4)	1.150(4)	O(1)-H(1A)	0.94(4)
Re-O(1)	2.431(2)	O(1)-H(1B)	0.94(3)
Bond angles (°)			
N(5)-Re-O(1)	178.06(1)	N(1)-C(1)-Re	176.0(3)
N(5)-Re-C(1)	97.60(1)	N(2)-C(2)-Re	177.6(3)
N(5)-Re-C(2)	100.73(1)	N(3)-C(3)-Re	177.1(3)
N(5)-Re-C(3)	96.96(1)	N(4)-C(4)-Re	179.4(3)
N(5)-Re-C(4)	99.22(1)	C(1)-Re-O(1)	83.53(1)
C(2)-Re-C(1)	87.79(1)	C(2)-Re-O(1)	77.71(1)
C(2)-Re-C(3)	87.87(1)	C(3)-Re-O(1)	81.86(1)
C(4)-Re-C(3)	89.94(1)	C(4)-Re-O(1)	82.34(1)
C(4)-Re-C(1)	89.47(1)	Re-O(1)-H(1B)	119(2)
C(2)-Re-C(4)	160.04(1)	Re-O(1)-H(1A)	117(2)
C(3)-Re-C(1)	165.34(1)		

5.3.1.3 Results and Discussion

At pH lower than 8.0, it was possible to isolate a Re(V) complex as a tetraphenylarsonium salt, $(AsPh_4)_2[ReN(H_2O)(CN)_4]\cdot 5H_2O$, with ν(Re≡N) and ν(C≡N) vibration frequencies at 1107, 1083 and 2104 cm^{-1} respectively (**Figure 4.6**, **Chapter 4**). The structure determination (**Figure 5.2**, and supplementary material) indicates that the $[ReN(H_2O)(CN)_4]^{2-}$ complex has the same geometrical arrangement as that previously reported by Purcell *et al*. (1992:387). This structure determination can thus be considered as a redetermination of the same product. There is, however, a difference in these structures: the previously reported structure by Purcell *et al*. (1992:387) reported a monoclinic crystal system whilst the present determination is based on a triclinic crystal system (**Table 5.1**).

The rhenium(V) atom is octahedrally coordinated to a nitrido ligand, an aqua ligand *trans* to the nitrido ligand and four cyano groups in an equatorial plane (**Figure 5.2**). The Re≡N(**5**) and Re-O(**1**) bond distances of 1.663(2) and 2.431(2)Å respectively, agree well with those in $[ReN(H_2O)(CN)_4]^{2-}$ (1.639(8)Å for Re≡N and 2.496(7)Å for Re-O) reported by Purcell *et al*. (1992:387). The long Re-O(**1**) bond distance is an indication of a very strong *trans*-influence of the nitrido ligand which is one of the strongest π-electron donors known. The average Re-C and C≡N bond distances of 2.112Å and 1.154Å respectively, also correspond well with those previously determined. The average N(**5**)-Re-C and O(**1**)-Re-C bond angles are 98.63(1)° and 81.36(1)° respectively. The N(**5**)-Re-C bond angle deviate by more than 8.63° and O(**1**)-Re-C bond angle deviate by less than 8.64° from the ideal value of 90°.

The Re-C-N bond angles are almost perfectly linear, the bond angles being in the range of 176.0(3) to 179.4(3)Å. The large *trans*-influence of the nitrido ligand is also evident by the mode of distortion from a regular octahedral geometry of the $[ReN(H_2O)(CN)_4]^{2-}$ ion. The rhenium atom is displaced by 0.309(2)Å out of the plane formed by four carbon atoms of the cyano ligands towards the nitrido ligand, whilst the average values for C-Re-N(**5**) and C-Re-O(**1**) bond angles are 99° and 81.4° respectively.

5.3.2 Crystal Structure Data of $(PPh_4)_4[ReN(H_2O)(CN)_3$-μ-CN-$ReN(CN)_4]\cdot 5H_2O$

5.3.2.1 Introduction

Suitable crystals of the $(PPh_4)_4[ReN(H_2O)(CN)_3$-μ-CN-$ReN(CN)_4]\cdot 5H_2O$ complex for X-ray analysis were selected from the material prepared as described in **Chapter 4**. These have ν(Re≡N) stretching frequencies at 1080 cm^{-1}, as well as the ν(C≡N) stretching frequency at 2102 cm^{-1} (see **Figure 4.7**, **Chapter 4**).

The partial projection of the $(PPh_4)_4[ReN(H_2O)(CN)_3$-μ-CN-$ReN(CN)_4]\cdot 5H_2O$ complex is shown in **Figure 5.3**, while the molecular diagram showing the numbering scheme of the anion is presented in **Figure 5.4.** Selected bond distances and angles are given in **Table 5.3**, with a discussion highlighting some of the important aspects of the $[ReN(H_2O)(CN)_3$-μ-CN-$ReN(CN)_4]^{4-}$ anion presented thereafter. Supplementary data containing a complete list of atomic coordinates, anisotropic displacement parameters, bond distances and angles as well as hydrogen bonds are given in **A2** (**Appendix A**).

5.3.2.2 Packing and Lattice Stabilization

The crystals of the $(PPh_4)_4[ReN(H_2O)(CN)_3$-μ-CN-$ReN(CN)_4]\cdot 5H_2O$ complex crystallize in the triclinic space group, Pī, with two molecules per unit cell. The structure consists of discrete PPh_4^+ cations and a $[ReN(H_2O)(CN)_3$-μ-CN-$ReN(CN)_4]^{4-}$ anion (**Figure 5.3**). The P atoms are tetrahedrally surrounded by four phenyl rings with average P-C bond distances of 1.795(4)Å whilst C-P-C bond angles range from 108.21(19)° to 112.0(2)°. These results, as well as the geometry of the phenyl ring, are in agreement with those found in other structures containing the tetraphenylphosphonium cations (1.80(1)Å, 106.3(6)° to 113.6(6)° in $(PPh_4)_3[ReN(CN)_5]$ and 1.80(1)Å, 104.5(6)° to 113.9(7)° in $(PPh_4)_4[\{ReN(CN)_4\}_2$(μ-en)]) (Purcell *et al*., 1991:473; Van der Westhuizen *et al*., 2002:506).

A drawing (**Figure 5.3**) of the packing within the unit cell also shows that four of the phosphonium cations are positioned interstitially between layers of Re-CN-Re units, the

latter being connected in chains by way of hydrogen bonding with water molecules. Pairs of cyano ligands, each bonded to an adjacent Re atom of the Re-CN-Re moiety, are bonded through hydrogen bonds to a common adjacent water molecules.

There are several kinds of hydrogen bonds in the structure:

(i) between anion and water molecules: the nitrogen atoms of the cyano ligands form hydrogen bonds with the oxygen atoms of water molecules (O(**3**)-H(**3**)….N(**2**) = 3.004(7)Å, O(**3**)-H(**3**)….N(**6**) = 2.990(7)Å, O(**4**)-H(**4**)….N(**2**) = 3.109(8)Å, O(**5**)-H(**5**)….N(**1**) = 2.898(5)Å, O(**5**)-H(**5**)….N(**8**) = 2.968(5)Å, O(**6**)-H(**6**)….N(**7**) = 2.874(5)Å, and O(**6**)-H(**6**)….N(**4**) = 2.880(5)Å. These bonds tend on average to be weaker than those between water molecules below.

(ii) between water molecules only: such interactions are observed for O(**1**)-H(**1**)….O(**2**) = 2.784(5)Å and O(**2**)-H(**2**)….O(**3**) = 2.750(7)Å.

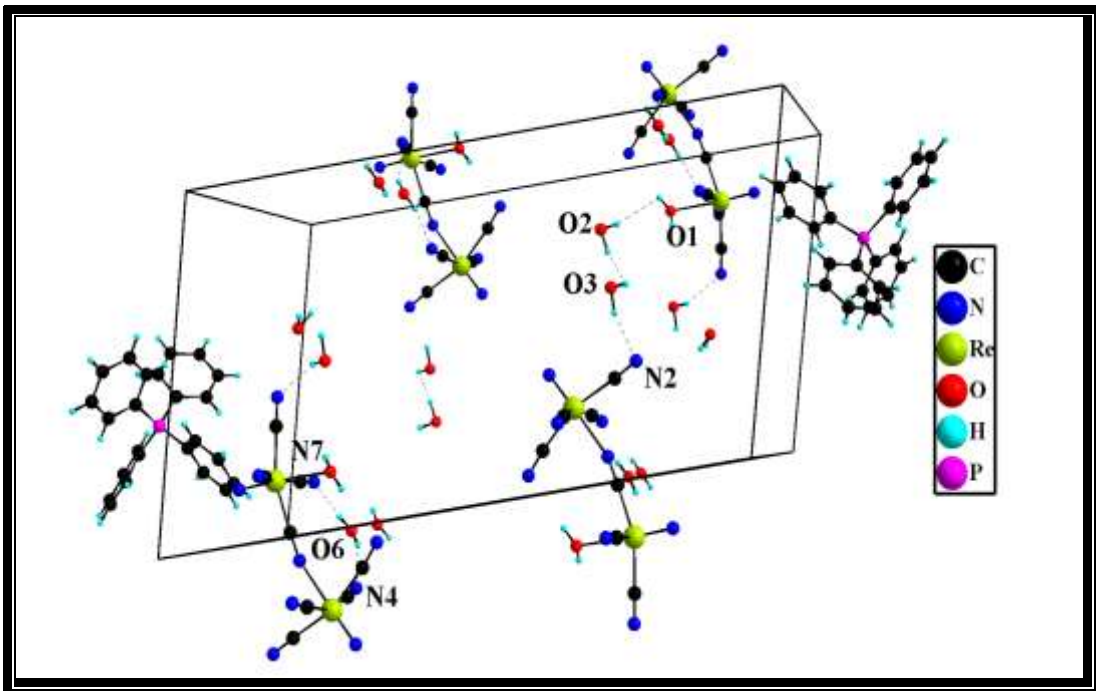

Figure 5.3: The partial projection of $(PPh_4)_4[ReN(H_2O)(CN)_3$-μ-CN-$ReN(CN)_4]\cdot 5H_2O$ complex (hydrogen bonding is shown).

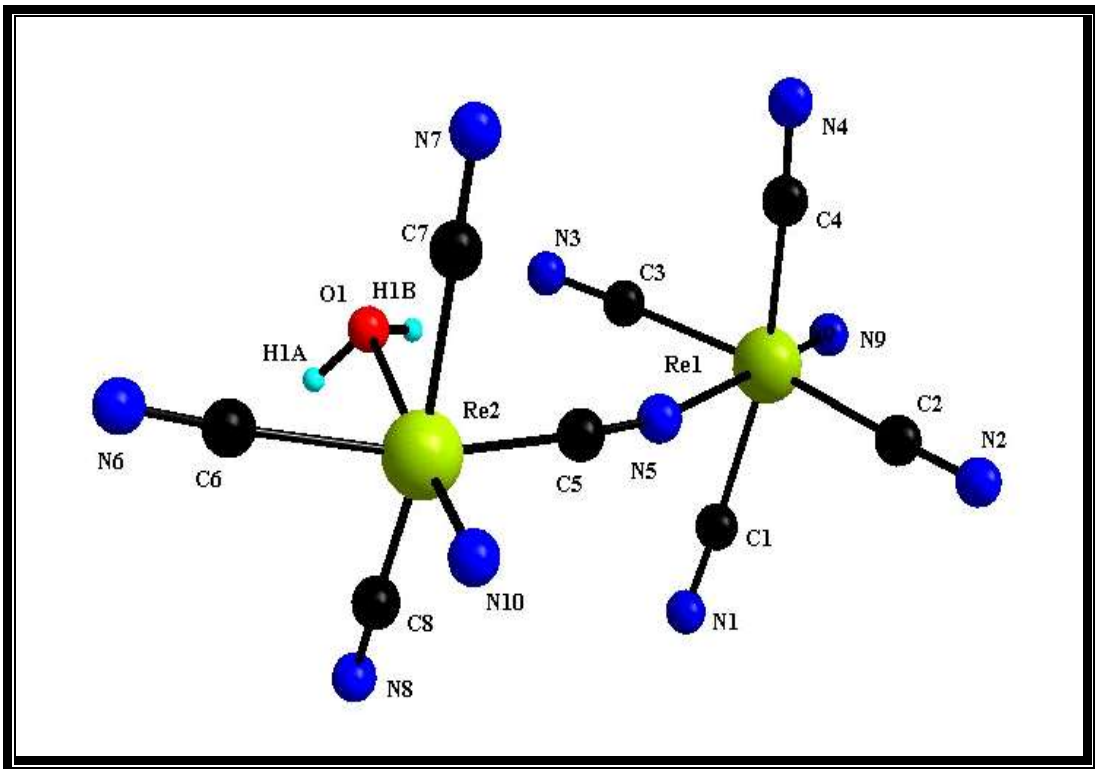

Figure 5.4: **Molecular diagram showing numbering scheme and displacement ellipsoids (50% probability) of the $[ReN(H_2O)(CN)_3$-μ-CN-$ReN(CN)_4]^{4-}$ anion.**

Table 5.3: Selected bond distances (Å) and angles (°) for the $[ReN(H_2O)(CN)_3$-μ-CN-$ReN(CN)_4]^{4-}$ anion.

Bond distances (Å)			
N(9)-Re(1)	1.657(4)	N(10)-Re(2)	1.656(5)
N(5)-Re(1)	2.348(4)	C(5)-Re(2)	2.083(4)
C(1)-Re(1)	2.104(4)	C(6)-Re(2)	2.112(5)
C(2)-Re(1)	2.109(5)	C(7)-Re(2)	2.099(4)
C(3)-Re(1)	2.115(4)	C(8)-Re(2)	2.095(4)
C(4)-Re(1)	2.102(4)	Re(2)-O(1)	2.462(4)
C(1)-N(1)	1.157(6)	C(5)-N(5)	1.137(6)
C(2)-N(2)	1.135(6)	C(6)-N(6)	1.138(7)
C(3)-N(3)	1.146(6)	C(7)-N(7)	1.150(5)
C(4)-N(4)	1.160(5)	C(8)-N(8)	1.160(5)
C(101)-P(1)	1.796(4)	C(121)-P(1)	1.794(4)
C(111)-P(1)	1.793(4)	C(131)-P(1)	1.793(4)
Bond angles (°)			
N(9)-Re(1)-N(5)	177.04(2)	N(10)-Re(2)-C(5)	97.3(2)
N(9)-Re(1)-C(1)	99.6(2)	N(10)-Re(2)-C(6)	101.0(3)
N(9)-Re(1)-C(2)	98.1(2)	N(10)-Re(2)-C(7)	100.5(2)
N(9)-Re(1)-C(3)	100.4(2)	N(10)-Re(2)-C(8)	98.44(2)
N(9)-Re(1)-C(4)	99.9(2)	N(5)-C(5)-Re(2)	176.5(4)
N(1)-C(1)-Re(1)	175.9(4)	N(6)-C(6)-Re(2)	176.7(5)
N(2)-C(2)-Re(1)	176.9(5)	N(7)-C(7)-Re(2)	178.8(4)
N(3)-C(3)-Re(1)	173.3(5)	N(8)-C(8)-Re(2)	179.1(4)
N(4)-C(4)-Re(1)	176.9(3)	N(10)-Re(2)-O(1)	176.4(2)
C(5)-N(5)-Re(1)	162.8(4)	C(5)-Re(2)-O(1)	79.3(2)
C(4)-Re(1)-N(5)	82.13(2)	C(8)-Re(2)-O(1)	80.68(1)
C(1)-Re(1)-N(5)	78.25(2)	C7)-Re(2)-O(1)	80.37(1)
C(2)-Re(1)-N(5)	84.13(2)	C(6)-Re(2)-O(1)	82.5(2)
C(3)-Re(1)-N(5)	77.6(2)	C(5)-Re(2)-C(8)	90.4(2)
C(4)-Re(1)-C(1)	160.3(2)	C(5)-Re(2)-C(7)	86.3(2)
C(4)-Re(1)-C(2)	89.73(2)	C(8)-Re(2)-C(7)	161.1(2)
C(1)-Re(1)-C(2)	90.53(2)	C(5)-Re(2)-C(6)	161.6(2)
C(4)-Re(1)-C(3)	85.1(2)	C(8)-Re(2)-C(6)	89.61(2)
C(1)-Re(1)-C(3)	88.5(2)	C(7)-Re(2)-C(6)	87.81(2)
C(2)-Re(1)-C(3)	161.5(2)		

5.3.2.3 Results and Discussion

The crystal structure determination of this complex shows a binuclear complex containing two rhenium atoms (**Figure 5.4**), with a cyano ligand (on the equatorial plane of the $ReN(H_2O)(CN)_4$ moiety) acting as a bridge between Re(**1**) and Re(**2**). An interesting feature of this structure is that the bridged cyano ligand is coordinated *trans* to the nitrido ligand *via* a nitrogen atom N(**5**) to Re(**1**). This bond probably formed by the substitution of the aqua ligand of $[ReN(H_2O)(CN)_4]^{2-}$ (**Figure 5.4**). Thus, it has to be mentioned that this is the first structure determination of rhenium(V) where a cyano ligand acts as a bridge within the bimetallic moiety.

The Re(**1**)≡N(**9**) bond distance of 1.657(4)Å and the Re(**2**)≡N(**10**) bond distance of 1.656(5)Å are in agreement with each other. This is indicative of a strong pπ-dπ ligand-to-metal interaction and may be compared with other nitridotetracyano complexes of Re(V), namely 1.663(2)Å in $[ReN(H_2O)(CN)_4]^{2-}$ reported above, 1.639(8)Å in $[ReN(H_2O)(CN)_4]^{2-}$, 1.68(1)Å in $[ReN(CN)_5]^{3-}$, 1.65(2)Å in $[ReN(N_3)(CN)_4]^{3-}$ and 1.73(2) and 1.62(2)Å in $[\{ReN(CN)_4\}_2(\mu\text{-en})]^{4-}$ (Purcell *et al*., 1991:473; 1992:387; 1992:217; Van der Westhuizen *et al*., 2002:506).

It is, however, interesting to note that the Re(**2**)≡N(**10**) bond leads to a somewhat longer *trans*-Re(**2**)-O(**1**) bond distance of 2.462(4)Å, whereas the Re(**1**)≡N(**9**) bond leads to a significant shorter *trans*-Re(**1**)-N(**5**) bond distance of 2.348(4)Å (**Table 5.3**) if compared with the corresponding Re-N bond distances of $[\{ReN(CN)_4\}_2(\mu\text{-en})]^{4-}$. The Re(**2**)-O(**1**) bond distance of 2.462(4)Å in $[ReN(H_2O)(CN)_3\text{-}\mu\text{-}CN\text{-}ReN(CN)_4]^{4-}$ corresponds very well with 2.496(7)Å found in the $[ReN(H_2O)(CN)_4]^{2-}$ anion (Purcell *et al*., 1992:387), but is considerably longer than the 2.142(7)Å and 2.32(4)Å distances found for the corresponding iso-electronic structures of $[ReO(H_2O)(CN)_4]^-$ and $(NEt_4)[ReO(Br)_4(H_2O)]$ respectively (Purcell *et al*., 1990:239; Cotton & Lippard, 1968:1621). This is an indication of a larger *trans*-influence of the nitrido ligand in the former, compared to that of the iso-electronic oxo ligand in the latter cases. The Re(**1**)-N(**5**) bond length of 2.348(4)Å (**Table 5.3**) is significantly shorter than the corresponding Re-N bond distances of 2.47(2)Å and 2.56(2)Å found in the $[\{ReN(CN)_4\}_2\text{-}\mu(en)]^{4-}$ anion (Van der Westhuizen *et al*., 2002:506). The ethylenediamine, en, only has σ-donating sp^3 nitrogen donor

atoms. In contrast, the present complex, $[ReN(H_2O)(CN)_3$-μ-CN-$ReN(CN)_4]^{4-}$, is different since the cyano ligand, apart from its nitrogen σ-donating electron pair in an sp-hybrid orbital of the cyano nitrogen atom, can also form d-π* bonding with the metal which will shorten the Re(**1**)-N(**5**) compared to the above $[\{ReN(CN)_4\}_2$-μ(en)$]^{4-}$ anion. However, the large *trans*-influence of the nitrido and oxo ligands were also observed in the iso-structural $[ReN(CN)_5]^{3-}$, $[ReN(N_3)(CN)_4]^{3-}$, $[MoO(HCN$-κN$)(CN)_4]^{2-}$ and $[MoO(dmap)(CN)_4]^{2-}$ anions (Purcell *et al*., 1991:473; 1992:387; 1992:217; Van der Westhuizen *et al*., 2002:506; Smit, 1995:71). It can thus be concluded that the significant shortening of the Re(**1**)-N(**5**) bond is ascribable to π* electron acceptance on N(**5**) in conjunction with the excellent π-donor properties of the *trans*-orientated nitrido ligand. This also manifests itself in π-shortening of the Re(**2**)-C(**5**) bond (2.083(4)Å) which is on the brink of being significantly shorter compared to the *trans*-Re(**2**)-C(**6**) bond length of 2.112(5)Å (**Table 5.3**).

The average Re(**1**)-CN bond distances of 2.108(4)Å and Re(**2**)-CN bond distances of 2.097(4)Å agree well with the same average cyano ligand values of 2.112(3)Å in $[ReN(H_2O)(CN)_4]^{2-}$ discussed above and 2.10(2)Å in $[\{ReN(CN)_4\}_2(\mu$-en$)]^{4-}$. The average C-N bond distances of 1.15(6)Å are similar to the bond distances found in $[ReN(H_2O)(CN)_4]^{2-}$, average 1.154(4)Å, $[\{ReN(CN)_4\}_2(\mu$-en$)]^{4-}$, average 1.17(3)Å and $[ReN(CN)_5]^{3-}$ average 1.14(2)Å (Purcell *et al*., 1991:473; 1992:387; Van der Westhuizen *et al*., 2002:506).

The Re(**1**)-C-N and Re(**2**)-C-N chains are nearly linear with average bond angles of 175.75(3)° and 177.78(2)°, respectively, with 4.25° and 2.22° deviations from expected linearity. The average bond angles (N≡Re-C = 99.4(2)°, N-Re-C = 80.5(2)° and O-Re-C = 80.7(2)°) in the $[ReN(H_2O)(CN)_3$-μ-CN-$ReN(CN)_4]^{4-}$ anion are in agreement with those of known nitridotetracyano complexes of rhenium(V) (Purcell *et al.*, 1991:473; 1992:387). The displacement of 0.348(2)Å for Re(**1**) and 0.3403(2)Å for Re(**2**) out of the equatorial plane formed by four carbon atoms of the cyano ligands towards the nitrido ligands showed that the Re(**1**) and Re(**2**) have distorted octahedral geometries. These out-of-plane values may be compared with those found in $[\{ReN(CN)_4\}_2(\mu$-en$)]^{4-}$ (0.34 and 0.31Å), $[ReN(H_2O)(CN)_4]^{2-}$ (0.35Å), $[ReN(CN)_5]^{3-}$ (0.31Å) and

$[ReN(N_3)(CN)_4]^{3-}$ (0.34Å) (Van der Westhuizen *et al*., 2002:506; Purcell *et al*., 1992:387; 1991:473; 1992:217). These distortions are indications of the relative metal-nitrido bond strength and thus also of the *trans*-influence of the nitrido ligand. The displacement of Re(**2**) out of the plane formed by C(**8**), C(**7**), O(**1**) and N(**10**) towards the cyano-bridge is significantly small (0.0309(1)Å) in comparison to Re(**1**) with 3.48(2)Å displacement formed by C(**1**), C(**2**), C(**3**) and C(**4**).

The isolation of this complex calls for an additional discussion. The aim of this preparation (**Chapter 4**, **Paragraph 4.3.5**) was to try and isolate the substituted $[ReN(\eta^2\text{-dipic})(CN)_3]^{2-}$ complex. The normal aqua complex, $[ReN(H_2O)(CN)_4]^{2-}$, and the cyano-bridge complex, $[ReN(H_2O)(CN)_3\text{-}\mu\text{-}CN\text{-}ReN(CN)_4]^{4-}$ should, in theory, have very similar IR spectra. This appears to be the case (see **Figures 4.6**, **4.7** and **4.8**). The only difference between the IR stretching frequencies of these complexes appears to be in the 1100 – 1000 cm^{-1} and 760 – 680 cm^{-1} regions. The normal aqua complex has Re≡N stretching frequency which splits into two distinguishable peaks namely at 1106 and 1089 cm^{-1}, while the cyano-bridge complex only exhibits one Re≡N stretching frequency at 1080 cm^{-1}. The other notable difference is that the normal aqua complex has strong peaks at 758, 721 and 688 cm^{-1}, while the cyano-bridge complex has only two stretching frequencies at 742 and 687 cm^{-1}. This difference in IR spectra for these two complexes was observed using both the PPh_4^+ and $AsPh_4^+$ cations.

Confirmation of the synthesis of the new cyano-bridge complex was done by repeating the preparation method in **Paragraph 4.3.5**, with 2,3-$dipic^-$ in solution and without 2,3-$dipic^-$ in solution. Results obtained from this experiment yielded the cyano-bridge complex, with one Re≡N stretching frequency at 1081 cm^{-1} and two peaks at 744 and 688 cm^{-1} with 2,3-$dipic^-$ in solution, and the normal aqua complex with a split in Re≡N stretching frequency into two at 1106 and 1089 cm^{-1} and three peaks at 758, 721 and 688 cm^{-1} without the 2,3-$dipic^-$ (**Figure 4.7**).

The crystals obtained for the first part of this experiment (with 2,3-$dipic^-$) were separated from the solution and the UV/VIS spectra were obtained for the solution. The absorption maxima at 410 and 388 nm confirm that the substitution was successfully followed with 2,3-$dipic^-$ (**Chapter 6**, **Paragraph 6.6**). These results clearly suggest that the presence of

2,3-dipic^{-} in solution somehow contributes to the formation of the cyano-bridge complex. The isolation of the $[\{ReN(CN)_4\}_2(\mu\text{-en})]^{4-}$ clearly indicates the ability of Re≡N moiety to bond with nitrogen donor ligands in the *trans*- position in these kind of complexes.

The isolation of this complex also reveals the very interesting bonding nature of the Re≡N moiety. The crystal structure determination of $[ReN(H_2O)(CN)_4]^{2-}$ complex (**I**) performed by Davies *et al*. (1969:736) indicated Re≡N·····Re≡N interaction with the nitrido ligand between the different metal complexes. On the other hand the $[ReN(H_2O)(CN)_4]^{2-}$ complex crystallizes into two different space groups (**II**) while under certain conditions the position *trans* to one of the Re≡N moiety is occupied by an adjacent molecule's ligand (**III**).

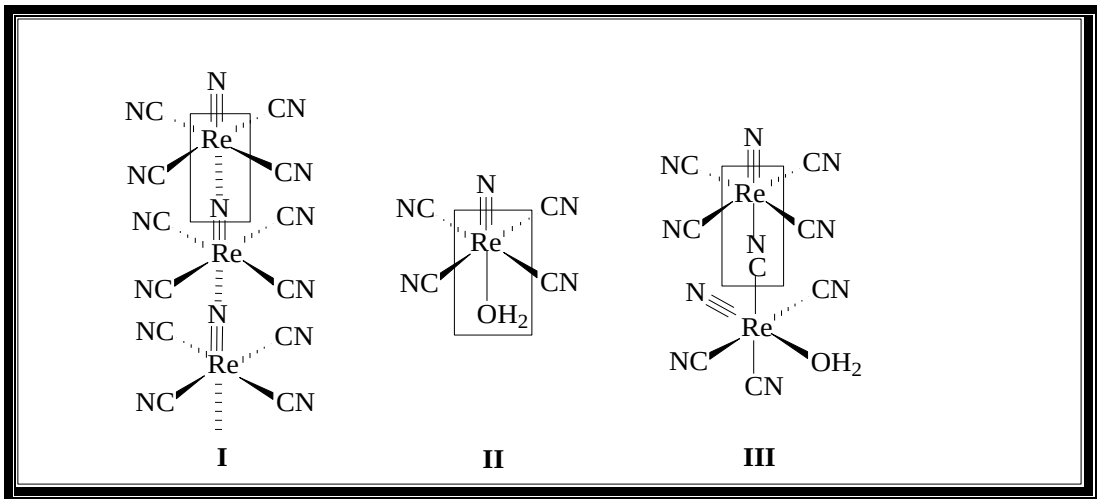

Bonding nature of the $[ReN(H_2O)(CN)_4]^{2-}$ complex.

5.4 CRYSTAL STRUCTURES OF $(AsPh_4)_2[ReN(\eta^2\text{-pic})(CN)_3]\cdot 4H_2O$ and $(AsPh_4)_2[ReN(\eta^2\text{-quin})(CN)_3]\cdot 2H_2O$

5.4.1 Crystal Structure Data of $(AsPh_4)_2[ReN(\eta^2\text{-pic})(CN)_3]\cdot 4H_2O$

(Mtshali *et al*., 2006: accepted for publication).

5.4.1.1 Introduction

The preparation of the $(AsPh_4)_2[ReN(\eta^2\text{-pic})(CN)_3]\cdot 4H_2O$ complex and the growth of the orange crystals used for data collection were reported in **Chapter 4**. This complex was isolated at a pH above the pK_a value of 2-picolinic acid (pK_a = 5.52) (Garcia *et al*., 1996:593).

The partial projection of $(AsPh_4)_2[ReN(\eta^2\text{-pic})(CN)_3]\cdot 4H_2O$ complex, is shown in **Figure 5.5** while the molecular diagram showing the numbering scheme of the anion is presented in **Figure 5.6** and selected bond distances and angles are given in **Table 5.4**, with a discussion highlighting some of the important aspects of the $[ReN(\eta^2\text{-pic})(CN)_3]^{2-}$ anion presented thereafter. A comparison with other relevant structures is given in **Table 5.5**. Supplementary data containing complete lists of atomic coordinates, anisotropic displacement parameters, bond distances and angles as well as hydrogen bonds are given in **A3** (**Appendix A**).

5.4.1.2 Packing and Lattice Stabilization

The $(AsPh_4)_2[ReN(\eta^2\text{-pic})(CN)_3]\cdot 4H_2O$ complex crystallizes in the triclinic space group, Pī, with two tetraphenylarsonium cations, $[ReN(\eta^2\text{-pic})(CN)_3]^{2-}$ anion and four water molecules in the asymmetric part of the unit cell. The structure consists of discrete $AsPh_4^+$ cations and a $[ReN(\eta^2\text{-pic})(CN)_3]^{2-}$ anion (**Figure 5.5**). The As atoms are tetrahedrally surrounded by four phenyl rings with the average As-C bond distance of 1.914(4)Å, while the C-As-C bond angles range between 107.3(2)° to 112.01(2)°. These results as well as the geometry of the phenyl rings are in agreement with those found in other structures containing $AsPh_4^+$ cations (1.906Å, 109.5° in

$(AsPh_4)_2[WO(\eta^2\text{-pic})(CN)_3]\cdot 2H_2O$, 1.912(11)Å, 107.3(4)° to 111.6(4)° and 1.907(7)Å, 107.6(3) to 113.0(3)° in $(AsPh_4)_2[ReN(H_2O)(CN)_4]\cdot 5H_2O$, and $(AsPh_4)_2[OsN(OH)(CN)_4]$ respectively (Leipoldt *et al*., 1986:323; Van der Westhuizen *et al*., 1994:582; Purcell *et al*., 1992:387).

The drawing of the packing within the unit cell shows several kinds of hydrogen bonding:

(i) between anions and water molecules: the nitrogen N(**3**) of the cyano ligand forms a hydrogen bond with O(**1**) of the water molecule (O(**1**)-H(**1**)….N(**3**) = 2.878(6)Å).

(ii) between cations and water molecules: the oxygen O(**2**) of the picolinate ligand forms a hydrogen bond with oxygen atoms O(**3**) of the water molecules (O(**3**)-H(**3**)….O(**2**) = 2.806(13)Å).

(iii) between water molecules only: such interactions are observed for O(**1**) and O(**4**) water molecules (O(**1**)-H(**1**)….O(**4**) = 2.751(16), and O(**1**)-H(**1**)….O(**4**) = 3.277(17)Å).

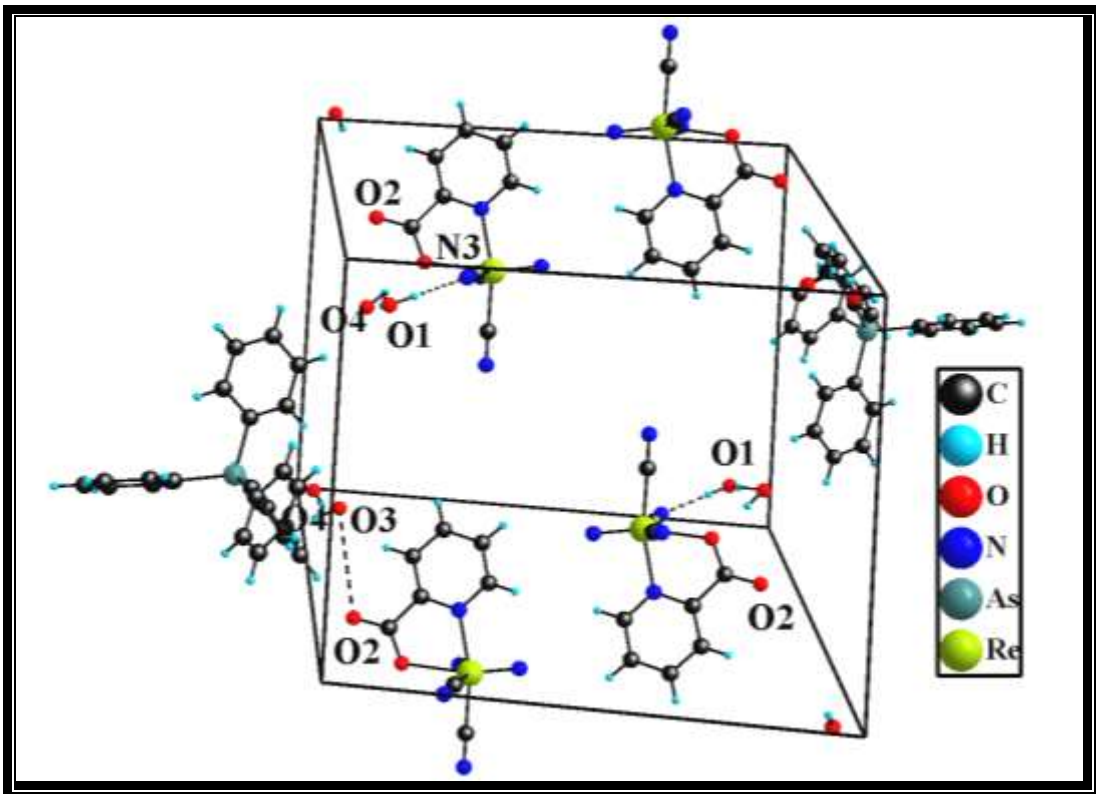

Figure 5.5: **The partial projection of $(AsPh_4)_2[ReN(\eta^2\text{-pic})(CN)_3]\cdot 4H_2O$. Displacement ellipsoids are shown at the 50% probability level (hydrogen bonding is shown).**

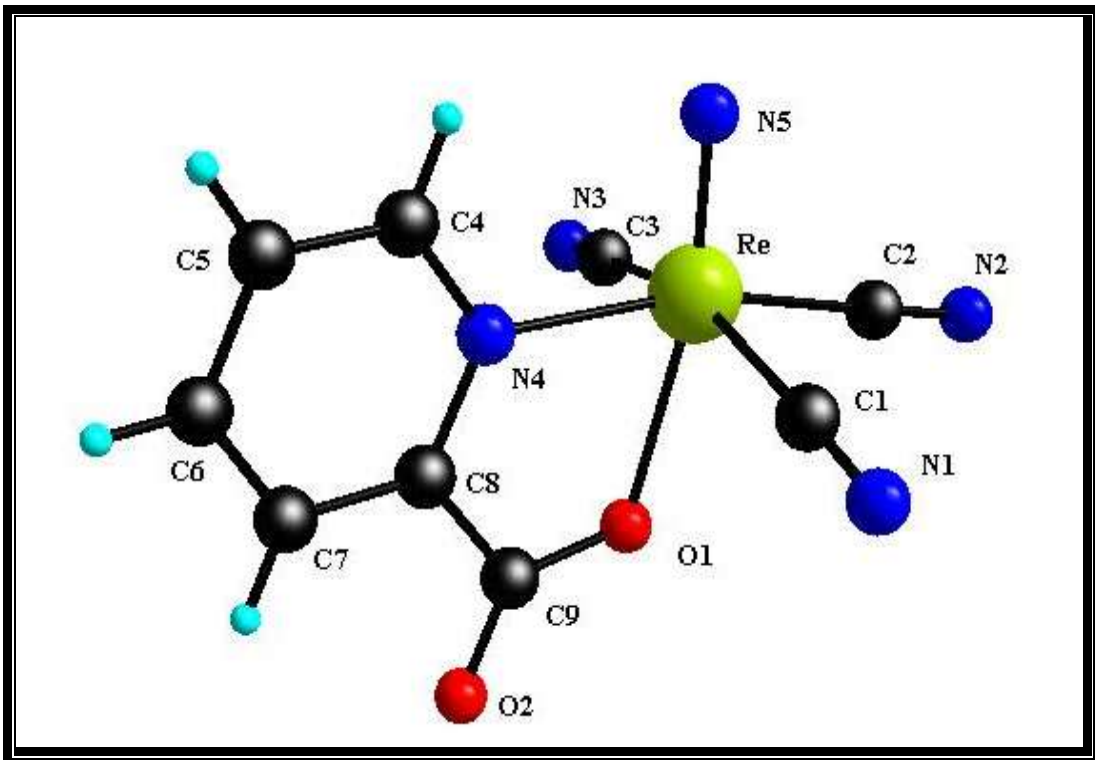

Figure 5.6: **Molecular diagram showing the numbering scheme and displacement ellipsoids (50 % probability) of the $[ReN(\eta^2\text{-pic})(CN)_3]^{2-}$ anion. The cations are omitted for clarity.**

Table 5.4: Selected bond distances (Å) and angles (°) for the $[ReN(\eta^2\text{-pic})(CN)_3]^{2-}$ anion.

Bond distances (Å)			
Re-N(5)	1.655(3)	As(2)-C(71)	1.921(4)
Re-C(2)	2.075(5)	O(2)-C(9)	1.222(6)
Re-C(1)	2.105(5)	O(1)-C(9)	1.281(7)
Re-C(3)	2.113(5)	N(4)-C(4)	1.353(6)
Re-N(4)	2.169(3)	C(2)-N(2)	1.152(7)
Re-O(1)	2.289(3)	C(8)-C(7)	1.392(8)
As(1)-C(21)	1.913(4)	C(8)-C(9)	1.501(8)
As(1)-C(31)	1.913(5)	C(6)-C(7)	1.344(9)
As(1)-C(41)	1.917(4)	C(6)-C(5)	1.395(9)
As(1)-C(11)	1.919(4)	N(4)-C(8)	1.364(6)
As(2)-C(81)	1.912(4)	N(3)-C(3)	1.141(6)
As(2)-C(61)	1.904(4)	N(1)-C(1)	1.150(6)
As(2)-C(51)	1.916(5)	C(4)-C(5)	1.378(8)
Bond angles (°)			
N(5)-Re-O(1)	166.5(1)	N(1)-C(1)-Re	175.7(4)
N(5)-Re-C(1)	100.6(2)	N(2)-C(2)-Re	178.0(4)
N(5)-Re-C(2)	99.62(2)	N(3)-C(3)-Re	174.8(4)
N(5)-Re-C(3)	99.1(2)	C(9)-O(1)-Re	117.8(3)
C(2)-Re-C(1)	87.6(2)	N(4)-C(8)-C(7)	121.1(4)
C(2)-Re-C(3)	86.1(2)	N(4)-C(8)-C(9)	115.5(4)
C(3)-Re-C(1)	160.1(2)	C(7)-C(8)-C(9)	123.5(4)
N(5)-Re-N(4)	94.2(2)	O(2)-C(9)-O(1)	125.2(5)
C(2)-Re-N(4)	166.1(1)	O(2)-C(9)-C(8)	119.5(4)
C(1)-Re-N(4)	88.6(1)	O(1)-C(9)-C(8)	115.3(4)
C(3)-Re-N(4)	93.1(1)	C(7)-C(6)-C(5)	119.1(5)
C(2)-Re-O(1)	93.9(1)	C(6)-C(7)-C(8)	120.2(5)
C(1)-Re-O(1)	80.7(1)	C(4)-C(5)-C(6)	119.1(5)
C(3)-Re-O(1)	80.9(1)	C(8)-N(4)-Re	119.0(3)
N(4)-Re-O(1)	72.4(1)	N(4)-C(4)-C(5)	123.1(4)
C(4)-N(4)-C(8)	117.5(4)	C(4)-N(4)-Re	123.4(3)

5.4.1.3 Results and Discussion

The rhenium(V) atom has distorted octahedral coordination geometry. The nitrido ligand is bonded normally to the original tetracyano equatorial plane, the latter now being constituted of three cyano ligands and a pyridine nitrogen of the picolinate ligand. The carboxylate oxygen completes the chelate ring *trans* to the nitrido ligand in the $[ReN(\eta^2\text{-pic})(CN)_3]^{2-}$ anion (**Figure 5.6**). The distortion has two main features:

(i) a displacement of 0.2979(2)Å of the rhenium from the equatorial C(**1**), C(**2**), C(**3**) and N(**4**) plane towards the nitrido ligand. This displacement is typical for $[MO(L)(CN)_4]^{n-}$ or $[MN(L)(CN)_4]^{m-}$ complexes (L = monodentate ligands) where different bond strengths along the *trans* O=M-L or N≡M-L moieties prevailed (Leipoldt *et al*., 1993:241).

(ii) a 13.3° distortion of the Re-O(**1**) bond from the expected linear N(**5**)≡Re-O(**1**) axis (90°). This is mainly the result of bite angle restrictions due to the five-membered chelate ring.

The Re≡N(**5**) bond distance (**Table 5.4**) is 1.655(3)Å and may be compared with the corresponding bond length of 1.65(2)Å in $[ReN(N_3)(CN)_4]^{3-}$, 1.639(8)Å in $[ReN(H_2O)(CN)_4]^{2-}$, and 1.68(1)Å in $[ReN(CN)_5]^{3-}$ (Purcell *et al*., 1991:473, 1992:217, 1992:387). This suggests a strong pπ-dπ ligand-to-metal interaction. The Re-O(**1**) bond length of 2.289(3)Å is significantly shorter than the 2.496(7)Å of the Re-O bond length in $[ReN(H_2O)(CN)_4]^{2-}$, but longer than the same bond in complexes containing κ^2-N,O ligands (2.171(8)Å in $[WO(\eta^2\text{-pic})(CN)_3]^{2-}$ and 2.191(2)Å in $[MoO(\eta^2\text{-pic})(CN)_3]^{2-}$) (Leipoldt *et al*., 1986:323; Szklarzewicz *et al*., 2005:1749). The latter results fit in well with the general tendency where the bond distances in rhenium nitrido complexes are longer than the corresponding bonds in the molybdenum(IV), tungsten(IV) and rhenium(V) oxo complexes (Leipoldt *et al*., 1986:323; Purcell *et al*., 1992:217; Murmann & Schlemper, 1971:2352). Furthermore, this long Re-O(**1**) bond distance is an indication of the large *trans*-influence of the nitrido ligand towards the oxygen atom of the carboxylic group of the picolinate ligand.

The carboxylate oxygen of the picolinate ligand is bonded *trans* to the nitrido ligand with a N(**5**)≡Re-O(**1**) bond angle of 166.5(1)°. This value corresponds well with bond angles of 164.7(5)° and 162.0(1)° which were obtained for the same bonds in $[WO(\eta^2\text{-pic})(CN)_3]^{2-}$ and the $[MoO(pic)(CN)_3]^{2-}$ respectively. The pyridine nitrogen atom of the picolinate ligand is bonded *cis* to the terminal nitrogen atom with a N(**5**)≡Re-N(**4**) bond angle of 94.2(2)° and a Re-N(**4**) bond distance of 2.169(3)Å which compares favourably with the data of $[WO(\eta^2\text{-pic})(CN)_3]^{2-}$ (92.2(5)° and 2.188(13)Å).

The rest of the bond distances and angles of the aromatic ring in the picolinate ligand are normal and correspond with those found in other complexes containing the same bidentate ligand (Leipoldt *et al*., 1986:323; Szklarzewicz *et al*., 2005:1749; Van der Westhuizen, 2004:90, a).

The Re-C-N chains are nearly linear (ranging between 174.8(4)° and 178.0(4)°). Another interesting aspect of the $[ReN(\eta^2\text{-pic})(CN)_3]^{2-}$ anion is that the rhenium-cyano bond length (2.075(5)Å in Re-C(**2**)) *trans* to the nitrogen atom of the picolinate ligand is significantly shorter than the other two cyano bond lengths (2.105(5)Å in Re-C(**1**) and 2.113(5)Å in Re-C(**3**)). The same tendency was observed for the corresponding cyano complexes of molybdenum(IV), tungsten(IV) and manganese(V) with κ^2-N,O ligand. The phenomenon is attributed to weak or no π-bonding capability of the pyridine nitrogen atom of the picolinate anion. This leads to extensive π-shortening of the *trans* Re-C bond due to back-bonding from the metal to the π*-orbital of the cyano ligand. This shortening of the metal-cyanide bond can also be explained in terms of the thermodynamic *trans*-influence of the different ligands. The cyanide ligand has a greater thermodynamic *trans*-influence than the nitrogen of the picolinate anion. This will also lead to a shortening of the Re-C bond *trans* to the nitrogen compared to the two *trans*-orientated cyanide ligands where equal sharing of π-electron density is operative.

5.4.2 Crystal Structure Data of $(AsPh_4)_2[ReN(\eta^2\text{-quin})(CN)_3]\cdot 2H_2O$

5.4.2.1 Introduction

The preparation of the $(AsPh_4)_2[ReN(\eta^2\text{-quin})(CN)_3]\cdot 2H_2O$ complex and the growth of the red crystals used for data collection were reported in **Chapter 4**. This complex was isolated at a pH above the pK_a value of quinoline-2-carboxylic acid (pK_a = 4.97) (Martell & Smith, 1982:129).

The partial projection of $(AsPh_4)_2[ReN(\eta^2\text{-quin})(CN)_3]\cdot 2H_2O$ complex, is shown in **Figure 5.7,** while the numbering scheme of $[ReN(\eta^2\text{-quin})(CN)_3]^{2-}$ anion is shown in **Figure 5.8.** Selected bond distances and angles are given in **Table 5.6**, with a discussion highlighting some of the important aspects of the $[ReN(\eta^2\text{-quin})(CN)_3]^{2-}$ anion presented thereafter. A comparison with other relevant cyano complexes containing κ^2-N,O ligands is given in **Table 5.7**. Supplementary data containing a complete list of atomic coordinates, anisotropic displacement parameters, bond distances and angles as well as hydrogen bonds are given in **A4** (**Appendix A**).

5.4.2.2 Packing and Lattice Stabilization

The $(AsPh_4)_2[ReN(\eta^2\text{-quin})(CN)_3]\cdot 2H_2O$ complex crystallizes in the triclinic space group, Pī, with two tetraphenylarsonium cations, $[ReN(\eta^2\text{-quin})(CN)_3]^{2-}$ anion and two water molecules in the asymmetric part of the unit cell. The structure consists of discrete $AsPh_4^+$ cations and a $[ReN(\eta^2\text{-quin})(CN)_3]^{2-}$ anion (**Figure 5.7**). The As atoms are tetrahedrally surrounded by four phenyl rings with the average As-C bond distance of 1.917(4)Å, while the C-As-C bond angles range between 106.3(4)° to 113.1(2)°. These results as well as the geometry of the phenyl rings are in good agreement with those found in other structures containing $AsPh_4^+$ cations (see **Paragraph 5.5.1**).

The drawing of the parking within the unit cell shows several kinds of hydrogen bonds in the structure (see **Figure 5.7**):

(i) between anions and water molecules: the nitrogen atoms N(**1**) and N(**3**) of the cyano ligand forms a hydrogen bond with oxygen atoms O(**3**) and O(**4**) of the water molecules (O(**3**)-H(**3**)…N(**1**) = 2.867(5), O(**4**)-H(**4**)….N(**3**) = 2.861(6)Å).

(ii) between cations and the water molecules: the oxygen atom O(**2**) of the quinolinate ligand form a hydrogen bond with oxygen atom O(**4**) of the water molecule (O(**4**)-H(**4**)…O(**2**) = 2.951(5) Å).

(iii) between water molecules only: such interactions are observed for O(**3**) and O(**4**) water molecules (O(**4**)-H(**4**)….O(**3**) = 2.815(6)Å).

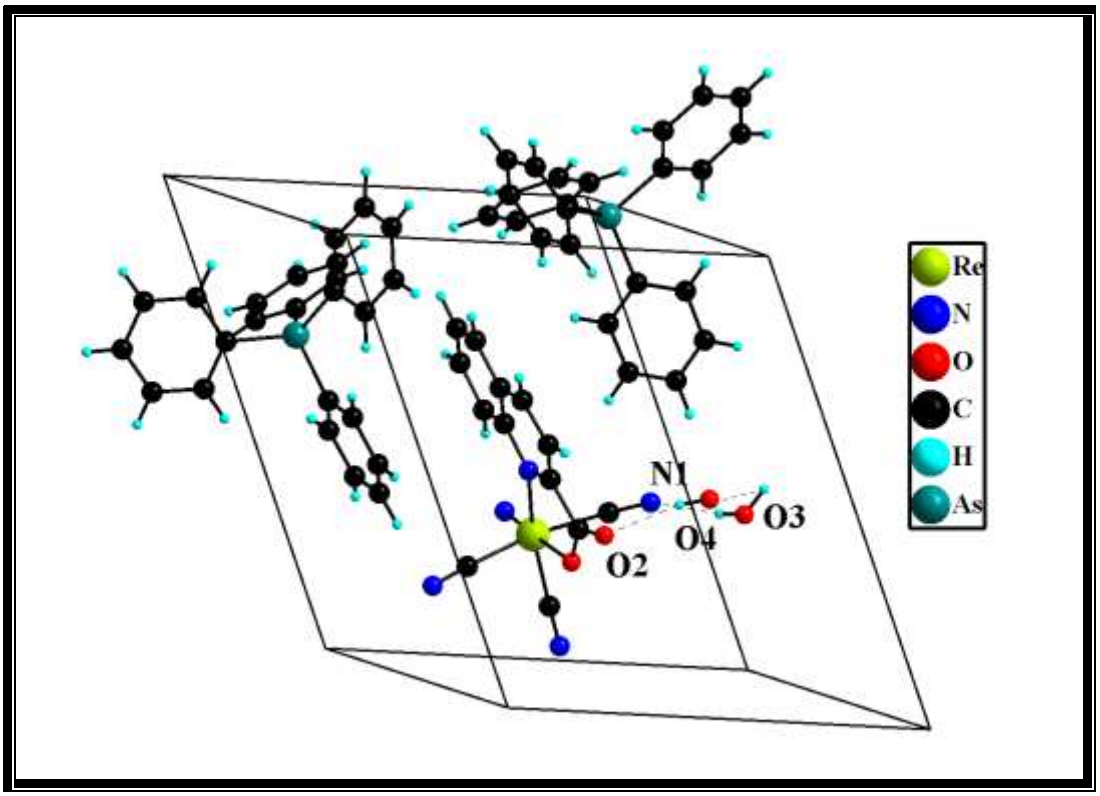

Figure 5.7: **The partial projection of $(AsPh_4)_2[ReN(\eta^2\text{-quin})(CN)_3]\cdot 2H_2O$. Displacement ellipsoids are shown at the 50% probability level (hydrogen bonding is shown).**

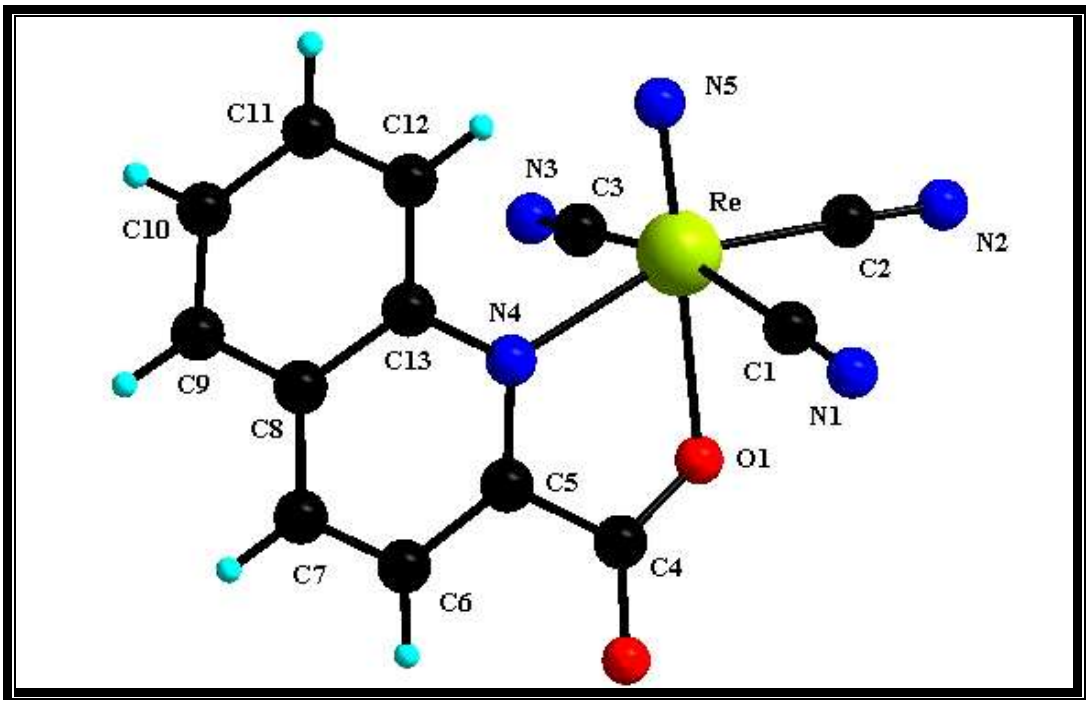

Figure 5.8: Molecular diagram showing the numbering scheme and displacement ellipsoids (50 % probability) of the $[ReN(\eta^2\text{-quin})(CN)_3]^{2-}$ anion. The cations are omitted for clarity.

Table 5.6: Selected bond distances (Å) and angles (°) for the $[ReN(\eta^2\text{-quin})(CN)_3]^{2-}$ complex.

Bond distances (Å)			
Re-N(5)	1.680(4)	As(1)-C(31)	1.916(4)
Re-C(2)	2.066(5)	As(1)-C(21)	1.920(5)
Re-C(3)	2.117(4)	As(2)-C(81)	1.908(4)
Re-C(1)	2.120(4)	As(2)-C(71)	1.910(4)
Re-N(4)	2.224(4)	As(2)-C(61)	1.914(4)
Re-O(1)	2.271(3)	As(2)-C(91)	1.915(4)
N(1)-C(1)	1.154(5)	C(4)-C(5)	1.517(6)
N(2)-C(2)	1.156(6)	C(5)-C(6)	1.404(6)
N(3)-C(3)	1.152(5)	C(6)-C(7)	1.358(7)
N(4)-C(13)	1.395(5)	C(7)-C(8)	1.402(7)
N(4)-C(5)	1.333(6)	C(8)-C(9)	1.416(7)
O(1)-C(4)	1.270(5)	C(8)-C(13)	1.425(7)
O(2)-C(4)	1.238(5)	C(9)-C(10)	1.360(8)
As(1)-C(51)	1.916(4)	C(10)-C(11)	1.398(8)
As(1)-C(41)	1.916(4)	C(11)-C(12)	1.394(7)
		C(12-C(13)	1.409(6)
Bond angles (°)			
N(5)-Re-O(1)	177.30(2)	N(4)-C(13)-C(12)	120.6(4)
N(5)-Re-C(1)	98.14(2)	N(4)-C(13)-C(8)	121.1(4)
N(5)-Re-C(2)	97.20(2)	C(5)-N(4)-Re	115.5(3)
N(5)-Re-C(3)	97.90(2)	O(2)-C(4)-O(1)	126.3(4)
C(2)-Re-C(1)	88.30(2)	O(2)-C(4)-C(5)	118.7(4)
C(2)-Re-C(3)	88.22(2)	O(1)-C(4)-C(5)	115.0(4)
C(3)-Re-C(1)	163.91(2)	C(6)-C(5)-C(4)	118.6(4)
N(5)-Re-N(4)	104.20(2)	C(7)-C(6)-C(5)	119.5(5)
C(2)-Re-N(4)	158.20(2)	C(6)-C(7)-C(8)	119.8(5)
C(1)-Re-N(4)	89.10(2)	C(13)-N(4)-Re	127.1(3)
C(3)-Re-N(4)	88.50(2)	C(7)-C(8)-C(9)	121.5(5)
C(2)-Re-O(1)	85.42(2)	C(9)-C(8)-C(13)	120.1(5)
C(1)-Re-O(1)	80.95(1)	C(10)-C(9)-C(8)	120.0(5)
C(3)-Re-O(1)	83.12(1)	C(9)-C(10)-C(11)	121.1(5)
N(4)-Re-O(1)	73.30(1)	C(12)-C(11)-C(10)	120.2(5)
C(5)-N(4)-C(13)	117.10(4)	C(11)-C(12)-C(13)	120.4(5)
C(3)-Re-C(1)	163.91(2)	C(13)-C(13)-C(8)	118.3(4)
N(1)-C(1)-Re	177.1(4)	C(4)-O(1)-Re	117.4(3)
N(2)-C(2)-Re	178.5(5)	N(4)-C(5)-C(4)	117.7(4)
N(3)-C(3)-Re	176.9(4)	N(4)-C(5)-C(6)	123.6(4)

5.4.2.3 Results and Discussion

The $[ReN(\eta^2\text{-quin})(CN)_3]^{2-}$ anion exhibits distorted octahedral geometry (**Figure 5.8**), with the nitrido ligand N(**5**) and the carboxylato oxygen O(**1**) of the quinolinate ligand occupying the apical positions, whereas the three cyano ligands (C(**1**)-N(**1**), C(**2**)-N(**2**) and C(**3**)-N(**3**)) together with the quinoline nitrogen (N(**4**)) are in an equatorial plane. These are similar to that found for $[ReN(\eta^2\text{-pic})(CN)_3]^{2-}$ (**Figure 5.6**). The distortion has two main features, namely:

(i) a displacement of 0.3461(2)Å of the rhenium from the equatorial C(**1**), C(**2**), C(**3**) and N(**4**) plane towards the nitrido ligand N(**5**). This out-of-plane displacement is typical for $[MO(L)(CN)_4]^{n-}$ or $[MN(L)(CN)_4]^{m-}$ complexes where different bond strengths along the O=M-L or N≡M-L moieties prevailed.

(ii) a 2.75° deviation from the expected linear N(**5**)-Re-O(**1**) axis. This deviation is much smaller than in the pic complex (**Figure 5.6**), but closer inspection of this structure shows that it is rather the N(**4**)-Re-C(**2**) axis with a bond angle of 158.69(16)° which deviates significantly from 180° in this case. The rather chelate ring is bent towards the N(**5**)-Re-O(**1**) axis which explains the deviation of only 2.75° and forces the *cis*-bonded cyano ligand C(**2**) and quinoline nitrogen N(**4**) atoms closer together (**Figure 5.8**).

The coordinated carboxylate oxygen and quinoline nitrogen form a N(**4**)-Re-O(**1**) bite angle of 73.30(1)° in comparison with 72.4(1) obtained in the $[ReN(\eta^2\text{-pic})(CN)_3]^{2-}$ complex (instead of the required 90°) and gives considerable distortion as evidenced in the shape-determining angle in **Table 5.5**. The terminal Re≡N(**5**) bond distance of 1.680(4)Å is comparatively short, and may be compared with other known nitrido complexes of rhenium(V). This short bond distance suggests strong pπ-dπ ligand-to-metal interaction and a large *trans*-influence of the nitrido ligand. The presence of such a strong Re≡N bond in nitridocyano complexes of Re(V) has been explained by the weak bonding of an atom in the *trans* position to the nitrido ligand. However, the oxygen-metal bond of the quinolinate ligand, Re-O(**1**) (2.271(3)Å), is

significantly shorter than the bond length of 2.496(7)Å in $[ReN(H_2O)(CN)_4]^{2-}$ (Purcell *et al.*, 1992:387), but slightly longer than the same bond length in other complexes containing κ^2-N,O ligands (see **Table 5.7**) (Leipoldt *et al.*, 1986:323; Szklarzewicz *et al.*, 2005:1749; Van der Westhuizen, 2004:90, a). The latter results agree with the general tendency where the bond distances in rhenium nitrido complexes are longer than the corresponding bonds in the molybdenum(IV), tungsten(IV) and rhenium(V) oxo complexes.

The carboxylate oxygen atom is bonded *trans* to the nitrido ligand with the N(**5**)≡Re-O(**1**) bond angle of 177.30(5)° and Re-O(**1**) bond length of 2.271(3)Å. This value corresponds well with the bond angle of 178.88(19)° and 2.168(4)Å which was obtained for the same oxygen bond in the $[MnN(\eta^2\text{-quin})(CN)_3]^{2-}$ anion (Van der Westhuizen, 2004:90, a). The nitrogen atom of the quinoline group is bonded *cis* to the nitrido ligand with the N(**5**)≡Re-N(**4**) bond angle of 104.20(2)° and a Re-N(**4**) bond distance of 2.224(4)Å, which compares favourably with the data of the $[MnN(\eta^2\text{-quin})(CN)_3]^{2-}$ complex (103.9(2)° and 2.110(4)Å).

The Re-C-N chains are linearly bonded with an average bond angle of 177.5(4)°. The two *trans*-oriented cyano ligands have comparable Re-C bond distances of 2.117(4)Å in Re-C(**3**) and 2.120(4)Å in Re-C(**1**), but the rhenium-cyano bond *trans* to the quinoline nitrogen (Re-C(**2**) = 2.066(5)Å) is significantly shorter than the other two. The same tendency was observed for the corresponding cyano complexes of molybdenum(IV), tungsten(IV) and manganese(V) with κ^2-N,O ligands. This phenomenon is attributed to weak or no π-bonding capacity of the nitrogen atom of the quinolinate anion. This leads to an extensive π-shortening of the Re-C bond due to back-bonding from the metal to the π^*-orbital of the cyanide ligand. The shortening of the Re-C(**2**) bond can also be explained in terms of the thermodynamic *trans*-influence of the different ligands. The cyanide ligand has a greater thermodynamic *trans*-influence than the nitrogen atom of the quinolinate anion. This will also lead to a shortening of the Re-C bond *trans* to the nitrogen in comparison to the two *trans*-orientated cyanide ligands.

5.5 STRUCTURE CORRELATIONS OF THE N,O-SUBSTITUTED CYANO COMPLEXES

In all the crystal structure determinations of $[ReN(L\text{-}L)(CN)_3]^{2-}$ complexes studied, bulky organic cations $AsPh_4^+$ (**Figure 5.9**) were used as counter ions for the isolation of complexes. These bulky organic cations are expected to show little influence on the chemistry of these systems, apart from making the anion soluble in aqueous solution or organic solvent, and are, therefore, not discussed separately from each structure.

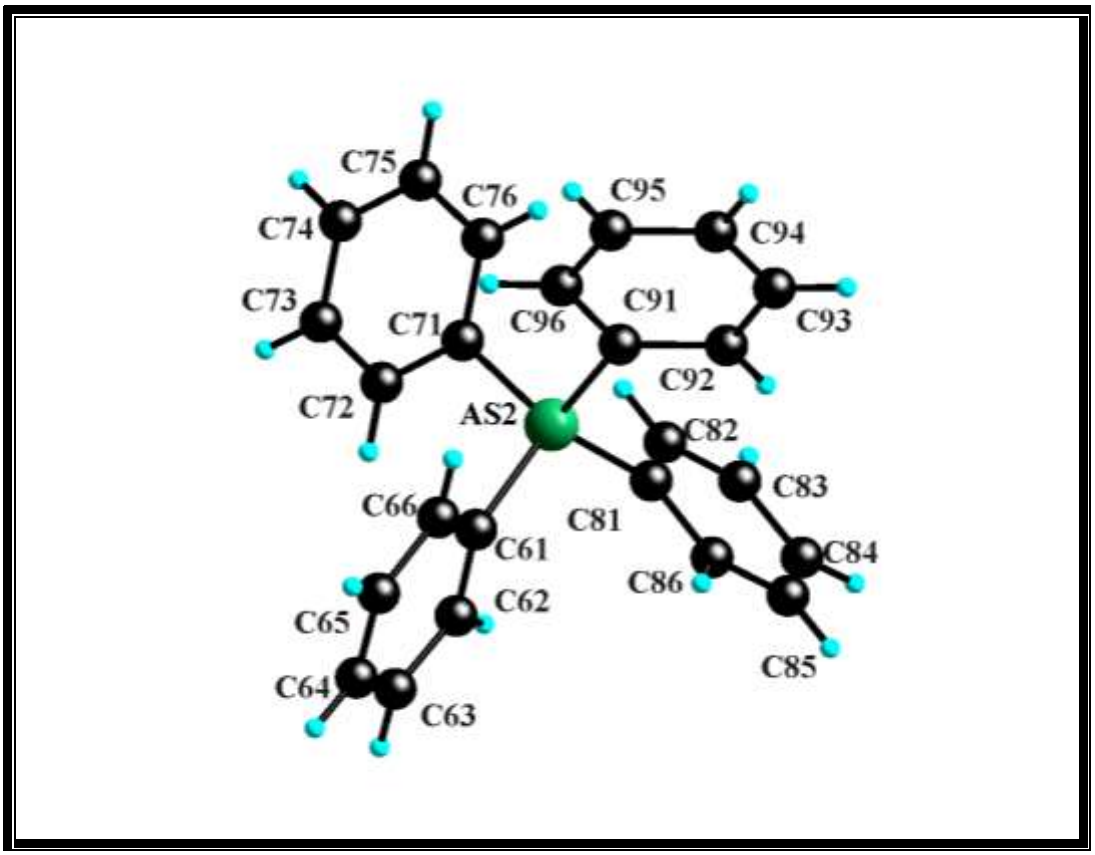

Figure 5.9: Numbering scheme for the $AsPh_4^+$ cation.

A brief discussion of some of the relevant points is given. It has been observed that these cations have a small influence on the IR stretching frequencies of some of the systems. No crystallographic evidence of substantial interactions is available, and this is, therefore, not discussed further. All the bond distances and angles within the tetraphenylarsonium cations are normal. The four phenyl groups in the cations are tetrahedrally bonded to the arsonium atom, with C-As-C bond angles ranging from 107.3(2) to 113.07(19)Å and

average As-C and C-C bond distances of 1.917(3) and 1.389(7)Å, respectively. These results are in agreement with those found in other structures containing the tetraphenylarsonium cation (Leipoldt *et al*., 1986:323; Szklarzewicz *et al*., 2005:1749; Van der Westhuizen, 2004:90, a).

A summary of the average bond lengths, bond angles, ligand bite angles, displacement of the central metal from the plane formed by three carbon atoms of the cyano ligands and the nitrogen atom of the different bidentate ligands as well as the IR stretching frequencies for the rhenium(V) metal centre described in this investigation are presented in **Table 5.7**. A comparison with the literature examples of the selected oxo and nitrido d^2 complexes of Mo(IV), W(IV) and Mn(V) are also presented in **Table 5.7**.

The determination of the crystal structures of the $[ReN(\eta^2\text{-pic})(CN)_3]^{2-}$ and $[ReN(\eta^2\text{-quin})(CN)_3]^{2-}$ were of importance due to the fact that this series of ligands have never been investigated with the same *trans* bonded ligand as well as the same metal centre. The rhenium-nitridocyano complexes with bidentate ligands (picolinate and quinolinate) were crystallized as the tetraphenylarsonium salts (see **Figures 5.5** and **5.7**). The structure determinations showed that the incoming bidentate ligands are coordinated *via* the carboxylate oxygen atom and a pyridine nitrogen atom (with the substitution of aqua and one cyano ligand in an equatorial plane) to the metal centre. It is expected that the aqua ligand will be substituted first in $[ReN(H_2O)(CN)_4]^{2-}$ anion, since the M-H_2O bond is much weaker than the M-CN bond (as indicated in **Chapter 2**), especially in these types of complexes as a result of the large *trans*-influence of the nitrido ligand.

Table 5.7: Bond data for selected isoelectronic N,O-substituted cyano complexes of groups 6 and 7 metal centres containing oxo and nitrido axial ligands.

Anion[a]	**M-X_t**[b] **(Å)**	**M-O**[c] **(Å)**	**M-C**[d] **(Å)**	**$\nu_{(MX)t}$**[e] **(cm^{-1})**	**D**[f] **(Å)**
ReN(pic)[1]	1.655(3)	2.289(3)	2.075(5)	1061	0.2979(2)
ReN(quin)[2]	1.680(4)	2.271(3)	2.066(5)	1080	0.346(2)
MnN(pic)[3]	1.538(3)	2.214(3)	1.931(5)	1033	0.259(2)
MnN(quin)[4]	1.523(5)	2.168(4)	1.984(5)	1032	0.286(3)
MoO(pic)[5]	1.679(2)	2.191(2)	2.137(4)	944	0.309(2)
WO(pic)[6]	1.676(9)	2.171(8)	2.043(2)	944	0.331(2)

Anion	**X_t-M-O**[g] **(°)**	**X_t-M-N**[h] **(°)**	**C-M-C**[i] **(°)**	**N-M-C**[j] **(°)**	**Bite angle (°)**
ReN(pic)[1]	166.5(1)	94.2(2)	160.1(2)	166.1(1)	72.4(1)
ReN(quin)[2]	177.30(2)	104.20(2)	163.91(2)	158.20(2)	73.30(1)
MnN(pic)[3]	171.94(2)	95.9(2)	162.5(2)	166.8(2)	76.1(1)
MnN(quin)[4]	178.9(2)	103.9(2)	166.3(2)	161.2(2)	76.4(2)
MoO(pic)[5]	162.04(1)	90.1(1)	158.3(1)	167.1(1)	72.5(4)
WO(pic)[6]	164.7(5)	92.2(5)	158.2(5)	165.3(4)	72.0(1)

[1] ReN(pic) = $(AsPh_4)_2[ReN(\eta^2\text{-pic})(CN)_3]\cdot 4H_2O$; [2] ReN(quin) = $[ReN(\eta^2\text{-quin})(CN)_3]^{2-}$; [3] MnN(pic) = $[MnN(\eta^2\text{-pic})(CN)_3]^{2-}$; [4] MnN(quin) = $[MnN(\eta^2\text{-qun})(CN)_3]^{2-}$; [5] MoO(pic) = $[MoO(\eta^2\text{-pic})(CN)_3]^{2-}$ and [6] WO(pic) = $[WO(\eta^2\text{-pic})(CN)_3]^{2-}$; [a] Complexes containing N,O-ligands, [b] M-X_t = terminal ligand (X_t = O^{2-} or N^{3-}); [c] M-O = *trans* to X_t; [d] M-C = C bond *trans* to the nitrogen atom of the bidentate ligand in the equatorial plane; [e] IR. stretching frequency of MX peak; [f] Displacement of the central metal atom from the plane formed by three carbon atoms of the cyano ligands and the nitrogen atom of the bidentate ligand; [g] N-M-O in the axial position; [h] X_t-M-N = N *cis* bonded; [i, j] Equatorial position; [1,2] this work; [3,4] Van der Westhuizen, (2004:90, a); [5] Szklarzewicz *et al*., (2005:1749); [6] Leipoldt *et al*., (1986:323).

The crystal structural determinations of the rhenium(V) system discussed in the previous sections showed similar behaviour. The incoming bidentate ligands (pic^- and $quin^-$) coordinate to the metal centre and form a five-membered chelate ring (see **Figures 5.6** and **5.8**). The Re(V) atom is located at the centre of the equatorial plane formed by three carbon atoms of the cyano ligands and a nitrogen atom of the pyridine or quinoline ring. The carboxylate oxygen and nitrido ligands coordinate normally to this

plane. Similar structures were observed for other iso-structural complexes of Mo(IV), W(IV) and Mn(V) (Leipoldt *et al*., 1986:323; Szklarzewicz *et al*., 2005:1749; Van der Westhuizen, 2004:90, a).

The large *trans*-influence of the nitrido ligand is also evident in the N,O-bidentate substitution complexes. The Re-O(**1**) bonds in these complexes (pic^- and $quin^-$) are longer than expected and correspond with other complexes of $[MX(L\text{-}L)(CN)_3]^{n-}$ type with κ^2-N,O ligands (see **Table 5.7**). The distortion has two main features. Firstly, the displacement of the rhenium atom from the equatorial plane formed by three carbon atoms of the cyano ligands and the nitrogen atom of the pyridine or quinoline rings towards the terminal nitrido ligand (0.2979(2)Å in $[ReN(\eta^2\text{-pic})(CN)_3]^{2-}$ and 0.346(2)Å in $[ReN(\eta^2\text{-quin})(CN)_3]^{2-}$). This displacement is substantially smaller for the $[ReN(\eta^2\text{-pic})(CN)_3]^{2-}$ complex compared to the $[ReN(\eta^2\text{-quin})(CN)_3]^{2-}$ anion. Secondly, there is also a deviation of the N≡Re-O(**1**) angles from the expected 180°. This deviation is coupled with the small bite angle of 72.4(1)° and 73.30(1)° respectively (see **Table 5.7**). These small bite angles are due to the fact that the coordinating groups are bonded *via* the same carbon backbone in the ligand molecule. The deviation of the N(**5**)-Re-N(**4**) bond angles of 94.2(2)° and 104.15(16)° respectively, as well as the N(**5**)-Re-C bond angles (range from 99.1(2)° to 100.6(2)° in $[ReN(\eta^2\text{-pic})(CN)_3]^{2-}$ and from 97.2(2)° to 98.14(17)° in $[ReN(\eta^2\text{-quin})(CN)_3]^{2-}$ complexes) from the angular 90° for the ideal octahedron is also an indication of the mode of distortion of the coordination octahedron. The displacement along the N(**5**)≡Re-(O(**1**) axes in these two anions can also be judged by the average angle between the two *cis* cyano ligands (Re-C(**1**)-N(**1**) and Re-C(**3**)-N(**3**)). Both C(**1**)-N(**1**) and C(**3**)-N(**3**) groups are considerably pushed away from the nitrido ligand with C(**1**)-Re-C(**3**) bond angles of 159.9(2) and 163.91(1)°, respectively.

Similar but weaker displacement has previously been observed for $[MoO((\eta^2\text{-pic})(CN)_3]^{2-}$ and $[WO(\eta^2\text{-pic})(CN)_3]^{2-}$ complexes (Leipoldt *et al*., 1986:323; Szklarzewicz *et al*., 2005:1749). As indicated in the previous discussions (**Paragraph 5.4.1.3**), this type of distortion can be attributed to a strong π-bonded ligand

such as oxo or nitrido in an axial position of the coordination octahedron of transition metal complexes.

Of interest in the picolinate and quinolinate structures is the fact that the Re-C(**2**) bond distance *trans* to the nitrogen atom of the pyridine or quinoline ring is more strongly bonded (short) when compared to the Re-C bond distances of the two weaker or (long) *trans*-bonded cyano ligands. This can be explained in terms of the large thermodynamic *trans*-influence of the cyano ligand on a *trans* bonded ligand. The cyano ligand has a larger thermodynamic *trans*-influence compared to the nitrogen atom of the quinolinate or picolinate ligand and this would lead to a shortening of the Re-C(**2**) bond distance in contrast to the two other *trans*-oriented cyano ligands with the longer Re-C bond distances. The shorter Re-C(**2**) bond distance can also be attributed to the fact that the nitrogen atom of the picolinate or quinolinate group has a very weak or no π-bonding capability and this leads to extensive π-shortening of the Re-C(**2**) bond. Thus the degree of the π-bonding has a large influence on the metal-carbon bond distances in cyano-complexes of groups 6 to 7 (see **Table 5.7**). Similar behaviour was observed for other iso-structural complexes reported in **Table 5.7**.

Another point worth mentioning is that the IR stretching frequencies of the Re≡N bonds in these two complexes are different (1061 cm^{-1} in $(AsPh_4)_2[ReN(\eta^2\text{-pic})(CN)_3]\cdot 4H_2O$ and 1080 cm^{-1} in $(AsPh_4)_2[ReN(\eta^2\text{-quin})(CN)_3]\cdot 2H_2O$ (**Table 5.7**). This is probably due to an extra aromaticity of the quinolinate ligand (containing naphthalene backbone) which can change the bonding capability of the pyridine nitrogen and carboxylic oxygen atoms to a large extent, compared to the pyridine nitrogen and carboxylic oxygen atoms of the picolinate ligand. The Re≡N bond length 1.680(4)Å in $[ReN(\eta^2\text{-quin})(CN)_3]^{2-}$ is significantly shorter than 1.655(3)Å in $[ReN(\eta^2\text{-pic})(CN)_3]^{2-}$, which is in line with the IR data showing a stronger bond for the quinolinate complex.

To conclude, it was imperative to determine the crystal structures of these N,O-substituted nitrido complexes of rhenium(V) since very little data is available on the bidentate substitution reactions of these nitrido complexes and the products thereof. Since the picolinate type of ligands have two different donor atoms, it was also important to

determine if these ligands will have the same bonding mode in the nitrido complexes as in the related oxo complexes. Thus, the characterization of these complexes gave valuable information on the coordination mode of the bidentate ligand studied, and, therefore, will also indirectly provide information about the determination of the reaction mechanism that these types of substitution reactions undergo. The bond distances would also play an integral role in the reaction rates if a dissociative pathway is an important part of the reaction.

These results will be used in the following chapter to assist in deriving a reaction mechanism for the bidentate substitution reactions of the $[ReN(H_2O)(CN)_4]^{2-}$ complexes (see **Chapter 6**)

6 KINETIC STUDY OF THE REACTION BETWEEN $[ReN(H_2O)(CN)_4]^{2-}$ AND DIFFERENT N,O-BIDENTATE LIGANDS

6.1 INTRODUCTION

One of the objectives of this study was to investigate the substitution reactions between the nitridotetracyanorhenate(V) complex, $[ReN(H_2O)(CN)_4]^{2-}$ with different κ^2-N,O bidentate ligands, and thus to determine the reaction mechanism for these reactions.

Kinetic studies over the past few years have shown that *trans*-dioxotetracyano complexes $[MO_2(CN)_4]^{n-}$ (M = molybdenum(IV), tungsten(IV), rhenium(V), technetium(V), manganese(V) and osmium(VI)) can undergo protonation and deprotonation reactions with the formation of the corresponding oxo-aqua and oxo-hydroxo complexes, except in case of the $[OsO_2(CN)_4]^{2-}$ complex. The iso-electronic $[MN(H_2O)(CN)_4]^{n-}$ complexes of rhenium(V), technetium(V) and osmium(VI) have also shown the tendency to undergo the same protonation reactions to form the hydroxo $[MN(OH)(CN)_4]^{3-}$ complexes and that these hydroxo species are inert towards substitution reactions. These protonated species (especially the aqua complex) can undergo aqua substitution reactions with monodentate nucleophiles such as F^-, N_3^-, NCS^-, pyridine (py) and substituted thiourea as for the W(IV) and Re(V) complexes (Smit *et al*., 1995:71; Leipoldt *et al*., 1986:4639; Roodt *et al*., 1988:336; Purcell *et al*., 1989:224; 1991:339).

The above-mentioned complexes (especially Mo(IV), W(IV) and Mn(V)) can also undergo substitution reactions by κ^2-N,N and κ^2-N,O ligands such as 1,10-phenanthroline (phen), pyridine-2-carboxylate (pic), and quinoline-2-carboxylate (quin) (Leipoldt *et al*., 1986:323; Szklarzewicz *et al*., 2005:1749; Van der Westhuizen, 2004:109, b).
The crystal structure determinations of the final products have showed that the aqua and one of the cyano ligands in the equatorial plane are substituted by the entering bidentate nucleophiles. The metal-aqua bond is usually much weaker than a metal-cyano bond, due

to the large *trans*-influence of the oxo or nitrido ligands bonded to the metal centre (in the terminal position).

The above-mentioned reactions of the corresponding rhenium(V) complexes have also been complemented by the crystallographic studies on the $[ReN(\eta^2\text{-pic})(CN)_3]^{2-}$ and $[ReN(\eta^2\text{-quin})(CN)_3]^{2-}$ complexes (see **Chapter 5**). The crystal structure determinations of these complexes showed that the oxygen atom of the carboxylic group is bonded *trans* to the nitrogen ligand while the nitrogen atom of the pyridine and quinoline ring is bonded *trans* to one of the equatorial cyano ligands. It is important to study this system and determine the reaction rates for these bidentate substitution reactions of the $[ReN(H_2O)(CN)_4]^{2-}$ complex to establish the mechanism of these reactions.

In this chapter, the kinetic results obtained from the reactions between $[ReN(H_2O)(CN)_4]^{2-}$ and different κ^2-N,O ligands such as pyridine-2-carboxylate (pic), quinoline-2-carboxylate (quin) and pyridine-2,3-dicarboxylate (2,3-dipic) anions are discussed.

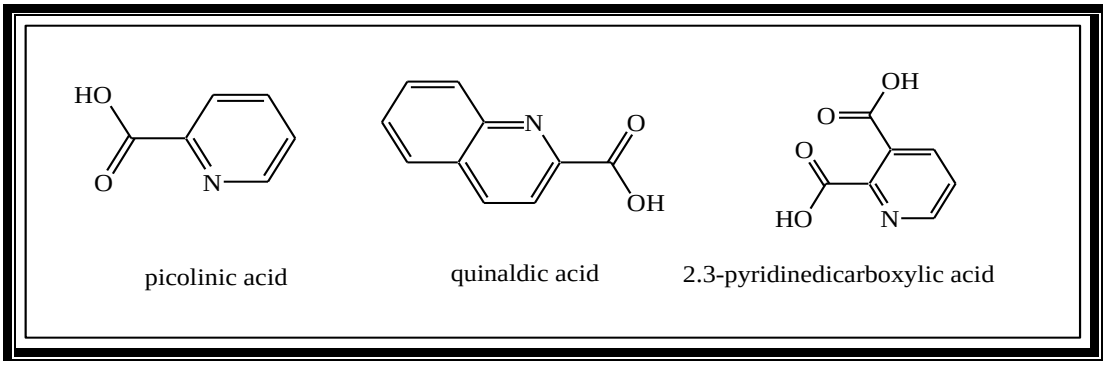

Bidentate ligands.

6.2 EXPERIMENTAL WORK

General: All reagents and chemicals used were of analytical grade. Pyridine-2-carboxylic and quinoline-2-carboxylic acids were purchased from Sigma Aldrich. Pyridine-2-carboxylic acid was recrystallized in hot ethanol and quinoline-2-carboxylic acid was recrystallized in hot water before use. All the experiments were performed aerobically and distilled water was used in all the preparations unless otherwise mentioned. All the pH measurements were performed on a Hanna model 8519 pH meter with a combined glass/calomel electrode using standard buffer solutions for calibration and an ionic strength 5.0M KCl.

Data collection and other measurements: Kinetic measurements and pH titration reactions for slow reactions were monitored on Hitachi (model 150-20) and Varian Carey (model 50Conc) spectrophotometers by using 1.00±0.001 cm double-sided tanderm quartz cells. Temperature control of the reaction solution was maintained by means of a Labcon CPE 50 circulating water bath system and APPA-51 Digital thermometer (accurate within 0.1°-1.0°). The kinetic reactions were measured aerobically under pseudo first-order conditions with at least 100 fold excess of the ligand concentration. Each kinetic run was performed at least twice and an average (k_{obs}) of both values was taken.

The kinetic runs and pH titration reactions for the fast reactions were monitored on a stopped-flow (model 05–109 Photophysics) spectrophotometer coupled with a personal computer (SX 18MV) capable of performing least-square analysis on absorbance *vs*. time data. Data of 150 points per trace were collected and at least 120-130 points for each trace were analyzed by the least-square fit to give the rate constants. The reported rate constants are the average of 4 to 12 runs. The Scientist-program was used to fit the data to selected functions. Linear plots of $\ln(A_\infty - A_t)$ *vs*. time were obtained for at least two half-lives under all conditions.

The pH of the solutions was adjusted with a freshly prepared 5.0M NaOH and concentrated $HClO_4$ with μ = 1.0M $NaClO_4$ ($KClO_4$, KNO_3 and HCl could not be used due to poor solubility and reactivity interference at high temperature). Dilution and

decomposition were avoided by the use of large volumes (50ml stock solution) of the complex and ligand solutions. The consecutive pH changes were varied by dipping a glass needle first into the saturated NaOH (5.0M) or $HClO_{4(conc)}$ and afterwards in the solution containing complex or ligand.

Table 6.1: Acid dissociation constants for the pyridine carboxylate type ligands.

Pyridine carboxylic acids	**pK_{a1}[a]**	**pK_{a2}[b]**	**Ref.**
Pyridine-2-carboxylate	1.03	5.02	**1**
Pyridine-2,3-dicarboxylate	2.78	5.02	**2**
Pyridine-2,4-dicarboxylate	2.17	5.09	**3**
Pyridine-2,5-dicarboxylate	2.31	5.06	**3**
Pyridine-2,6-dicarboxylate	-0.81	4.97	**4**
Quinoline-2-carboxylate	1.9	4.97	**5**

[a] Dissociating group = -COOH; [b] Dissociating group = $-NH^+$, [1] Garcia *et al*., (1996:593); [2] Harmon *et al*., (1998:43); [3] Canic, (1955:35); [4] Tichane & Benet, (1957:1293); [5] Martell & Smith, (1982: 129).

6.3 RESULTS

6.3.1 Reaction Scheme and the Determination of the Rate Laws

During the kinetic reactions of all the bidentate ligands studied, two different reactions were observed on close inspection of the absorbance *vs*. time spectra under the conditions employed. The first reaction was relatively fast, followed by a much slower second reaction that yielded the UV/VIS spectrum which was identical to that of the final product. The following reaction **Scheme 6.1** may be constructed for all the reactions which are possible under the experimental conditions that prevailed during this study.

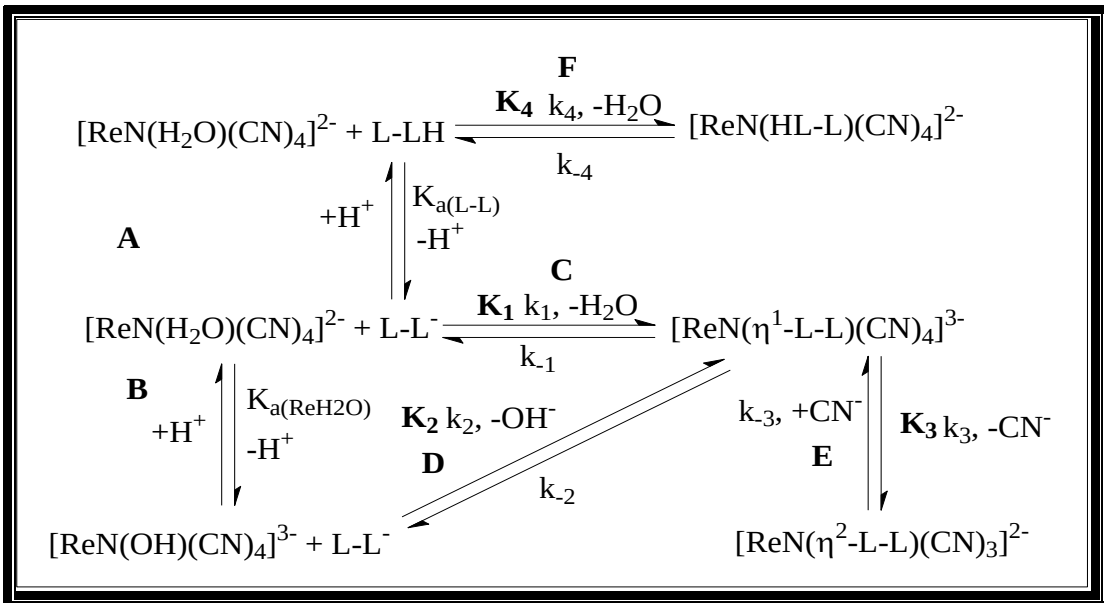

Scheme 6.1: Protonation reactions and bidentate substitution behaviour of the $[ReN(H_2O)(CN)_4]^{2-}$ complex (L-L = bidentate ligand).

In **Scheme 6.1**, the first step (reaction **C**) is regarded as the substitution of the aqua ligand by an oxygen atom of the carboxylate group (K_1 path) with the formation of $[ReN(\eta^1\text{-L-L})(CN)_4]^{3-}$ anion. The second ring-closure step (reaction **E**) is regarded as the substitution of the cyano ligand by the nitrogen atom of the pyridine moiety with the formation of the $[ReN(\eta^2\text{-L-L})(CN)_3]^{2-}$ complex. The protonation reactions of the $[ReN(H_2O)(CN)_4]^{2-}$ complex and the ligand (where the ligands change from N,OH to free anions N-O$^-$) are presented by the reactions **A** and **B,** respectively.

In all the ligands studied, a slow reaction was also followed at high pH were the hydroxo $[ReN(OH)(CN)_4]^{3-}$ species are dominated in solution (reaction **D,** K_2 path).

The low solubility of the pyridine-2-carboxylate (pic^-), quinoline-2-carboxylate ($quin^-$) and pyridine-2,3-dicarboxylate ($2,3\text{-}dipic^-$) at pH values lower than 5 ($pK_{a2(picH)}$ = 5.52, $pK_{a2(quin)}$ = 4.97 and $pK_{a2(2,3\text{-}dipic)}$ = 5.02) (Garcia *et al*., 1996:593; Martel & Smith, 1982:129; Harmon *et al*., 1998:43) restricted the concentration range in which the reactions could be performed and no reactions were observed between the rhenium(V) complex and these bidentate ligands at or below a pH of 3.5. This completely eliminates the reaction **F** (K_4 path) from the final rate law.

The rate equation from **Scheme 6.1** may have different forms depending on the rate-determining step, i.e., aqua/hydroxo substitution or CN^- substitution and ring closure. Since two reactions were observed, despite the fact that the reaction yield of the first step is very low with small absorbance change as mentioned above, the total reaction can be interpreted in terms of the two rate-determining steps (k_1 + k_2 and k_3) in **Scheme 6.1**.

Reaction rates for the first fast reactions:

The rate law corresponding to the fast reaction in the biphasic time-concentration data, taking into account that the formation of the final product ($[ReN(\eta^2\text{-L-L})(CN)_3]^{2-}$) is much slower (more so at the lower temperatures at which these reactions were followed) and does not influence the rate of the $[ReN(\eta^1\text{-L-L})(CN)_4]^{3-}$ formation, is given in **Eq. 6.1**.

$$\begin{aligned}\text{Rate} = {} & k_1[ReN(H_2O)(CN)_4^{2-}][L\text{-}L^-] + k_2[ReN(OH)(CN)_4^{3-}][L\text{-}L^-] + \\ & k_4[ReN(H_2O)(CN)_4^{2-}][L\text{-}LH] - k_{-1}[ReN(\eta^1\text{-L-L})(CN)_4^{3-}] - \\ & k_{-2}[ReN(\eta^1\text{-L-L})(CN)_4^{3-}][OH^-] - k_{-4}[ReN(\eta^1\text{-L-LH})(CN)_4^{2-}] \qquad \textbf{(6.1)}\end{aligned}$$

More accurate values for the different rate constants were determined as described according to **Eq. 6.1** which was derived from the reaction **Scheme 6.1.**

At a pH between 4 and 6 ($[H^+] >> K_{a(L\text{-}LH)}$, and k_2, $k_{-2} \approx 0$), the pseudo first-order rate constant is given by **Eq. 6.2**.

$$k_{obs} = \left(k_1 + k_4 \frac{[H^+]}{K_{a(L\text{-}LH)}} \right) \left(1 + \frac{[H^+]}{K_{a(L\text{-}LH)}} \right) [L\text{-}L]_T + \frac{\left(k_{-1} + k_{-4} \frac{[H^+]}{K_{a(L\text{-}LH)}} \right)}{\left(1 + \frac{[H^+]}{K_{a(L\text{-}LH)}} \right)} \qquad (\mathbf{6.2})$$

where $[L\text{-}L]_T$ represents the total ligand concentration.

The pseudo first-order rate constant ($[L\text{-}L]_T > [Re]_T$) for the substitution of the aqua/hydroxo ligand with the formation of $[ReN(\eta^1\text{-}L\text{-}L)(CN)_4]^{3-}$ species in the first step in **Scheme 6.1** (at higher pH between 8 and 13) is given by **Eq. 6.3**.

$$k_{obs} = \frac{k_1 + k_2 \frac{K_{a(ReH_2O)}}{[H^+]}}{1 + \frac{K_{a(ReH_2O)}}{[H^+]}} [L\text{-}L]_T + k_{-1} + k_{-2}[OH^-] \qquad (\mathbf{6.3})$$

This equation is similar to the rate equation derived for monodentate substitution reactions of the $[MN(H_2O)(CN)_4]^{n-}$ complexes (M = rhenium(V), osmium(VI) and manganese(V)) (Damoense *et al*., 1994:619; Van der Westhuizen *et al*., 1994:717; 2004:109, b).

Eq. 6.3 simplifies to **Eq. 6.4** at a pH < 9 ($pK_{a(ReH2O)}$) ~ 11.6**).**

$$k_{obs} = k_1[L\text{-}L]_T + k_{-1} \qquad (\mathbf{6.4})$$

Eq. 6.4 predicts a straight line with a slope k_1 and an intercept of k_{-1} (with $k_{-2}[OH^-]$ very small).

In all the ligands studied, an attempt was made to determine the rate of the fast reaction at high pH (*ca*. 12.4) where the hydroxo $[ReN(OH)(CN)_4]^{3-}$ complex is the main species in solution. The results obtained were dubious due to small absorbance change

(see **Figure 6.1**, small change of absorbance (**A**) at $[pic]_T$ = 1.0 M, pH *ca*. 8.0), and accurate rate constants could not be determined.

Reaction rates for the second slow reactions:

The second chelate ring-closing step (substitution of the cyano ligand) is much slower than the first aqua/hydroxo substitution step. From **Scheme 6.1** (reaction **E**) the overall rate law for the slow reaction is given by **Eq. 6.5**.

$$\text{Rate} = k_3[ReN(\eta^1\text{-L-L})(CN)_4^{3-}] - k_{-3}[ReN(\eta^2\text{-L-L})(CN)_3^{2-}][CN^-] = k_{obs}([ReN(\eta^1\text{-L-L})(CN)_4^{3-}] + [ReN(H_2O)(CN)_4^{2-}] + [ReN(OH)(CN)_4^{3-}] - k_{-3}[CN^-] \quad (\mathbf{6.5})$$

The pseudo first-order rate constant ($[L\text{-}L]_T > [Re]_T$) is given by **Eq. 6.6**.

$$k_{obs} = \frac{k_3K_1 + k_3K_2\dfrac{K_{a(ReH_2O)}}{[H^+]}}{K_1[L\text{-}L]_T + K_2[L\text{-}L]_T\dfrac{K_{a(ReH_2O)}}{[H^+]} + \dfrac{K_{a(ReH_2O)}}{[H^+]} + 1}[L\text{-}L]_T + k_{-3} \quad (\mathbf{6.6})$$

Eq. 6.6 predicts a non-linear relationship between k_{obs} and $[L\text{-}L]_T$. At pH ≈ 8 (**Figure 6.8** for $[pic]_T$), where the slow reactions were followed, clearly showed a linear relationship between these two variables indicating that the term $K_1[L\text{-}L]_T << 1$, **Eq. 6.6** simplifies to **Eq. 6.7**.

$$k_{obs} = \frac{k_3K_1 + k_3K_2\dfrac{K_{a(ReH_2O)}}{[H^+]}}{\left(K_2[L\text{-}L]_T\dfrac{K_{a(ReH_2O)}}{[H^+]}\right) + \dfrac{K_{a(ReH_2O)}}{[H^+]} + 1}[L\text{-}L]_T + k_{-3} \quad (\mathbf{6.7})$$

From **Eq. 6.7,** different rate constants (k_3K_1, K_2, k_3, k_{-3} and $pK_{a(ReH2O)}$) can be obtained. At pH values below the $pK_{a(ReH2O)}$ (pH < 11.7), **Eq. 6.7** simplifies to **Eq. 6.8**.

$$k_{obs} = k_3K_1[L - L]_T + k_{-3} \quad (\mathbf{6.8})$$

This equation predicts a straight line with slope k_3K_1 and an intercept k_{-3}. The reactions between these two species were also followed at a pH (pH between 4 and 8) where the incoming ligands changed from the protonated acid (L-LH) to the free anions ($L\text{-}L^-$). All the results obtained for these reactions can be fitted into **Eq. 6.9.**

$$k_{obs} = \frac{k_3K_1[L - L]_T}{1 + \frac{[H^+]}{K_{a(L\text{-}LH)}}} + k_{-3} \quad (\mathbf{6.9})$$

where $[L\text{-}L]_T = [L\text{-}L^-] + [L\text{-}LH]$. From this equation, the values of k_3, k_{-3}, K_1, and $pK_{a(L\text{-}LH)}$ can be obtained.

Effect of temperature on the rate:

The temperature dependencies for both fast and slow reactions were used to calculate the activation parameters of the bidentate substitution reactions of the $[ReN(H_2O)(CN)_4]^{2-}$ complex using the Eyring Equation (**Eq. 6.10**).

$$\ln\frac{k}{T} = \ln\frac{k_B}{h} + \frac{\Delta S^{\neq}}{R} - \frac{\Delta H^{\neq}}{RT} \quad (\mathbf{6.10})$$

In **Eq. 6.10**, k_B is the Boltzmann constant, h is the Planck constant, R is the gas constant, $\Delta S^{\neq}$ and $\Delta H^{\neq}$ are the entropy and enthalpy of activation respectively.

In all the following figures, the solid line represents a computer least-square fit of the data to selected equation, while the experimentally determined values are represented by the dots. More complete derivations for **Eqs. 6.3** and **6.10** as well as some general kinetic considerations are given in supplementary material **B5** and **B4** (**Appendix B**).

6.3.2 Kinetic Results of the Reaction between $[ReN(H_2O)(CN)_4]^{2-}$ Complex and Pyridine-2-carboxylate ion (pic) (Mtshali *et al*., 2006: in press)

6.3.2.1 Identification of the Product

Pyridine-2-carboxylic acid has been observed to react with $[ReN(H_2O)(CN)_4]^{2-}$ complex in aqueous solution at an appropriate pH value of *ca* 8.0, yielding the substitution of aqua and cyanide ligands in $[ReN(H_2O)(CN)_4]^{2-}$ with the formation of $[ReN(\eta^2\text{-pic})(CN)_3]^{2-}$ anion (see **Chapter 5**, crystal structure).

The UV/VIS spectra taken at 80ºC for the reaction between $[ReN(H_2O)(CN)_4]^{2-}$ complex and pyridine-2-carboxylate (pic^-) showed the formation of two distinctive peaks, one at 355 nm and the other at 400 nm (**Figure 6.1**).

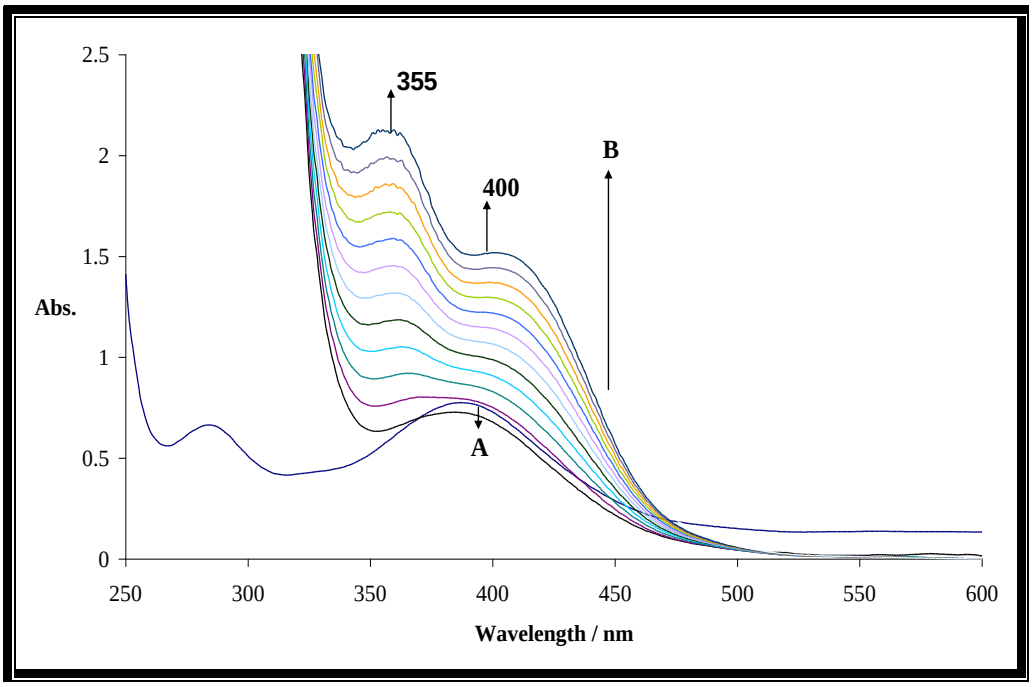

Figure 6.1: UV/VIS spectral changes during the reaction between $[ReN(H_2O)(CN)_4]^{2-}$ and pyridine-2-carboxylate (pic^-), T = 80.3°C, pH = 8.04, $[[ReN(H_2O)(CN)_4]^{2-}]$ = 1.0×10^{-3}M, $[pic]_T$ = 1.0M: A = absorbance decrease for the initial fast reaction, B = subsequent absorbance increase for the slow reaction. Time intervals 1.0 min.

The formation of these peaks corresponds to the formation of the final complex, $[ReN(\eta^2\text{-pic})(CN)_3]^{2-}$. On close inspection of the absorbance *vs*. time spectrum, two different reactions were observed during the reaction between these two species. The first reaction was relatively fast and resulted in a decrease in absorbance at 400 nm (**A** in **Figure 6.1**) with a half-life of few seconds. The second reaction was much slower (**B** in **Figure 6.1**) with half-life of 5 to 15 minutes.

6.3.2.2 Stability and Acid Dissociation Constants

The effect of absorbance changes due to picolinate concentration is shown in **Figure 6.2**. The concentration of the incoming ligand $[pic]_T$ was varied from 0.1 to 1.0M at constant complex concentration ($[[ReN(H_2O)(CN)_4]^{2-}]$ complex = 1.0×10^{-3}M).

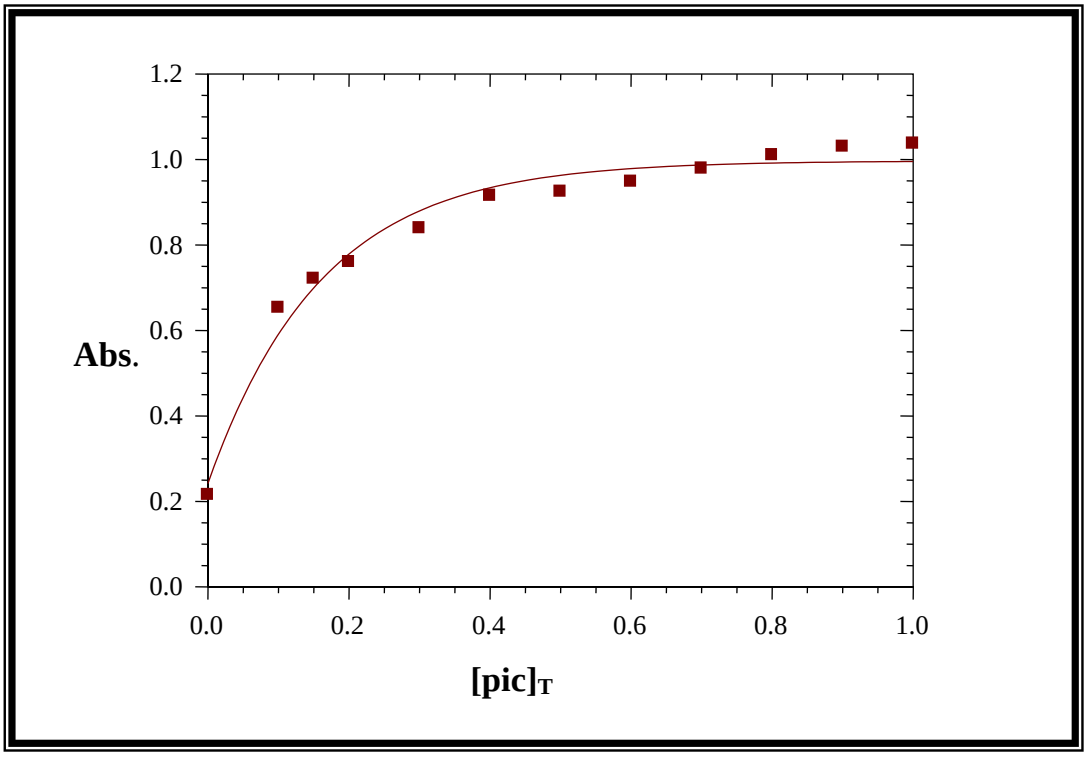

Figure 6.2: Plot of Abs. *vs*. $[pic]_T$ at T = 79.8°C, pH 8.06, $[[ReN(H_2O)(CN)_4]^{2-}]$ = 1.0×10^{-3}M, λ = 400 nm, μ = 1.0M $NaClO_4$.

The stability constant for the overall reaction between $[ReN(H_2O)(CN)_4]^{2-}$ complex and pyridine-2-carboxylate was determined spectrophotometrically at 400 nm by a least-

square fit of the absorbance *vs.* the concentration of the entering ligand (**Figure 6.2)** to **Eq. 6.11**. The K' value obtained is given in **Table 6.3**.

$$A_{obs} = \frac{A_{ReH_2O} + A_{Repic}K'[pic]_T}{1 + K'[pic]_T} \quad (\mathbf{6.11})$$

This equation is derived from Beer's law, mass balance as well as the definition of K' for the overall reaction. In **Eq. 6.11**, A_{ReH2O} = absorbance of $[ReN(H_2O)(CN)_4]^{2-}$, A_{Repic} = absorbance of $[ReN(\eta^2\text{-pic})(CN)_3]^{2-}$, $[pic]_T$ = analytical concentration of pyridine-2-carboxylic acid, A_{obs} = observed absorbance and K' = stability constant of the reaction.

Figure 6.3 illustrates the effect of pH on the absorbance of a reaction mixture. From the reaction **Scheme 6.1** (reaction **B**), the acid/base behaviour for the reaction between $[ReN(H_2O)(CN)_4]^{2-}$ and $[pic]_T$ proceed as depicted in **Eq. 6.12**, and it is important that these values be determined as the $pK_{a(ReH2O)}$.

$$[ReN(H_2O)(CN)_4]^{2-} \underset{+H^+}{\overset{K_a, -H^+}{\rightleftharpoons}} [ReN(OH)(CN)_4]^{3-} \quad (\mathbf{6.12})$$

From the definition of K_a, mass balance and Beer's law, **Eq. 6.13** can be derived for the determination of one pK_a value (see **Appendix B** for derivation).

$$A_{obs} = \frac{A_{ReH_2O}K_{a(ReH_2O)} + A_{ROH}[H^+]}{K_{a(ReH_2O)} + [H^+]} \quad (\mathbf{6.13})$$

In **Eq. 6.13,** A_{ReH2O} = absorbance for $[ReN(H_2O)(CN)_4]^{2-}$ and A_{ReOH} = absorbance for $[ReN(OH)(CN)_4]^{3-}$ and $pK_{a(ReH2O)}$ = acid dissociation constant of $[ReN(H_2O)(CN)_4]^{2-}$.

The acid dissociation constant for the $[ReN(\eta^2\text{-pic})(CN)_4]^{2-}$ complex, $pK_{a(ReH2O)}$, was calculated from the experimental data in **Figure 6.3**, which was fitted to **Eq. 6.13** and reported in **Table 6.3**.

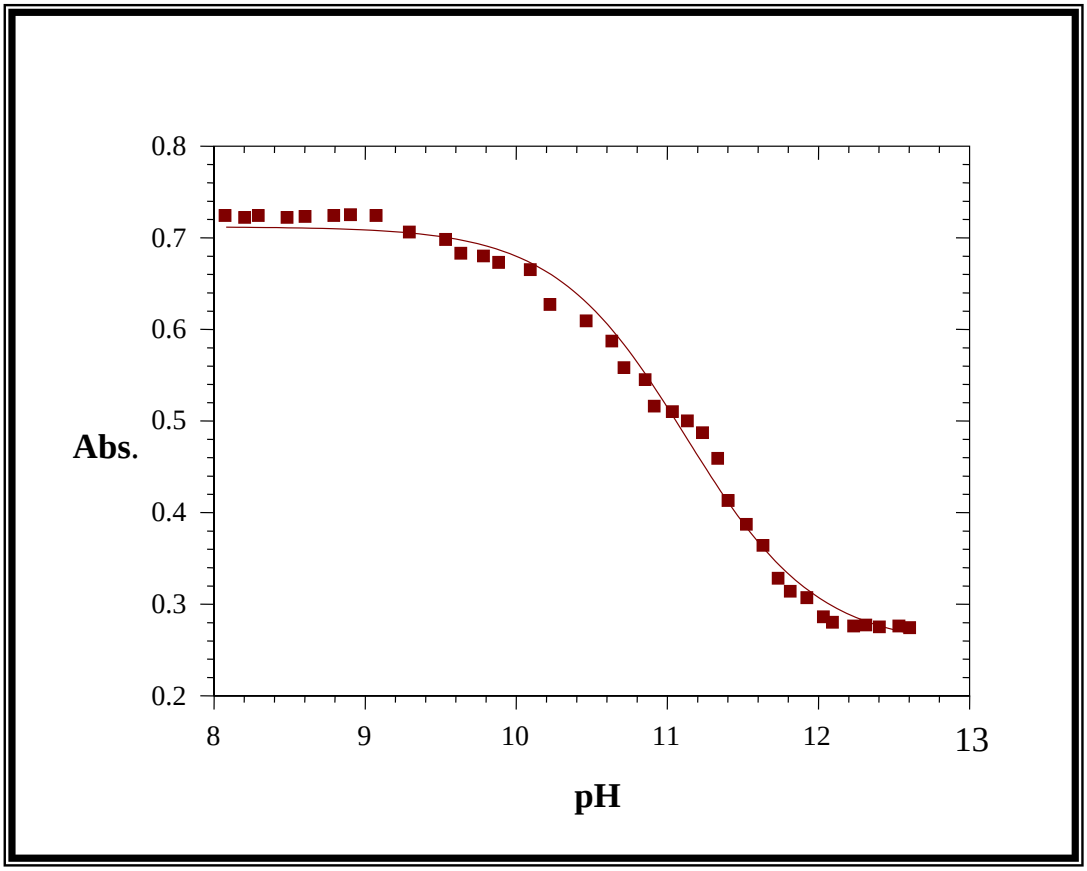

Figure 6.3: Plot of Abs. *vs*. pH at T = 80.2°C, $[pic]_T$ = 0.1M, $[[ReN(H_2O)(CN)_4]^{2-}]$ = 1.0×10^{-3}M, λ = 400 nm, μ = 1.0M $NaClO_4$.

6.3.2.3 Fast Reaction

Figure 6.4 shows the temperature and $[pic]_T$ dependence of the pseudo first-order rate constant (k_{obs}) for the first fast reactions between $[ReN(H_2O)(CN)_4]^{2-}$ and $[pic^-]$ anions at 400 nm. The experimental k_{obs} *vs*. $[pic]_T$ data obtained at three different temperatures were used to calculate the values for k_1 and k_{-1} using least-square fit to **Eq. 6.4** and are reported in **Table 6.2**.

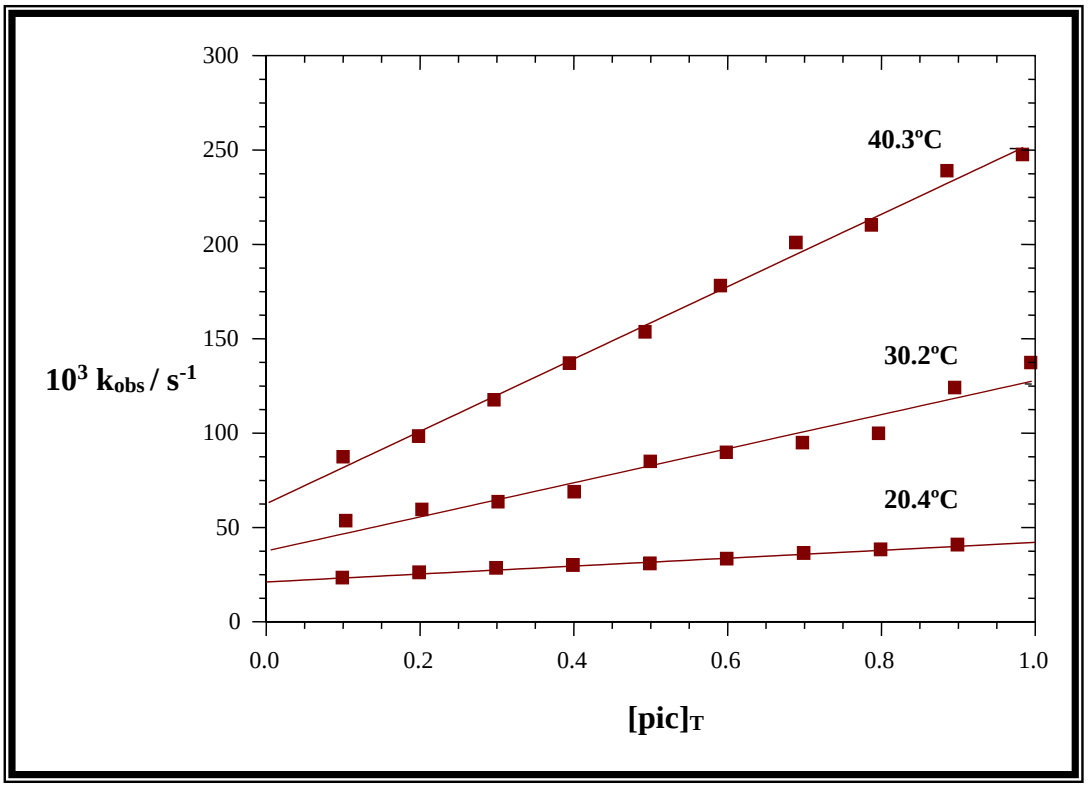

Figure 6.4: **Plot of k_{obs} *vs*. $[pic]_T$ at different temperatures, pH = 8.05, $[[ReN(H_2O)(CN)_4]^{2-}] = 1.0\times10^{-2}$M, λ = 400 nm, μ = 1.0M $NaClO_4$.**

The pH dependence of the pseudo first-order rate constant for the fast reactions is illustrated in **Figure 6.5.** The values of the different rate constants and the acid dissociation constant (k_2, k_{-2} and $pK_{a(ReH2O)}$) were obtained from the least-square fit of the data in **Figure 6.5** to **Eq. 6.3**, using k_1 and k_{-1} values from the temperature variations. These values are reported in **Table 6.2**.

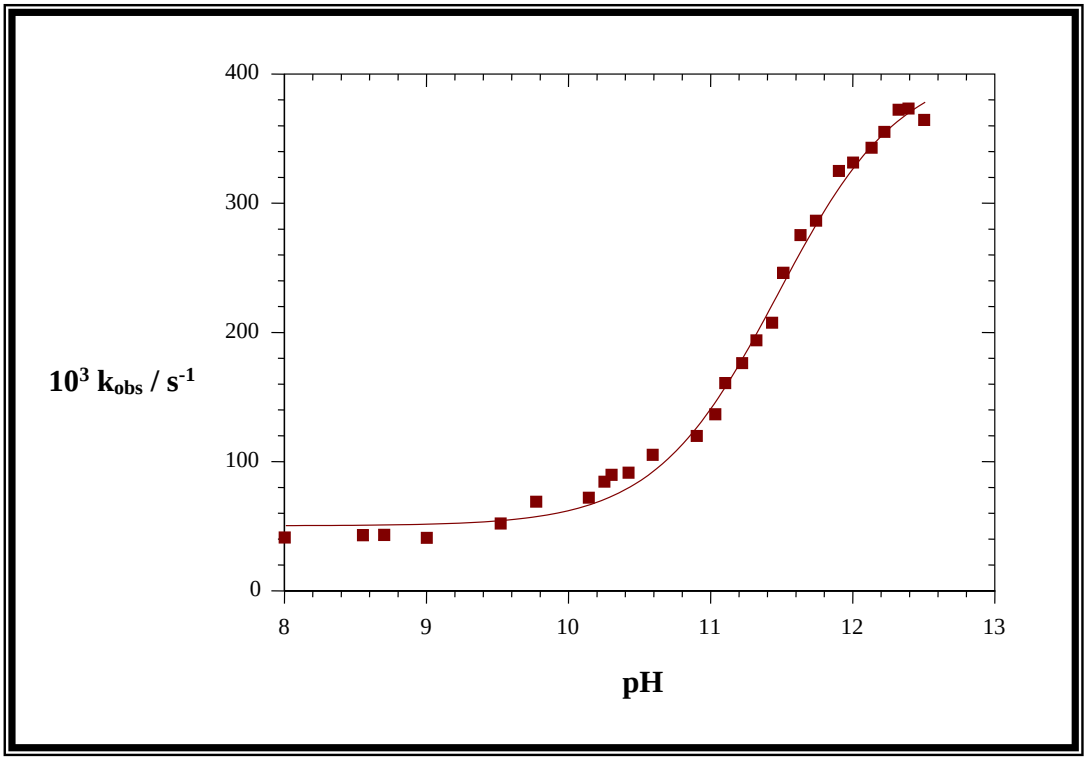

Figure 6.5: **Plot of k_{obs} *vs*. pH at T = 40.3°C, $[[ReN(H_2O)(CN)_4]^{2-}] = 1.0\times10^{-2}$M, $[pic]_T$ = 0.1M, λ = 400 nm, μ = 1.0M $NaClO_4$.**

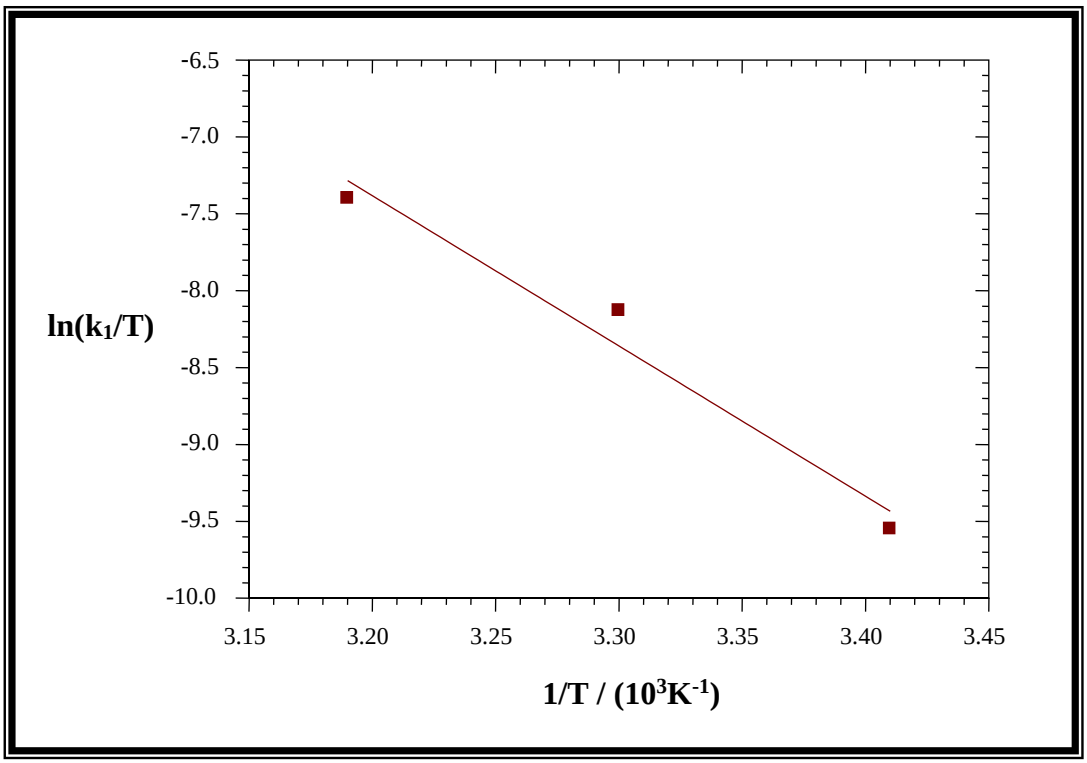

Figure 6.6: **Plot of ln(k_1/T) *vs*. 1/T for the fast reaction between $[ReN(H_2O)(CN)_4]^{2-}$ and picolinate anions.**

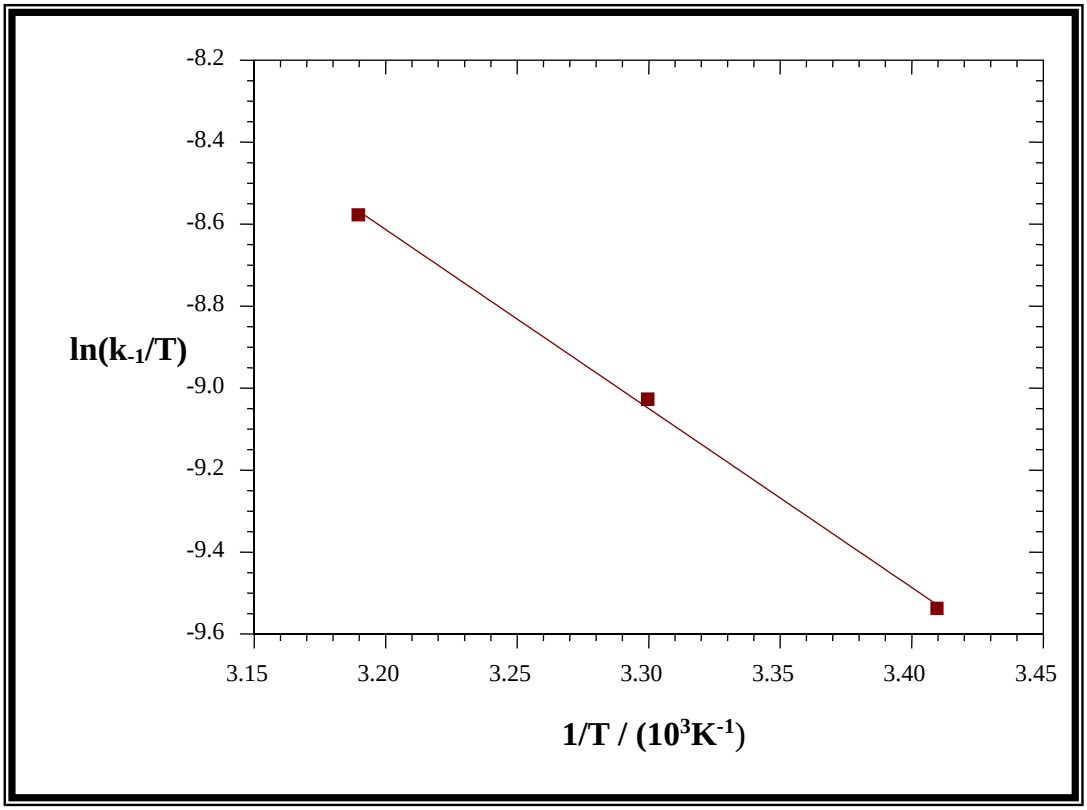

Figure 6.7: Plot of $\ln(k_{-1}/T)$ *vs.* 1/T for the fast reaction between $[ReN(H_2O)(CN)_4]^{2-}$ and picolinate anions.

The activation parameters ($\Delta H^{\neq}$ and $\Delta S^{\neq}$) for fast reaction between $[ReN(H_2O)(CN)_4]^{2-}$ complex and $[pic]_T$ were determined by least-square fit of the temperature dependency of the pseudo first-order rate constants (k_1 and k_{-1}) to the Eyring **Eq. 6.10**, and are reported in **Table 6.2**.

Table 6.2: Kinetic data for the fast reaction between $[ReN(H_2O)(CN)_4]^{2-}$ and $[pic]_T$, λ = 400 nm, μ = 1.0M $NaClO_4$.

Temperature °C	Constant	Value
40.3	$k_1(M^{-1}s^{-1})$[a]	$1.92(5) \times 10^{-1}$
	$k_1(M^{-1}s^{-1})$[b]	$5.3(3) \times 10^{-1}$
	$k_{-1}(s^{-1})$[a]	$5.9(3) \times 10^{-2}$
	$k_{-1}(s^{-1})$[b]	$5.9(3) \times 10^{-2}$
	$K_1(M^{-1})$[c]	3.3(1)
	$k_2(M^{-1}s^{-1})$[b]	4.1(2)
	$k_{-2}(s^{-1})$[b]	$1.0(1) \times 10^{-3}$
30.2	$k_1(M^{-1}s^{-1})$[a]	$8.98(7) \times 10^{-2}$
	$k_{-1}(s^{-1})$[a]	$3.65(5) \times 10^{-2}$
	$K_1(M^{-1})$[c]	2.46(1)
20.4	$k_1(M^{-1}s^{-1})$[a]	$2.1(1) \times 10^{-2}$
	$k_{-1}(s^{-1})$[a]	$2.11(5) \times 10^{-2}$
	$K_1(M^{-1})$[c]	1.0(2)
	$pK_{a(ReH2O)}$[b]	11.43(2)
	$\Delta H^{\neq}$ (k_1)[d] $kJmol^{-1}$	82.5(2)
	$\Delta S^{\neq}$ (k_1)[d] $JK^{-1}mol^{-1}$	5.01(6)
	$\Delta H^{\neq}$ (k_{-1})[d] $kJmol^{-1}$	36.8(1)
	$\Delta S^{\neq}$ (k_{-1})[d] $JK^{-1}mol^{-1}$	-151.4(1)

[a] Slope and intercept, Fig. 6.4, Eq. 6.4.

[b] Data in Fig. 6.5, Eq. 6.3.

[c] $K_1 = k_1/k_{-1}$.

[d] Temperature dependence, Figures 6.6 and 6.7, Eq. 6.10.

6.3.2.4 Slow Reaction

The slow reaction that was observed in this study at 400 nm is thus regarded as the substitution of the cyano ligand with chelate ring-closure of the bidentate ligand to form $[ReN(\eta^2\text{-pic})(CN)_3]^{2-}$ (see **Scheme 6.1**, reaction **E**).

The temperature and $[pic]_T$ dependence of the pseudo first-order rate constants for the second slow reaction between the $[ReN(H_2O)(CN)_4]^{2-}$ complex with pyridine-2-carboxylate anion are shown in **Figure 6.8**. As indicated above (**Paragraph 6.3.1**), **Eq. 6.8** predicts a straight line with a slope k_3K_1 and an intercept k_{-3}. The experimental results in **Figure 6.8** were fitted to **Eq. 6.8** to yield the slopes and intercepts. The values of k_3K_1 and k_{-3} obtained at different temperatures are reported in **Table 6.3**. The term k_{-3} represents the contribution of the reverse reaction or the coordination of the cyanide anion.

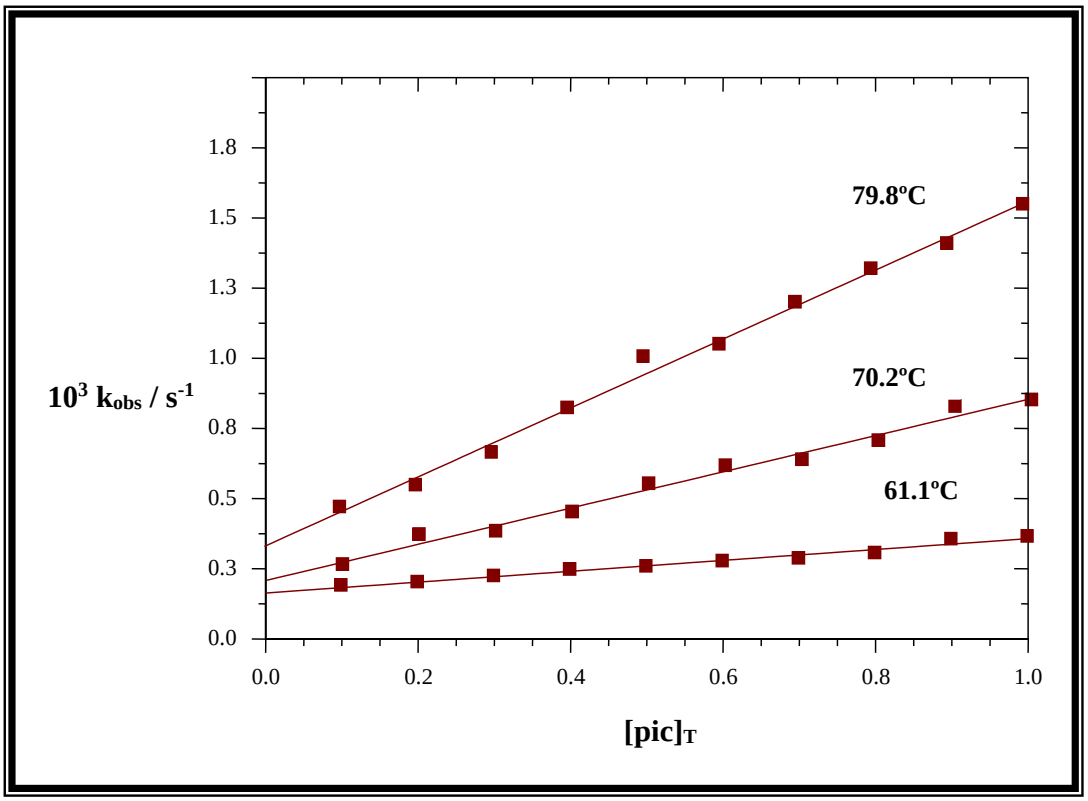

Figure 6.8: Plot of k_{obs} *vs.* $[pic]_T$ at different temperatures, pH = 8.06, $[[ReN(H_2O)(CN)_4]^{2-}] = 1.0\times10^{-3}$M, λ = 400 nm, μ = 1.0M $NaClO_4$.

The pH dependence of the pseudo first-order rate constant for the second reaction is illustrated in **Figure 6.9**. The values of the different rate constants and acid dissociation constant (k_3, k_{-3}, K_1, K_2 and $pK_{a(ReH2O)}$) were obtained from the least-square fit of the k_{obs} *vs*. pH data in **Figure 6.9** to **Eq. 6.7**, using k_3K_1 value and are reported in **Table 6.3**.

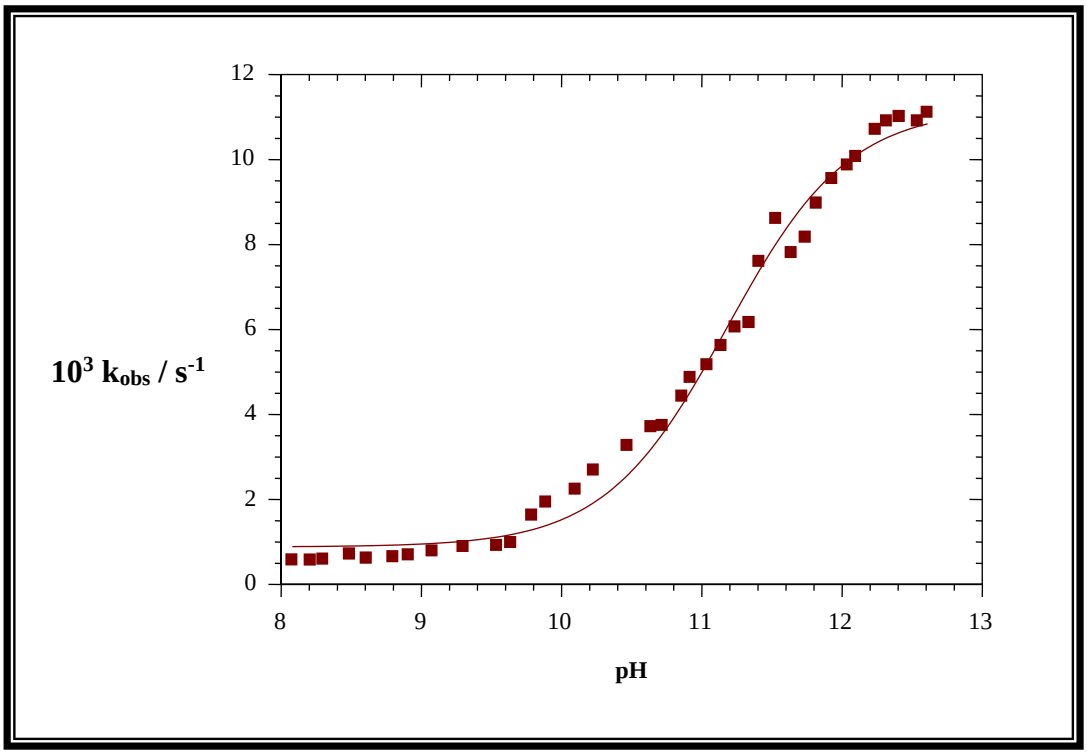

Figure 6.9: Plot of k_{obs} *vs*. pH at T = 80.2°C, $[ReN(H_2O)(CN)_4]^{2-}$ = 1.0×10^{-3}M, $[pic]_T$ = 0.1M, λ = 400 nm, μ = 1.0M $NaClO_4$.

Figure 6.10 illustrates the temperature and $[pic]_T$ dependence of the pseudo first-order rate constant (k_{obs}) for the slow reactions at high pH (pH *ca.* 12.6). The non-linear experimental data reported in **Figure 6.10** were fitted to **Eq. 6.7** and the final rate and equilibrium constant (k_3 and K_2) calculated, are reported in **Table 6.3.** The reaction between $[ReN(H_2O)(CN)_4]^{2-}$ complex and $[pic]_T$ was also followed at a pH (pH between 4 and 8) where the incoming ligand changed from the protonated picolinic acid (picH) to the free picolinate anion (pic^-).

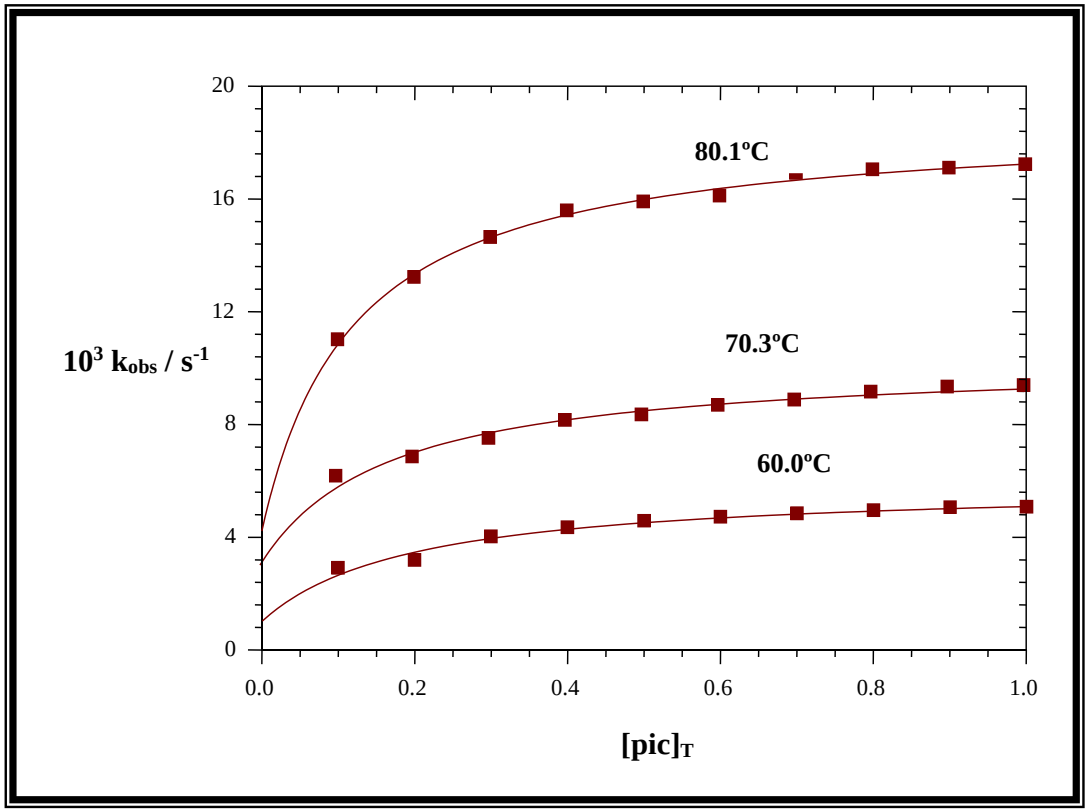

Figure 6.10: Plot of k_{obs} *vs*. $[pic]_T$ at different temperatures, pH = 12.6, $[[ReN(H_2O)(CN)_4]^{2-}] = 1.0\times10^{-3}$M, λ = 400 nm, μ = 1.0M $NaClO_4$.

Figure 6.11 illustrates the pH dependence of the pseudo first-order rate constant. The values for the different rate constants and acid dissociation constant (k_3, k_{-3} and $pK_{a(picH)}$) were obtained from a least-square fit of the data in **Figure 6.11** to **Eq. 6.9** and are reported in **Table 6.3**.

The reactivity of the final product, $[ReN(\eta^2\text{-pic})(CN)_3]^{2-}$, towards CN^- ions was confirmed with the addition of free CN^- to a solution containing the final product (**Figure 6.12**). These results not only point to the reverse reaction, k_{-3}, but also to additional cyanide substitution of probably the complete picolinate anion from the coordination sphere (Damoense *et al*., 1994:619).

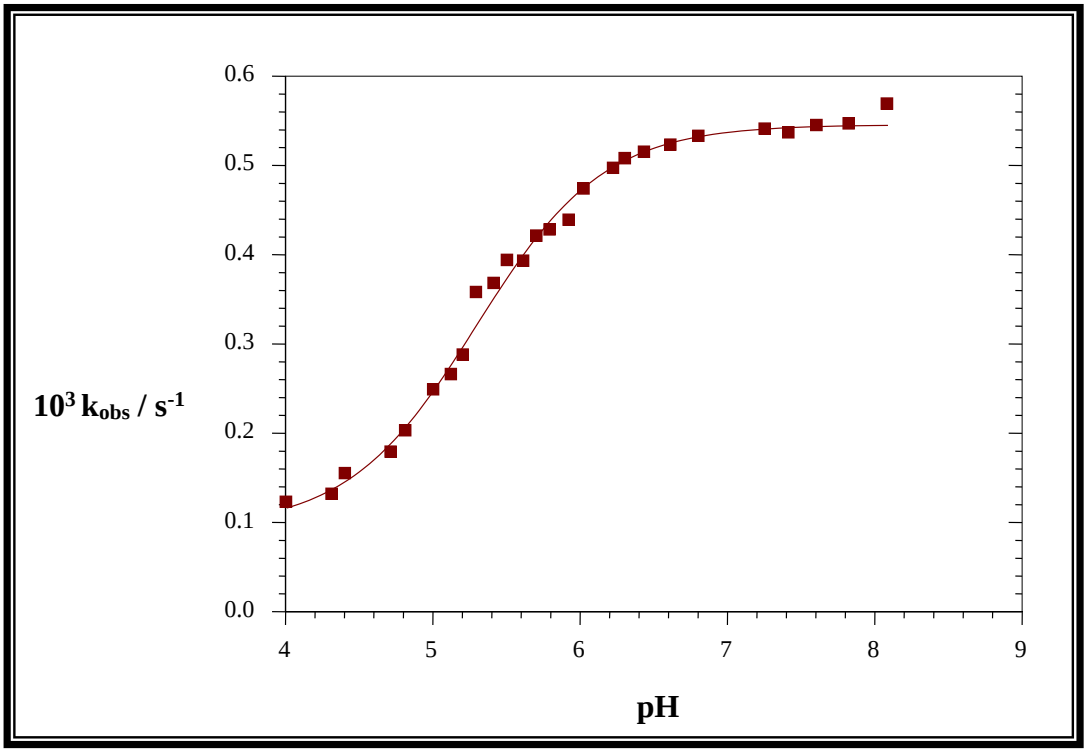

Figure 6.11: **Plot of k_{obs} *vs.* pH at T = 80.3°C, $[[ReN(H_2O)(CN)_4]^{2-}]$ = 1.0×10^{-3}M, $[pic]_T$ = 0.1M, λ = 400 nm, μ = 1.0M $NaClO_4$.**

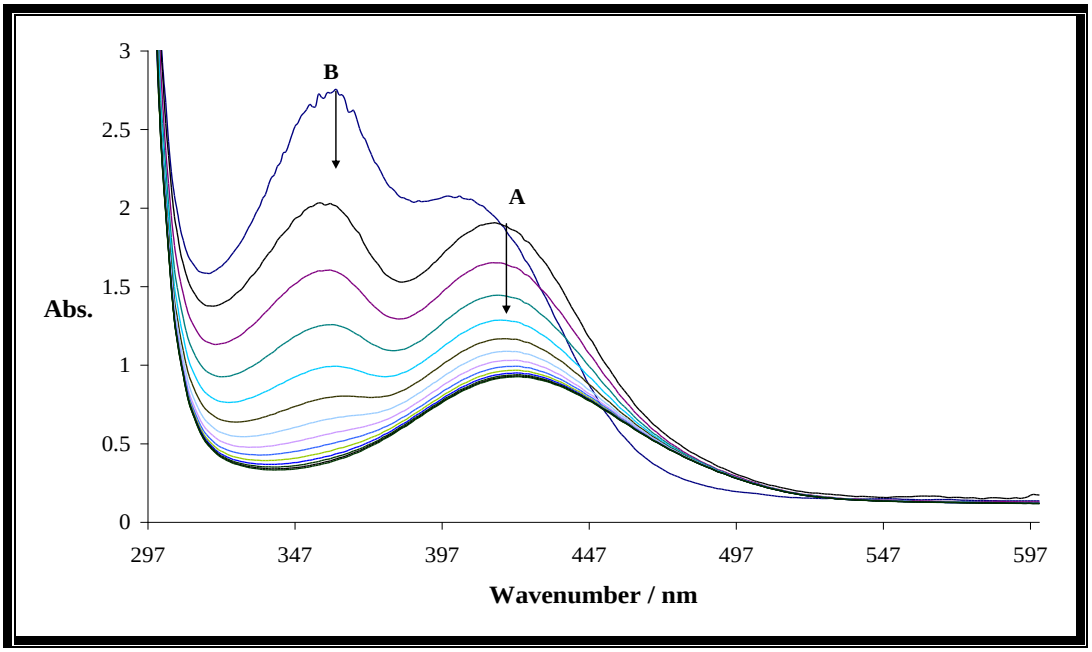

Figure 6.12: **UV/VIS spectrum changes during the reaction between $[[ReN(pic)(CN)_3]^{2-}]$ = 1.0×10^{-3}M, with $[CN^-]_T$ = 1.0M, T = 70.3°C, pH ≈ 8.01, $[CN^-]$ = 1.0M, time intervals of every 6 seconds.**

The activation parameters ($\Delta H^{\neq}$ and $\Delta S^{\neq}$ for k_3) of the overall reaction between $[ReN(H_2O)(CN)_4]^{2-}$ complex and $[pic]_T$ were determined by a least-square fit of the temperature dependency data of the pseudo first-order rate constant (k_3, see **Figure 6.13**) to the Eyring equation (**Eq. 6.10**) and are reported in **Table 6.3**.

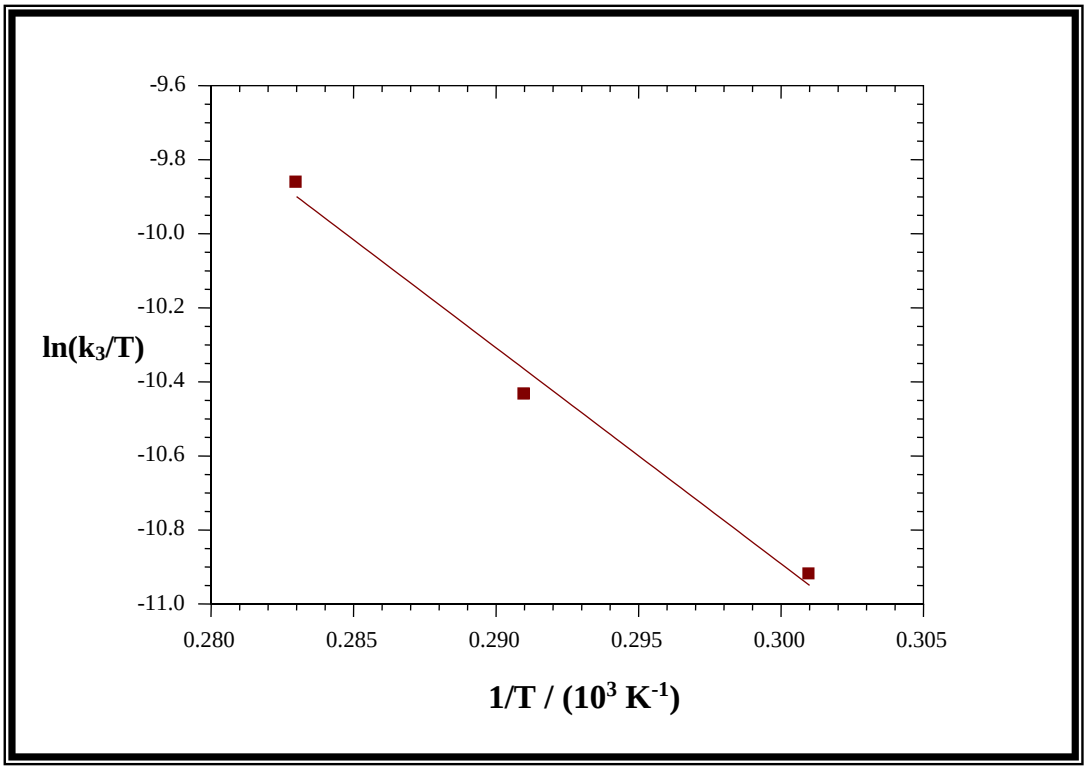

Figure 6.13: Plot of $\ln(k_3/T)$ *vs.* 1/T for the slow reaction between $[ReN(H_2O)(CN)_4]^{2-}$ and picolinate anions.

Table 6.3: Kinetic data for the slow reaction between $[ReN(H_2O)(CN)_4]^{2-}$ and $[pic]_T$, λ = 400 nm, μ = 1.0M $NaClO_4$.

Temperature °C	Constant	Value
80.0	k_3K_1 $(M^{-1}s^{-1})^e$	$1.23(3)\times10^{-3}$
	$k_3(s^{-1})^g$	$1.84(2)\times10^{-2}$
	$k_3(s^{-1})^f$	$1.85(2)\times10^{-2}$
	$k_3(s^{-1})^h$	$6.8(1)\times10^{-2}$
	k_{-3} $(M^{-1}s^{-1})^e$	$4.2(2)\times10^{-4}$
	k_{-3} $(M^{-1}s^{-1})^f$	$7.72(1)\times10^{-4}$
	$k_{-3}(M^{-1}s^{-1})^h$	$9.3(1)\times10^{-5}$
	K_1 $(M^{-1})^f$	$6.61(1)\times10^{-2}$
	$K_1(M^{-1})^h$	$6.60(1)\times10^{-2}$
	$K_1(M^{-1})^j$	$6.62(1)\times10^{-2}$
	$K_2(M^{-1})^g$	14.8(1)
	K_2 $(M^{-1})^f$	13.99(3)
	K_3 $(M^{-1})^i$	731.2(1)
	K' [l]	8.01(1)
	$pK_{a(Re\text{-}H2O)}{}^f$	11.54(6)
	$pK_{a(picH)}{}^h$	5.29(2)
	$pK_{a(pic)}{}^m$	5.52
	$pK_{a(ReH2O)}{}^k$	11.09(3)
70.0	$k_3K_1(M^{-1}s^{-1})^e$	$6.3(3)\times10^{-4}$
	$k_3(s^{-1})^g$	$1.01(2)\times10^{-2}$
	$k_{-3}(M^{-1}s^{-1})^e$	$2.8(1)\times10^{-4}$
	$K_1(M^{-1})^j$	$6.2(1)\times10^{-2}$
	K_2 $(M^{-1})^g$	14.1(2)
60.0	k_3K_1 $(M^{-1}s^{-1})^e$	$1.96(6)\times10^{-4}$
	$k_3(M^{-1}s^{-1})^g$	$6.04(1)\times10^{-3}$
	k_{-3} $(M^{-1})^e$	$1.7(4)\times10^{-4}$
	$K_1(M^{-1})^j$	$3.2(5)\times10^{-2}$
	K_2 $(M^{-1})^g$	9.5(1)
	$\Delta S^{\neq}$ $(k_3)^d$ $JK^{-1}mol^{-1}$	-133.4(3)
	$\Delta H^{\neq}$ $(k_3)^d$ $kJmol^{-1}$	51.7(5)

[d] Temperature dependence in Fig. 6.13, Eq. 6.10; [e] From slope and intercept, Fig. 6.8, Eq. 6.8; [f] Data in Fig. 6.9, Eq. 6.7; [g] Data in Fig. 6.10, Eq. 6.7; [h] Data in Fig. 6.11, Eq. 6.9; [i] $K_3 = k_3/k_{-3}$; [j] $K_1 = k_3K_1/k_3$; [K] Data in Fig. 6.3, Eq. 6.13; [l] Data in Fig. 6.2, Eq. 6.11; [m] Garcia *et al*., (1996:593).

6.3.3 Kinetic Results of the Reaction between $[ReN(H_2O)(CN)_3]^{2-}$ Complex with Quinoline-2-carboxylic acid (quin)

6.3.3.1 Identification of the Product

The reaction between quinoline-2-carboxylic acid and the $[ReN(H_2O)(CN)_4]^{2-}$ complex in aqueous solution was initially investigated at pH values between 8.0 and 12.4. The UV/VIS spectrum (absorbance *vs.* wavelength) of the reaction between the two species taken at 80.1°C show only one absorption maximum at 450 nm (**Figure 6.14**).

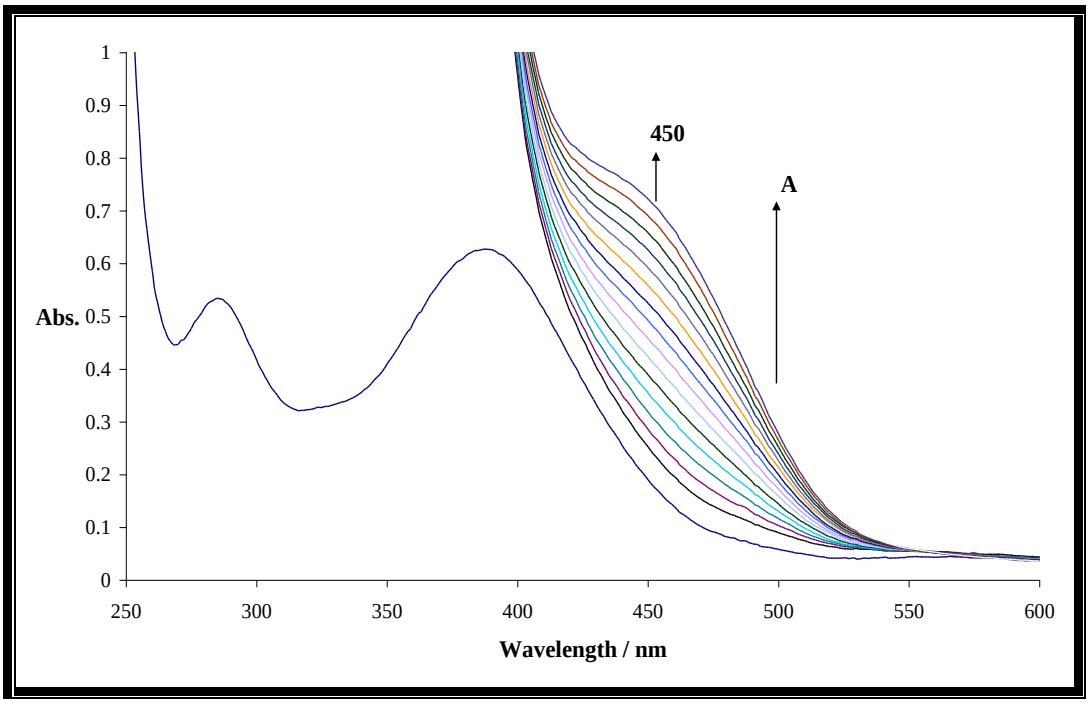

Figure 6.14: UV/VIS spectral changes during the reaction between $[ReN(H_2O)(CN)_4]^{2-}$ and quinoline-2-carboxylate (quin), at T = 80.1°C, pH = 8.10, $[[ReN(H_2O)(CN)_4]^{2-}] = 1.0\times10^{-3}$M, $[quin]_T$ = 1.0M: A = Absorbance increase due to the slow reaction. Time intervals 1.0 min.

This absorption maximum corresponds to the formation of the final complex, $[ReN(\eta^2\text{-quin})(CN)_3]^{2-}$. The crystal structure determination of $(AsPh_4)_2[ReN(\eta^2\text{-quin})(CN)_3]\cdot 2H_2O$ showed that the quinolinate anion coordinates *via* the carboxylate oxygen and quinoline nitrogen atom to the rhenium(V) with the substitution of both aqua and one cyano ligand

(see **Chapter 5**). The absorbance *vs*. time spectrum showed two different reactions. A relatively fast reaction with a half-life of few seconds followed by the second much slower reaction with the half-life of 10 to 25 minutes.

6.3.3.2 Stability and Acid Dissociation Constants

The stability constant or equilibrium constant (K') for the overall reaction between the $[ReN(H_2O)(CN)_4]^{2-}$ complex and quinoline-2-carboxylate anions was determined spectrophotometrically at 450 nm. The absorbance change due to the addition of the quinolinate concentration is shown in **Figure 6.15**. The stability constant of $[ReN(\eta^2\text{-quin})(CN)_3]^{2-}$ was obtained by a least-square fit of the absorbance *vs*. $[quin]_T$ data shown in **Figure 6.15** to **Eq. 6.11** and reported in **Table 6.5**.

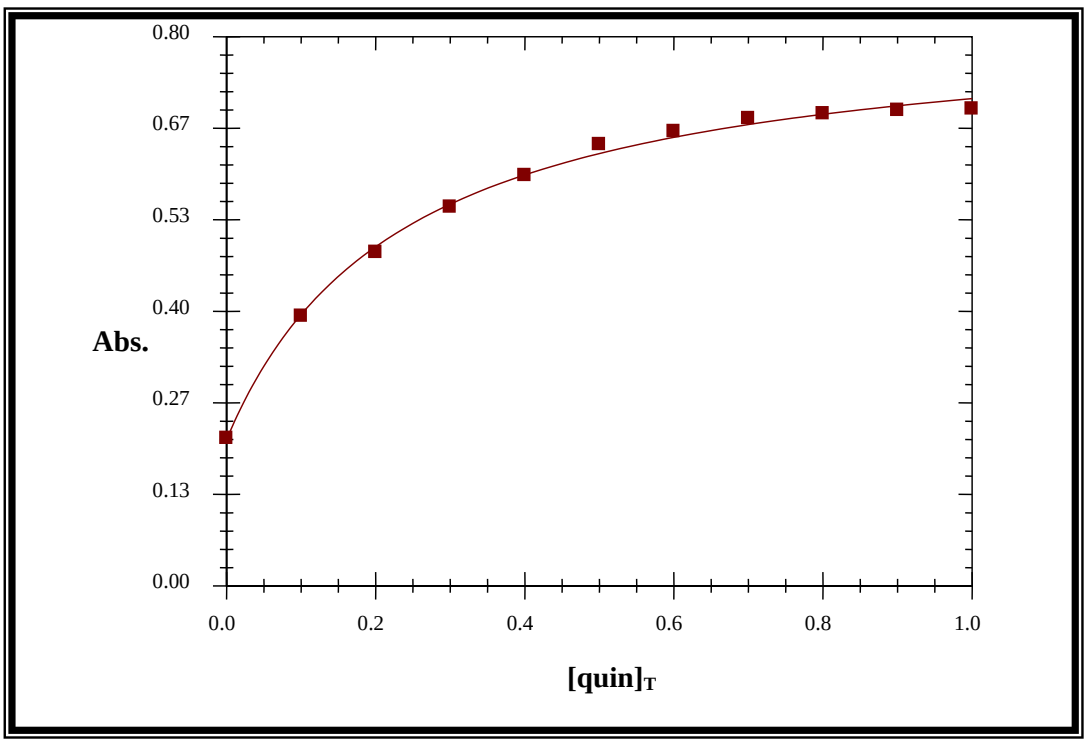

Figure 6.15: Plot of Abs. *vs*. $[quin]_T$ at T = 80.2°C, pH 8.11, $[[ReN(H_2O)(CN)_4]^{2-}] = 1.0\times10^{-3}$M, λ = 450 nm, μ = 1.0M $NaClO_4$.

The acid/base behaviour for the reaction between $[ReN(H_2O)(CN)_4]^{2-}$ and $[quin]_T$ proceed as depicted in **Eq. 6.12** (see reaction **B**, **Scheme 6.1**).

The effect of pH on the absorbance of the reaction mixture is illustrated by the results in **Figure 6.16**. The acid dissociation constant, $pK_{a(ReH2O)}$, was calculated by a least-square fit of the absorbance *vs*. pH to **Eq. 6.13** and this value is reported in **Table 6.5**.

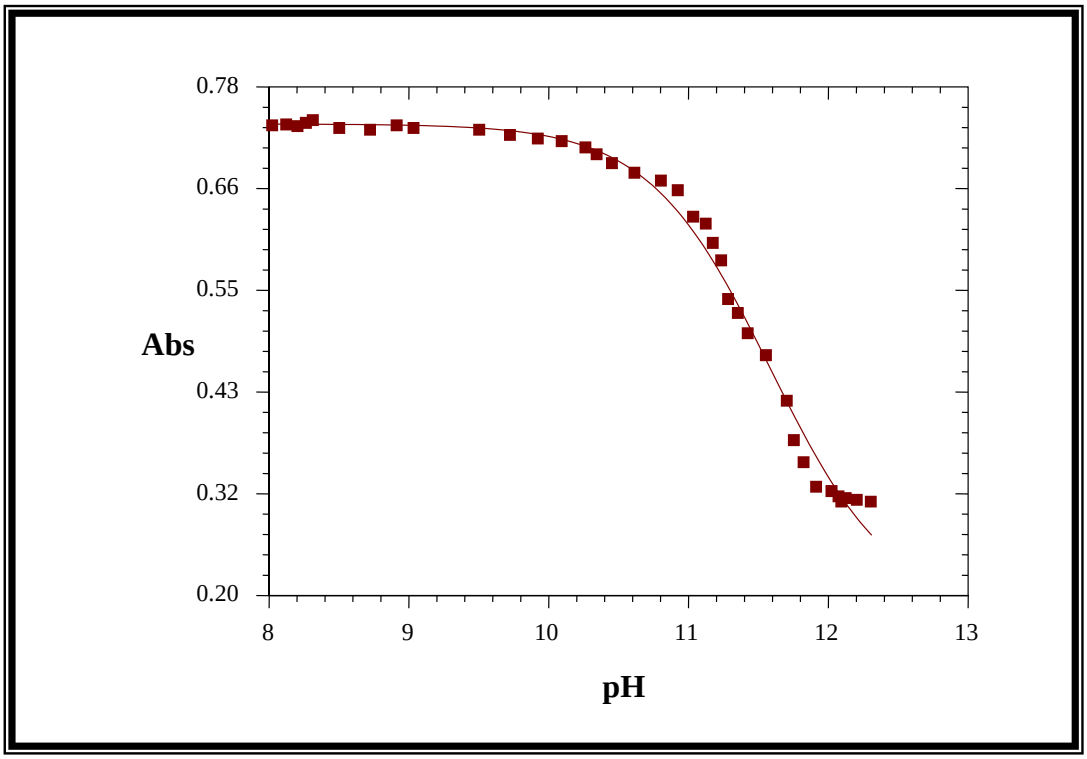

Figure 6.16: Plot of Abs. *vs*. pH at T = 80.4°C, $[quin]_T$ = 0.1M, $[[ReN(H_2O)(CN)_4]^{2-}]$ = 1.0×10^{-3}M, λ = 450 nm, μ = 1.0M $NaClO_4$.

6.3.3.3 Fast Reaction

As indicated above (**Paragraph 6.3.2.1**), two reactions were observed at 450 nm. The rate of the fast reactions could not be determined at 450 nm, due to a small absorbance change. The UV/VIS spectra of the reaction between these two species was again drawn at low temperatures (*ca*. 40ºC), and showed a change in absorbance at 400 nm. It was, therefore, decided to follow the rate of the fast reactions at this wavelength (400 nm), and the kinetic results obtained are reported in **Table 6.4**. The same reaction **Scheme 6.1** is predicted for the reactions between $[ReN(H_2O)(CN)_4]^{2-}$ and quinolinate ligand (quin). The first fast reaction that was observed in this study is also regarded as the aqua ligand substitution with the formation of $[ReN(\eta^1\text{-quin})(CN)_4]^{3-}$.

The quinolinate anion concentration, $[quin]_T$, and temperature dependencies of the pseudo first-order rate constant (k_{obs}) for the first fast reactions between $[ReN(H_2O)(CN)_4]^{2-}$ and $[quin]_T$ anion is presented in **Figure 6.17**. The values of k_1 and k_{-1} at three different temperatures were calculated from the k_{obs} *vs.* $[quin]_T$ data in **Figure 6.17** fitted to **Eq. 6.4** by using a least-square fit program**,** and are reported in **Table 6.4**.

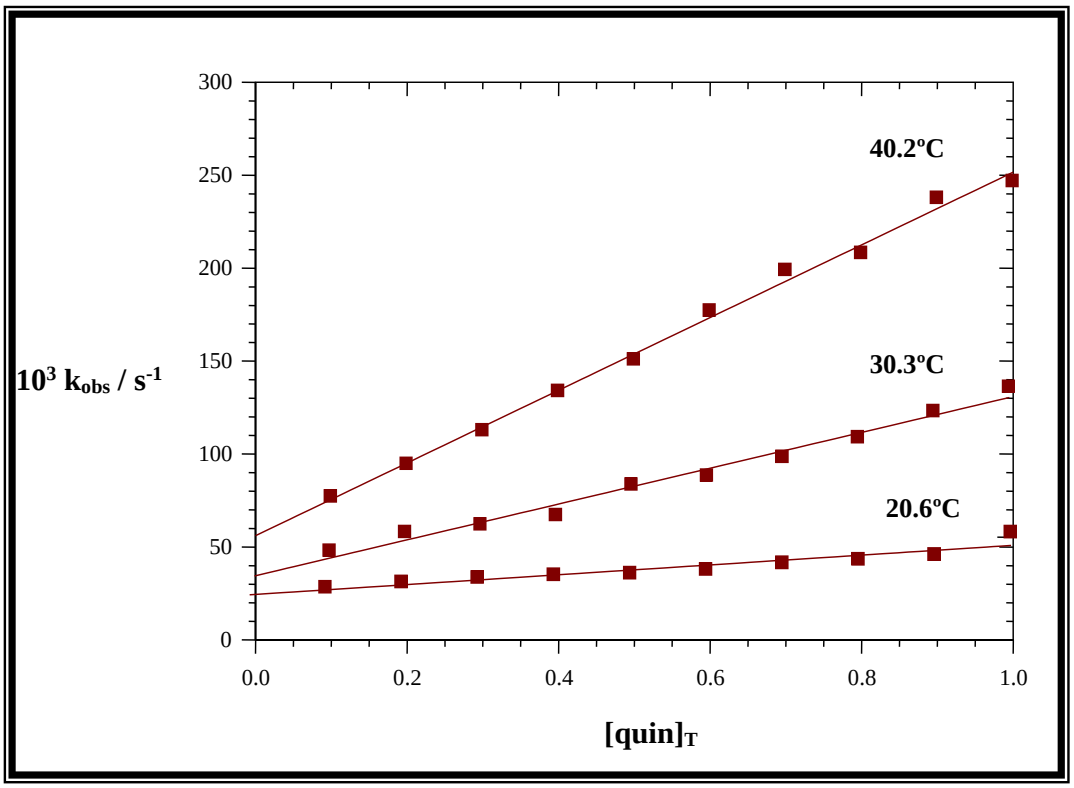

Figure 6.17: Plots of k_{obs} *vs.* $[quin]_T$ at different temperatures, pH = 8.02, $[[ReN(H_2O)(CN)_4]^{2-}] = 1.0\times10^{-2}$M, λ = 400 nm, μ = 1.0M $NaClO_4$.

The pH dependence of the pseudo first-order rate constant for the fast reactions is illustrated in **Figure 6.18.** The values of the different rate constants and the acid dissociation constant (k_2, k_{-2} and $pK_{a(ReH2O)}$) were obtained from the least-square fit of the data in **Figure 6.18** to **Eq. 6.3**, using k_1 and k_{-1} values from the temperature variations (**Figure 6.17**). These values are reported in **Table 6.4**.

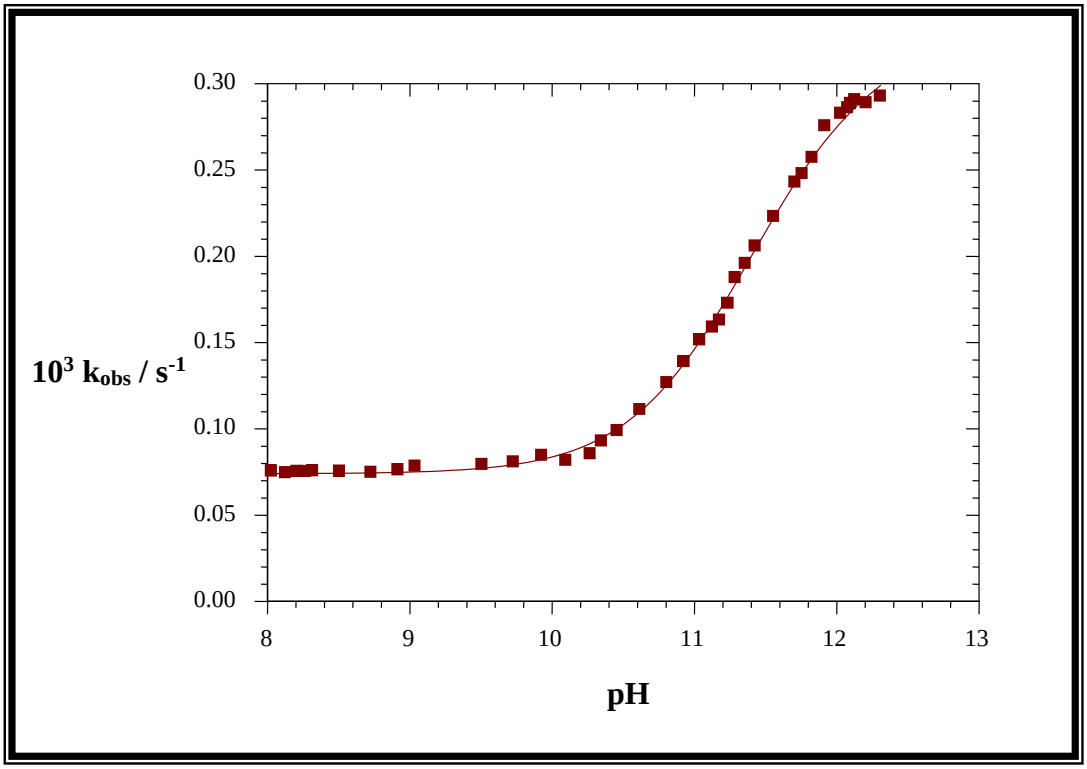

Figure 6.18: Plot of k_{obs} *vs.* pH at T = 40.3°C, $[ReN(H_2O)(CN)_4]^{2-}$ = 1.0×10^{-2}M, $[quin]_T$ = 0.1M, λ = 400 nm, μ = 1.0M $NaClO_4$.

The activation parameters ($\Delta H^{\neq}$ and $\Delta S^{\neq}$ for k_1 and k_{-1}) for the fast reaction between $[ReN(H_2O)(CN)_4]^{2-}$ complex and $[quin]_T$ were determined by least-square fit of the data in **Figures 6.19** and **6.20** respectively to Eyring equation, and are reported in **Table 6.4**.

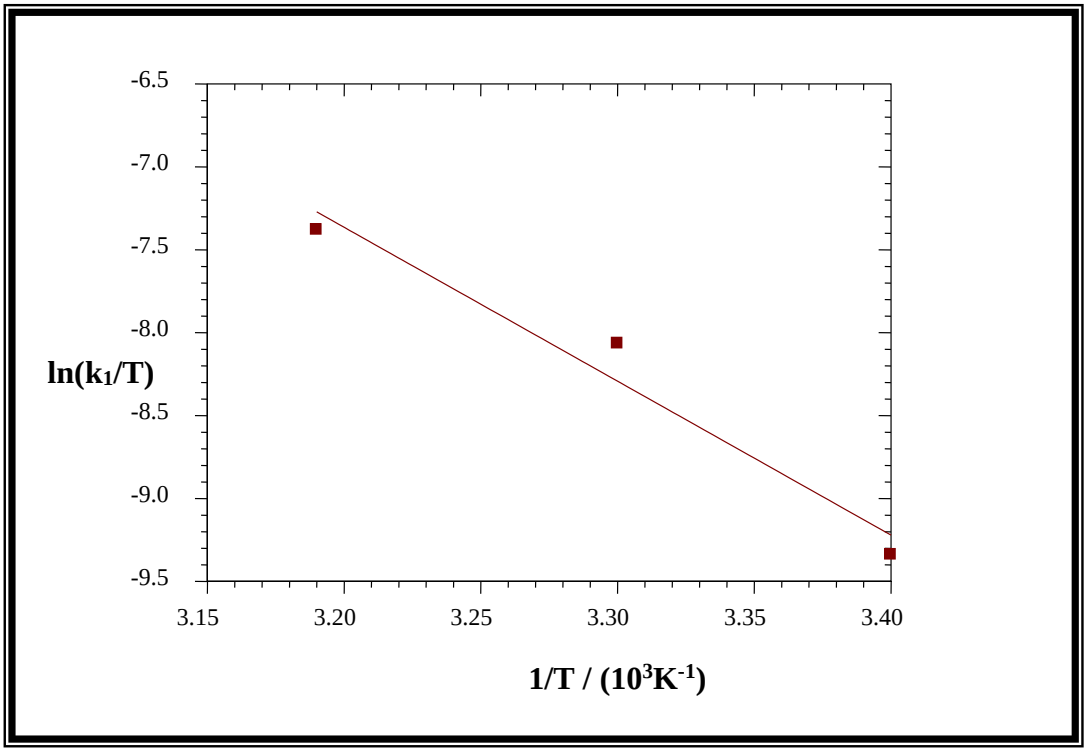

Figure 6.19: Plot of $\ln(k_1/T)$ *vs.* 1/T for the fast reaction between $[ReN(H_2O)(CN)_4]^{2-}$ and quinolinate anions.

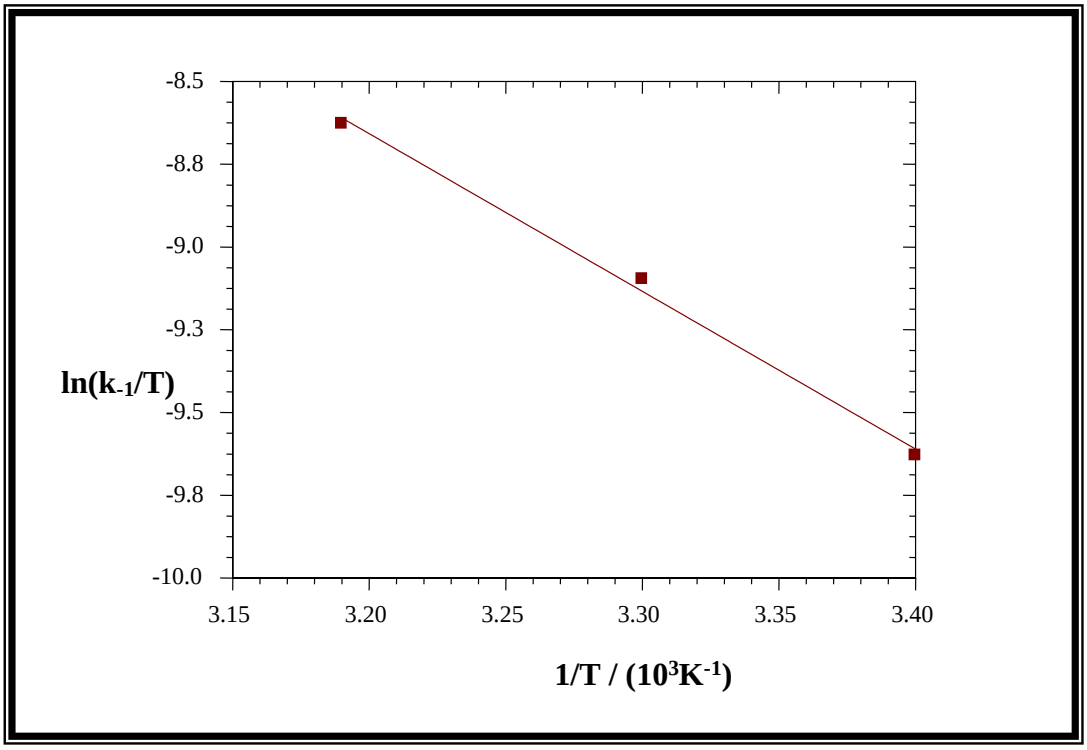

Figure 6.20: Plot of $\ln(k_{-1}/T)$ *vs.* 1/T for the fast reaction between $[ReN(H_2O)(CN)_4]^{2-}$ and quinolinate anions.

Table 6.4: Kinetic data for the fast reaction between $[ReN(H_2O)(CN)_4]^{2-}$ and $[quin]_T$, λ = 400 nm, μ = 1.0M $NaClO_4$.

Temperature °C	Constant	Value
40.2	$k_1(M^{-1}s^{-1})$[a]	$1.96(5) \times 10^{-1}$
	$k_1(M^{-1}s^{-1})$[b]	$1.65(2) \times 10^{-1}$
	$k_{-1}(s^{-1})$[a]	$5.6(3) \times 10^{-2}$
	$k_{-1}(s^{-1})$[b]	$5.74(1) \times 10^{-2}$
	$K_1(M^{-1})$[c]	3.5(4)
	$k_2(M^{-1}s^{-1})$[b]	2.64(3)
	$k_{-2}(s^{-1})$[b]	$2.15(2) \times 10^{-5}$
30.3	$k_1(M^{-1}s^{-1})$[a]	$9.6(5) \times 10^{-2}$
	$k_{-1}(s^{-1})$[a]	$3.41(3) \times 10^{-2}$
	$K_1(M^{-1})$[c]	2.82(4)
20.6	$k_1(M^{-1}s^{-1})$[a]	$2.17(1) \times 10^{-2}$
	$k_{-1}(s^{-1})$[a]	$2.05(5) \times 10^{-2}$
	$K_1(M^{-1})$[c]	1.06(3)
	$pK_{a(ReH2O)}$[b]	11.39(1)
	$\Delta H^{\neq}$ (k_1)[d] $kJmol^{-1}$	77.2(3)
	$\Delta S^{\neq}$ (k_1)[d] $JK^{-1}mol^{-1}$	-11.8(3)
	$\Delta H^{\neq}$ (k_{-1})[d] $kJmol^{-1}$	39.6(2)
	$\Delta S^{\neq}$ (k_{-1})[d] $JK^{-1}mol^{-1}$	-142.8(1)

[a] Slope and intercept, Fig. 6.17, Eq. 6.4.

[b] Data in Fig. 6.18, Eq. 6.3.

[c] $K_1 = k_1/k_{-1}$.

[d] Temperature dependence, Fig. 6.19 and 6.20, Eq. 6.10.

6.3.3.4 Slow Reaction

The UV/VIS spectrum changes of the reaction between $[ReN(H_2O)(CN)_4]^{2-}$ complex and quinolinate anions show only one maximum at 450 nm, and the experimental data for the slow reactions were investigated at this wavelength (see **Figure 6.14**). The slow reaction that was observed during the reaction between $[ReN(H_2O)(CN)_4]^{2-}$ and quinolinate anions is regarded as the chelate ring-closure with the substitution of the cyano ligand (see **Scheme 6.1**, reaction **E**)

Figure 6.21 shows the temperature and $[quin]_T$ dependence of the pseudo first-order rate constant for the second slow reaction between $[ReN(H_2O)(CN)_4]^{2-}$ complex and quinolinate anions. The values of k_3K_1 and k_{-3} were obtained from a least-square fit of k_{obs} *vs*. $[quin]_T$ data (determined at pH 8.02) to **Eq. 6.8**. The k_3K_1 and k_{-3} values obtained at three different temperatures are reported in **Table 6.5**. The term k_{-3} represents the contribution of the reverse reaction or the coordination of the cyanide anion.

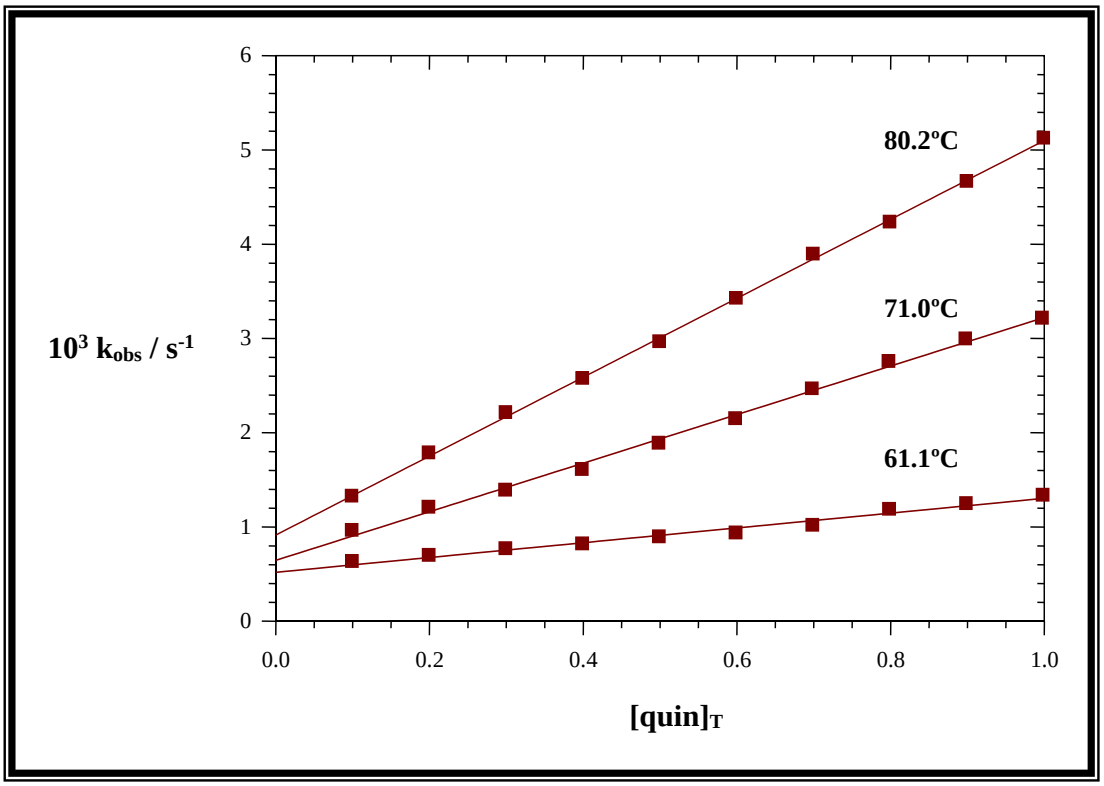

Figure 6.21: Plot of k_{obs} *vs*. $[quin]_T$ at different temperatures, pH = 8.02, $[[ReN(H_2O)(CN)_4]^{2-}] = 1.0\times10^{-3}$M, λ = 450 nm, μ = 1.0M $NaClO_4$.

Figure 6.22 illustrates the pH dependence of the pseudo first-order rate constant for the overall reaction mixture between $[ReN(H_2O)(CN)_4]^{2-}$ and $[quin]_T$ anions. The k_{obs} *vs*. pH data in **Figure 6.22** was fitted to **Eq. 6.7** and the values for different rate constants (k_3, k_{-3}, K_1, K_2 and $pK_{a(ReH2O)}$) were obtained by means of a least-square fit program and are reported in **Table 6.5**.

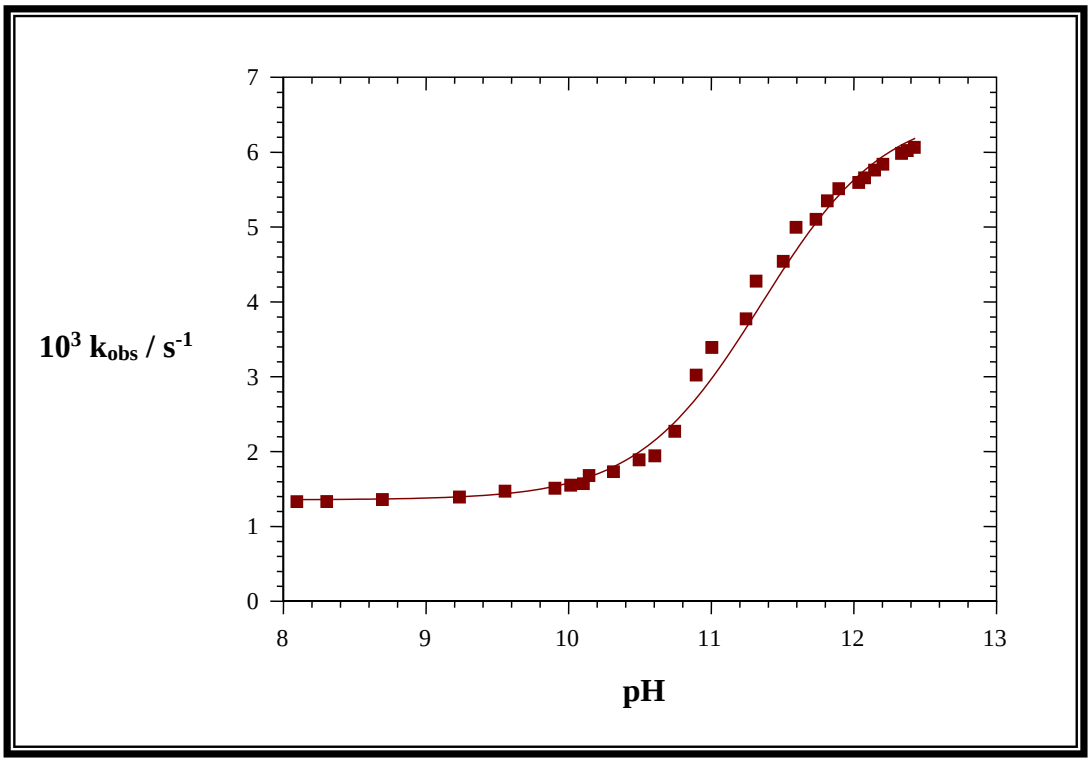

Figure 6.22: Plot of k_{obs} *vs*. pH at T = 80.4°C, $[[ReN(H_2O)(CN)_4]^{2-}] = 1.0\times10^{-3}$M, $[quin]_T = 0.1$M, $\lambda = 450$ nm, $\mu = 1.0$M $NaClO_4$.

The plots in **Figure 6.23** illustrate the temperature and quinolinate anion dependence of the pseudo first-order rate constant (k_{obs}) at high pH (*ca*. 12.0). As was the case for the slow reactions between $[ReN(H_2O)(CN)_4]^{2-}$ and $[pic]_T$ anions, discussed above (**Paragraph 6.3.1**), it appeared that the complex is also reactive at high pH where $[ReN(OH)(CN)_4]^{3-}$ is the predominant species in solution (pH *ca*. 12.0). The final rate and equilibrium constant (k_3 and K_2) were calculated by means of a least-square fit program of the k_{obs} *vs*. $[quin]_T$ data in **Figure 6.23** to **Eq. 6.7** and these values are reported in **Table 6.5.**

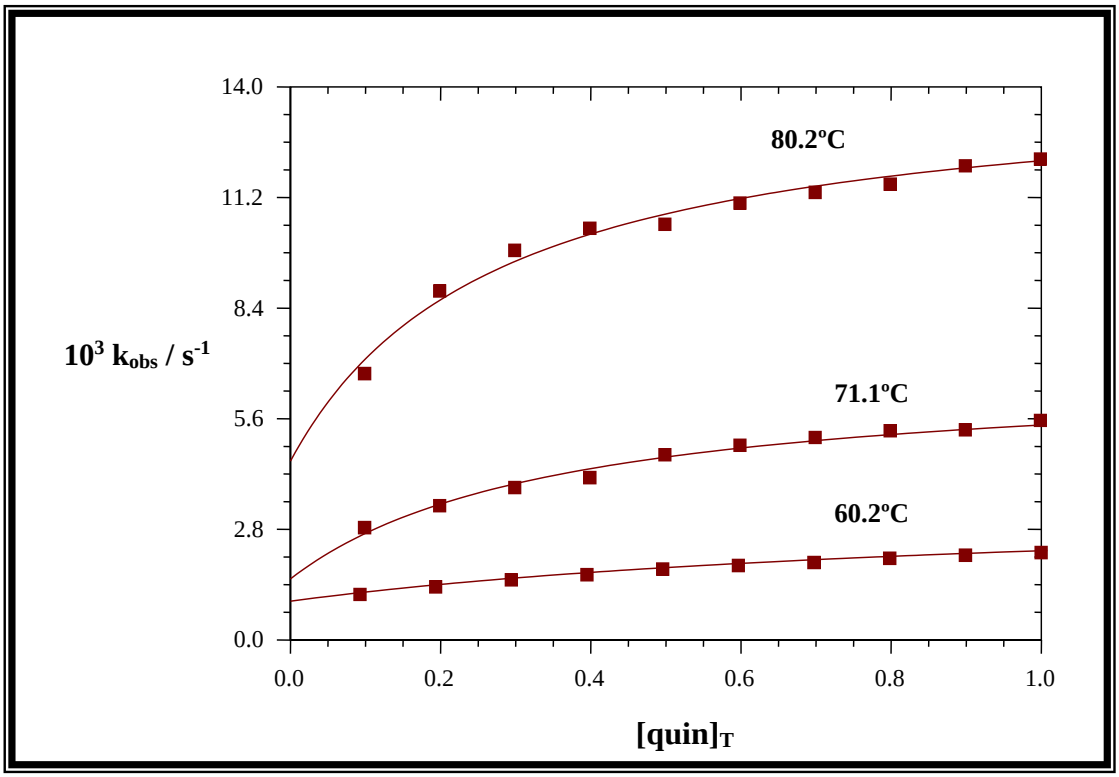

Figure 6.23: Plot of k_{obs} *vs.* $[quin]_T$ at different temperatures, pH = 12.34, $[[ReN(H_2O)(CN)_4]^{2-}] = 1.0\times10^{-3}$M, λ = 400 nm, μ = 1.0M $NaClO_4$.

The reaction between $[ReN(H_2O)(CN)_4]^{2-}$ complex and $[quin]_T$ was also followed at a pH between 3.5 and 8 where the incoming ligand changed from the protonated quinaldic acid (quinH) to the free quinolinate anion ($quin^-$). **Figure 6.24** illustrates the pH dependence of the pseudo first-order rate constant. The values for the different rate constants and acid dissociation constant (k_3, K_1, k_{-3} and $pK_{a(quinH)}$) were obtained from a least-square fit of the data in **Figure 6.24** to **Eq. 6.9** and are reported in **Table 6.5**.

The activation parameters ($\Delta H^{\neq}$ and $\Delta S^{\neq}$ for k_3) of the overall reaction between the $[ReN(H_2O)(CN)_4]^{2-}$ complex and quinolinate anions were determined by a least-square fit of the temperature dependence data of the pseudo first-order rate constant (k_3, see **Figure 6.25**) to the Eyring equation (**Eq. 6.10**) and are reported in **Table 6.5**.

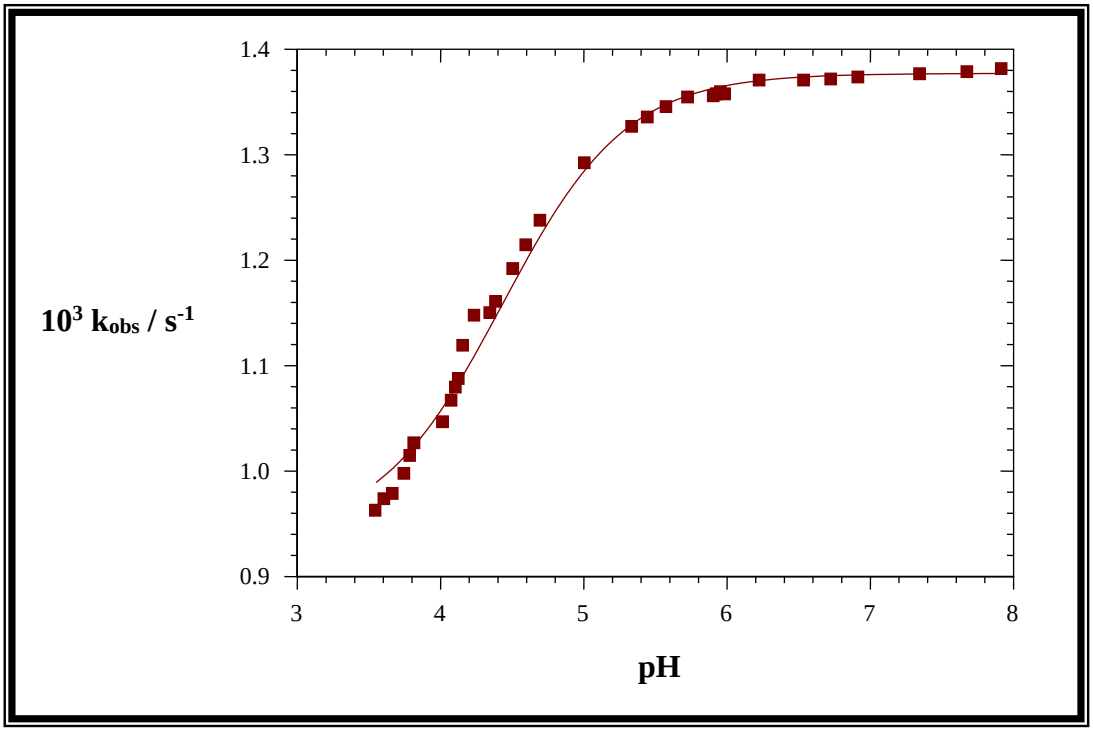

Figure 6.24: Plot of k_{obs} *vs.* pH at T = 80.6°C, $[[ReN(H_2O)(CN)_4]^{2-}]$ = 1.0×10^{-3}M, $[quin]_T$ = 0.1M, λ = 450 nm, μ = 1.0M $NaClO_4$.

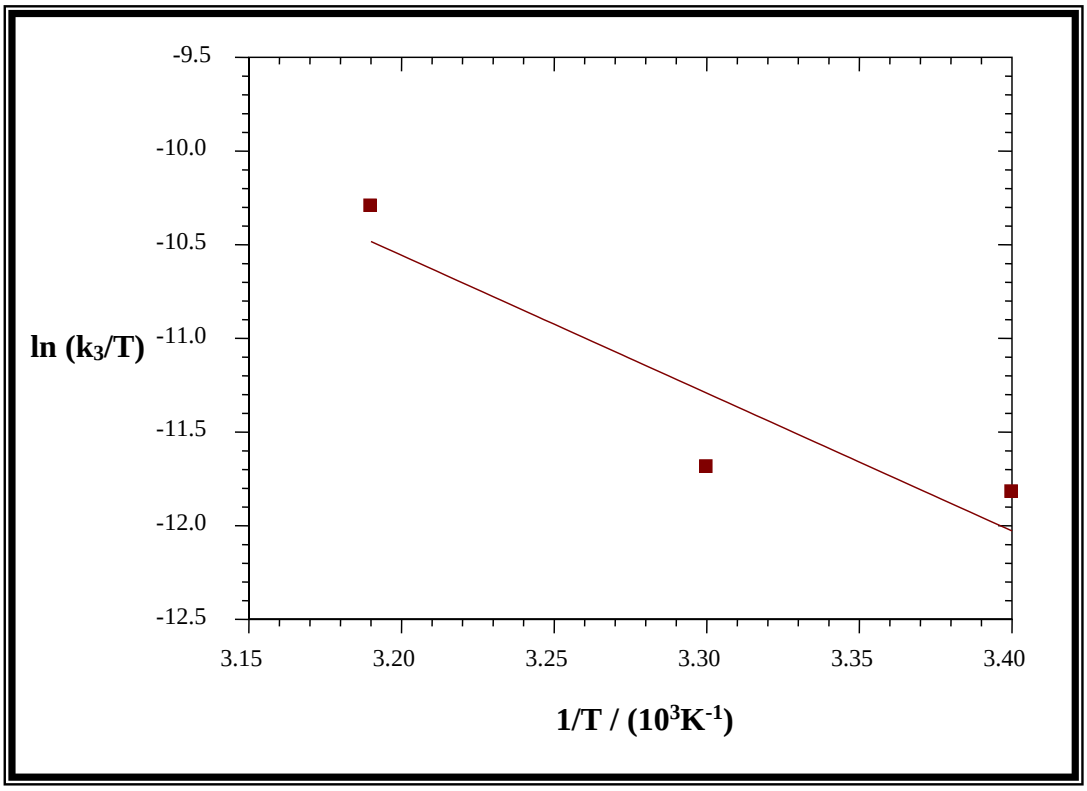

Figure 6.25: Plot of ln(k_3/T) *vs.* 1/T for the slow reaction between $[ReN(H_2O)(CN)_4]^{2-}$ and quinolinate anions.

Table 6.5: Kinetic data for the slow reaction between $[ReN(H_2O)(CN)_4]^{2-}$ and $[quin]_T$, λ = 450 nm, μ = 1.0M $NaClO_4$.

Temperature °C	Constant	Value
80.0	k_3K_1 $(M^{-1}s^{-1})^{e}$	$4.17(4)\times10^{-3}$
	$k_3(s^{-1})^{f}$	$2.12(3)\times10^{-2}$
	$k_3(s^{-1})^{g}$	$8.7(1)\times10^{-3}$
	$k_3(s^{-1})^{h}$	$7.5(4)\times10^{-2}$
	k_{-3} $(M^{-1}s^{-1})^{e}$	$9.2(2)\times10^{-4}$
	k_{-3} $(M^{-1}s^{-1})^{f}$	$1.39(3)\times10^{-3}$
	$k_{-3}(M^{-1}s^{-1})^{h}$	$9.2(2)\times10^{-4}$
	K_1 $(M^{-1})^{f}$	$3.9(1)\times10^{-2}$
	$K_1(M^{-1})^{h}$	$6.1(3)\times10^{-2}$
	$K_1(M^{-1})^{j}$	$5.6(2)\times10^{-2}$
	$K_2(M^{-1})^{g}$	4.33(1)
	K_2 $(M^{-1})^{f}$	3.3(1)
	$K_3(M^{-1})^{i}$	82.0(2)
	K'^{l}	5.06(3)
	$pK_{a(Re\text{-}H2O)}{}^{f}$	11.51(8)
	$pK_{a(ReH2O)}{}^{k}$	11.58(3)
	$pK_{a(quinH)}{}^{h}$	4.36(1)
	$pK_{a(quin)l}{}^{m}$	4.97
70.0	$k_3K_1(M^{-1}s^{-1})^{e}$	$2.58(5)\times10^{-3}$
	$k_3(s^{-1})^{g}$	$5.2(1)\times10^{-3}$
	$k_{-3}(M^{-1}s^{-1})^{e}$	$6.38(3)\times10^{-4}$
	$K_1(M^{-1})^{j}$	$6.5(4)\times10^{-1}$
	K_2 $(M^{-1})^{g}$	3.2(1)
60.0	k_3K_1 $(M^{-1}s^{-1})^{e}$	$7.84(4)\times10^{-4}$
	$k_3(M^{-1}s^{-1})^{g}$	$2.5(1)\times10^{-3}$
	k_{-3} $(M^{-1})^{e}$	$5.15(3)\times10^{-4}$
	$K_1(M^{-1})^{j}$	$6.3(5)\times10^{-1}$
	K_2 $(M^{-1})^{g}$	1.14(7)
	$\Delta S^{\neq}$ $(k_3)^{d}$ $JK^{-1}mol^{-1}$	-83.5(2)
	$\Delta H^{\neq}$ $(k_3)^{d}$ $kJmol^{-1}$	71.4(3)

[d] Temperature dependence in Fig. 6.25, Eq. 6.10; [e] From slope and intercept, Fig. 6.21, Eq. 6.8; [f] Data in Fig. 6.22, Eq. 6.7; [g] Data in Fig. 6.23, Eq. 6.7; [h] Data in Fig. 6.24, Eq. 6.9; [i] $K_3 = k_3/k_{-3}$; [j] $K_1 = k_3K_1/k_3$; [K] Data in Fig. 6.16, Eq. 6.13; [l] Data in Fig. 6.15, Eq. 6.11; [m] Martell & Smith, (1982:129).

6.3.4 Kinetic Results of the Reaction between $[ReN(H_2O)(CN)_3]^{2-}$ Complex with Pyridine-2,3-dicarboxylate (2,3dipic)

6.3.4.1 Identification of the Product

The reaction between pyridine-2,3-dicarboxylate anion and the $[ReN(H_2O)(CN)_4]^{2-}$ complex in aqueous solution was initially investigated at pH values between 8.0 and 12.4. The UV/VIS spectrum change of the reaction between these two species taken at 80.1°C showed two absorption maxima at 410 and 360 nm (**Figure 6.26**).

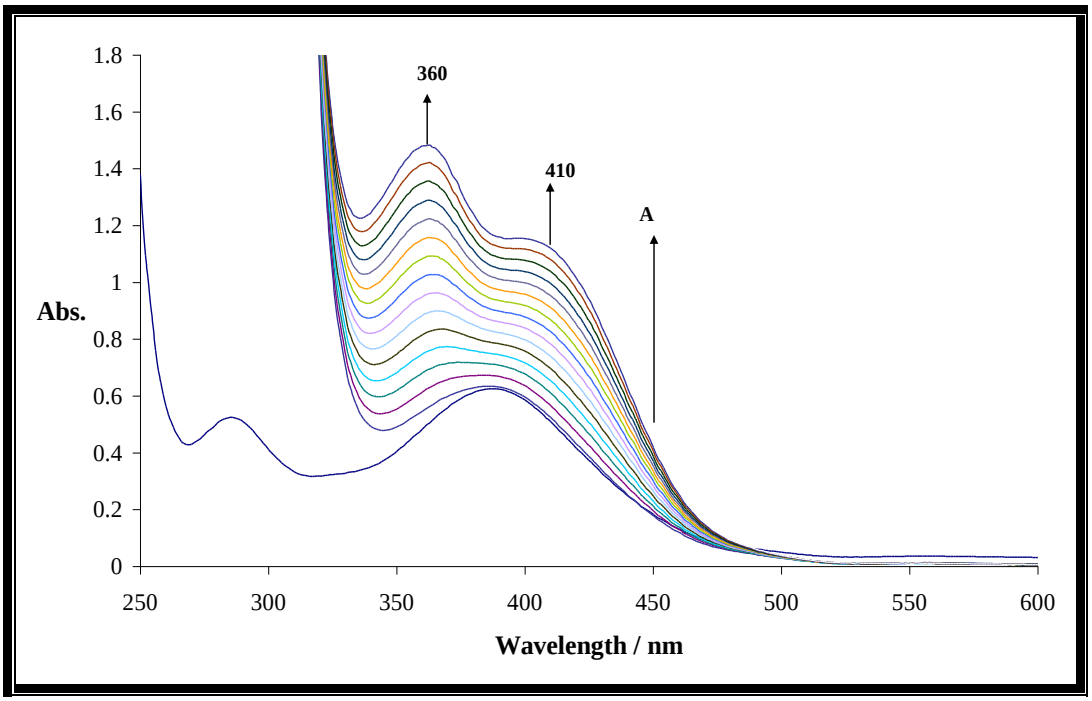

Figure 6.26: UV/VIS spectral changes during the reaction between $[ReN(H_2O)(CN)_4]^{2-}$ and pyridine-2,3-dicarboxylate ($2,3\text{-dipic}^-$), at T = 80.1°C, pH = 8.10, $[[ReN(H_2O)(CN)_4]^{2-}] = 1.0\times10^{-3}$M, $[2,3\text{-dipic}]_T$ = 1.0M: A = Absorbance increase due to the slow reaction. Time intervals 1.0 min.

The kinetic reactions between these two species (**Eq. 4.3, Chapter 4**) were investigated at 410 nm, and the same reaction scheme, **Scheme 6.1,** was predicted based on the following observations:

(i) on close inspection of absorbance *vs.* time spectrum of the reaction between $[ReN(H_2O)(CN)_4]^{2-}$ and pyridine-2,3-dicarboxylate at this temperature, two different reactions were observed. A relatively first fast reaction with a half-life of few seconds followed by the second much slower reaction with the half-life of 10 to 25 minutes.

(ii) the rate of reactions shows a dependence on the pyridine-2,3-dicarboxylate concentration.

6.3.4.2 Stability and Acid Dissociation Constants

The stability constant (K', **Table 6.6**) for the reaction between the $[ReN(H_2O)(CN)_4]^{2-}$ complex and pyridine-2,3-dicarboxylate was determined by means of spectrophotometry from a least-square fit of the absorbance *vs.* $[2,3\text{-dipic}]_T$ data in **Figure 6.27** to **Eq. 6.11** and reported in **Table 6.6**.

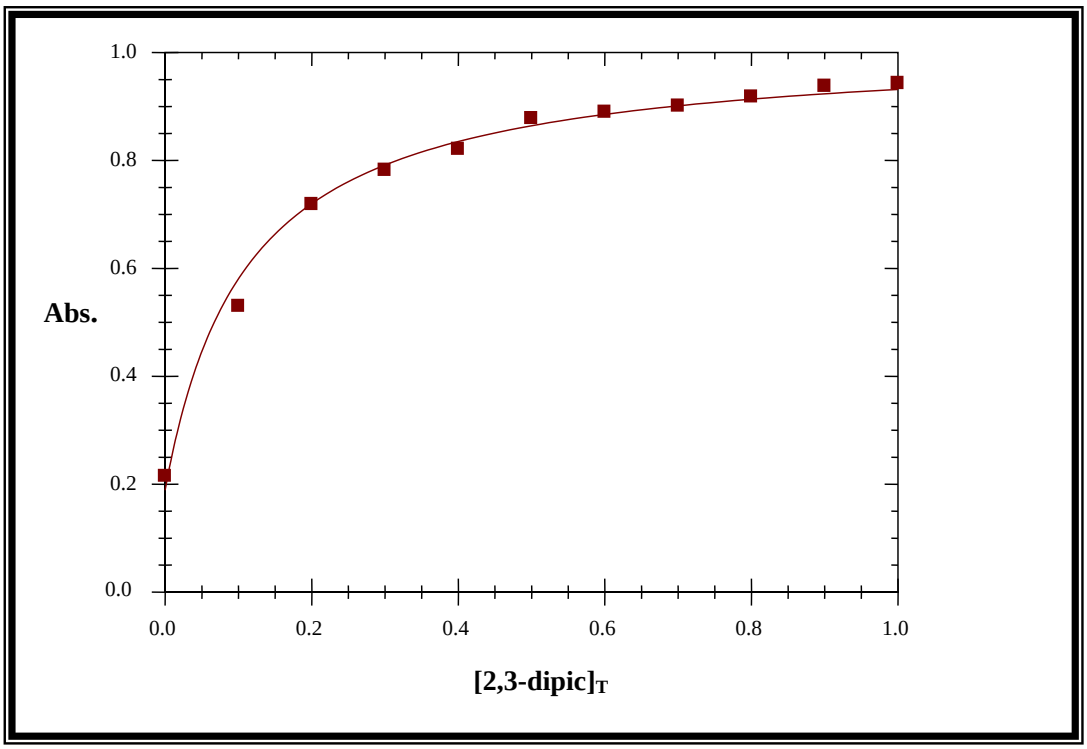

Figure 6.27: Plot of Abs. *vs.* $[2,3\text{-dipic}]_T$ at T = 80.5°C, pH = 8.03, $[[ReN(H_2O)(CN)_4]^{2-}] = 1.0\times10^{-3}$M, λ = 410 nm, μ = 1.0M $NaClO_4$.

The acid/base behaviour for the reaction between $[ReN(H_2O)(CN)_4]^{2-}$ and 2,3-dipicolinate also proceed as depicted in **Eq. 6.12** (see reaction **B**, **Scheme 6.1**).

The plot of absorbance *vs*. pH for the overall reaction between $[ReN(H_2O)(CN)_4]^{2-}$ and 2,3-dipicolinate anions is illustrated in **Figure 6.28**. The acid dissociation constant, $pK_{a(ReH2O)}$, was calculated by a least-square fit of the data in **Figure 6.28** to **Eq. 6.13** and is reported in **Table 6.6**.

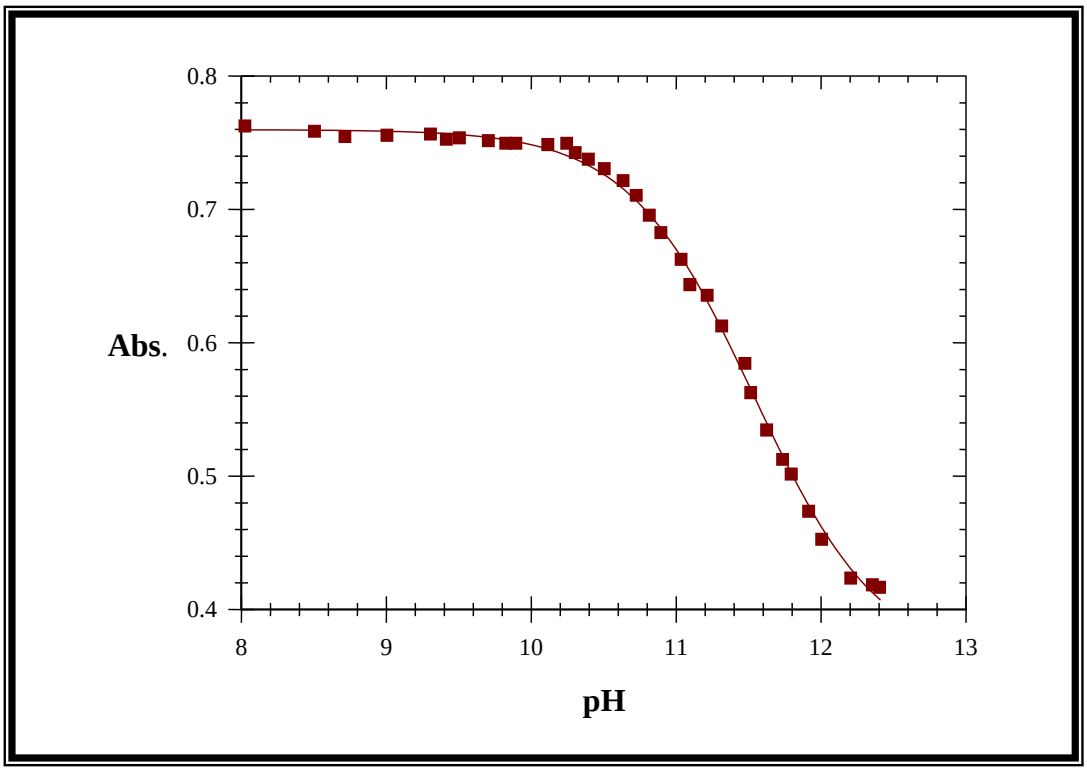

Figure 6.28: Plot of Abs. *vs*. pH at T = 80.4°C, [2,3-dipic] = 0.1M, $[[ReN(H_2O)(CN)_4]^{2-}] = 1.0\times10^{-3}$M, λ = 410 nm, μ = 1.0M $NaClO_4$.

An attempt was made to investigate the rate of the fast reaction between these two species at the chosen wavelength (410 nm). The observed rate constants of these reactions (below 40°C) were less accurate and as a result are not included in this study.

6.3.4.3 Slow Reaction

The UV/VIS spectra (**Figure 6.26**) of the reaction between $[ReN(H_2O)(CN)_4]^{2-}$ complex and 2,3-dipicolinate anions show two absorption maxima at 410 and 360 nm, and reaction rate for the slow reactions were investigated at 410 nm.

Figure 6.29 shows the temperature and $[2,3\text{-dipic}]_T$ dependence of the pseudo first-order rate constant for the second slow reaction between $[ReN(H_2O)(CN)_4]^{2-}$ complex and pyridine-2,3-dicaboxylate anions. The values of k_3K_1 and k_{-3} were obtained from a least-square fit of k_{obs} *vs.* $[2,3\text{-dipic}]_T$ data in **Figure 6.29** to **Eq. 6.8**. The k_3K_1 and k_{-3} values obtained at three different temperatures are reported in **Table 6.6**.

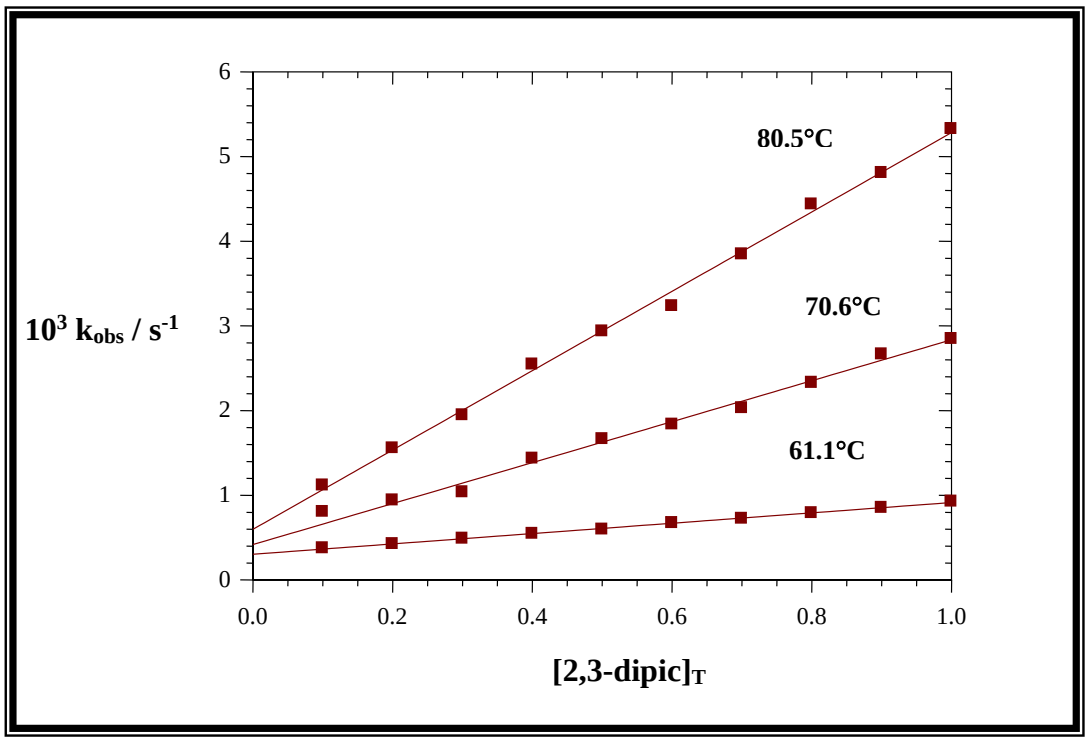

Figure 6.29: Plot of k_{obs} *vs.* $[2,3\text{-dipic}]_T$ at different temperatures, pH = 8.03, $[[ReN(H_2O)(CN)_4]^{2-}] = 1.0\times10^{-3}$M, λ = 410 nm, μ = 1.0M $NaClO_4$.

Figure 6.30 illustrates the pH dependence of the pseudo first-order rate constant variation for the overall reaction mixture. The k_{obs} *vs.* pH data in **Figure 6.30** were fitted to **Eq. 6.7** and the values for different rate constants and acid dissociation constant (k_3, k_{-3}, K_1, K_2

and $pK_{a(ReH2O)}$) were obtained by means of a least-square fit program and are reported in **Table 6.6**.

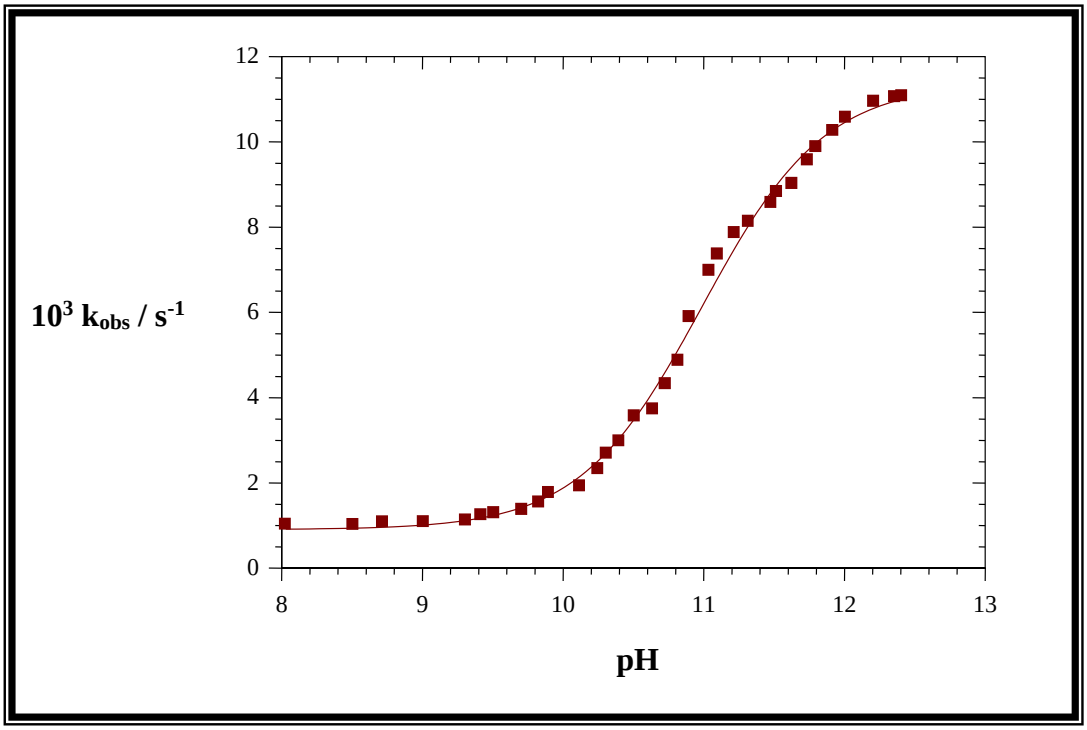

Figure 6.30: Plot of k_{obs} *vs.* pH, T = 80.4°C, $[[ReN(H_2O)(CN)_4]^{2-}] = 1.0\times10^{-3}$M, $[2,3\text{-dipic}]_T = 0.1$M, $\lambda = 410$ nm, $\mu = 1.0$M $NaClO_4$.

The data in **Figure 6.31** illustrates the temperature and 2,3-dipicolinate anion concentration dependence of the pseudo first-order rate constant (k_{obs}) at high pH (pH *ca*. 12.0). As was the case for the slow reactions between the $[ReN(H_2O)(CN)_4]^{2-}$ with $[pic]_T$ and $[quin]_T$ anions respectively, it appeared that the complex is also reactive at high pH. The final rate and equilibrium constants (k_3 and K_2) were calculated by means of a least-square fit program of the k_{obs} *vs.* $[2,3\text{-dipic}]_T$ data in **Figure 6.31** to **Eq. 6.7** and these values are reported in **Table 6.6.**

The reaction between $[ReN(H_2O)(CN)_4]^{2-}$ complex and 2,3-dipicolinate was also followed at a pH between 4 and 8, where the incoming ligand changed from the protonated pyridine-2,3-dicarboxylic acid (2,3-dipicH) to the free pyridine-2,3-dicarboxylate anion ($2,3\text{-dipic}^-$). **Figure 6.32** illustrates the pH dependence of the pseudo first-order rate constant. The values for the different rate constants and acid dissociation constant (k_3, K_1,

k_{-3} and $pK_{a(2,3\text{-dipic})}$) were obtained from a least-square fit of the data in **Figure 6.31** to **Eq. 6.9** and are reported in **Table 6.6**.

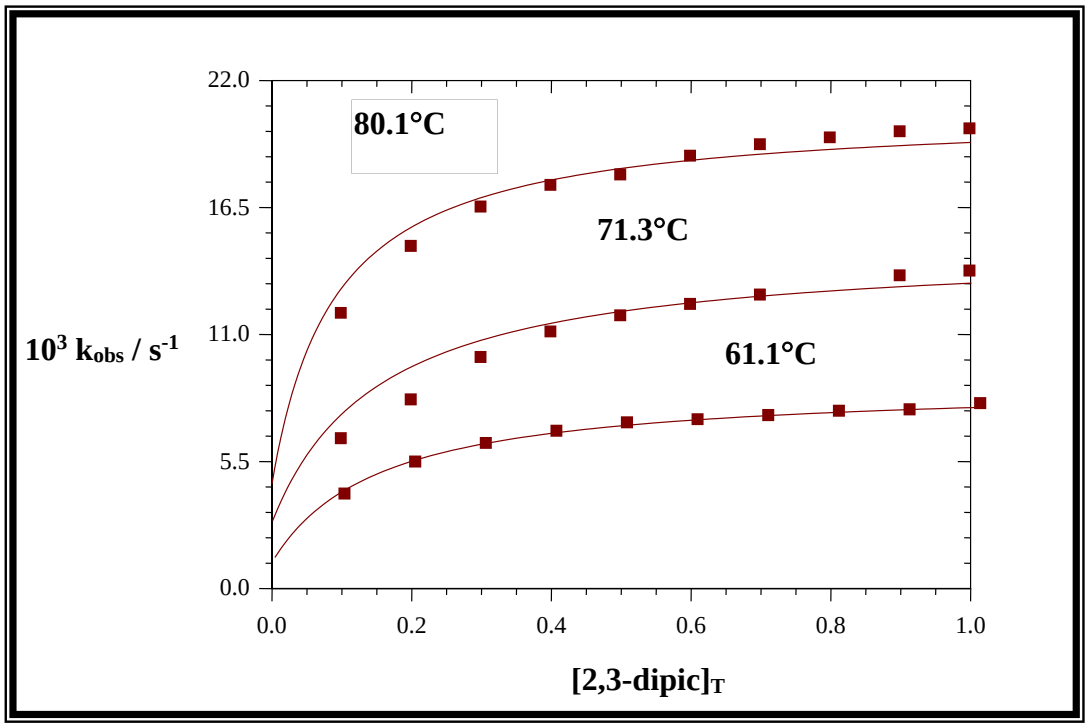

Figure 6.31: Plot of k_{obs} *vs.* $[2,3\text{-dipic}]_T$ at different temperatures, pH = 12.41, $[ReN(H_2O)(CN)_4]^{2-}] = 1.0\times10^{-3}$M, λ = 410 nm, μ = 1.0M $NaClO_4$.

The activation parameters ($\Delta H^{\neq}$ and $\Delta S^{\neq}$ for k_3) of the overall reaction between the $[ReN(H_2O)(CN)_4]^{2-}$ complex and 2,3-dipicolinate anions were determined by a least-square fit of the temperature dependence data of the pseudo first-order rate constant (k_3, see **Figure 6.33**) to the Eyring equation (**Eq. 6.10**) and are reported in **Table 6.6**.

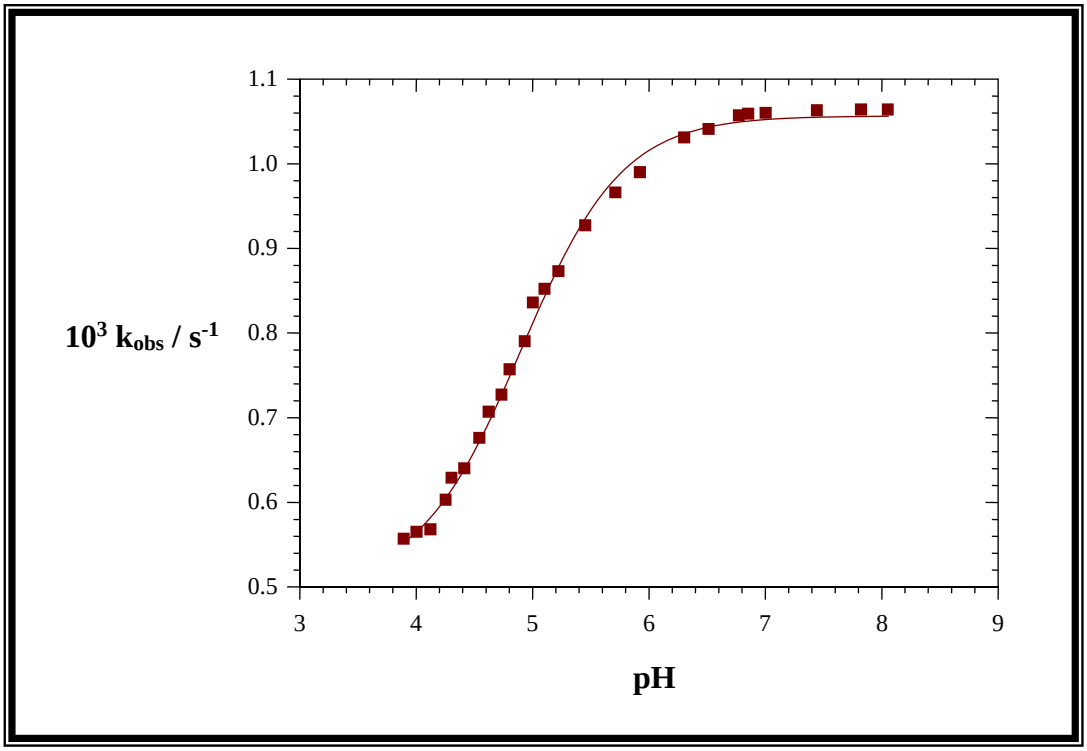

Figure 6.32: Plot of k_{obs} *vs.* pH at T = 80.6°C, $[[ReN(H_2O)(CN)_4]^{2-}]$ = 1.0×10^{-3}M, $[2,3\text{-dipic}]_T$ = 0.1M, λ = 410 nm, μ = 1.0M $NaClO_4$.

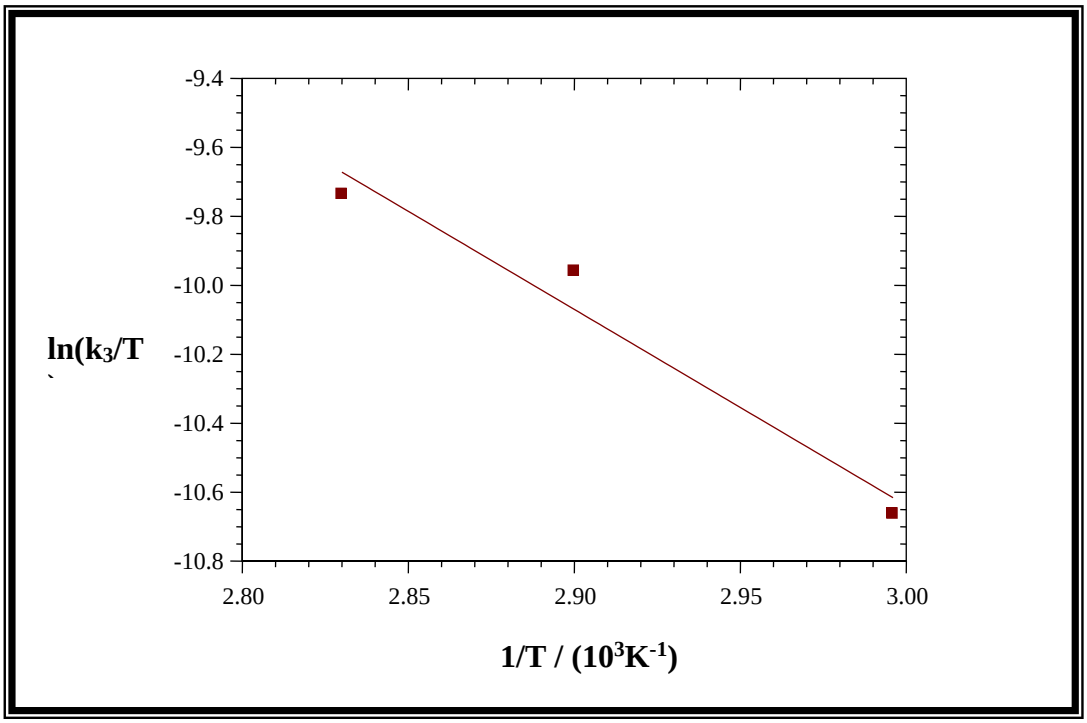

Figure 6.33: Plot of $\ln(k_3/T)$ *vs.* 1/T for the slow reaction between $[ReN(H_2O)(CN)_4]^{2-}$ and 2,3-dipicolate anions.

Table 6.6: Kinetic data for the slow reaction between $[ReN(H_2O)(CN)_4]^{2-}$ and $[2,3\text{-dipic}]_T$, $\lambda = 410$ nm, $\mu = 1.0$M.

Temperature °C	Constant	Value
80.0	k_3K_1 $(M^{-1}s^{-1})^e$	$4.68\ (7)\times10^{-3}$
	$k_3(s^{-1})^f$	$1.83(1)\times10^{-2}$
	$k_3(s^{-1})^g$	$2.1(2)\times10^{-2}$
	$k_3(s^{-1})^h$	$6.7(3)\times10^{-2}$
	k_{-3} $(M^{-1}s^{-1})^e$	$5.13(4)\times10^{-4}$
	k_{-3} $(M^{-1}s^{-1})^f$	$7.95(4)\times10^{-4}$
	$k_{-3}(M^{-1}s^{-1})^h$	$4.94(2)\times10^{-4}$
	K_1 $(M^{-1})^f$	$1.03(4)\times10^{-1}$
	$K_1(M^{-1})^h$	$8.36(4)\times10^{-2}$
	$K_1(M^{-1})^j$	$1.3(1)\times10^{-2}$
	$K_2(M^{-1})^g$	12.26(6)
	K_2 $(M^{-1})^f$	14.56(2)
	K_3 $(M^{-1})^i$	135.6(1)
	K'^l	9.03(5)
	$pK_{a(Re\text{-}H2O)}{}^f$	11.41(1)
	$pK_{a(2,3\text{-}dipicH)}{}^h$	4.87(1)
	$pK_{a(2,3\text{-}dipic)}{}^m$	5.02
	$pK_{a(ReH2O)}{}^k$	11.54(2)
70.0	$k_3K_1(M^{-1}s^{-1})^e$	$2.35(3)\times10^{-3}$
	$k_3(s^{-1})^g$	$1.63(4)\times10^{-2}$
	$k_{-3}(M^{-1}s^{-1})^e$	$3.8(1)\times10^{-4}$
	$K_1(M^{-1})^j$	$1.44(1)\times10^{-1}$
	K_2 $(M^{-1})^g$	7.27(6)
60.0	k_3K_1 $(M^{-1}s^{-1})^e$	$6.1(9)\times10^{-4}$
	$k_3(M^{-1}s^{-1})^g$	$7.8(1)\times10^{-3}$
	k_{-3} $(M^{-1})^e$	$3.03(5)\times10^{-4}$
	$K_1(M^{-1})^j$	$7.8(2)\times10^{-2}$
	K_2 $(M^{-1})^g$	6.83(2)
	$\Delta S^{\neq}$ $(k_3)^d$ $JK^{-1}mol^{-1}$	-144.1(2)
	$\Delta H^{\neq}$ $(k_3)^d$ $kJmol^{-1}$	47.3(3)

[d] Temperature dependence in Fig. 6.33, Eq. 6.10; [e] From slope and intercept, Fig. 6.29, Eq. 6.8; [f] Data in Fig. 6.30, Eq. 6.7; [g] Data in Fig. 6.31, Eq. 6.7; [h] Data in Fig. 6.32, Eq. 6.9; [i] $K_3 = k_3/k_{-3}$; [j] $K_1 = k_3K_1/k_3$; [K] Data in Fig. 6.28, Eq. 6.13; [l] Data in Fig. 6.27, Eq. 6.11; [m] Harmon *et al*., (1998:43).

6.4 DISCUSSION

The substitution reactions between $[ReN(H_2O)(CN)_4]^{2-}$ with picolinate, quinolinate and 2,3-dipicolinate anions were investigated in this study. In all the reactions studied two reaction steps were observed during the substitution reaction. The first reaction was relatively fast which resulted in a decrease in absorbance followed by a subsequent slow reaction which resulted in the UV/VIS spectra that were identical to those of the final products (**Figures 6.1, 6.14** and **6.26**). The crystal structure determinations of both $(AsPh_4)_2[ReN(\eta^2\text{-pic})(CN)_3]\cdot 4H_2O$ and $(AsPh_4)_2[ReN(\eta^2\text{-quin})(CN)_3]\cdot 2H_2O$ complexes showed that the aqua ligand and one of the cyano ligands are substituted by incoming bidentate ligands (pic^- and $quin^-$, respectively). The reaction **Scheme 6.1** was proposed for all the reactions which are possible under experimental conditions that prevailed during this study.

It has to be mentioned that during the reaction between $[ReN(H_2O)(CN)_4]^{2-}$ and 2,3-dipicolinate anions, a cyano-bridged binuclear rhenium(V) complex $[ReN(H_2O)(CN)_3\text{-}\mu\text{-}CN\text{-}ReN(CN)_4]^{4-}$ as product was isolated. It was expected that a bidentate ligand (2,3-dipic) will behave similarly to the picolinate and quinolinate anions and result in the substitution of both aqua and cyano ligands to form the $[ReN(\eta^x\text{-dipic})(CN)_m]^{n-}$ type of complex. All the kinetic results obtained between $[ReN(H_2O)(CN)_4]^{2-}$ and $2,3\text{-dipic}^-$ were of the same magnitude, and followed the same reaction scheme (**Scheme 6.1**) as those of the other two bidentate ligands studied (pic^- and $quin^-$). Therefore, it is concluded that the same reaction was followed in this study. The inability to isolate the substitution product can be attributed to the high solubility of the $2,3\text{-dipic}^-$ ligand (2 carboxylate groups bonded to pyridine ring) under the experimental conditions that prevailed during the crystallization process.

The results obtained in this study were compared with the previous kinetics (monodentate and bidentate ligands substitutions) and structural studies of $Na[MoO(\eta^2\text{-phen})(CN)_3]\cdot 2phen\cdot CH_3OH\cdot H_2O$, $(AsPh_4)_2[WO(\eta^2\text{-pic})(CN)_3]\cdot 3H_2O$, $(AsPh_4)_2[MnN(\eta^2\text{-pic})(CN)_3]\cdot 2H_2O$ and $(AsPh_4)_2[MnN(\eta^2\text{-quin})(CN)_3]\cdot 2H_2O$ complexes (Leipoldt *et al*., 1987:57; Roodt *et al*., 1994:599; Van der Westhuizen, 2004:109, b)

(**Table 6.7**). These results correlate very well with those of the previous kinetic studies of the reactions of $[MX(H_2O)(CN)_4]^{n-}$ (M = W(IV), Mo(IV), and Mn(V), X = O^{2-} or N^{3-}) with different bidentate ligands (1,10-phenanthroline, pyridine-2-carboxylate, quinoline-2-carboxylate and pyridine-2,3-dicarboxylate) which indicated a two-step reaction process (Leipoldt *et al*, 1987:57; Roodt *et al*., 1994:599; Van der Westhuizen, 2004:109, b). The kinetic results of, for example, the substitution reaction between $[WO(H_2O)(CN)_4]^{2-}$ complex and bidentate ligand, pyridine-2-dicarboxylate anions, suggested that the first step is the substitution of the aqua ligand followed by the second chelate ring-closure step with the substitution of a cyano ligand as the rate-determining step.

The monodentate substitution reactions between $[ReN(H_2O)(CN)_4]^{2-}$ with CN^- and N^{3-} clearly indicated that only the aqua ligand is substituted in a relatively fast reaction and that the rest of the coordinated sphere is left unchanged (except for an increase in octahedral distortion) (Damoense *et al*., 1994:619; Purcell *et al*., 1992:217). A comparison between the aqua substitution rate for the $[ReX(H_2O)(CN)_4]^{n-}$ complexes (k_1 = 3.48(4)×10^{-3} $M^{-1}s^{-1}$ for NCS^- at 25ºC for X = O^{2-} and k_1 = 7.2(4)×$10^3M^{-1}s^{-1}$ for CN^- at 25ºC for X = N^{3-}) indicated that the weak Re-H_2O bond length of 2,142(7)Å for $[ReO(H_2O)(CN)_4]^-$ and 2.496(7)Å for $[ReN(H_2O)(CN)_4]^{2-}$ is a very good indicator of the lability of the complex towards substitution reactions. Thus, the fast reactions that were observed in this study are also regarded as the substitution of the aqua ligand to form a mono-substituted $[ReN(\eta^1\text{-L-L})(CN)_4]^{3-}$ complex (**Scheme 6.1**, reaction **C**).

The results obtained for the first fast reactions (first step, reaction **C** in **Scheme 6.1**) between $[ReN(H_2O)(CN)_4]^{2-}$ with picolinate and quinolinate ligands, were interpreted in terms of **Eqs. 6.3** and **6.5,** the same way as for the monodentate substitution reactions and the pH and ligand dependence could be explained satisfactory using these equations. The rates of aqua substitutions from the $[ReN(H_2O)(CN)_4]^{2-}$ complex by the picolinate and quinolinate anions were determined as 1.92(5)×10^{-1} and 1.96(5)×10^{-1} $M^{-1}s^{-1}$ at 40ºC respectively. These values are in agreement with each other (**Table 6.7**), and also substantially slower (factor 10^5) than the corresponding reaction when CN^- was the incoming group. This is due to the difference in the coordination capability of these

ligands (monodentate *vs*. bidentate) which is also manifested in the stability constants of these different complexes. The stability constant for the $[ReN(CN)_5]^{3-}$ ion was determined as 471(1) M^{-1} during the previous kinetic study and the values of 1.0(2) and 1.06(3) M^{-1} (at 20ºC) were obtained for the first step in $[ReN(\eta^2\text{-pic})(CN)_3]^{2-}$ and $[ReN(\eta^2\text{-quin})(CN)_3]^{2-}$ anions respectively. This is indicative of weak σ-donating ability of the COO^- group compared to that of the cyano group. The same tendency was observed for the corresponding reaction between $[WO(H_2O)(CN)_4]^{2-}$ and the picolinate anion where a decrease in substitution rate of a factor of 2.5 was observed when compared to the rate with CN^- as an incoming group (Smith, 1995:71; Roodt *et al*., 1994:599). A decrease of a factor of 10^3 was also observed for the stability constant of $[WO(H_2O)(CN)_4]^{2-}$ and picolinate when compared to that of the reaction between $[WO(H_2O)(CN)_4]^{2-}$ with CN^-.

It is, however, interesting to note that in both ligands studied, the results obtained in the pH variation indicate acceleration in the substitution rate with an increase in pH (**Figures 6.5** and **6.18)**. However, the reaction between $[WO(H_2O)(CN)_4]^{2-}$ with pic^- anions showed a decrease in substitution rate with an increase in pH (Roodt *et al*., 1994:599). The calculated k_2 values of 4.1(2) and 2.64(3)$M^{-1}s^{-1}$ are a factor 10^3 faster than k_1 pathway (aqua substitution) (**Tables 6.6**). These results are quite novel in the sense that all the previous studies, except maybe for the substitution between $[ReN(H_2O)(CN)_4]^{2-}$ and CN^-, indicated that the hydroxo complexes are normally inert with respect to substitution. There are, however, examples where the substitution of a hydroxo ligand has about the same effect as the substitution of the aqua ligand. For example, it was reported during the reaction between $[MoO(H_2O)(CN)_4]^{2-}$ and 1,10-phenanthroline that the value of k_2 is about four times greater than the value of k_1 (Leipoldt *et al*., 1987:57). In the case of the reaction between $[ReN(H_2O)(CN)_4]^{2-}$ and CN^- a hydroxo substitution rate of $1.5(4)\times10^1$ $M^{-1}s^{-1}$ was obtained, but due to the large error, this value was interpreted as zero and, therefore, non-reactive towards incoming ligand.

As mentioned earlier (**Paragraph 6.3.1**), the rate of fast reactions at high pH (*ca.* 12.0) could not be determined accurately due to very small absorbance change. Therefore, these results were not included in this study. A possible explanation for this

novel observation is a change from a largely dissociated mechanism during the aqua substitution, from the coordinated sphere to more associated mechanism with the hydroxo substituent. However, this is speculative and more accurate information is needed to substantiate this fact.

The acid dissociation constants, $pK_{a(ReH2O)}$, for the $[ReN(\eta^2\text{-pic})(CN)_3]^{2-}$ and $[ReN(\eta^2\text{-quin})(CN)_3]^{2-}$ complexes were kinetically determined as 11.43(2) and 11.39(1), respectively (**Figures 6.5 and 6.18**). These values correspond very well with the 11.6(2) that was previously determined by Damoense *et al*. (1994:619).

The activation enthalpy and entropy for these two reactions were calculated by using both forwards and reverse rate constants values (k_1 and k_{-1}) obtained at three different temperatures (see **Table 6.2** and **6.4**). The relatively small activation enthalpies and entropies obtained for the first fast reaction in this study are compatible with the $\Delta H^{\neq}$ = 70(9) $kJmol^{-1}$ and $\Delta S^{\neq}$ = -12(31) $JK^{-1}mol^{-1}$ for k_1 and $\Delta H^{\neq}$ = 70(16) $kJmol^{-1}$ and $\Delta S^{\neq}$ = -14(50) $JK^{-1}mol^{-1}$ for k_{-1} values obtained for the corresponding reaction between $[WO(H_2O)(CN)_4]^{2-}$ with picolinate anions (Roodt *et al*., 1994:599).

Correlation of the kinetic results for aqua/hydroxo ligand reaction with other known $[MX(L\text{-}L)(CN)_3]^{n-}$ complexes (M = Mo(IV), W(IV) and Mn(V), X = O^{2-} or N^{3-}) are given in **Table 6.7**.

Table 6.7: Kinetic data for the reaction of $[MX(H_2O)(CN)_4]^{n-}$ complexes with different bidentate ligands (L-L) at 25.0, 20.0°C and 40°C.

M	X	L-L	pK_{a1}	k_1 / $M^{-1}s^{-1}$	K_1 / M^{-1}	k_2 / $M^{-1}s^{-1}$	K_2[j] M^{-1}	K' [d] / M^{-1}
Mo(IV)	O	phen[e]	10.24(7)	$2.68(2)\times10^{-1}$[a]	558(20)[a]	-	-	560(30)[a]
	O	bipy[f]		0.26(1)[a]	$3.8(3)\times10^{2}$[a]	-	-	1.1(1)[a]
W(IV)	O	pic[g]	7.4(2)	0.45(5)[b]	1.0(2)[b]	-	9.4(2)[b]	13(2)[a]
Mn(V)	N	pic [g]	13.6(6)	$1.15(4)\times10^{-3}$[a]	37[a]	-	-	33(4)[a]
	N	2,3-dip[g]	13.3(2)	$1.1(1)\times10^{-3}$[a]	15[a]	-	-	6.4(6)[a]
	N	2,4-dip [g]		$8.5(5)\times10^{-4}$[a]	27[a]	-	-	30(4)[a]
	N	2,5-dip[g]		$1.98(4)\times10^{-3}$[a]	20[a]	-	-	43(4)[a]
Re(V)	N	pic[h]	11.43(2)	$2.1(1)\times10^{-2}$[b]	1.0(2)[b]	4.1(2)[c]	-	8.01(1)
	N	quin[h]	11.39(1)	$2.17(5)\times10^{-2}$[b]	1.06(3)[b]	2.64(3)[c]	-	5.06(3)

[a] 25°C; [b] 20°C; [c] 40°C; [d] K_{eq} = overall equilibrium constant; [e] Leipoldt *et al*., (1987:57); [f] Somatus *et al*., (1991:614); Roodt *et al*., (1994:599); [g] Van der Westhuizen, (2004:109, b); [h] This work; [j] k_2 = hydroxo substitution reaction (reaction **D**, **Scheme 6.1**).

The final products of these reactions, as well as a number of iso-electronic complexes all revealed that the pyridine or quinoline nitrogen atom of the incoming group is situated *trans* with respect to the cyano ligand in an equatorial plane. The kinetic results of all the ligands studied showed that the substitution of the CN^- group (ring-closing step) by the pyridine or quinoline nitrogen atom of the pic^-, $quin^-$ and 2,3-$dipic^-$ was substantially slower than the aqua substitution and these reactions were studied at higher temperatures. It is anticipated that the more strongly bonded cyano ligand would be much more difficult to substitute than the more labile aqua ligand, hence the slower ring-closure step.

Correlation of the kinetic results obtained for the slow reactions between the $[ReN(H_2O)(CN)_4]^{2-}$ complex with picolinate, quinolinate and 2,3-dipicolinate respectively, are shown in **Table 6.8**.

Table 6.8: Kinetic data for the reactions of $[ReN(H_2O)(CN)_4]^{2-}$ complex with pic^-, $quin^-$ and 2,3-$dipic^-$ ligands (see also Scheme 6.1).

Constants	pic^-	$quin^-$	2,3-$dipic^-$
80.0°C			
k_3K_1[a] ($M^{-1}s^{-1}$)	$1.23(3)\times10^{-3}$	$4.17(4)\times10^{-3}$	$4.68(7)\times10^{-3}$
k_{-3}[a] ($M^{-1}s^{-1}$)	$4.2(2)\times10^{-4}$	$9.2(2)\times10^{-4}$	$5.13(4)\times10^{-4}$
k_3[b] (s^{-1})	$1.85(2)\times10^{-2}$	$2.12(3)\times10^{-2}$	$1.83(1)\times10^{-2}$
k_{-3}[b] ($M^{-1}s^{-1}$)	$7.72(1)\times10^{-4}$	$1.39(3)\times10^{-3}$	$7.95(4)\times10^{-4}$
K_1[b] (M^{-1})	$6.61(1)\times10^{-2}$	$3.9(1)\times10^{-2}$	$1.03(4)\times10^{-1}$
K_2[b] (M^{-1})	13.99(3)	3.3(1)	14.56(2)
$pK_{a(ReH2O)}$[b]	11.54(6)	11.51(8)	11.41(1)
$pK_{a(ReH2O)}$[h]	11.09(3)	11.58(3)	11.54(2)
k_3[c] (s^{-1})	$1.84(2)\times10^{-2}$	$8.7(1)\times10^{-3}$	$2.1(2)\times10^{-2}$
K_2[c] (M^{-1})	14.8(1)	4.33(1)	12.26(6)
k_3[d] (s^{-1})	$6.8(1)\times10^{-2}$	$7.5(4)\times10^{-2}$	$6.7(3)\times10^{-2}$
k_{-3}[d] ($M^{-1}s^{-1}$)	$9.3(1)\times10^{-5}$	$9.2(2)\times10^{-4}$	$4.94(2)\times10^{-4}$
K_1[d] (M^{-1})	$6.60(1)\times10^{-2}$	$6.1(3)\times10^{-2}$	$8.36(4)\times10^{-2}$
$pK_{a(L-L)}$[d]	5.29(2)	4.36(1)	4.87(1)
K'_3[e] (M^{-1})	731.2(1)	82.0(2)	135.6(1)
K_{eq}[f]	8.01(1)	5.06(3)	9.03(5)
K_1[g] (M^{-1})	$6.62(1)\times10^{-2}$	$5.6(2)\times10^{-2}$	$1.3(1)\times10^{-1}$
70.0°C			
k_3K_1[a] ($M^{-1}s^{-1}$)	$6.3(3)\times10^{-4}$	$2.58(5)\times10^{-3}$	$2.35(3)\times10^{-3}$
k_{-3}[a] ($M^{-1}s^{-1}$)	$2.8(1)\times10^{-4}$	$6.38(3)\times10^{-4}$	$3.8(1)\times10^{-4}$
k_3[c] (s^{-1})	$1.01(2)\times10^{-2}$	$5.2(1)\times10^{-3}$	$1.63(4)\times10^{-2}$
K_2[c] (M^{-1})	14.1(2)	3.2(1)	7.27(6)
K_1[g] (M^{-1})	$6.3(1)\times10^{-2}$	$6.5(4)\times10^{-1}$	$1.44(1)\times10^{-1}$
60.0°C			
k_3K_1[a] ($M^{-1}s^{-1}$)	$1.96(6)\times10^{-4}$	$7.84(4)\times10^{-4}$	$6.1(9)\times10^{-4}$
k_{-3}[a] ($M^{-1}s^{-1}$)	$1.7(4)\times10^{-4}$	$5.15(3)\times10^{-4}$	$3.03(5)\times10^{-4}$
k_3[c] (s^{-1})	$6.04(1)\times10^{-3}$	$2.5(1)\times10^{-3}$	$7.8(1)\times10^{-2}$
K_2[c] (M^{-1})	9.5(1)	1.14(7)	6.83(2)
K_1[g] (M^{-1})	$3.2(5)\times10^{-2}$	$6.3(5)\times10^{-1}$	$7.8(2)\times10^{-2}$
$\Delta H^{\neq}$ ($kJmol^{-1}$)[i]	51.7(5)	71.4(3)	47.3(2)
$\Delta S^{\neq}$ ($JK^{-1}mol^{-1}$)[i]	-133.4(3)	-83.5(2)	-144.1(3)

[a] Slope and intercept, Figure 6.8, 6.21 and 6.29, Eq. 6.8; [b] Data in Fugure 6.9, 6.22 and 6.30, Eq. 6.7; [c] Data in Figure 6.10, 6.23 and 6.31, Eq. 6.7; [d] Data in Figure 6.11, 6.24 and 6.32, Eq. 6.9; [e] $K_3=k_3/k_{-3}$; [f] Data in Figure 6.2 and 6.15, Eq. 6.11; [g] $K_1=k_3K_1/k_3$; [h] Data in Figure 6.2 and 6.15, Eq. 6.13; [i] Temperature dependence, Figure 6.13, 6.25 and 6.33, Eq. 6.10.

The values for the cyano substitution (k_3K_1) for the $[ReN(\eta^1\text{-L-L})(CN)_4]^{3-}$ to form the final $[ReN(\eta^2\text{-L-L})(CN)_3]^{2-}$ complex (see **Eq. 6.8**) at 80ºC was determined as $1.23(3)\times10^{-3}$, $4.17(4)\times10^{-3}$ and $4.68(7)\times10^{-3}$ $M^{-1}s^{-1}$ respectively (**Table 6.8**). These values emphasize the relative difficulty of the CN^- substitution by these bidentate ligands. Furthermore, k_3 values were determined as $1.85(2)\times10^{-2}$, $2.12(3)\times10^{-2}$ and $1.83(1)\times10^{-2}$ (s^{-1}) respectively. As indicated above, it is clear that the displacement of an equatorial cyano ligand and the ring-closure by the pyridine or quinoline nitrogen atom is much slower than the substitution of the aqua ligand by the carboxylate oxygen atom of the picolinate and quinolinate anions. This can be seen by comparing the k_1 and k_3 values. The value of k_3 is a factor 10 slower than the value of k_1 (**Tables 6.2, 6.4** and **6.8**).

The pH variation as indicated in **Figures 6.9**, **6.22** and **6.30**, clearly shows an increase in substitution rate with an increase in pH. Similar behaviour was observed for the fast reactions. The stability constants calculated from the kinetic results of $[ReN(\eta^2\text{-L-L})(CN)_3]^{2-}$ clearly show that the k_2 pathway, with K_2 = 13.99(3), 3.3(1), and 14.56(2) M^{-1} compared to K_1 = $6.61(1)\times10^{-2}$, $3.9(1)\times10^{-2}$ and $1.03(4)\times10^{-1}$ M^{-1}, respectively, is favoured above the k_1 pathway for the fast reactions (**Tables 6.8**), while the equilibrium constants, K_3 values of 731.2(1), 82.0(2) and 135.6(1) M^{-1}, respectively, are substantially larger than the previous two equilibrium constants (K_1 and K_2) (see **Table 6.8**). These results indicate an increase towards thermodynamic stability which is normally associated with chelation reactions.

The equilibrium constant values of 8.01(1), 5.06(3) and 9.03(5) M^{-1} obtained in this study can be compared with 1.0(2) M^{-1} and $5.6(3)\times10^2$ M^{-1} values obtained for the reaction between $[WO(H_2O)(CN)_4]^{2-}$ with pic^- and between $[MoO(H_2O)(CN)_4]^{2-}$ with phen (Roodt *et al*., 1994:599; Leipoldt *et al*., 1987:57). The large overall equilibrium constants reported for the molybdenum(IV) system is the overall equilibrium constant (K'). Since only one reaction was observed and it was thought that the aqua substitution is the rate-determining step of the two-step process.

The relative difference in metal-ligand bond strength of the equatorial cyano ligand compared to the aqua ligand *trans* to the nitrido ligand can be illustrated by the difference

in bond distances of the $[ReN(CN)_5]^{2-}$ complex with cyano ligands in both equatorial position and *trans* to the terminal nitrido ligand (Purcell *et al*., 1991:473). The $Re\text{-}CN_{(eq)}$ bond distance for cyano ligand (bonded equatorial plane) is 2.12(1)Å (average), while the $Re\text{-}CN_{(trans)}$ bond distance (bonded *trans* to the terminal nitrogen ligand) is 2.39(1)Å. It is also expected that the $Re\text{-}OH_2$ bond distance will be even longer than the $Re\text{-}CN_{(trans)}$ bond distance. The same tendency was found for the manganese(V) system in the $[MnN(CN)_5]^{3-}$ complex, with $Mn\text{-}CN_{(eq)}$ = 1.990(6)Å (average) compared to $Mn\text{-}CN_{(trans)}$ = 2.243(7)Å and the even longer $Mn\text{-}OH_2$ bond distance of 2.001(1)Å in the $[MnN(H_2O)(CN)_4]^{2-}$ complex (Van der Westhuizen, 2004:109, b).

The acid dissociation constants, $pK_{a(ReH2O)}$ values for $[ReN(H_2O)(CN)_4]^{2-}$ complex, were kinetically determined as 11.54(6), 11.51(8) and 11.41(1) and spectrophotometrically as 11.09(3), 11.58(3) and 11.54(2) respectively (**Table 6.8**). These values are in good agreement with each other as well as with those values obtained for the fast reactions.

The reaction of $[ReN(H_2O(CN)_4]^{2-}$ with picolinate, quinolinate and 2,3-dipicolinate anions respectively, was also performed at lower pH values (pH *ca*. 4.0) where the incoming bidentate ligands changed from the acid form to the free anion. The kinetic results obtained at low pH values (k_4, $k_{-4} \sim 0$) yielded a $pK_{a(picH)}$, $pK_{a(quinH)}$ and $pK_{a(2,3\text{-}dipic)}$ values of 5.29(2), 4.36(1) and 4.87(1) for the picolinate, quinolinate and 2,3-dipicolinate anions respectively. These pK_a values agree very well with the literature values of 5.02, 4.97 and 5.02 for these different acids (see **Table 6.1**).

The activation entropies, $\Delta S^{\neq}$, for the slow reaction for the different bidentate ligands are clearly negative (-133.4(3), -83.5(2) and -144.1(2) $JK^{-1}mol^{-1}$), indicating an associative activation during the last step of these reactions. It is anticipated that the strongly bonded cyano group will not dissociate easily and that substantial bond formation between the bidentate ligands (pic^-, $quin^-$ and $2,3\text{-}dipic^-$) and the metal complex takes place before the dissociation of the cyanide group. An increase in coordination number for these transition metal complexes is well known, for example the isolation of the $[Re(CN)_7]^{4-}$ complex (Manoli *et al*., 1980:192). The free energy of activation, $\Delta G^{\neq}$, for the fast reaction (81.03 $kJmol^{-1}$) between, for example, $[ReN(H_2O)(CN)_4]^{2-}$ and $[pic]_T$, has a very large contribution from the activation enthalpy (82.5 $kJmol^{-1}$), indicating that this particular

reaction is mainly enthalpy driven. The $\Delta G^{\neq}$ for the slow reaction of 98.8 kJmol^{-1}, on the other hand, has a large activation entropy component (47.1 kJmol^{-1}), pointing to a substantial entropy contribution in the final reaction. These results also tie in strongly with the suggestion that an increase in substitution rate at high pH suggests an increase in the associative nature of the mechanism.

Additional free cyanide ions were added to different solutions containing $[ReN(\eta^2\text{-pic})(CN)_3]^{2-}$, $[ReN(\eta^2\text{-quin})(CN)_3]^{2-}$ and $[ReN(\eta^2\text{-dipic})(CN)_3]^{2-}$complex in an effort to investigate the reverse reaction of the slow chelating step (k_{-3} in **Scheme 6.1**). A relatively fast reaction was observed (similar to that in **Figure 6.12**), and a $[CN^-]$ variation clearly showed a linear dependence in cyanide concentration. The slope (supposed to be k_3) is, however, an order of magnitude smaller than the values obtained for the k_{-3} pathway. The UV/VIS spectra of the final products $[ReN(\eta^2\text{-pic})(CN)_3]^{2-}$, $[ReN(\eta^2\text{-quin})(CN)_3]^{2-}$ and $[ReN(\eta^2\text{-dipic})(CN)_3]^{2-}$ complexes with the addition of the CN^- also show absorption maxima at 273 and 422nm for $[ReN(\eta^2\text{-pic})(CN)_3]^{2-}$, 275 and 430 nm for $[ReN(\eta^2\text{-dipic})(CN)_3]^{2-}$ and at 400 nm for $[ReN(\eta^2\text{-quin})(CN)_3]^{2-}$. These results suggest that the reaction sequence between $[ReN(\eta^2\text{-L-L})(CN)_3]^{2-}$ and CN^- ions was as follows:

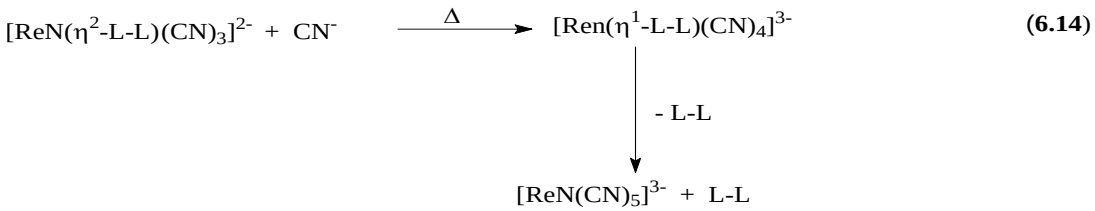

(6.14)

The bidentate anions (L-L) have thus been completely substituted in a two-step process from the coordination sphere. Further research and information is needed to verify this reaction process. A research or more information is needed to verify these types of reactions (**Eq. 6.14**, ring-opening).

7 EVALUATION OF THE STUDY

7.1 SCIENTIFIC RELEVANCE OF THIS STUDY

The chemical relevance and results of this study are briefly discussed according to the goals which were established in **Chapter1**.

This study was initiated by conducting a thorough literature search, gathering all applicable practical and theoretical information. This research revealed that a number of nitridocyano complexes of rhenium(V) with different monodentate nucleophiles, such as CN^- and N^{3-}, has already been reported and none of the bidentate nucleophiles has been reported in literature. The reported procedure for the synthesis of nitridotetracyanorhenate(V) complex ($[ReN(H_2O)(CN)_4]^{2-}$) was subsequently used as a starting compound for the synthesis of the substituted products that contain the bidentate ligands of choice. The model complexes were thoroughly characterized using a variety of techniques, including IR, UV/VIS spectroscopy and X-ray crystallography.

The ligand systems included in this study were the different bidentate nucleophiles [pyridine-2-carboxylate (pic^-), quinoline-2-carboxylate ($quin^-$), 2,2'bipyridine (bipy), 1,10-phenanthroline (phen) and pyridine-2,3-dicarboxylate ($2,3\text{-}dipic^-$)]. Most of the isolated complexes were studied structurally and kinetically (see **Chapter 4**). An attempt to prepare and isolate the $[ReN(\eta^2\text{-phen})(CN)_3]^{2-}$ and $[ReN(\eta^2\text{-bipy})(CN)_3]^{2-}$ complexes was unsuccessful, due to the low solubility of these ligands in aqueous solution.

The complexes containing the above-mentioned bidentate ligands gave valuable information about the bonding capabilities of the ligands in this system, as well as the geometry of the complexes investigated. The crystallographic studies of the $[ReN(\eta^2\text{-pic})(CN)_3]^{2-}$ and $[ReN(\eta^2\text{-quin})(CN)_3]^{2-}$ complexes showed that both aqua and cyano ligands in an equatorial plane are substituted by an incoming N,O ligands. The nitrido ligand is bonded normally to the original tetracyano equatorial plane, the latter being constituted of three cyano ligands and a pyridine nitrogen of the picolinate or

quinolinate ligand. The carboxylate oxygen completes the chelate ring *trans* to the terminal nitrido ligand (see **Chapter 5**). This is the first study of a nitridotetracyano rhenium(V) complex in which bidentate ligands are bonded to the metal centre.

An interesting result obtained in this study is the first crystal structure determination of rhenium(V) containing a cyano-bridge between two rhenium atoms, ($[ReN(H_2O)(CN)_3$-μ-CN-$ReN(CN)_4]^{4-}$), which was isolated during the reaction between $[ReN(H_2O)(CN)_4]^{2-}$ complex and pyridine-2,3-dicarboxylate. It was expected that a bidentate ligand such as 2,3-dipic$^-$ will behave similarly to picolinic acid and coordinate to the metal centre (Re(V)), with the substitution of both aqua and one cyano ligand in $[ReN(H_2O)(CN)_4]^{2-}$. A second crystal modification of the $[ReN(H_2O)(CN)_4]^{2-}$ complex was also isolated.

Kinetic investigation of the ligand systems was limited to the ligands with a high solubility in an aqueous medium (pyridine-2-carboxylate (pic$^-$), quinoline-2-carboxylate (quin$^-$) and pyridine-2,3-dicarboxylate (2,3-dipic$^-$)). The kinetic investigations were undertaken to correlate the behaviour of these complexes with the structural properties as well as with the previously studied systems. All the kinetic reactions between $[ReN(H_2O)(CN)_4]^{2-}$ complex and different bidentate ligands showed a two-step reaction process. The first reaction was relatively fast with a decrease in absorbance followed by a much slower reaction with an increase in absorbance. These two different reactions were monitored at different temperatures (see **Chapter 6**).

The fast reaction between $[ReN(H_2O)(CN)_4]^{2-}$ with 2,3-dipic$^-$ could not be studied due to small absorbance change of the reaction progress. The same reaction **Scheme 6.1** was proposed for all the bidentate ligands studied, and the kinetic results obtained correspond very well with each other and with those of the other known cyano complexes of the type $[MX(L\text{-}L)(CN)_3]^{n-}$ with κ^2-N,O ligands. The kinetically and spectrophotometrically determined acid dissociation constants ($pK_{a(ReH2O)}$) are in agreement with each other and with those reported in literature.

This study succeeded in describing the substitution between nitridotetracyano complexes of rhenium(V), the first 3rd-row element investigated containing a nitrido axial ligand, as

well as some of the N,O-bidentate ligand systems chosen. The existing knowledge concerning the reactivity of the nitridocyano complexes of group 7 was expanded by the crystallographic and kinetic investigation of the bidentate substituted complexes containing the rhenium(v) metal centre.

In general, it is concluded that the study, based on the goals set in **Chapter 1**, was successfully completed and much new scientific knowledge was gained in this process.

7.2 FUTURE RESEARCH

Although an associative mechanism for the reaction of $[ReN(H_2O)(CN)_4]^{2-}$ with bidentate ligands is predicted (chelate-ring closure step) based on the other known complexes, more evidence is needed to confirm its existence. More complete studies of other transition metal complexes of groups 6 and 7 performed at high temperatures is needed to help in verifying the proposed reaction scheme as well as some of the kinetic results obtained in this study.

Crystallographic and kinetic studies of the reaction between the $[ReN(H_2O)(CN)_4]^{2-}$ and pyridine-2,3-carboxyalte is needed in order to isolate the formation of the final product.

An investigation of the effect of added free cyanide ligands onto the final reaction mixture of $[ReN(L\text{-}L)(CN)_3]^{2-}$ would provide more information on the reverse rate of these substitution reaction (k_{-3} in **Scheme 6.1**).

An investigation of electrochemical properties (electrochemistry) of the formed products by means of cyclic voltammetry in several solvents would provide information on the redox reaction process.

LIST OF REFERENCES

ABOU-HAMDAN, A., ROODT, A. & MERBACH, A.E. 1998. *Inorg. Chem*., **37**:1278.

ARZOUMANIANN, H., PIERROT, M., RIDOUANE, F. & SANCHEZ, J. 1991. *Transition Met. Chem.*, **16**:422.

ASCHROFT, S.J. & MORTIMER, C.T. 1970. *Thermochemistry of Transition Metal Complexes*. New York: Academic Press. p. 445.

BAILAR, J.C. & BUSCH, D.H. 1956. *Chemistry of the Coordination Compounds.* New York. London: Chapman and Hall. Ltd.
(a) p. 115 (b) p. 244 (c) p. 251 (d) p. 227 (e) p. 237.

BALDAS, J., BOAS, J.F., COLMANET, S.F. & MACKAY, M.F. 1990. *Inorg. Chim. Acta*, **170**:233.

BASOLO, F. & JOHNSON, R.C. 1986. *Coordination Chemistry*. Northwood: Science Review.
(a) p. 2 (b) p. 3 (c) p. 7.

BASOLO, F. & MURMANN, R.K. 1954. *J. Am. Chem. Soc*., **76**:211.

BASOLO, F. & MURMANN, R.K. 1952. *J. Am. Chem. Soc*., **74**:5243.

BASOLO, F. & PEARSON, R.G. 1967. *Mechanism of Inorganic Chemistry*. 2nd Edition. New York: John Wiley and Sons. Inc. p. 225.

BASSON, S.S., LEIPOLDT, J.G. & POTGIETER, I.M. 1984. *Inorg. Chim. Acta*, **87**:71.

BASSON, S.S., LEIPOLDT, J.G. & POTGIETER, I.M. 1984. *Inorg. Chim. Acta*, **90**:57.

BASSON, S.S., LEIPOLDT, J.G., POTGIETER, I.M. & ROODT, A. 1985. *Inorg. Chim. Acta*, **103**:121.

BASSON, S.S., LEIPOLDT, J.G., ROODT, A. & PURCELL, W. 1987. *Transition Met. Chem*., **12**:82.

BOTHA, J.M. 1995. *Mechanistic Aspects of Model Tc(V) and Re(V) Complexes of Relevance to Nuclear Medicine*. University of the Orange Free State: Department of chemistry. Faculty of Science. Ph.D. Thesis. (a) p. 20, (b) p. 35

BRANDENBURG, K. & PUTZ, H. 2005. *Version 3.0* (Crystal Impact GbR). Germany: Postfach 2151. D-53002.

BRESLOW, R., BELVELDERE, S., GERSHELL, L. & LEUNG, D. 2000. *Pure Appl. Chem*., **72**, 3:333.

BRUKER. 1999. SAINT+. *Version 6.02* (includes XPREP and SADABS). Madison. USA: Bruker AXS Inc.

BRUKER. 1999. SHELXTL. *Version 5.1* (includes XS, XL, XP, XSHELL). Madison. Wisconsin. USA: Bruker AXS Inc.

BUCKNALL, W.R. & WARDLOW, W. 1927. *J. Chem. Soc*., p. 2981.

CALVIN, M. & BAILES, R.H. 1946. *J. Am. Chem. Soc*., **68**:949.

CALVIN, M. & WILSON, K.W. 1945. *J. Am. Chem. Soc*., **67**:2003.

CANIC, G. 1955. *Glas. Hem. Drus. Beograd*., **29**:35.

CHAKRAVORTI, M.C. 1972. *J. Inorg. Nucl. Chem*., **34**:893.

CHATT, J. & ROWE, G.A. 1962. *J. Chem. Soc*., **A**:4019.

CHATT, J., FALK, C.D., LEIGH, G.J. & ROSEMARY, J.P. 1969. *J. Chem. Soc*., **A.** p. 2288.

CHATT, J., GARFORTH, J.D. & ROWE, G.A. 1963. *Chem. and Ind*., p. 332.

CHATT, J., GARFORTH, J.D., JOHNSON, N.P. & ROWE, G.A. 1964. *J. Chem. Soc*., p. 1012.

CHE, C.-M., LAM, M.H. & MAK, T.C.W. 1989. *J. Chem. Soc., Chem. Commun*., p. 1529.

CLIFFORD, A.F. & OLSEN, R.R. 1960. *Inorg. Synth*., **6**:167.

COLLENBERG, O. 1924. *Z. Anorg. Allg. Chem*., **136**:246.

COTTON, F.A. & LIPPARD, S.J. 1968. *Inorg. Chem*., **7:**1621.

COTTON, F.A., WILKINSON, G. & GAUS, P.L. 1995. *Basic Inorganic Chemistry*. 3rd Edition. USA: John Wiley and Sons. Inc. p. 186.

DAMOENSE, L.J., PURCELL, W. & LEIPOLDT, J.G. 1994. *Transition Met. Chem*., **19**:619.

DAVIES, D.D. & WATT, G.W. 1948. *J. Am. Chem. Soc*., **70**:2041.

DAVIES, W.O. & MORGAN, G. 1938. *J. Chem. Soc.*, p. 1858.

DAVIES, W.O., JOHNSON, N.P., JOHNSON, P. & GRAHAM, A.J. 1969. *Chem. Commum*., p. 736.

DAY, V.W. & HOARD, J.L. 1968. *J. Am. Chem. Soc*., **90**:3374.

DEY, A.K. 1947. *Chem. Abs*., **41**:6169.

DIEBLER, H. & ROSEN, P.H. 1972. *Ber. Bunsenges. Phys. Chem*., **76**:1031.

DIEHL, H. 1937. *Chem. Rev*., **21**:39.

DUDEK, M. & SAMOTUS, A. 1985. *J. Inorg. Nucl. Chem*., **42**:1701.

DUDEK, M. & SAMOTUS, A. 1985. *Transition Met. Chem*., **10**:271.

DUDEK, M., KANAS, A. & SAMOTUS, A. 1980. *J. Inorg. Nucl. Chem*., **42**:1710.

DWYER, F.P. & MELLOR, D.P. 1964. *Chelating Agents and Metal Chelates*. New York. London: Academic Press.

(a) p. 7 (b) p. 17 (c) p. 42 (d) p. 43 (e) p. 44 (f) p. 45 (g) p. 31 (h) p. 19.

EIGEN, M. 1963. *Pure Appl. Chem*., **6**:97.

EISENHUT, M. 1982. *Int. J. Appl. Radiat. Isot*., **33**:99.

FRITSCHE, J. & STRUVE, H. 1847. *J. prakt. Chem*., **41:**97.

GARCIA, B., IBEAS, S. & LEAL, J.M. 1996. *J. Phys. Org. Chem.*, **9**:593.

GERBER, T.I.A., BRUWER, J., BANDOLI, G., PERILS, J. & DU PREEZ, J.G.H. 1995. *J. Chem. Soc. Dalton Trans*., p. 2189.

GRIFFITH, W.P. & PAWSON, D. 1973. *J. Chem. Soc., Dalton Trans*., p. 1315.

HARMON, K.M., BROWN, P.W. & GILL, S.H. 1988. *J. Mol. Struct*., **448**:43.

HEMJO, E., KANAS, A. & SAMOTUS, A. 1973. *Bull. Acad. Pol. Sci., Sci. Chim*., **21**:311.

HOFFMAN, R. 1988. *A Chemist's View of Bonding in Extended Structures*. VCH. New York: p. 16.

IRVING, H. & WILLIAMS, R.J.P. 1948. *Nature*, **162**:746.

JOHNSON, N.P. 1969. *J. Chem. Soc.*, **A**:1843.

JONES, M.M. 1964. *Elemental Coordination Chemistry*. Englewood Cliffs: Prentice Hall.

(a) p. 1 (b) p. 19.

KEISSLING, D., NAGORSNIK, E., THOMAS, P. & HENNING, H. 1980. *J. Prakt. Chem*., **322**:843.

KIRSCHENBAUM, L.J. & KUSTIN, K. 1970. *J. Chem. Soc*., **A**:684.

KOWAL, A., KUSTIN, K., PASTERNACK, R.F. & PETRUCI, S. 1967. *J. Am. Chem. Soc.*, **89**:3126.

KRAUS, F., & SCHRADER, G. 1928. *J. Prakt. Chem*., **30**:36.

KUSTIN, K. & PASTERNACK, R.F. 1968. *J. Am. Chem. Soc*., **90**:2805.

KUSTIN, K., PASTERNACK, R.F. & WEINSTOCK, E.M. 1966. *J. Am. Chem. Soc.*, **88**:4610.

LEIPOLDT, J.G., BASSON, S.S. & ROODT, A. 1993. *Adv. Inorg. Chem.*, **40**:289.

LEIPOLDT, J.G., BASSON, S.S. & ROODT, A. 1993. *Adv. Inorg. Chem.*, **40**:241.

LEIPOLDT, J.G., BASSON, S.S., POTGIETER, I.M. & ROODT, A. 1987. *Inorg. Chem.*, **26**:57.

LEIPOLDT, J.G., BASSON, S.S., ROODT, A. & POTGIETER, I.M. 1986. *Transition Met. Chem.*, **11**:323.

LEIPOLDT, J.G., BASSON, S.S., ROODT, A. & POTGIETER, I.M. 1986. *S. Afr. J. Chem.*, **39**:179.

LEIPOLDT, J.G., BASSON, S.S., ROODT, A. & PURCELL, W. 1987. *Transition Met. Chem.*, **12**:209.

LEIPOLDT, J.G., BASSON, S.S., ROODT, A. & PURCELL, W. 1992. *Polyhedron*, **11**:2277.

LEIPOLDT, J.G., BOK, L.D.C. & CILLIERS, P.J. 1974. *Z. Anorg. Allg. Chem.*, **407**:350.

LEIPOLDT, J.G., VAN ELDIK, R., BASSON, S.S. & ROODT, A. 1986. *Inorg. Chem.*, **25**:4639.

LEIPOLDT, J.G., BOK, L.D.C. & CILLIERS, P.J. 1974. *Z. Anorg. Allg. Chem.*, **409**:343.

LIN, C. & RORABACHER, D.B. 1973. *Inorg. Chem.*, **12**:2402.

LIPPARD, S.J. & RUSS, B. 1967. *Inorg. Chem.*, **6**:1943.

LOCK, C. J. L. & WILKINSON, G. 1964. *J. Chem. Soc.*, p. 2281.

LUMME, P.O., TURPEINEN, U. & STASICKA, Z. 1991. *Acta Crystallogr., Sect. C: Cryst. Struct. Commun.*, **C47**:501.

MANOLI, J.-M., POTVIN, C. & BRĚGEAULT, J.C.S. 1980. *J. Chem. Soc. Dalton Trans.* 192.

MARGERUM, D.W., CALEY, G.R., WEATHERBURN, D.C. & PAKENKOPF, G.W. 1978. *Coordination Chemistry*. **2**. *American Chemical Siciety*. Washington. D.C: p. 42.

MARTELL, A.E. & CALVIN, M. 1952. *Chemistry of the Metal Chelate Compounds*. New York: Prentice Hall.
(a) p. 150 (b) p. 151.

MARTELL, A.E. & SMITH, R.M. 1982. *Critical Stability Constants*. New York: Plenum Press. p. 129.

MARTELL, E.A. 1978. *Coordination Chemistry*. American Chemical Society. Washington. D.C:
(a) p. 2 (b) p. 26 (c) p. 32 (d) p. 48.

MATHIEU, L., CHEVALIER, P., GALY, G. & BERGER, M. 1979. *Int. J. Appl. Radiat. Isot*., **30**:725.

MORGAN, G. & DAVIES, G.R. 1938. *J. Chem. Soc*., p. 1858.

MORGAN, G.T. & DREW, H.D.K. 1920. *J. Chem. Soc*., **117**:1456.

MTSHALI, T.N., PURCELL, W., VISSER, H.G. & BASSON, S.S. 2006. *Polyhedron*. accepted for publication.

MURMANN, R.K. & SCHLEMPER, E.O. 1971. *Inorg. Chem*., **10**:2352.

NAGORSIK, E., THOMAS, P. & HOYER, E. 1974. *Inorg. Nucl. Chem. Lett*., **10**:353.

NAKAMOTO, K. 1963. *Infrared Spectra of Inorganic and Coordination Compounds*. 2nd Edition. New York: John Wiley and Sons. p. 222.

PASTERNACK, R.F., ANGWIN, M., GIPP, L. & REINGOLD, R. 1972. *J. Inorg. Nucl. Chem*., **34**:2329.

PASTERNACK, R.F., GIBBS, E. & CASSETT, J.C. 1969. *J. Phys. Chem*., **73**:3814.

PASTERNACK, R.F. & KUSTIN, K. 1968. *J. Am. Chem. Soc*., **90**:2295.

PERILS, J. 1995. *Complexes of Rhenium(V) with Bidentate Nitrogen and Oxygen Donor Ligands*. University of Port Elizabeth: Faculty of Science. M.Sc. Thesis. p. 5.

POTGIETER, I.M., BASSON, S.S., ROODT, A. & LEIPOLDT, J.G. 1988. *Transition Met. Chem.*, **13**:209.

PURCELL, K.F. & KOTZ, J.C. 1977. *Inorganic Chemistry*. Japan: Holt-Saunders International Edition.
(a) p. 739 (b) p. 736 (c) p. 740 (d) p. 738.

PURCELL, W., ROODT, A., BASSON, S.S. & LEIPOLDT, J.G. 1990. *Transition Met. Chem*., **15**:239.

PURCELL, W., ROODT, A., BASSON, S.S. & LEIPOLDT, J.G. 1989. *Transition Met. Chem*., **14**:369.

PURCELL, W., DAMOENSE, L.J. & LEIPOLDT, J.G. 1992. *Inorg. Chim. Acta*, **195**:217.

PURCELL, W., POTGIETER, I.M., DAMOENSE, L.J. & LEIPOLDT, J.G. 1992. *Transition Met. Chem*., **17**:387.

PURCELL, W., POTGIETER, I.M., DAMOENSE, L.J. & LEIPOLDT, J.G. 1991. *Transition Met. Chem*., **16**:473.

PURCELL, W., ROODT, A., BASSON, S.S. & LEIPOLDT, J.G. 1989**.** *Transition Met. Chem*., **14**:5.

PURCELL, W., ROODT, A. & LEIPOLDT, J.G. 1991. *Transition Met. Chem*., **16**:339.

PURCELL, W., ROODT, A., BASSON, S.S. & LEIPOLDT, J.G. 1989. *Transition Met. Chem*., **14**:224.

PURCELL, W., ROODT, A., BASSON, S.S. & LEIPOLDT, J.G. 1991. *Transition Met. Chem*., **16**:60.

PURCELL, W., ROODT, A., BASSON, S.S. & LEIPOLDT, J.G. 1989. *Transition Met. Chem*., **14**:369.

PURCELL, W., VAN DER WESTHUIZEN, H.J., LEIPOLDT, J.G. & BASSON, S.S. 1994. *Transition Met. Chem*., **13**:717.

ROBINSON, P.R., SCHLEMPER, E.O. & MURMANN, R.K. 1995. *Inorg. Chem*., **34**:2035.

ROMEO, R., GRASSI, A. & MONSÙ SCOLARO, L. 1992. *Inorg. Chem*., **31**:4383.

ROODT, A., BASSON, S.S. & LEIPOLDT, J.G. 1994. *Polyhedron*, **13**:599.

ROODT, A., LEIPOLDT, J.G., BASSON, S.S. & POTGIETER, I.M. 1988. *Transition Met. Chem.*, **13**:336.

ROODT, A., LEIPOLDT, J.G., BASSON, S.S. & POTGIETER, I.M. 1990. *Transition Met. Chem.*, **15**:439.

ROODT, A., LEIPOLDT, J.G., DEUTSCH, E.A. & SULLIVAN, J.C. 1992. *Inorg. Chem*., **31**:1080.

ROODT, A., LEIPOLDT, J.G., HELM, L., ABOU-HAMDAN, A. & MERBACH, A.E. 1995. *Inorg. Chem*., **34**:350.

ROODT, A., LEIPOLDT, J.G., HELM, L. & MERBACH, A.E. 1992. *Inorg. Chem*., **31**:2864.

RORABACHER, D.B. 1966. *Inorg. Chem*., **5**:1891.

RORABACHER, D.B. & MELENDEZ-CEPEDA, C.A. 1971. *J. Am. Chem. Soc*., **93**:6071.

SAMOTUS, A., KANAS, A. & DUDEK, M. 1979. *J. Inorg. Nucl. Chem*., **41**:1129.

SAMOTUS, A., KANAS, A., GLUG, W. & SZKLARZEWICZ, J. 1991. *Transition Met. Chem*., **16**:614.

SAMOTUS, A., SZKLARZEWICZ, J. & ALCOCK, N.W. 1990. *Inorg. Chim. Acta*, **172**:129.

SHANDLESS, R., SCHLEMPER, E.O. & MURMANN, R.K. 1971. *Inorg. Chem*., **10**:2785.

SMIT, J.P., PURCELL, W., ROODT, A. & LEIPOLDT, J.G. 1993. *Polyhedron*, **12**:2271.

SMIT, J.P., PURCELL, W., ROODT, A. & LEIPOLDT, J.G. 1995. *Polyhedron*, **14**:1795.

SMIT, J.P. 1995. *Mechanistic study of the Formation and Molecular Oxygen Activation reaction of Oxocyano Molybdate(IV) and Tungsten(IV) Complexes*. University of Free State: Department of Chemistry. Faculty of Science. Ph.D. Thesis. p. 71.

SMITH, J.P., PURCELL, W., LAMPRECHT, G.J. & ROODT, A. 1996. *Polyhedron*, **15**:1389.

SPEK, A.L. 2003. *J. Apply. Cryst*., **36**:7.

SPIKE, C.G. & PARRY, R.W. 1953. *J. Am. Chem. Soc*., **75**:2726 and 3770.

SZKLARZEWICZ, J., MAKULA, A., MATOGA, D. & FAWCETT, J. 2005. *Inorg. Chim. Acta*, **358**:1749.

SZKLARZEWICZ, J., SAMOTUS, A., ALCOCK, N.W. & MOLL, M. 1990. *J. Chem. Soc., Dalton Trans*., p. 2959.

TAYLOR, R.W., STEPIEN, H.K. & RORABACHER, D.B. 1974. *Inorg. Chem*., **13**:1282.

TICHANE, S. & BENNET, T. 1957. *J. Am. Chem. Soc.,* **79**:1293.

TOPPEN, D.L. & MURMANN, R.K. 1970. *Inorg. Nucl. Chem. Lett*., **6**:139.

TROP, H.S., JONES, A.G. & DAVISON, A.N. 1980. *Inorg. Chem*., **19**:1993.

VAN DER POEL, J. & NEUMANN, H.M. 1968. *Inorg. Chem*., **7**:2086.

List of references

VAN DER WESTHUIZEN, H.J. 2004. *Reactivity and Mechanism of Manganese and Related group 6, 7 and 8 Metal Complexes as Models in Homogeneous Oxygen, Nitrogen and Ligand Transfer Reactions*. University of Johannesburg: Faculty of Science. Ph.D. Thesis.
(a) p. 90 (b) p. 109.

VAN DER WESTHUIZEN, H.J., BASSON, S.S. & PURCELL, W. 1994. *Transition Met. Chem*., **19**:582.

VAN DER WESTHUIZEN, H.J., BASSON, S.S., LEIPOLDT, J.G. & POTGIETER, I.M. 1994. *Polyhedron*, **13**:717.

VAN DER WESTHUIZEN, H.J., PURCELL, W. & BASSON, S.S. 2002. *Transition Met. Chem*., **27**:506.

WATT, G.W. & DAVIES, D.D. 1948. *J. Am. Chem. Soc*., **70**:2041.

WIEGHARDT, K., BACKES-DAHMANN, G., HOLZBACH, W.J., SWIRIDOFF, W.J. & WEISS, J. 1983. *Z. Anorg. Allg. Chem*., **499**:44.

WILKINS, R.G., 1970. *Acc. Chem. Res*., **3**:408.

WILKINS, R.G. 1974. *The Study of Kinetics and Mechanism of Reactions of Transition Metal Complexes*. USA: Allyn and Bacon. Inc. p. 196.

WILKINSON, G., GILLARD, R.D. & McCLEVERTY, T.A. 1987. *Comprehensive Coordination Chemistry*. 1st Edition. Oxford. Great Britain: Pergamon Press. **1**:2.

APPENDIX A: SUPPLEMENTARY DATA

1 SUPPLEMENTARY DATA FOR STRUCTURE DETERMINATIONS

Supplementary data for structures discussed in **Chapter 5** are given in this section. For each structure, five table are given under a heading consisting of the formular of the complex for which the structure was studied: (**1**) complete set of atomic coordinates, (**2**) bond distances and angles, (**3**) anisotropic parameters, (**4**) hydrogen coordinated and (**5**) hydrogen bonds.

A1: Crystal Data for $(AsPh_4)_2[ReN(H_2O)(CN)_4]\cdot 5H_2O$ (Paragraph 5.3.1)

Table 1.1: Atomic coordinates ($\times 10^4$) and equivalent isotropic displacement parameters ($Å \times 10^3$) for $(AsPh_4)_2[ReN(H_2O)(CN)_4]5H_2O$. $U_{(eq)}$ is defined as one third of the trace of the orthogonalized U_{ij} tensor.

	x/a	y/b	z/c	U(eq)
Re	7497(1)	290(1)	2897(1)	22(1)
N(1)	5786(2)	3107(2)	2484(2)	35(1)
N(2)	7204(3)	1018(3)	753(2)	45(1)
N(3)	9604(3)	-2307(3)	3075(2)	44(1)
N(4)	8475(3)	-152(3)	4870(2)	42(1)
N(5)	6531(2)	-131(2)	3154(2)	30(1)
O(1)	8924(2)	878(2)	2482(2)	37(1)
C(1)	6421(2)	2122(3)	2637(2)	28(1)
C(2)	7283(3)	767(3)	1515(2)	31(1)
C(3)	8873(2)	-1395(3)	3034(2)	29(1)
C(4)	8136(2)	0(3)	4173(2)	30(1)
As(1)	749(1)	4344(1)	1888(1)	22(1)
C(11)	1896(2)	3030(3)	1650(2)	26(1)
C(12)	1595(3)	2354(3)	1376(2)	32(1)
C(13)	2451(3)	1326(3)	1296(2)	42(1)
C(14)	3593(3)	996(3)	1488(2)	44(1)

C(15)	3886(3)	1676(3)	1747(2)	43(1)
C(16)	3038(3)	2701(3)	1840(2)	35(1)
C(21)	653(2)	5831(2)	1169(2)	24(1)
C(22)	1470(3)	5852(3)	639(2)	31(1)
C(23)	1381(3)	6944(3)	131(2)	40(1)
C(24)	508(3)	7986(3)	156(2)	42(1)
C(25)	-302(3)	7960(3)	674(2)	39(1)
C(26)	-240(3)	6882(3)	1189(2)	31(1)
C(31)	-710(2)	4489(3)	1687(2)	24(1)
C(32)	-908(3)	3615(3)	2289(2)	31(1)
C(33)	-1956(3)	3692(3)	2152(2)	34(1)
C(34)	-2783(3)	4620(3)	1429(2)	35(1)
C(35)	-2577(3)	5477(3)	835(2)	35(1)
C(36)	-1531(3)	5414(3)	956(2)	30(1)
C(41)	1161(2)	3953(3)	3120(2)	24(1)
C(42)	773(2)	4874(3)	3420(2)	28(1)
C(43)	1044(3)	4587(3)	4320(2)	37(1)
C(44)	1677(3)	3410(3)	4901(2)	39(1)
C(45)	2065(3)	2495(3)	4606(2)	36(1)
C(46)	1805(3)	2763(3)	3706(2)	31(1)
As(2)	5665(1)	6454(1)	3386(1)	22(1)
C(51)	5442(2)	7204(3)	4204(2)	24(1)
C(52)	5753(2)	6505(3)	5119(2)	28(1)
C(53)	5477(3)	7073(3)	5709(2)	36(1)
C(54)	4910(3)	8300(3)	5397(2)	40(1)
C(55)	4630(3)	8984(3)	4492(2)	44(1)
C(56)	4897(3)	8435(3)	3890(2)	38(1)
C(61)	5962(2)	7377(2)	2326(2)	24(1)
C(62)	6706(3)	7779(3)	2406(2)	30(1)
C(63)	6934(3)	8442(3)	1645(2)	32(1)
C(64)	6410(3)	8719(3)	816(2)	33(1)
C(65)	5663(3)	8318(3)	739(2)	33(1)
C(66)	5441(3)	7643(3)	1492(2)	30(1)
C(71)	6897(2)	4836(2)	3903(2)	25(1)
C(72)	8003(3)	4605(3)	4081(2)	32(1)
C(73)	8879(3)	3421(3)	4408(2)	39(1)
C(74)	8657(3)	2495(3)	4678(2)	38(1)
C(75)	7562(3)	2729(3)	4488(2)	36(1)

C(76)	6664(3)	3912(3)	4101(2)	30(1)
C(81)	4291(2)	6466(3)	3112(2)	26(1)
C(82)	4265(3)	5892(3)	2574(2)	29(1)
C(83)	3258(3)	5923(3)	2363(2)	37(1)
C(84)	2305(3)	6501(3)	2715(2)	39(1)
C(85)	2342(3)	7046(4)	3263(2)	40(1)
C(86)	3350(3)	7028(3)	3465(2)	32(1)
O(2)	4518(2)	6502(2)	298(2)	47(1)
O(3)	4220(2)	4518(2)	847(2)	45(1)
O(4)	290(3)	99535(3)	1597(3)	83(1)
O(5)	2365(3)	8958(3)	974(2)	58(1)
O(6)	850(3)	531(4)	3401(2)	75(1)

Table 1.2: Bond lengths (Å) and angles (°) for $(AsPh_4)_2[ReN(H_2O)(CN)_4]\cdot 5H_2O$.

Bond lengths	**(Å)**	**Bond lengths**	**(Å)**
Re(1)-N(5)	1.663(2)	C(24)-H(24)	0.9500
Re(1)-C(2)	2.104(3)	C(25)-C(26)	1.391(4)
Re(1)-C(4)	2.108(3)	C(25)-H(25)	0.9500
Re(1)-C(3)	2.117(3)	C(26)-H(26)	0.9500
Re(1)-C(1)	2.118(3)	C(31)-C(36)	1.386(4)
Re(1)-O(1)	2.431(2)	C(31)-C(32)	1.400(4)
N(1)-C(1)	1.147(4)	C(32)-C(33)	1.390(4)
N(2)-C(2)	1.163(4)	C(32)-H(32)	0.9500
N(3)-C(3)	1.155(4)	C(33)C(34)	1.382(4)
N(4)-C(4)	1.150(4)	C(33)-H(33)	0.9500
O(1)-H(1A)	0.94(4)	C(34)-C(35)	1.383(5)
O(1)-H(1B)	0.94(3)	C(34)-H(34)	0.9500
As(1)-C(31)	1.913(3)	C(35)-C(36)	1.393(4)
As(1)-C(41)	1.915(3)	C(35)-H(35)	0.9500
As(1)-C(11)	1.916(3)	C(36)-H(36)	0.9500
As(1)-C(21)	1.916(3)	C(41)-C(46)	1.393(4)
C(11)-C(12)	1.387(5)	C(41)C(42)	1.396(4)
C(11)-C(16)	1.396(4)	C(42)-C(43)	1.392(4)
C(12)-C(13)	1.395(5)	C(42)-H(42)	0.9500
C(12)-H(12)	0.9500	C(43)-C(44)	1.378(5)

C(13)-C(14)	1.396(5)	C(43)-H(43)	0.9500
C(13)-H(13)	0.9500	C(44)-C(45)	1.385(5)
C(14)-C(15)	1.372(6)	C(44)-H(44)	0.9500
C(14)-H(14)	0.9500	C(45)-C(46)	1.395(4)
C(15)-C(16)	1.398(5)	C(45)-H(45)	0.9500
C(15)-H(15)	0.9500	C(46)-H(46)	0.9500
C(16)-H(16)	0.9500	As(2)-C(51)	1.913(3)
C(21)-C(26)	1.395(4)	As(2)-C(81)	1.917(3)
C(21)-C(22)	1.395(4)	As(2)-C(71)	1.917(3)
C(22)-C(23)	1.390(4)	As(2)-C(61)	1.919(3)
C(22)-H(22)	0.9500	C(51)-C(56)	1.384(4)
C(23)-C(24)	1.378(5)	C(51)-C(52)	1.402(4)
C(23)-H(23)	0.9500	C(52)-C(53)	1.395(4)
C(24)-C(25)	1.378(5)	C(52)-H(52)	0.9500
C(54)-C(53)	1.386(5)	C(63)-H(63)	0.9500
C(54)-H(54)	0.9500	C(64)-C(65)	1.394(5)
C(55)-C(56)	1.394(5)	C(64)-H(64)	0.9500
C(55)-H(55)	0.9500	C(65)-C(66)	1.383(4)
C(56)-H(56)	0.9500	C(65)-H(65)	0.9500
C(61)-C(66)	1.393(4)	C(66)-H(66)	0.9500
C(61)-C(62)	1.394(4)	C(71)-C(72)	1.390(4)
C(62)C(63)	1.388(4)	C(71)-C(76)	1.390(4)
C(62)-H(62)	0.9500	C(72)-C(73)	1.394(5)
C(63)-C(64)	1.383(4)	C(72)-H(72)	0.9500
C(73)-C(74)	1.383(5)	C(82)-H(82)	0.9500
C(73)-H(73)	0.9500	C(83)-C(84)	1.398(5)
C(74)-C(75)	1.376(5)	C(83)-H(83)	0.9500
C(74)-H(74)	0.9500	C(84)-C(85)	1.381(5)
C(75)-C(76)	1.401(4)	C(84)-H(84)	0.9500
C(75)-H(75)	0.9500	C(85)-C(86)	1.400(4)
C(76)-H(76)	0.9500	C(85)-H(85)	0.9500
C(81)-C(86)	1.382(4)	C(86)-H(86)	0.9500
C(81)-C(82)	1.396(4)	O(2)-H(2A)	0.95(4)
C(82)-C(83)	1.392(4)	O(2)-H(2B)	0.94(3)
O(3)-H(3A	0.94(4)	O(5)-H(5A)	0.94(3)
O(3)-H(3B)	0.94(3)	O(5)-H(5B)	0.94(4)

O(4)-H(4A)	0.95(6)	O(6)-(H6A)	0.941(13)
O(4)-H(4B)	0.94(5)	O(6)-H(6B)	0.94(5)
Bond angles	**(°)**	**Bond angles**	**(°)**
N(5)-Re-C(2)	100.73(12)	C(13)-As(1)-C(41)	109.19(12)
N(5)-Re-C(4)	99.22(12)	C(31)-As(1)-C(11)	109.90(13)
C(2)-Re-C(4)	160.04(12)	C(41-As(1)-C(11)	105.74(12)
N(5)-Re-C(3)	96.96(12)	C(31)-As(1)-C(21)	108.63(11)
C(2)-Re-C(3)	87.87(11)	C(41)-As(1)-C(21)	110.54(12)
C(4)-Re-C(4)	89.84(11)	C(11)-As(1)-C(21)	112.78(12)
N(5)-Re-C(1)	97.60(12)	C(12)-C(11)-As(1)	119.9(2)
C(2)-Re-C(1)	87.79(11)	C(16)-C(11)-As(1)	118.8(2)
C(4)-Re-C(1)	89.47(11)	C(26)-C(21)-As(1)	118.8(2)
C(3)-Re-C(1)	165.34(11)	C(22)-C(21)-As(1)	120.2(2)
N(5)-Re-O(1)	178.06(11)	C(36)-C(31)-As(1)	121.0(2)
C(2)-Re-O(1)	77.71(10)	C(32)-C(31)-As(1)	117.8(2)
C(4)-Re-O(1)	82.34(10)	C(46)-C(41)-As(1)	119.9(2)
C(3)-Re-O(1)	81.86(10)	C(42)-C(41)-As(1)	119.0(2)
C(1)-Re-O(1)	83.53(10)	C(51)-As(2)-C(81)	108.56(12)
Re-O(1)-H(1A)	117(2)	C(51)-As(2)-C(71)	110.21(12)
Re-O(1)-H(1B)	119(2)	C(81)-As(2)-C(71)	109.15(12)
H(1A)-O(1)-H(1B)	102.6(18)	C(51)-As(2)-C(61)	107.67(12)
N(1)-C(1)-Re	176.0(3)	C(81)-As(2)-C(61)	109.46(12)
N(2)-C(2)-Re	177.6(3)	C(71)-As(2)-C(61)	111.73(12)
N(3)-C(3)-Re	177.1(3)	C(56)-C(51)-As(2)	119.6(2)
N(4)-C(4)-Re	179.4(3)	C(52)-C(51)-As(2)	119.5(2)
H(2A)-O(2)-H(2B)	102(4)	C(72)-C(71)-As(2)	119.6(2)
H(3A)-O(3)-H(3B)	103(4)	C(76)-C(71)-As(2)	119.2(2)
H(4A)-O(4)-H(4B)	103(6)	C(66)-C(61)-As(2)	120.6(2)
H(5A)-O(5)-H(5B)	102(4)	C(62)-C(61)-As(2)	118.8(2)
H(6A)-O(6)-H(6B)	103(5)	C(86)-C(81)-As(2)	119.1(2)
		C(82)-C(81)-As(2)	119.6(2)

Table 1.3: Anisotropic displacement parameters ($Å^2 \times 10^3$) for $(AsPh_4)_2[ReN(H_2O)(CN)_4]\cdot 5H_2O$. The anisotropic displacement factor exponent takes the form: $2\pi^2[h^2a^{*2}U^{11} + ... + 2hka^*b^*U^{12}]$.

	U^{11}	U^{22}	U^{33}	U^{23}	U^{13}	U^{12}
Re	20(1)	19(1)	23(1)	-6(1)	2(1)	-8(1)
N(1)	35(1)	24(1)	35(1)	-9(1)	-6(1)	-8(1)
N(2)	58(2)	38(2)	30(1)	-8(1)	6(1)	-2(2)
N(3)	35(2)	32(2)	57(2)	-20(1)	4(1)	-9(1)
N(4)	46(2)	34(2)	37(2)	-13(1)	-6(1)	-15(1)
N(5)	28(1)	29(1)	31(1)	-11(1)	2(1)	-15(1)
O(1)	35(1)	40(1)	45(1)	-18(1)	11(1)	-24(1)
C(1)	30(1)	32(2)	21(1)	-10(1)	6(1)	-16(1)
C(2)	31(2)	22(1)	33(2)	-8(1)	5(1)	-10(1)
C(3)	26(1)	28(2)	31(1)	-11(1)	3(1)	-13(1)
C(4)	27(1)	23(1)	34(2)	-11(1)	3(1)	-9(1)
As(1)	20(1)	21(1)	21(1	-6(1)	2(1)	-9(1)
C(11)	24(1)	23(1)	23(1)	-7(1)	4(1)	-7(1)
C(12)	35(2)	32(2)	28(1)	-13(1)	6(1)	-15(1)
C(13)	55(2)	32(2)	37(2)	-20(1)	11(2)	-17(2)
C(14)	46(2)	30(2)	32(2)	-11(1)	8(1)	-1(2)
C(15)	26(2)	40(2)	38(2)	-12(1)	4(1)	-2(1)
C(16)	26(2)	37(2)	34(2)	-13(1)	2(1)	-11(1)
C(21)	24(1)	24(1)	20(1)	-5(1)	1(1)	-12(1)
C(22)	28(1)	33(2)	27(1)	-8(1)	4(1)	-15(1)
C(23)	41(2)	46(2)	34(2)	-9(1)	10(1)	-28(2)
C(24)	50(2)	33(2)	37(2)	0(1)	-2(1)	-26(2)
C(25)	41(2)	23(2)	38(2)	-4(1)	0(1)	-11(1)
C(26)	30(2)	27(2)	30(1)	-7(1)	4(1)	-12(1)
C(31)	22(1)	24(1)	23(1)	-8(1)	2(1)	-10(1)
C(32)	28(1)	28(2)	30(1)	-7(1)	3(1)	-13(1)
C(33)	33(2)	36(2)	38(2)	-14(1)	10(1)	-22(1)
C(34)	24(1)	43(2)	43(2)	-22)1)	7(1)	-16(1)
C(35)	26(1)	39(2)	32(2)	-13(1)	-2(1)	-12(1)
C(36)	30(1)	31(2)	25(1)	-7(1)	1(1)	-15(1)
C(41)	25(1)	27(1)	21(1)	-6(1)	1(1)	-16(1)
C(42)	29(1)	32(2)	26(1)	-11(1)	5(1)	-17(1)

C(43)	43(2)	48(2)	31(2)	-19(1)	9(1)	-28(2)
C(44)	43(2)	57(2)	22(1)	-10(1)	2(1)	-33(2)
C(45)	33(2)	36(2)	29(2)	0(1)	-4(1)	-20(1)
C(46)	29(1)	27(2)	30(2)	-5(1)	1(1)	-14(1)
As(2)	22(1)	22(1)	21(1)	-8(1)	3(1)	-12(1)
C(51)	24(1)	25(1)	26(1)	-12(1)	7(1)	-14(1)
C(52)	31(1)	29(2)	26(1)	-11(1)	7(1)	-18(1)
C(53)	44(2)	48(2)	28(2)	-17(1)	13(1)	-13(2)
C(54)	48(2)	52(2)	40(2)	-30(2)	22(2)	-33(2)
C(55)	57(2)	30(2)	46(2)	-21(2)	16(2)	-20(2)
C(56)	49(2)	30(2)	31(2)	-12(1)	6(1)	-16(2)
C(61)	28(1)	24(1)	20(1)	-8(1)	5(1)	-13(1)
C(62)	33(2)	31(2)	26(1)	-9(1)	1(1)	-17(1)
C(63)	33(2)	30(2)	36(2)	-13(1)	9(1)	-19(1)
C(64)	40(2)	30(2)	26(1)	-8(1)	11(1)	-18(1)
C(65)	40(2)	36(2)	21(1)	-9(1)	2(1)	-17(1)
C(66)	30(1)	32(2)	27(1)	-10(1)	2(1)	-16(1)
C(71)	23(1)	24(1)	23(1)	-9(1)	3(1)	-9(1)
C(72)	28(1)	34(2)	37(2)	-15(1)	4(1)	-16(1)
C(73)	23(1)	44(2)	42(2)	-18(2)	2(1)	-10(1)
C(74)	32(2)	28(2)	35(2)	-10(1)	0(1)	-4(1)
C(75)	41(2)	26(2)	38(2)	-10(1)	7(1)	-17(1)
C(76)	28(1)	27(2)	32(2)	-8(1)	3(1)	-14(1)
C(81)	25(1)	28(1)	23(1)	-6(1)	1(1)	-14(1)
C(82)	29(1)	31(2)	30(1)	-13(1)	6(1)	-16(1)
C(83)	38(2)	43(2)	36(2)	-13(1)	2(1)	-27(2)
C(84)	31(2)	47(2)	41(2)	-11(2)	2(1)	-25(2)
C(85)	27(2)	55(2)	40(2)	-19(2)	11(1)	-22(2)
C(86)	30(2)	41(2)	29(1)	-16(1)	7(1)	-19(1)
O(2)	44(1)	42(2)	42(1)	-13(1)	-2(1)	-13(1)
O(3)	33(1)	43(1)	46(1)	-9(1)	0(1)	-16(1)
O(4)	81(2)	49(2)	95(3)	-18(2)	40(2)	-23(2)
O(5)	55(2)	64(2)	44(2)	-20(1)	12(1)	-23(2)
O(6)	66(2)	109(3)	49(2)	-30(2)	-3(2)	-44(2)

Table 1.4: Hydrogen coordinates ($\times 10^4$) and isotropic displacement parameters ($Å^2 \times 10^3$) for $(AsPh_4)_2[ReN(H_2O)(CN)_4]\cdot 5H_2O$.

	x	y	z	U(eq)
H(1A)	9420(2)	530(3)	2130(20)	45
H(1B)	9420(2)	780(30)	2931(18)	45
H(12)	815	2588	1245	38
H(13)	2257	853	1112	50
H(14)	4175	291	1438	53
H(15)	4666	1449	1865	51
H(16)	3237	3168	2028	42
H(22)	2075	5133	626	37
H(23)	1928	6974	-236	47
H(24)	464	8725	-185	50
H(25)	-908	8684	680	46
H(26)	-796	6863	1548	37
H(32)	-336	2980	2784	37
H(33)	-2104	3107	2556	41
H(34)	-3498	4669	1340	42
H(35)	-3153	6112	342	41
H(36)	-1383	5994	543	36
H(42)	330	5683	3016	34
H(43)	793	5204	4534	45
H(44)	1850	3223	5515	47
H(45)	2507	1688	5014	43
H(46)	2062	2142	3496	37
H(52)	6145	5658	5334	33
H(53)	5683	6610	6331	43
H(54)	4709	8678	5804	48
H(55)	4255	9829	4281	52
H(56)	4707	8903	3270	46
H(62)	7053	7602	2976	36
H(63)	7452	7602	2976	36
H(64)	6558	9184	297	40
H(65)	5305	8510	168	40
H(66)	4938	7363	1441	36
H(72)	8159	5240	3934	39

H(73)	9638	3247	4618	47
H(74)	9264	1692	4947	45
H(75)	7416	2090	4618	43
H(76)	5905	4081	3976	36
H(82)	4927	5183	2354	35
H(83)	3220	5557	1984	44
H(84)	1619	6519	2575	47
H(85)	1689	7430	3501	48
H(86)	3387	7399	3841	38
H(2A)	4920(30)	6390(40)	-170(20)	71
H(2B)	3990(30)	7325(15)	50(30)	67
H(3A)	4190(40)	5250(20)	540(20)	67
H(3B)	4730(30)	4190(30)	1375(16)	67
H(4A)	900(40)	9510(50)	1290(40)	125
H(4B)	350(50)	8800(30)	1690(40)	125
H(5A)	2460(40)	9030(40)	389(13)	87
H(5B)	3020(30)	8230(30)	1310(30)	87
H(6A)	1110(40)	260(50)	4010(12)	112
H(6B)	1460(30)	-20(40)	3230(30)	112

Table 1.5: Hydrogen bonds for $(AsPh_4)_2[ReN(H_2O)(CN)_4]\cdot 5H_2O$ [Å and °].

D-H…A	**d(D-H)**	**d(H…A)**	**d(D…A)**	**<(DHA)**
O(1)-H(1A)…O(4)	0.94(4)	1.82(4)	2.744(5)	164(4)
O(1)-H(1B)…O(6)	0.94(3)	1.93(5)	2.790(4)	153(3)
O(2)-H(2A)…O(3)	0.93(5)	1.93(5)	2.811(4)	155(4)
O(2)-H(2B)…N(2)	0.94(3)	2.01(4)	2.921(4)	165(4)
O(3)-H(3A)…O(2)	0.94(4)	1.90(4)	2.797(4)	159(3)
O(3)-H(3B)…N(1)	0.94(3)	1.931(16)	2.843(4)	163(3)
O(4)-H(4A)…O(5)	0.95(6)	1.89(6)	2.810(5)	162(5)
O(5)-H(5A)…N(2)	0.94(3)	1.932(15)	2.870(4)	173(4)
O(6)-H(6A)…N(4)	0.941(13)	1.87(2)	2.784(4)	164(6)

A2: Crystal Data for $(PPh_4)_4[ReN(H_2O)(CN)_3$-μ-CN-$ReN(CN)_4]\cdot 5H_2O$ (Paragraph 5.3.2).

Table 2.1: Atomic coordinates ($\times 10^4$) and equivalent isotropic displacement parameters ($Å \times 10^3$) for $(PPh_4)_4[ReN(H_2O)(CN)_3$-μ-CN-$ReN(CN)_4]\cdot 5H_2O$. $U_{(eq)}$ is defined as one third of the trace of the orthogonalized U_{ij} tensor.

	x/a	y/b	z/c	U(eq)
Re(1)	7785(1)	9685(1)	6873(1)	19(1)
Re(2)	11601(3)	10372(1)	8168(1)	23(1)
C(1)	8027(3)	8296(3)	7011(2)	29(1)
C(2)	7180(4)	10014(3)	7573(2)	35(1)
C(3)	8812(4)	9527(3)	6381(2)	32(1)
C(4)	8033(3)	11181(3)	6922(2)	25(1)
C(5)	10110(3)	10116(3)	7786(2)	24(1)
C(6)	13145(3)	10619(3)	8284(3)	53(2)
C(7)	11518(3)	11782(3)	8041(2)	26(1)
C(8)	11710(3)	8870(3)	8013(2)	26(1)
N(1)	8217(3)	7554(3)	7103(2)	38(1)
N(2)	6816(4)	10197(4)	7933(2)	56(1)
N(3)	9437(4)	9479(3)	6163(2)	60(2)
N(4)	8212(3)	1999(3)	6944(2)	33(1)
N(5)	9293(3)	10018(3)	7567(2)	31(1)
N(6)	13964(4)	10795(4)	8341(4)	91(3)
N(7)	11462(3)	12547(3)	7961(2)	33(1)
N(8)	11750(3)	8037(3)	7928(2)	37(1)
N(9)	6742(3)	9400(3)	6367(2)	34(1)
N(10)	11549(3)	10565(3)	8832(2)	40(1)
O(1)	11601(3)	10038(2)	7160(2)	39(1)
C(101)	7712(3)	1309(3)	9969(2)	26(1)
C(102)	7533(3)	829(3)	10374(2)	29(1)
C(103)	6692(4)	167(3)	10235(2)	35(1)
C(104)	6062(4)	-20(4)	9700(3)	44(1)
C(105)	6229(5)	468(6)	9309(3)	71(2)
C(106)	7070(4)	1122(5)	9444(2)	56(2)

C(111)	9858(3)	1725(3)	10515(2)	25(1)
C(112)	10585(4)	1465(3)	10241(2)	34(1)
C(113)	11418(4)	1122(4)	10527(3)	44(1)
C(114)	11534(4)	1049(3)	11074(2)	40(1)
C(115)	10800(4)	1304(4)	11349(2)	40(1)
C(116)	9984(3)	1647(3)	11076(2)	32(1)
C(121)	8561(3)	3250(3)	10640(2)	24(1)
C(122)	9327(3)	3821(3)	11070(2)	30(1)
C(123)	9155(4)	4684(3)	11401(2)	34(1)
C(124)	8226(4)	4999(3)	11293(2)	36(1)
C(125)	7472(4)	4433(3)	10863(2)	35(1)
C(126)	7619(3)	3559(3)	10540(2)	29(1)
C(131)	8943(3)	2520(3)	9545(2)	24(1)
C(132)	9019(3)	3491(3)	9532(2)	29(1)
C(133)	9125(4)	3755(4)	9049(2)	36(1)
C(134)	9154(4)	3052(4)	8578(2)	37(1)
C(135)	9085(4)	2083(4)	8580(2)	44(1)
C(136)	8982(4)	1810(3)	9068(2)	37(1)
P(1)	8778(1)	2184(1)	10167(1)	21(1)
C(201)	4820(3)	5180(3)	1225(2)	24(1)
C(202)	4677(4)	5557(4)	754(2)	40(1)
C(203)	5339(4)	6331(4)	757(3)	51(2)
C(204)	6118(4)	6703(4)	1230(3)	45(1)
C(205)	6268(4)	6309(3)	1692(2)	37(1)
C(206)	5615(3)	5541(3)	1691(2)	32(1)
C(211)	3246(3)	4723(3)	1726(2)	24(1)
C(212)	2470(4)	4117(4)	1771(2)	36(1)
C(213)	1898(4)	4504(5)	2129(2)	46(1)
C(214)	2060(4)	5458(5)	2400(2)	50(2)
C(215)	2804(4)	6072(4)	2354(2)	41(1)
C(216)	3407(3)	5699(3)	2009(2)	31(1)
C(221)	3133(3)	3741(3)	576(2)	23(1)
C(222)	3248(3)	2866(3)	324(2)	32(1)
C(223)	2597(4)	2517(4)	-297(2)	42(1)
C(224)	1834(4)	3028(4)	-483(2)	38(1)
C(225)	1724(4)	3909(4)	-141(2)	40(1)
C(226)	2361(4)	4259(3)	384(2)	35(1)
C(231)	4638(3)	3285(3)	1472(2)	27(1)

C(232)	4338(5)	2724(4)	1796(3)	48(1)
C(233)	4832(5)	1939(5)	1899(3)	62(2)
C(234)	5614(4)	1713(4)	1685(3)	50(2)
C(235)	5923(4)	2271(4)	1369(3)	47(1)
C(236)	5442(4)	3057(3)	1257(2)	38(1)
P(2)	3962(1)	4232(1)	1257(1)	21(1)
C(301)	6914(3)	5396(3)	3336(2)	21(1)
C(302)	6729(3)	4446(3)	3003(2)	27(1)
C(303)	7346(4)	4100(4)	2674(2)	37(1)
C(304)	8136(4)	4711(4)	2662(2)	43(1)
C(305)	8321(4)	5649(4)	2989(2)	39(1)
C(306)	7726(3)	6005(3)	3332(2)	29(1)
C(311)	6915(3)	6384(3)	4478(2)	22(1)
C(312)	7723(3)	5918(3)	4689(2)	30(1)
C(313)	8299(4)	6279(4)	5237(2)	36(1)
C(314)	8093(4)	7103(4)	5572(2)	37(1)
C(315)	7306(4)	7573(4)	5367(2)	44(1)
C(316)	6721(4)	7225(3)	4818(2)	35(1)
C(321)	5327(3)	4869(3)	3801(2)	26(1)
C(322)	4524(3)	4506(3)	3336(2)	27(1)
C(323)	3947(3)	3659(3)	3305(2)	35(1)
C(324)	4173(4)	3197(4)	3745(3)	54(2)
C(325)	4948(5)	3564(5)	4201(3)	72(2)
C(326)	5541(4)	4422(4)	4243(2)	48(2)
C(331)	5457(3)	6778(3)	3541(2)	28(1)
C(332)	5759(4)	7279(4)	3180(2)	40(1)
C(333)	5264(5)	8047(4)	3036(3)	54(2)
C(334)	4483(4)	8312(4)	3260(3)	56(2)
C(335)	4181(4)	7812(4)	3608(3)	51(2)
C(336)	4658(4)	7035(4)	3748(2)	40(1)
P(3)	6148(1)	5863(1)	3785(1)	20(1)
C(401)	160(3)	8081(3)	4461(2)	22(1)
C(402)	48(3)	8101(3)	3895(2)	28(1)
C(403)	-779(4)	8430(3)	3603(2)	34(1)
C(404)	-1490(4)	8754(3)	3872(2)	38(1)
C(405)	-1388(4)	8735(4)	4427(2)	40(1)
C(406)	-571(4)	8403(3)	473(2)	33(1)
C(411)	1561(3)	6646(3)	4384(2)	24(1)

C(412)	815(3)	6042(3)	3936(2)	30(1)
C(413)	1102(4)	5208(3)	3614(2)	36(1)
C(414)	2048(4)	4970(3)	3749(2)	38(1)
C(415)	2753(4)	5564(4)	4186(2)	39(1)
C(416)	2527(3)	6415(3)	4510(2)	32(1)
C(421)	2258(3)	8605(3)	5073(2)	30(1)
C(422)	2446(4)	9122(3)	4691(2)	33(1)
C(423)	3273(4)	9800(4)	4853(2)	46(1)
C(424)	3871(6)	9981(5)	5379(3)	78(3)
C(425)	3681(6)	9481(6)	5780(3)	91(3)
C(426)	2868(5)	8801(5)	5623(2)	57(2)
C(431)	1032(3)	7279(3)	5442(2)	26(1)
C(432)	1036(3)	6296(3)	5448(2)	33(1)
C(433)	878(4)	6002(4)	5913(2)	41(1)
C(434)	706(4)	6661(4)	6360(2)	42(1)
C(435)	676(4)	7619(4)	6346(2)	40(1)
C(436)	850(4)	7946(4)	5892(2)	34(1)
P(4)	1239(1)	7670(1)	4841(1)	21(1)
O(2)	2880(3)	8660(3)	6945(2)	55(1)
O(3)	4660(4)	9796(4)	7350(3)	104(2)
O(4)	5908(5)	2081(4)	8356(3)	97(2)
O(5)	9932(3)	6655(2)	7554(2)	36(1)
O(6)	9875(2)	3466(2)	7404(2)	31(1)

Table 2.2: Bond lengths (Å) and angles (°) for $(PPh_4)_4[ReN(H_2O)(CN)_3$-μ-CN-$ReN(CN)_4]\cdot 5H_2O$.

Bond lengths	**(Å)**	**Bond lengths**	**(Å)**
C(1)-N(1)	1.157(6)	C(233)-H(233)	0.9500
C(2)-N(2)	1.135(6)	C(234)-C(235)	1.365(9)
C(3)-N(3)	1.146(6)	C(234)-H(234)	0.9500
C(4)-N(4)	1.160(5)	C(235)-C(236)	1.382(6)
C(5)-N(5)	1.137(6)	C(235)-H(235)	0.9500
C(6)-N(6)	1.138(7)	C(236)-H(236)	0.9500
C(7)-N(7)	1.150(5)	C(301)-C(302)	1.393(6)
C(8)-N(8)	1.160(5)	C(301)-C(306)	1.404(5)
C(1)-Re(1)	2.104(4)	C(301)-P(3)	1.795(4)

C(2)-Re(1)	2.109(5)	C(302)-C(303)	1.378(6)
C(3)-Re(1)	2.115(4)	C(302)-H(302)	0.9500
C(4)-Re(1)	2.102(4)	C(303)-C(304)	1.389(8)
C(5)-Re(2)	2.083(4)	C(303)-H(303)	0.9500
C(6)-Re(2)	2.112(5)	C(304)-C(305)	1.373(8)
C(7)-Re(2)	2.099(4)	C(304)-H(304)	0.9500
C(8)-Re(2)	2.095(4)	C(305)-C(306)	1.380(7)
N(5)-Re(2)	2.348(4)	C(305)-H(305)	0.9500
N(9)-Re(1)	1.657(4)	C(306)-H(306)	0.9500
N(10)-Re(2)	1.656(5)	C(311)-C(316)	1.378(6)
Re(2)-O(1)	2.462(4)	C(311)-C(312)	1.399(4)
O(1)-H(1A)	0.93(4)	C(311)-H(311)	1.781(4)
O(1)-H(1B)	0.91(4)	C(312)-C(313)	1.382(7)
C(101)-C(106)	1.365(7)	C(312)-H(312)	0.9500
C(101)-C(102)	1.407(6)	C(313)-C(314)	1.369(7)
C(101)-P(1)	1.796(4)	C(313)-H(313)	0.9500
C(102)-C(103)	1.397(6)	C(314)-C(315)	1.377(8)
C(102)-H(102)	0.9500	C(314)-H(314)	0.9500
C(103)-C(104)	1.379(8)	C(315)-C(316)	1.386(7)
C(103)-H(103)	0.9500	C(315)-H(315)	0.9500
C(104)-C(105)	1.377(8)	C(316)-H(316)	0.9500
C(104)-H(104)	0.9500	C(321)-C(326)	1.376(6)
C(105)-C(106)	1.392(7)	C(321)-C(322)	1.395(6)
C(105)-H(105)	0.9500	C(321)-P(3)	1.791(4)
C(106)-H(106)	0.9500	C(322)-C(323)	1.392(6)
C(111)-C(112)	1.394(6)	C(322)-H(322)	0.9500
C(111)-C(116)	1.404(6)	C(323)-C(324)	1.386(7)
C(111)-P(1)	1.793(4)	C(323)-H(323)	0.9500
C(112)-C(113)	1.391(7)	C(324)-C(325)	1.358(9)
C(112)-H(112)	0.9500	C(324)-H(324)	0.9500
C(113)-C(114)	1.372(8)	C(325)-C(326)	1.410(7)
C(113)-H(113)	0.9500	C(325)-H(325)	0.9500
C(114)-C(115)	1.400(7)	C(326)-H(326)	0.9500
C(114)-H(114)	0.9500	C(331)-C(332)	1.398(7)
C(115)-C(116)	1.363(7)	C(331)-C(336)	1.388(7)
C(115)-H(115)	0.9500	C(331)-P(3)	1.789(4)

C(116)-H(116)	0.9500	C(332)-C(333)	1.390(7)
C(121)-C(122)	1.394(6)	C(332)-H(332)	0.9500
C(121)-C(126)	1.405(6)	C(333)-C(334)	1.388(9)
C(121)-P(1)	1.794(4)	C(333)-H(333)	0.9500
C(122)-C(123)	1.387(6)	C(334)-C(335)	1.368(9)
C(122)-H(122)	0.9500	C(334)-H(334)	0.9500
C(123)-C(124)	1.392(7)	C(335)-C(336)	1.387(7)
C(123)-H(123)	0.9500	C(335)-H(335)	0.9500
C(124)-C(125)	1.383(7)	C(336)-H(336)	0.9500
C(124)-H(124)	0.9500	C(401)-C(402)	1.399(6)
C(125)-C(126)	1.378(6)	C(401)-C(406)	1.411(6)
C(125)-H(125)	0.9500	C(401)-P(4)	1.788(4)
C(126)-H(126)	0.9500	C(402)-C(403)	1.382(6)
C(131)-C(132)	1.384(6)	C(402)-H(402)	0.9500
C(131)-C(136)	1.397(6)	C(403)-C(404)	1.385(7)
C(131)-P(1)	1.793(6)	C(403)-H(403)	0.9500
C(132)-C(133)	1.383(6)	C(404)-C(405)	1.372(7)
C(132)-H(132)	0.9500	C(404)-H(404)	0.9500
C(133)-C(134)	1.378(7)	C(405)-C(406)	1.387(7)
C(133)-H(133)	0.9500	C(405)-H(405)	0.9500
C(134)-C(135)	1.373(7)	C(406)-H(406)	0.9500
C(134)-H(134)	0.9500	C(411)-C(412)	1.391(6)
C(135)-C(136)	1.402(6)	C(411)-C(416)	1.398(6)
C(135)-H(135)	0.9500	C(411)-P(4)	1.794(4)
C(136)-H(136)	0.9500	C(412)-C(413)	1.392(6)
C(201)-C(202)	1.378(6)	C(412)-H(412)	0.9500
C(201)-C(206)	1.387(6)	C(413)-C(414)	1.376(7)
C(201)-P(2)	1.792(4)	C(413)-H(413)	0.9500
C(202)-C(203)	1.403(7)	C(414)-C(415)	1.369(8)
C(202)-H(202)	0.9500	C(414)-H(414)	0.9500
C(203)-C(204)	1.385(8)	C(415)-C(416)	1.396(7)
C(203)-H(203)	0.9500	C(415)-H(415)	0.9500
C(204)-C(205)	1.371(8)	C(416)-H(416)	0.9500
C(204)-H(204)	0.9500	C(421)-C(422)	1.394(6)
C(205)-C(206)	1.391(6)	C(421)-C(426)	1.396(7)
C(205)-H(205)	0.9500	C(421)-P(4)	1.794(5)

C(206)-H(206)	0.9500	C(422)-C(423)	1.391)7)
C(211)-C(216)	1.387(6)	C(422)-H(422)	0.9500
C(211)-C(212)	1.400(6)	C(423)-C(424)	1.344(9)
C(211)-P(2)	1.785(4)	C(423)-H(423)	0.9500
C(212)-C(213)	1.394(7)	C(424)-C(425)	1.419(8)
C(212)-H(212)	0.9500	C(424)-H(424)	0.9500
C(213)-C(214)	1.358(9)	C(425)-C(426)	1.379(8)
C(213)-H(213)	0.9500	C(425)-H(425)	0.9500
C(214)-C(215)	1.386(8)	C(426)-H(426)	0.9500
C(214)-H(214)	1.9500	C(431)-C(436)	1.389(6)
C(215)-C(216)	1.400(6)	C(431)-C(432)	1.398(6)
C(215)-H(215)	0.9500	C(431)-P(4)	1.798(4)
C(216)-H(216)	0.9500	C(432)-C(433)	1.387(4)
C(221)-C(222)	0.385(6)	C(432)-H(432)	0.9500
C(221)-C(226)	1.395(6)	C(433)-C(434)	1.372(8)
C(221)-P(2)	1.786(6)	C(433)-H(433)	0.9500
C(222)-C(223)	1.389(7)	C(434)-C(435)	1.369(7)
C(222)-H(222)	0.9500	C(434)-H(434)	0.9500
C(223)-C(224)	1.375(8)	C(435)-C(436)	1.390(6)
C(223)-H(223)	1.9500	C(435)-H(435)	0.9500
C(224)-C(225)	1.391(7)	C(436)-H(436)	0.9500
C(224)-H(224)	0.9500	O(2)-H(2A)	0.94(5)
C(225)-C(226)	1.369(7)	O(2)-H(2B)	0.94(6)
C(225)-H(225)	0.9500	O(3)-H(3A)	0.971(18)
C(226)-H(226)	0.9500	O(3)-H(3B)	0.99(5)
C(231)-C(232)	1.377(7)	O(4)-H(4A)	0.9488
C(231)-C(236)	1.396(7)	O(4)-H(4B)	0.95(6)
C(231)-P(2)	1.790(4)	O(5)-H(5A)	0.94(4)
C(232)-C(233)	1.382(7)	O(5)-H(5B)	0.92(5)
C(232)-H(232)	0.9500	O(6)-H(6A)	0.92(5)
C(233)-C(234)	1.364(9)	O(6)-H(6B)	0.93(2)
Bond angles	**(°)**	**Bond angles**	**(°)**
N(1)-C(1)-Re(1)	175.9(4)	C(132)-C(131)-P(1)	119.9(3)
N(2)-C(2)-Re(1)	176.9(5)	C(136)-C(131)-P(1)	120.8(3)
N(3)-C(3)-Re(1)	173.3(5)	C(131)-P(1)-C(111)	110.6(2)
N(4)-C(4)-Re(1)	176.9(3)	C(131)-P(1)-C(121)	108.21(19)

N(5)-C(5)-Re(2)	176.5(4)	C(111)-P(1)-C(121)	108.8(2)
N(6)-C(6)-Re(2)	176.7(5)	C(131)-P(1)-C(101)	108.8(2)
N(7)-C(7)-Re(2)	178.8(4)	C(111)-P(1)-C(101)	112.0(2)
N(8)-C(8)-Re(2)	179.1(4)	C(121)-P(1)-C(101)	108.3(2)
C(5)-N(5)-Re(1)	162.8(4)	C(202)-C(202)-P(2)	120.6(4)
N(9)-Re(1)-C(4)	99.92(17)	C(206)-C(201)-P(2)	118.4(3)
N(9)-Re(1)-C(1)	99.60(18)	C(232)-C(231)-P(2)	122.2(4)
C(4)-Re(1)-C(1)	160.25(17)	C(236)-C(231)-P(2)	118.1(3)
N(9)-Re(1)-C(2)	98.0(2)	C(211)-P(2)-C(221)	107.2(2)
C(4)-Re(1)-C(2)	89.73(17)	C(211)-P(2)-C(231)	112.9(2)
C(1)-Re(1)-C(2)	90.53(18)	C(221)-P(2)-C(231)	108.7(2)
N(9)-Re(1)-C(2)	100.4(2)	C(211)-P(2)-C(201)	109.53(19)
C(4)-Re(1)-C(3)	85.10(15)	C(221(-P(2)-C(201)	110.35(19)
C(1)-Re(1)-C(3)	88.45(16)	C(231)-P(2)-C(201)	108.1(2)
C(2)-Re(1)-C(3)	161.5(2)	C(302)-C(301)-P(3)	121.5(3)
N(9)-Re(1)-N(5)	177.04(17)	C(306)-C(301)-P(3)	118.7(3)
C(4)-Re(1)-N(5)	82.13(15)	C(316)C(311)-P(3)	121.8(3)
C(1)-Re(1)-N(5)	78.25(15)	C(312)-C(311)-P(3)	119.0(3)
C(2)-Re(1)-N(5)	84.13(17)	C(326)-C(321)-P(3)	120.1(4)
C(3)-Re(1)-N(5)	77.55(18)	C(322)-C(321)-P(3)	118.8(3)
N(10)-Re(2)-C(5)	97.3(2)	C(336)-C(331)-P(3)	119.0(4)
N(10)-Re(2)-C(8)	98.43(18)	C(332)-C(331)-P(3)	120.6(4)
C(5)-Re(2)-C(8)	90.37(15)	C(311)-P(3)-C(331)	108.8(2)
N(10)-Re(2)-C(7)	100.49(18)	C(311)P(3)-C(321)	109.9(2)
C(5)-Re(2)-C(7)	86.25(15)	C(331)-P(3)-C(321)	109.7(2)
C(8)-Re(2)-C(7)	161.05(18)	C(311)-P(3)-C(301)	108.21(19)
N(10)-Re(2)-C(6)	101.0(3)	C(331)-P(3)-C(301)	112.0(2)
C(5)-Re(2)-C(6)	161.6(2)	C(321)-P(3)-C(301)	108.27(19)
C(8)-Re(2)-C(6)	89.61(17)	C(402)-C(401)-P(4)	119.8(3)
C(7)-Re(2)-C(6)	87.81(17)	C(406)-C(401)-P(4)	120.5(3)
N(10)-Re(2)-O(1)	176.39(18)	C(412)-C(411)-P(4)	121.0(3)
C(5)-Re(2)-O(1)	79.25(15)	C(416)-C(411)-P(4)	118.8(4)
C(8)-Re(2)-O(1)	80.68(16)	C(422)-C(421)-P(4)	119.0(4)
C(7)-Re(2)-O(1)	80.37(14)	C(426)-C(421)-P(4)	120.8(3)
C(6)-Re(2)-O(1)	82.5(2)	C(436)-C(431)-P(4)	120.3(3)
Re(2)-O(1)-H(1A)	122(4)	C(432-C(431)-P(4)	119.6(3)

Re(2)-O91)-H(1B)	97(4)	C(401)P(4)-C(411)	109.1(2)
H(1A)-O(1)-H(1B)	100(3)	C(401)-P(4)-C(421)	111.2(2)
C(102)-C(101)-P(1)	118.4(3)	C(411)-P(4)-C(421)	108.0(2)
C(112)-C(111)-P(1)	120.8(3)	C(401)-P(4)-C(431)	111.28(19)
C(116)-C(111)-P(1)	119.8(3)	C(411)-P(4)-C(431)	107.53(19)
C(122)-C(121)-P(1)	121.2(3)	C(421)-P(4)-C(431)	109.5(2)
C(126)-C(121)-P(1)	118.9(3)	H(2A)-O(2)-H(2B)	97(3)
C(216)-C(211)-P(2)	120.9(3)	H(3A)-O(3)-H(3B)	92(6)
C(212)-C(211)-P(2)	118.4(3)	H(4A)-O(4)-H(4B)	95.5
C(222)-C(221)-P(2)	121.4(3)	H(5A)-O(5)-H(5B)	99(3)
C(226)-C(221)-P(2)	119.0(3)	H(6A)-O(6)-H(6B)	99(3)

Table 2.3: Anisotropic displacement parameters ($Å^2 \times 10^3$) for $(PPh_4)_4[ReN(H_2O)(CN)_3$-μ-CN-$ReN(CN)_4]\cdot 5H_2O$. The anisotropic displacement factor exponent takes the form: $2\pi^2[h^2a^{*2}U^{11} + \ldots + 2hka^*b^*U^{12}]$.

	U^{11}	U^{22}	U^{33}	U^{23}	U^{13}	U^{12}
Re(1)	15(1)	21(1)	19(1)	2(1)	5(1)	-1(1)
Re(2)	19(1)	18(1)	26(1)	2(1)	-4(1)	-1(1)
C(1)	20(2)	29(2)	32(3)	1(2)	2(2)	-6(2)
C(2)	32(2)	41(2)	33(3)	10(2)	13(2)	6(2)
C(3)	41(3)	21(2)	40(3)	7(2)	23(2)	6(2)
C(4)	18(2)	30(2)	26(2)	3(2)	7(2)	5(2)
C(5)	20(2)	22(2)	23(2)	3(2)	-4(2)	-2(1)
C(6)	13(2)	27(2)	100(5)	16(3)	-17(3)	-6(2)
C(7)	20(2)	26(2)	24(2)	0(2)	-2(2)	0(2)
C(8)	18(2)	26(2)	24(2)	0(2)	02(2)	0(2)
N(1)	35(2)	28(2)	45(3)	10(2)	-3(2)	-4(2)
N(2)	49(3)	83(4)	48(3)	17(3)	33(3)	14(3)
N(3)	799(4)	39(2)	83(4)	12(2)	64(3)	12(2)
N(4)	27(2)	26(2)	43(3)	5(2)	9(2)	3(1)
N(5)	26(2)	25(2)	38(2)	3(2)	4(2)	-2(1)
N(6)	31(3)	40(3)	178(8)	16(4)	-6(4)	3(2)
N(7)	34(2)	24(2)	34(2)	6(2)	-1(2)	-1(2)
N(8)	31(2)	26(2)	46(3)	3(2)	2(2)	2(2)

N(9)	29(2)	34(2)	37(2)	9(2)	2(2)	4(2)
N(10)	49(3)	27(2)	28(2)	4(2)	-12(2)	-3(2)
O(1)	45(2)	37(2)	38(2)	10(2)	13(2)	8(2)
C(101)	27(2)	28(2)	22(2)	4(2)	7(2)	-2(2)
C(102)	26(2)	33(2)	25(2)	9(2)	4(2)	-2(2)
C(103)	30(2)	38(2)	42(3)	16(2)	12(2)	-1(2)
C(104)	31(3)	49(3)	50(4)	10(2)	9(2)	-12(2)
C(105)	47(3)	113(6)	40(4)	33(4)	-16(3)	-47(4)
C(106)	47(3)	80(4)	32(3)	24(3)	-10(3)	-36(3)
C(111)	26(2)	25(2)	24(2)	5(2)	9(2)	3(2)
C(112)	41(3)	40(2)	29(3)	13(2)	19(2)	13(2)
C(113)	42(3)	46(3)	55(4)	18(3)	25(3)	19(2)
C(114)	39(3)	36(2)	43(3)	15(2)	5(2)	9(2)
C(115)	38(3)	45(3)	35(3)	15(2)	6(2)	-2(2)
C(116)	30(2)	42(2)	25(2)	10(2)	12(2)	-3(2)
C(121)	27(2)	27(2)	18(2)	2(2)	11(2)	-1(2)
C(122)	29(2)	34(2)	25(2)	0(2)	10(2)	1(2)
C(123)	39(3)	32(2)	27(2)	-3(2)	12(2)	-4(2)
C(124)	53(3)	25(2)	34(3)	3(2)	25(2)	5(2)
C(125)	35(3)	37(2)	39(3)	7(2)	21(2)	7(2)
C(126)	26(2)	31(2)	31(3)	5(2)	12(2)	2(2)
C(131)	29(2)	30(2)	16(2)	5(2)	9(2)	3(2)
C(132)	33(2)	31(2)	28(2)	8(2)	17(2)	9(2)
C(133)	40(3)	39(2)	40(3)	20(2)	21(2)	14(2)
C(134)	39(3)	59(3)	24(2)	20(2)	16(2)	15(2)
C(135)	64(4)	51(3)	20(3)	3(2)	20(3)	9(3)
C(136)	25(1)	23(1)	16(1)	3(1)	8(1)	0(1)
P(1)	25(1)	23(1)	16(1)	3(1)	8(1)	0(1)
C(201)	24(2)	24(2)	25(2)	2(2)	11(2)	2(2)
C(202)	38(3)	44(3)	37(3)	13(2)	7(2)	-4(2)
C(203)	49(3)	53(3)	58(4)	29(3)	14(3)	-5(3)
C(204)	38(3)	36(3)	61(4)	8(2)	18(3)	-5(2)
C(205)	25(2)	41(3)	40(3)	-3(2)	11(2)	-3(2)
C(206)	24(2)	39(2)	31(3)	4(2)	9(2)	2(2)
C(211)	23(2)	35(2)	18(2)	9(2)	7(2)	6(2)
C(212)	31(2)	42(3)	41(3)	18(2)	16(2)	4(2)
C(213)	33(3)	77(4)	45(3)	38(3)	22(3)	14(3)
C(214)	49(3)	85(4)	36(3)	30(3)	28(3)	40(3)

C(215)	40(3)	54(3)	25(3)	0(2)	10(2)	22(2)
C(216)	27(2)	38(2)	22(2)	-3(2)	5(2)	7(2)
C(221)	22(2)	25(2)	19(2)	4(2)	4(2)	-2(2)
C(222)	29(2)	27(2)	33(3)	-4(2)	4(2)	-1(2)
C(223)	46(3)	35(2)	32(3)	-10(2)	6(2)	-3(2)
C(224)	37(3)	48(3)	22(2)	3(2)	1(2)	-11(2)
C(225)	36(3)	50(3)	28(3)	12(2)	-2(2)	6(2)
C(226)	34(3)	36(2)	29(3)	4(2)	2(2)	8(2)
C(231)	29(2)	25(2)	24(2)	4(2)	2(2)	7(2)
C(232)	55(4)	48(3)	53(4)	27(3)	22(3)	18(3)
C(234)	54(4)	32(3)	52(4)	9(2)	-10(3)	17(2)
C(235)	36(3)	40(3)	53(4)	-1(2)	-1(3)	16(2)
C(236)	35(3)	37(2)	41(3)	7(2)	9(2)	12(2)
P(2)	22(1)	22(1)	17(1)	2(1)	6(1)	3(1)
C(301)	18(2)	26(2)	20(2)	6(2)	5(2)	1(1)
C(302)	27(2)	28(2)	21(2)	1(2)	5(2)	4(2)
C(303)	42(3)	43(2)	26(3)	4(2)	11(2)	19(2)
C(304)	39(3)	75(4)	26(3)	23(3)	18(2)	25(3)
C(305)	26(2)	66(3)	36(3)	28(3)	14(2)	5(2)
C(306)	26(2)	43(2)	26(2)	9(2)	8(2)	-4(2)
C(311)	22(2)	25(2)	17(2)	2(2)	4(2)	-3(2)
C(312)	32(2)	30(2)	25(2)	3(2)	3(2)	4(2)
C(313)	27(2)	42(3)	35(3)	11(2)	-1(2)	1(2)
C(314)	38(3)	45(3)	19(2)	3(2)	0(2)	-11(2)
C(315)	48(3)	43(3)	32(3)	-7(2)	9(3)	4(2)
C(316)	38(3)	35(2)	26(3)	-3(2)	5(2)	8(2)
C(321)	21(1)	32(2)	28(2)	8(2)	11(2)	0(2)
C(322)	21(2)	36(2)	23(2)	5(2)	6(2)	-1(2)
C(323)	25(2)	42(3)	32(3)	3(2)	6(2)	-8(2)
C(324)	40(3)	54(3)	62(4)	27(3)	-1(3)	-23(3)
C(325)	51(4)	88(5)	73(5)	58(4)	-16(3)	-33(3)
C(326)	33(3)	66(4)	41(3)	31(3)	-11(2)	-18(2)
C(331)	27(2)	26(2)	26(2)	5(2)	-2(2)	5(2)
C(332)	39(3)	39(3)	43(3)	18(2)	6(2)	7(2)
C(333)	56(4)	54(3)	56(4)	33(3)	4(3)	11(3)
C(334)	49(3)	35(3)	70(5)	15(3)	-11(3)	13(2)
C(335)	38(3)	49(3)	54(4)	4(3)	-7(3)	21(2)
C(336)	33(3)	42(3)	43(3)	7(2)	5(2)	14(2)

P(3)	18(1)	21(1)	18(1)	3(1)	4(1)	0(1)
C(401)	25(2)	24(2)	18(2)	5(2)	7(2)	3(2)
C(402)	30(2)	32(2)	23(2)	7(2)	9(2)	4(2)
C(403)	44(3)	37(2)	22(2)	11(2)	6(2)	6(2)
C(404)	29(2)	37(2)	52(3)	21(2)	8(2)	8(2)
C(405)	32(3)	46(3)	46(3)	15(2)	16(2)	10(2)
C(406)	36(3)	37(2)	34(3)	12(2)	19(2)	9(2)
C(411)	27(2)	27(2)	20(2)	6(2)	11(2)	3(2)
C(412)	28(2)	31(2)	31(3)	5(2)	9(2)	1(2)
C(413)	47(3)	30(2)	27(3)	1(2)	11(2)	-1(2)
C(414)	51(3)	36(2)	35(3)	9(2)	26(3)	11(2)
C(415)	32(2)	50(3)	42(3)	12(2)	21(2)	12(2)
C(416)	25(2)	43(2)	29(3)	8(2)	10(2)	4(2)
C(421)	33(2)	31(2)	25(2)	4(2)	10(2)	-3(2)
C(422)	33(2)	34(2)	32(2)	10(2)	6(2)	-4(2)
C(423)	50(3)	45(3)	43(3)	13(2)	12(3)	-11(2)
C(424)	87(5)	87(5)	44(4)	17(4)	1(4)	-57(4)
C(425)	89(6)	128(7)	34(4)	34(4)	-20(4)	-17(5)
C(426)	60(4)	74(4)	25(3)	15(3)	-5(3)	-35(3)
C(431)	27(2)	38(2)	15(2)	11(2)	8(2)	4(2)
C(432)	33(2)	42(2)	36(3)	18(2)	21(2)	14(2)
C(433)	39(3)	54(3)	49(3)	33(3)	23(3)	19(2)
C(434)	31(3)	72(4)	32(3)	30(3)	12(2)	13(2)
C(435)	31(3)	69(3)	19(2)	6(2)	9(2)	0(2)
C(436)	37(3)	43(3)	21(2)	4(2)	10(2)	0(2)
P(4)	24(1)	25(1)	15(1)	4(1)	7(1)	1(1)
O(2)	42(2)	71(3)	48(3)	14(2)	4(2)	9(2)
O(3)	43(3)	106(4)	175(7)	98(4)	-5(3)	-12(3)
O(4)	101(5)	98(4)	96(5)	35(4)	21(4)	20(4)
O(5)	31(2)	32(2)	44(2)	11(2)	10(2)	0(1)
O(6)	28(2)	30(2)	35(2)	9(1)	9(1)	2(1)

Table 2.4: Hydrogen coordinates ($\times 10^4$) and isotropic displacement parameters ($Å^2 \times 10^3$) for $(PPh_4)_4[ReN(H_2O)(CN)_3\text{-}\mu\text{-}CN\text{-}ReN(CN)_4]\cdot 5H_2O$.

	x	y	z	U(eq)
H(1A)	11060(3)	9710(3)	6875(19)	59
H(1B)	12010(30)	9560(30)	7160(20)	59
H(102)	7979	953	10739	34
H(103)	6555	-151	10508	42
H(104)	5506	-491	9599	53
H(105)	5772	360	8948	86
H(106)	7199	1440	9169	68
H(112)	10514	1522	9863	40
H(113)	11912	937	10340	53
H(114)	12112	825	11267	47
H(115)	10871	1239	11725	47
H(116)	9494	1835	11266	38
H(122)	9967	3619	11137	36
H(123)	9673	5061	11702	41
H(124)	8111	5598	11513	43
H(125)	6839	4650	10789	42
H(126)	7090	3170	10252	35
H(132)	8999	3979	9855	34
H(133)	9179	4423	9043	43
H(134)	9222	3240	8248	45
H(135)	9107	1602	8253	53
H(136)	8939	1142	9075	44
H(202)	4139	5298	433	48
H(203)	5254	6600	436	61
H(204)	6554	7238	1234	54
H(205)	6813	6560	2010	44
H(206)	5713	5263	2009	39
H(212)	2336	3457	1562	43
H(213)	1388	4095	2177	55
H(214)	1657	5707	2650	59
H(215)	2905	6741	2548	49
H(216)	3922	6112	1969	37
H(222)	3770	2507	362	39

H(223)	2680	1920	-533	50
H(224)	1385	2780	-844	46
H(225)	1204	4270	-271	47
H(226)	2277	4858	618	42
H(232)	3796	2875	1948	57
H(233)	4624	1551	2122	74
H(234)	5942	1167	1757	60
H(235)	6474	2118	1225	56
H(236)	5656	3441	1034	45
H(302)	6176	4035	3003	32
H(303)	7231	3445	2456	44
H(304)	8550	4479	2426	51
H(305)	8866	6059	2980	47
H(306)	7864	6652	3561	34
H(312)	7876	5353	4456	36
H(313)	8840	5954	5381	43
H(314)	8495	7352	5946	44
H(315)	7162	8140	5603	53
H(316)	6189	7563	4676	42
H(322)	4370	4835	3040	33
H(323)	3405	3401	2986	42
H(324)	3782	2620	3728	64
H(325)	5093	3236	4498	86
H(326)	6073	4683	4567	58
H(332)	6299	7096	3033	48
H(333)	5458	8387	2788	65
H(334)	4154	8847	3170	67
H(335)	3642	7999	3754	61
H(336)	4438	6681	3984	48
H(402)	540	7890	3711	34
H(403)	-861	8435	3216	41
H(404)	-2015	8990	3671	46
H(405)	-1885	8953	4606	48
H(406)	-504	8393	5116	40
H(412)	194	6199	3851	37
H(413)	622	4805	3301	43
H(414)	2213	4388	3538	45
H(415)	3405	5395	4270	47

H(416)	3020	6829	4810	38
H(422)	2013	9011	4323	40
H(423)	3415	10138	4590	55
H(424)	4430	10450	5484	93
H(425)	4108	9614	6151	109
H(426)	2725	8467	5888	69
H(432)	1145	5835	5137	39
H(433)	888	5336	5923	50
H(434)	609	6453	6679	50
H(435)	534	8068	6651	48
H(436)	845	8615	5890	41
H(2A)	3552(19)	8830(50)	7120(30)	82
H(2B)	2760(40)	8240(40)	7170(30)	82
H(3A)	5371(13)	9830(50)	7450(30)	157
H(3B)	4680(50)	10360(40)	7670(20)	157
H(4A)	6182	1504	8227	145
H(4B)	6320(40)	2500(30)	8240(30)	145
H(5A)	9470(30)	7020(30)	7380(20)	53
H(5B)	10410(30)	7160(30)	7760(20)	53
H(6A)	10350(30)	3120(30)	7570(20)	46
H(6B)	9430(30)	2950(30)	7164(19)	46

Table 2.5: Hydrogen bonds for $(PPh_4)_4[ReN(H_2O)(CN)_3$-μ-CN-$ReN(CN)_4]\cdot 5H_2O$ [Å and °].

D-H…A	d(D-H)	d(H…A)	d(D…A)	<(DHA)
O(1)-H(1B)…O(2)	0.91	1.90(3)	2.784(5)	161(6)
O(2)-H(2A)…O(3)	0.94(5)	1.91(4)	2.750(7)	148(5)
O(3)-H(3A)…..N(2)	0.971(18)	2.08(4)	3.004(7)	158(5)
O(3)-H(3B)…..N(6)	0.99(5)	2.16(6)	2.990(7)	140(4)
O(4)-H(4A)…..N(2)	0.95	2.16	3.109(8)	179.6
O(5)-H(5A)…..N(1)	0.94(4)	1.99(2)	2.898(5)	162(5)
O(5)-H(5B)…..N(8)	0.92(5)	2.10(3)	2.968(5)	155(5)
O(6)-H(6A)…..N(7)	0.92(5)	1.95(2)	2.874(5)	173(5)
O(6)-H(6B)…..N(4)	0.93(2)	2.02(3)	2.880(5)	154(5)

A3: Crystal Data for $(AsPh_4)_2[ReN(\eta^2\text{-pic})(CN)_3]\cdot 4H_2O$ (Paragraph 5.3.3)

Table 3.1: Atomic coordinates ($\times 10^4$) and equivalent isotropic displacement parameters ($Å \times 10^3$) for $(AsPh_4)_2[ReN(\eta^2\text{-pic})(CN)_3]\cdot 4H_2O$. $U_{(eq)}$ is defined as one third of the trace of the orthogonalized U_{ij} tensor.

	x/a	y	z	$U_{(eq)}$
Re(1)	5225(1)	1856(1)	3338(1)	42(1)
As(1)	630(1)	5032(1)	8062(1)	40(1)
As(2)	8494(1)	2047(1)	6604(1)	40(1)
N(4)	5384(3)	256(3)	3033(2)	48(1)
N(5)	5037(3)	1724(3)	4338(2)	49(1)
C(81)	10116(3)	1771(3)	6149(2)	42(1)
C(11)	1152(3)	5062(3)	6871(2)	41(1)
C(2)	5089(3)	3420(4)	3335(3)	49(1)
C(51)	7570(3)	3216(3)	7553(2)	45(1)
C(71)	8453(4)	698(3)	6895(3)	47(1)
C(41)	483(3)	3720(3)	8296(2)	41(1)
C(61)	7868(3)	2497(3)	5736(3)	43(1)
C(21)	-886(3)	6314(3)	8657(2)	42(1)
N(3)	8097(3)	964(3)	2532 (3)	67(1)
N(2)	5039(4)	4285(4)	3343(3)	70(1)
C(3)	7095(4)	1231(3)	2831(3)	48(1)
N(1)	2472(3)	3067(3)	3422(3)	69(1)
C(4)	5288(4)	-433(3)	3605(3)	54(1)
C(82)	10323(4)	2663(3)	5968(3)	52(1)
C(16)	312(4)	5572(3)	6499(2)	46(1)
C(12)	2381(4)	4514(4)	6383(3)	55(1)
C(13)	2750(4)	4490(5)	5511(3)	62(1)
C(1)	3429(4)	2624(3)	3422(3)	50(1)
C(42)	1284(4)	2749(3)	7718(3)	57(1)
C(52)	7405(4)	2962(4)	8370(3)	63(1)
C(66)	3644(5)	2092(4)	4904(3)	57(1)
C(22)	-957(4)	7112(3)	9183(3)	56(1)
C(31)	1843(4)	4949(4)	8430(2)	51(1)
C(26)	-1894(4)	6443(3)	8538(3)	51(1)
C(15)	711(4)	5528(4)	5632(3)	59(1)

C(62)	6640(4)	3158(3)	5945(3)	57(1)
C(56)	7103(4)	4317(3)	7418(3)	52(1)
C(14)	1919(4)	4987(4)	5145(3)	56(1)
C(72)	7923(4)	311(4)	6518(3)	59(1)
O(2)	5829(4)	480(3)	889(2)	100(1)
C(54)	6343(4)	4916(4)	8897(3)	61(1)
C(86)	11075(4)	698(4)	5953(3)	53(1)
C(55)	6485(4)	5169(4)	8087(3)	60(1)
C(46)	-340(4)	3728(4)	9043(3)	56(1)
C(25)	-2986(4)	7394(4)	8938(3)	67(1)
O(1)	5554(3)	1619(3)	1935(2)	59(1)
C(85)	12229(4)	532(4)	5576(4)	65(1)
C(8)	5510(4)	-49(3)	2245(3)	57(1)
C(43)	1264(5)	1775(4)	7903(3)	70(1)
C(76)	8988(4)	106(4)	7443(3)	63(1)
C(65)	8197(5)	2352(4)	4266(3)	72(1)
C(66)	8654(4)	2094(3)	4902(3)	56(1)
C(32)	2301(4)	4115(4)	8891(3)	61(1)
C(83)	11470(4)	2487(4)	5575(3)	61(1)
C(63)	6232(5)	3404(4)	5280(4)	75(2)
C(9)	5640(4)	729(4)	1628(3)	62(1)
C(84)	12420(4)	1433(4)	5385(3)	62(1)
C(53)	6790(5)	3826(5)	9039(3)	72(1)
C(44)	443(5)	1777(4)	8653(4)	73(1)
C(6)	5379(5)	-1689(4)	2637(4)	79(2)
C(64)	6996(5)	2994(4)	4459(4)	75(2)
C(45)	-358(5)	2744(4)	9231(3)	71(1)
C(7)	5509(4)	-1024(4)	2040(3)	73(1)
C(24)	-3063(5)	8187(4)	9462(3)	70(1)
C(5)	5273(4)	-1397(4)	3429(3)	71(1)
C(73)	7885(5)	-661(4)	6731(4)	73(1)
C(23)	-2064(5)	8045(4)	9590(3)	71(1)
C(74)	8377(5)	-1227(4)	7284(4)	80(2)
C(75)	8939(5)	-860(4)	7630(4)	80(2)
C(33)	3221(5)	4022(6)	9107(4)	89(2)
C(36)	2266(6)	5697(6)	8213(3)	92(2)
OW1	9525(5)	1208(5)	922(3)	146(2)
C(34)	3663(6)	4740(8)	8890(4)	109(3)

C(35)	3188(7)	5589(8)	8456(4)	124(3)
OW2	8315(9)	713(7)	-229(6)	276(5)
OW4	6929(14)	2309(13)	709(10)	404(8)
OW3	5961(10)	1382(9)	-618(7)	306(5)

Table 3.2: Bond lengths (Å) and angles (°) for $(AsPh_4)_2[ReN(\eta^2\text{-pic})(CN)_3]\cdot 4H_2O$.

Bond lengths	**(Å)**	**Bond lengths**	**(Å)**
Re(1)-N(5)	1.655(3)	C(22)-H(22)	0.9300
Re(1)-C(2)	2.067(5)	C(31)-C(32)	1.390(6)
Re(1)-C(1)	2.111(4)	C(31)-C(36)	1.378(7)
Re(1)-C(3)	2.105(4)	C(26)-C(25)	1.387(6)
Re(1)-N(4)	2.169(3)	C(25)-H(25)	0.9300
Re(1)-O(1)	2.289(3)	C(26)-H(26)	0.9300
As(1)-C(21)	1.914(4)	C(15)-C(14)	1.377(6)
As(1)-C(31)	1.914(4)	C(14)-H(14)	0.9300
As(1)-C(41)	1.916(4)	C(62)-C(63)	1.396(6)
As(1)-C(11)	1.917(4)	C(62)-H(62)	0.9300
As(2)-C(81)	1.912(4)	C(56)-C(55)	1.376(6)
As(2)-C(61)	1.907(4)	C(55)-H(55)	0.9300
As(2)-C(51)	1.916(4)	C(56)-H(56)	0.9300
As(2)-C(71)	1.921(4)	C(72)-C(73)	1.390(6)
N(4)-C(4)	1.352(5)	C(72)-H(72)	0.9300
N(4)-C(8)	1.355(5)	O(2)-C(9)	1.226(5)
C(81)-C(82)	1.382(5)	C(54)-C(53)	1.376(7)
C(81)-C(86)	1.385(5)	C(53)-H(53)	0.9300
C(11)-C(16)	1.387(5)	C(54)-C(55)	1.385(6)
C(11)-C(12)	1.398(5)	C(54)-H(54)	0.9300
C(2)-N(2)	1.158(5)	C(86)-C(85)	1.378(6)
C(51)-C(56)	1.386(5)	C(85)-H(85)	0.9300
C(51)-C(52)	1.395(6)	C(86)-H(86)	0.9300
C(71)-C(76)	1.391(6)	C(46)-C(45)	1.387(6)
C(71)-C(72)	1.386(6)	C(45)-H(45)	0.9300
C(41)-C(46)	1.371(6)	C(46)-H(46)	0.9300
C(41)-C(42)	1.389(5)	C(25)-C(24)	1.378(7)
C(61)-C(62)	1.390(6)	C(24)-H(24)	0.9300

C(61)-C(66)	1.387(6)	O(1)-C(9)	1.285(5)
C(21)-C(22)	1.388(6)	C(85)-C(84)	1.384(6)
C(21)-C(26)	1.383(6)	C(84)-H(84)	0.9300
N(3)-C(3)	1.146(5)	C(8)-C(7)	1.395(7)
N(1)-C(1)	1.150(5)	C(7)-H(7)	0.9300
C(4)-C(5)	1.378(6)	C(8)-C(9)	1.501(7)
C(4)-H(4)	0.9300	C(43)-C(44)	1.376(7)
C(82)-C(83)	1.368(6)	C(43)-H(43)	0.9300
C(82)-H(82)	0.9300	C(76)-C(75)	1.379(7)
C(16)-C(15)	1.384(6)	C(75)-H(75)	0.9300
C(15)-H(15)	0.9300	C(76)-H(76)	0.9300
C(16)-H(16)	0.9300	C(65)-C(64)	1.361(7)
C(12)-C(13)	1.394(6)	C(64)-H(64)	0.9300
C(12)-H(12)	0.9300	C(32)-C(33)	1.374(7)
OW1-HW1A	0.9000	C(32)-H(32)	0.9300
OW1-HW1B	0.9000	C(83)-C(84)	1.365(6)
C(13)-C(14)	1.370(6)	C(83)-H(83)	0.9300
C(13)-H(13)	0.9300	C(63)-C(64)	1.364(8)
C(42)-C(43)	1.374(6)	C(63)-H(63)	0.9300
C(42)-H(42)	0.9300	C(44)-C(45)	1.385(7)
C(52)-C(53)	1.384(7)	C(44)-H(44)	0.9300
C(52)-H(52)	0.9300	C(6)-C(7)	1.366(8)
C(66)-C(65)	1.391(6)	C(6)-H(6)	0.9300
C(65)-H(65)	0.9300	C(6)-C(5)	1.365(7)
C(66)-H(66)	0.9300	C(5)-H(5)	0.9300
C(22)-C(23)	1.388(6)	C(24)-C(23)	1.374(7)
C(36)-H(36)	0.9300	C(23)-H(23)	0.9300
C(34)-C(35)	1.377(10)	C(73)-C(74)	1.360(8)
C(34)-H(34)	0.9300	C(73)-H(73)	0.9300
OW2-HW2A	0.9002	C(74)-C(75)	1.372(8)
OW3-HW3A	0.9000	C(74)-H(74)	0.9300
C(36)-C(35)	1.396(8)	C(33)-C(34)	1.356(9)
C(35)-H(35)	0.9300	C(33)-H(33)	0.9300
Bond angles	**(°)**	**Bond angles**	**(°)**
N(5)-Re(1)-C(2)	99.62(16)	C(81)-C(82)-C(83)	120.1(4)
N(5)-Re(1)-C(1)	100.56(15)	C(83)-C(82)-H(82)	120.0
C(2)-Re(1)-C(1)	82.57(16)	C(81)-C(82)-H(82)	120.0
N(5)-Re(1)-C(3)	99.08(16)	C(15)-C(16)-C(11)	118.8(4)

C(2)-Re(1)-C(3)	86.13(15)	C(15)-C(16)-H(16)	120.6
C(1)-Re(1)-C(3)	160.12(16)	C(11)-C(16)-H(16)	120.6
N(5)-Re(1)-N(4)	94.17(15)	C(13)-C(12)-C(11)	118.7(4)
C(2)-Re(1)-N(4)	166.14(14)	C(13)-C(12)-H(12)	120.7
C(1)-Re(1)-N(4)	88.59(14)	C(11)-C(12)-H(12)	120.7
C(3)-Re(1)-N(4)	93.05(14)	C(14)-C(13)-C(12)	120.3(4)
N(5)-Re(1)-O(1)	166.48(14)	C(14)-C(13)-H(13)	119.9
C(2)-Re(1)-O(1)	93.88(14)	C(12)-C(13)-H(13)	119.9
C(1)-Re(1)-O(1)	80.72(13)	N(1)-C(1)-Re(1)	175.7(4)
C(3)-Re(1)-O(1)	80.92(13)	C(43)-C(42)-C(41)	119.5(4)
N(4)-Re(1)-O(1)	72.35(12)	C(43)-C(42)-H(42)	120.3
C(21)-As(1)-C(31)	11.24(17)	C(41)-C(42)-H(42)	120.3
C(21)-As(1)-C(41)	108.84(16)	C(53)-C(52)-C(51)	118.8(4)
C(31)-As(1)-C(41)	107.48(17)	C(51)-C(52)-H(52)	120.6
C(21)-As(1)-C(11)	111.32(16)	C(53)-C(52)-H(52)	120.6
C(31)-As(1)-C(11)	107.85(16)	C(61)-C(66)-C(65)	119.0(4)
C(41)-As(1)-C(11)	110.04(16)	C(61)-C(66)-H(66)	120.5
C(81)-As(2)-C(61)	107.12(16)	C(65)-C(66)-H(66)	120.5
C(81)-As(2)-C(51)	109.97(16)	C(21)-C(22)-C(23)	118.6(5)
C(61)-As(2)-C(51)	109.64(16)	C(23)-C(22)-H(22)	120.7
C(81)-As(2)-C(71)	110.09(16)	C(21)-C(22)-H(22)	120.7
C(61)-As(2)-C(71)	107.87(17)	C(32)-C(31)-C(36)	121.4(4)
C(51)-As(2)-C(71)	112.01(17)	C(32)-C(31)-As(1)	119.2(3)
C(4)-N(4)-C(8)	117.5(4)	C(36)-C(31)-As(1)	119.4(4)
C(4)-N(4)-Re(1)	123.4(3)	C(21)-C(26)-C(25)	119.4(4)
C(8)-N(4)-Re(1)	119.0(3)	C(21)-C(26)-H(26)	120.3
C(82)-C(81)-C(86)	119.9(4)	C(25)-C(26)-H(26)	120.3
C(82)-C(81)-As(2)	118.5(3)	C(14)-C(15)-C(16)	120.7(4)
C(86)-C(81)-As(2)	121.5(3)	C(14)-C(15)-H(15)	119.7
C(16)-C(11)-As(1)	119.9(3)	C(16)-C(15)-H(15)	119.7
C(12)-C(11)-As(1)	119.1(3)	C(63)-C(62)-C(61)	117.2(5)
N(2)-C(2)-Re(1)	178.0(4)	C(61)-C(62)-H(62)	121.4
C(56)-C(51)-C(52)	120.2(4)	C(63)-C(62)-H(62)	121.4
C(16)-C(11)-C(12)	121.0(4)	C(55)-C(56)-C(51)	120.4(4)

Table 3.3: Anisotropic displacement parameters ($Å^2 \times 10^3$) for $(AsPh_4)_2[ReN(\eta^2\text{-pic})(CN)_3]\cdot 4H_2O$. The anisotropic displacement factor exponent takes the form: $2\pi^2[h^2a^{*2}U^{11} + \ldots. + 2hka^*b^*U^{12}]$.

	U^{11}	U^{22}	U^{33}	U^{23}	U^{13}	U^{12}
Re	27(1)	19(1)	22(1)	-5(1)	0(1)	-6(1)
N(1)	33(2)	30(2)	39(3)	-9(2)	2(2)	-9(2)
N(2)	35(2)	38(2)	53(3)	-17(2)	-7(2)	-5(2)
N(3)	44(2)	27(2)	38(3)	-9(2)	-1(2)	-12(2)
N(4)	27(2)	24(2)	22(2)	-5(2)	2(2)	-7(2)
N(5)	33(2)	30(2)	30(2)	-9(2)	0(2)	-5(2)
O(1)	26(2)	28(2)	-8(1)	6(1)	-10(1)	-6(2)
O(2)	46(2)	52(2)	24(2)	-6(2)	4(2)	-21(2)
C(1)	22(2)	22(2)	24(2)	-5(2)	-1(2)	-4(2)
C(2)	31(3)	18(2)	31(3)	-8(2)	-2(2)	-2(2)
C(3)	30(2)	25(2)	25(2)	-8(2)	2(2)	-11(2)
C(4)	32(2)	22(2)	25(3)	-7(2)	7(2)	-9(2)
C(5)	27(2)	27(2)	27(3)	-3(2)	1(2)	-8(2)
C(6)	38(3)	54(3)	24(3)	-5(2)	-7(2)	-20(3)
C(7)	38(3)	58(4)	38(3)	-3(3)	-7(3)	-24(3)
C(8)	30(3)	28(2)	40(3)	-2(2)	1(2)	-10(2)
C(9)	33(3)	35(3)	57(4)	-1(3)	0(3)	-17(2)
C(10)	34(3)	29(3)	64(4)	-8(3)	15(3)	-13(2)
C(11)	53(3)	37(3)	48(3)	-15(3)	22(3)	-22(3)
C(12)	42(3)	32(3)	33(3)	-10(2)	13(2)	-20(2)
C(13)	28(2)	18(2)	32(3)	-2(2)	4(2)	-9(2)
As(1)	19(1)	25(1)	29(1)	-11(1)	5(1)	-8(1)
C(21)	26(2)	29(2)	37(3)	-16(2)	7(2)	-10(2)
C(22)	26(2)	44(3)	33(3)	-7(2)	7(2)	-11(2)
C(23)	25(2)	45(3)	36(3)	-12(2)	-1(2)	-6(2)
C(24)	37(3)	44(3)	39(3)	-17(3)	-6(2)	-10(2)
C(25)	44(4)	103(5)	28(3)	-15(3)	4(3)	-12(4)
C(26)	29(3)	94(5)	36(3)	-22(3)	6(3)	-4(3)
C(31)	21(2)	27(2)	30(3)	-6(2)	6(2)	-10(2)
C(32)	30(3)	39(3)	39(3)	-17(2)	10(2)	-17(2)
C(33)	34(3)	49(3)	42(3)	-15(3)	16(2)	-18(2)
C(34)	27(3)	43(3)	53(4)	-7(3)	11(2)	-19(2)

C(35)	31(3)	34(3)	47(3)	-4(2)	-4(2)	-17(2)
C(36)	28(2)	26(2)	37(3)	-8(2)	5(2)	-13(2)
C(41)	22(2)	27(2)	30(3)	13(2)	8(2)	-13(2)
C(42)	42(3)	22(2)	36(3)	-8(2)	9(2)	-15(2)
C(43)	44(3)	31(3)	41(3)	-18(2)	13(2)	-17(2)
C(44)	30(2)	44(3)	33(3)	-22(2)	8(2)	-17(2)
C(45)	30(3)	44(3)	30(3)	-9(2)	-4(2)	-11(2)
C(46)	28(2)	31(2)	34(3)	-13(2)	-2(2)	-3(2)
C(51)	26(2)	24(2)	29(3)	-9(2)	5(2)	-11(2)
C(52)	27(2)	34(3)	48(3)	-17(2)	12(2)	-14(2)
C(53)	50(3)	49(3)	48(3)	-21(3)	19(3)	-35(3)
C(54)	61(4)	33(3)	46(3)	-17(3)	13(3)	-25(3)
C(55)	42(3)	28(3)	49(3)	-14(2)	8(3)	-6(2)
C(56)	28(2)	26(2)	47(3)	-13(2)	9(2)	-9(2)
As(2)	22(1)	22(1)	23(1)	-7(1)	5(1)	-11(1)
C(61)	19(2)	31(2)	23(2)	-8(2)	7(2)	-11(2)
C(62)	37(3)	28(2)	29(3)	-6(2)	7(2)	-13(2)
C(63)	35(3)	46(3)	32(3)	6(2)	1(2)	-19(2)
C(64)	39(3)	76(4)	26(3)	-14(3)	8(2)	-34(3)
C(65)	35(3)	62(4)	38(3)	-31(3)	14(2)	-25(3)
C(66)	26(2)	32(2)	31(3)	-12(2)	4(2)	-14(2)
C(71)	21(2)	33(2)	26(2)	-13(2)	9(2)	-15(2)
C(72)	31(3)	29(2)	33(3)	-5(2)	2(2)	-12(2)
C(73)	25(2)	42(3)	48(3)	-15(3)	1(2)	-13(2)
C(74)	28(3)	64(4)	49(4)	-19(3)	15(3)	-25(3)
C(75)	49(3)	71(4)	40(3)	-2(3)	12(3)	-40(3)
C(76)	30(3)	46(3)	34(3)	-1(2)	3(2)	-17(2)
C(81)	31(2)	24(2)	26(2)	-7(2)	4(2)	-15(2)
C(82)	43(3)	40(3)	27(3)	-13(2)	10(2)	-23(2)
C(83)	59(4)	48(3)	37(3)	-22(3)	11(3)	-23(3)
C(84)	73(4)	39(3)	35(3)	-12(2)	-4(3)	-30(3)
C(85)	64(4)	49(3)	40(3)	-13(3)	6(3)	-42(3)
C(86)	46(3)	41(3)	40(3)	-15(2)	14(2)	-29(3)
C(91)	21(2)	24(2)	24(2)	-2(2)	3(2)	-7(2)
C(92)	28(2)	37(3)	30(3)	-8(2)	4(2)	-14(2)
C(93)	29(3)	50(3)	32(3)	-3(2)	-5(2)	-12(2)
C(94)	38(3)	33(3)	36(3)	0(2)	1(2)	-2(2)
C(95)	43(3)	23(2)	40(3)	-4(2)	5(2)	-8(2)

C(96)	33(3)	26(2)	31(3)	-8(2)	1(2)	-10(2)
O(3)	47(2)	49(2)	41(2)	2(2)	7(2)	-21(2)
O(4)	78(3)	41(2)	53(3)	-8(2)	2(2)	-17(2)

Table 3.4: Hydrogen coordinates ($\times 10^4$) and isotropic displacement parameters ($Å^2 \times 10^3$) for $(AsPh_4)_2[ReN(\eta^2\text{-pic})(CN)_3]\cdot 4H_2O$.

	x	y	z	U(eq)
H(6)	4956	4378	4499	48
H(7)	6469	4656	3989	55
H(9)	7594	4850	2825	53
H(10)	7866	4893	1483	53
H(11)	6531	4905	610	54
H(12)	4923	4796	1106	41
H(22)	9313	7467	1825	44
H(23)	10620	6256	2970	46
H(24)	10093	6003	4275	50
H(25)	8216	6656	4462	81
H(26)	6876	7841	3321	72
H(32)	5202	9483	2635	41
H(33)	3627	9211	3029	50
H(34)	3011	8197	2426	50
H(35)	3920	7471	1401	46
H(36)	5539	7691	1018	36
H(42)	8322	6479	1298	40
H(43)	8773	5778	166	44
H(44)	8089	7040	-1170	40
H(45)	6996	8997	-1397	45
H(46)	6511	9708	-279	40
H(52)	8228	9965	963	42
H(53)	7909	11895	305	52
H(54)	6133	13381	166	53
H(55)	4681	12948	648	51
H(56)	4964	11024	1235	41
H(62)	9271	2982	1657	39
H(63)	9225	3521	217	50
H(64)	9968	2117	-436	53

H(66)	10786	-419	1772	34
H(72)	7630	2132	2234	39
H(73)	5928	2119	2555	46
H(74)	5841	756	3739	54
H(75)	7448	-629	4590	62
H(76)	9165	-643	4294	47
H(82)	8816	2089	4127	41
H(83)	9046	3410	4662	55
H(84)	10512	3922	4311	56
H(85)	11669	3216	3387	54
H(86)	11407	1932	2824	46
H(92)	11953	-146	4182	38
H(93)	13371	-1992	4838	50
H(94)	13365	-3609	4580	52
H(95)	11947	-3425	3711	47
H(96)	10487	-1604	3079	37
H(3A)	4376	-193	4332	75
H(3B)	3727	826	3679	75
H(4A)	4028	2282	5103	94
H(4B)	4082	1348	4843	94

Table 3.5: Hydrogen bonds for $(AsPh_4)_2[ReN(\eta^2\text{-pic})(CN)_3]\cdot 4H_2O$ [Å and °].

D-H…A	**d(D-H)**	**d(H…A)**	**d(D…A)**	**<(DHA)**
O(1)-H(1A)…O(4)	0.90	2.38	3.277(17)	179.5
O(1)-H(1B)…N(3)	0.90	1.98	2.878(6)	179.0
O(3)-H(3A)…O(2)	0.90	1.91	2.806(13)	179.4
O(4)-H(4B)…O(1)	0.90	1.85	2.751(16)	176.0

A4: Crystal Data for $(AsPh_4)_2[ReN(\eta^2\text{-quin})(CN)_3]\cdot 2H_2O$ (Paragraph 5.3.4)

Table 4.1: Atomic coordinates ($\times 10^4$) and equivalent isotropic displacement parameters ($Å \times 10^3$) for $(AsPh_4)_2[ReN(\eta^2\text{-quin})(CN)_3]\cdot 2H_2O$. $U_{(eq)}$ is defined as one third of the trace of the orthogonalized U_{ij} tensor.

	x/a	y/b	z/c	U(eq)
Re	2881(1)	4796(1)	1872(1)	24(1)
N(1)	3779(3)	1978(3)	2604(3)	36(1)
N(2)	469(4)	4922(4)	1505(3)	45(1)
N(3)	1646(3)	7555(3)	1676(3)	38(1)
N(4)	4330(3)	4654(3)	2591(2)	26(1)
N(5)	3245(3)	4908(3)	914(2)	34(1)
O(1)	2476(2)	4605(3)	3190(2)	28(1)
O(2)	3221(3)	4103(3)	4488(2)	43(1)
C(1)	3483(3)	2968(4)	2331(3)	25(1)
C(2)	1330(4)	4891(4)	1628(3)	29(1)
C(3)	2109(4)	6586(4)	1740(3)	27(1)
C(4)	3243(4)	4380(4)	3731(3)	27(1)
C(5)	4252(4)	4514(4)	3392(3)	29(1)
C(6)	5047(4)	4491(5)	3931(3)	40(1)
C(7)	5947(4)	4631(5)	3635(3)	46(1)
C(8)	6101(4)	4739(4)	2806(3)	36(1)
C(9)	7058(4)	4822(4)	2484(4)	44(1)
C(10)	7210(4)	4863(4)	1688(4)	44(1)
C(11)	6417(5)	4862(4)	1167(4)	45(1)
C(12)	5459(4)	4796(4)	1463(3)	35(1)
C(13)	5282(4)	4732(4)	2289(3)	28(1)
As(1)	6872(1)	8724(1)	1517(1)	24(1)
C(21)	7966(4)	7810(4)	2464(3)	30(1)
C(22)	9085(4)	7317(4)	2361(3)	37(1)
C(23)	9859(4)	6613(4)	3040(3)	39(1)
C(24)	9545(4)	6426(5)	3809(3)	42(1)
C(25)	8431(5)	6846(6)	3925(4)	67(2)
C(26)	7640(5)	7544(6)	3250(4)	60(2)
C(31)	5527(3)	8593(4)	1801(3)	26(1)
C(32)	4955(4)	9062(4)	2392(3)	34(1)

C(33)	4017(4)	8905(5)	2621(3)	42(1)
C(34)	3649(4)	8308(4)	2259(3)	42(1)
C(35)	4195(4)	7868(4)	1657(3)	38(1)
C(36)	5151(4)	8001(4)	1426(3)	30(1)
C(41)	7349(3)	8149(4)	607(3)	25(1)
C(42)	8039(4)	6987(4)	752(3)	33(1)
C(43)	8311(4)	6576(4)	78(3)	37(1)
C(44)	7910(4)	7326(4)	-714(3)	33(1)
C(45)	7254(4)	8484(4)	-849(3)	37(1)
C(46)	6965(4)	8908(4)	-188(3)	34(1)
C(51)	6619(4)	10318(4)	1145(3)	26(1)
C(52)	7502(4)	10571(4)	884(3)	35(1)
C(53)	7316(5)	11715(5)	505(3)	43(1)
C(54)	6260(5)	12596(4)	419(3)	44(1)
C(55)	5398(4)	12339(4)	699(3)	43(1)
C(56)	5566(4)	11200(4)	1055(3)	34(1)
As(2)	9939(1)	794(1)	3003(1)	22(1)
C(61)	10015(3)	1227(4)	1839(3)	24(1)
C(62)	9560(4)	2410(4)	1387(3)	33(1)
C(63)	9544(4)	2724(5)	536(3)	41(1)
C(64)	9984(4)	1892(5)	148(3)	44(1)
C(65)	10447(4)	736(5)	605(3)	40(1)
C(66)	10470(4)	380(4)	1459(3)	29(1)
C(71)	8554(3)	742(4)	3233(3)	24(1)
C(72)	7593(4)	1571(4)	271(3)	33(1)
C(73)	6588(4)	1563(4)	2906(3)	39(1)
C(74)	6537(4)	751(5)	3606(3)	45(1)
C(75)	7491(5)	-67(5)	4114(4)	52(2)
C(76)	8509(4)	-83(4)	3940(3)	39(1)
C(81)	10086(4)	1902(4)	3427(3)	26(1)
C(82)	9390(4)	2326(4)	3974(3)	34(1)
C(83)	9532(5)	3096(5)	4296(3)	46(1)
C(84)	10399(5)	3408(5)	4078(3)	47(1)
C(85)	11089(5)	2988(5)	3535(3)	45(1)
C(86)	10935(4)	2228(4)	3203(3)	38(1)
C(91)	11097(3)	-703(4)	3561(3)	25(1)
C(92)	11950(4)	-811(4)	4088(3)	32(1)
C(93)	12791(4)	-1903(5)	4473(3)	42(1)

C(94)	12781(4)	-2865(4)	4322(3)	42(1)
C(95)	11939(4)	-2757(4)	3807(3)	39(1)
C(96)	11079(4)	-1679(4)	3426(3)	31(1)
O(3)	3787(3)	434(3)	4181(2)	50(1)
O(4)	4198(4)	1561(3)	5241(3)	62(1)

Table 4.2: Bond lengths (Å) and angles (°) for $(AsPh_4)_2[ReN(\eta^2\text{-quin})(CN)_3]\cdot 2H_2O$.

Bond lengths	**(Å)**	**Bond lengths**	**(Å)**
Re-N(5)	1.680(4)	C(45)-H(45)	0.9500
Re-C(2)	2.066(5)	C(51)-C(56)	1.384(6)
Re-C(3)	2.117(4)	C(51)-C(52)	1.390(6)
Re-C(4)	2.120(4)	C(52)-C(53)	1.389(7)
Re-N(4)	2.224(4)	C(52)-H(52)	0.9500
Re-O(1)	2.271(3)	C(53)-C(54)	1.389(8)
N(1)-C(1)	1.154(5)	C(53)-H(53)	0.9500
N(2)-C(2)	1.156(6)	C(54)-C(55)	1.373(7)
N(3)-C(3)	1.152(5)	C(54)-H(54)	0.9500
N(4)-C(5)	1.333(6)	C(55)-C(56)	1.384(7)
N(4)-c(13)	1.395(5)	C(55)-H(55)	0.9500
O(1)-C(4)	1.270(5)	C(56)-H(56)	0.9500
O(2)-C(4)	1.238(5)	As(2)-C(81)	1.908(4)
C(4)-C(5)	1.517(6)	As(2)-C(71)	1.910(4)
C(5)-C(6)	1.404(6)	As(2)-C(61)	1.914(4)
C(6)-C(7)	1.358(7)	As(2)-C(91)	1.915(4)
C(6)-H(6)	0.9500	C(61)-C(66)	1.386(6)
C(7)-C(8)	1.402(7)	C(61)-C(62)	1.403(6)
C(7)-H(7)	0.9500	C(62)-C(63)	1.387(7)
C(8)-C(9)	1.416(7)	C(62)-H(62)	0.9500
C(8)-C(13)	1.425(7)	C(63)-C(64)	1.378(7)
C(9)-C(10)	1.360(8)	C(63)-H(63)	0.9500
C(9)-H(9)	0.9500	C(64)-C(65)	1.376(8)
C(10)-C(11)	1.398(8)	C(64)-H(64)	0.9500
C(10)-H(10)	0.9500	C(65)-C(66)	1.391(7)
C(11)-C(12)	1.394(7)	C(65)-H(65)	0.9500

C(11)-H(11)	0.9500	C(66)-H(66)	0.9500
C(12)-C(13)	1.409(6)	C(71)-C(72)	1.395(6)
C(12)-H(12)	0.9500	C(71)-C(76)	1.395(6)
As(1)-C(51)	1.916(4)	C(72)-C(73)	1.382(6)
As(1)-C(41)	1.914(4)	C(72)-H(72)	0.9500
As(1)-C(31)	1.916(4)	C(73)-C(74)	1.381(7)
As(1)-C(21)	1.920(5)	C(73)-H(73)	0.9500
C(21)-C(26)	1.394(7)	C(74)-C(75)	1.379(8)
C(21)-C(22)	1.394(6)	C(74)-H(79)	0.9500
C(22)-C(23)	1.376(7)	C(75)-C(76)	1.380(7)
C(22)-H(22)	0.9500	C(75)-H(75)	0.9500
C(23)-C(24)	1.355(7)	C(76)-H(76)	0.9500
C(23)-H(23)	0.9500	C(81)-C(82)	1.378(6)
C(24)-C(25)	1.389(8)	C(81)-C(86)	1.386(6)
C(24)-H(24)	0.9500	C(82)-C(83)	1.377(6)
C(25)-C(26)	1.382(8)	C(82)-H(82)	0.9500
C(25)-H(25)	0.9500	C(83)-C(84)	1.397(8)
C(26)-H(26)	0.9500	C(83)-H(83)	0.9500
C(31)-C(36)	1.390(6)	C(84)-C(85)	1.369(8)
C(31)-C(32)	1.394(6)	C(84)-H(84)	0.9500
C(32)-C(33)	1.386(6)	C(85)-C(86)	1.383(6)
C(32)-H(32)	0.9500	C(85)-H(85)	0.9500
C(33)-C(34)	1.374(7)	C(86)-H(86)	0.9500
C(33)-H(33)	0.9500	C(91)-C(96)	1.399(6)
C(34)-C(35)	1.382(7)	C(91)-C(92)	1.400(6)
C(34)-H(34)	0.9500	C(92)-C(93)	1.388(7)
C(35)-C(36)	1.396(6)	C(92)-H(92)	0.9500
C(35)-H(35)	0.9500	C(93)-C(94)	1.390(7)
C(36)-H(36)	0.9500	C(93)-H(93)	0.9500
C(41)-C(46)	1.385(6)	C(94)-C(95)	1.375(7)
C(41)-C(42)	1.385(6)	C(94)-H(94)	0.9500
C(42)-C(43)	1.396(6)	C(95)-C(96)	1.387(6)
C(42)-H(42)	0.9500	C(95)-H(95)	0.9500
C(43)-C(44)	1.380(7)	C(96)-H(96)	0.9500
C(43)-H(43)	0.9500	O(3)-H(3A)	0.8491
C(44)-C(45)	1.375(7)	O(3)-H(3B)	0.8482
C(44)-H(44)	0.9500	O(4)-H(4A)	0.8502
C(45)-C(46)	1.387(7)	O(4)-H(4B)	0.8502

Appendix A

Bond angles	(°)	Bond angles	(°)
N(5)-Re-C(2)	97.16(19)	N(4)-C(13)-C(12)	120.6(4)
N(5)-Re-C(3)	97.88(17)	N(4)-C(13)-C(8)	121.1(4)
N(5)-Re-C(1)	98.14(17)	C(12)-C(13)-C(8)	118.3(4)
N(5)-Re-O(1)	177.25(15)	C(51)-As(1)-C(41)	106.26(18)
C(2)-Re-C(3)	88.22(16)	C(51)-As(1)-C(31)	110.42(18)
C(2)-Re-C(1)	88.28(16)	C(41)-As(1)-C(311)	109.25(18)
C(3)-Re-C(1)	163.91(16)	C(51)-As(1)-C(21)	113.07(19)
N(5)-Re-N(4)	104.15(16)	C(41)-As(1)-C(21)	110.04(19)
C(2)-Re-N(4)	158.69(16)	C(31)-As(1)-C(21)	107.76(19)
C(3)-Re-N(4)	88.48(15)	C(26)-C(21)-As(1)	120.2(4)
C(1)-Re-N(4)	89.10(15)	C(22)-C(21)-As(1)	120.1(4)
N(5)-Re-O(1)	177.25(15)	C(36)-C(31)-As(1)	119.1(3)
C(2)-Re-O(1)	85.42(15)	C(32)-C(21)-As(1)	120.1(3)
C(3)-Re-O(1)	83.12(14)	C(46)-C(41)-As(1)	118.7(3)
C(1)-Re-O(1)	80.95(14)	C(42)-C(41)-As(1)	120.0(4)
N(4)-Re-O(1)	73.28(12)	C(56)-C(51)-As(1)	121.3(3)
C(5)-N(4)-C(13)	117.4(4)	C(52)-C(51)-As(1)	117.9(3)
C(5)-N(4)-Re	115.5(3)	C(81)-As(2)-C(71)	109.13(18)
C(13)-N(4)-Re	127.1(3)	C(81)-As(2)-C(61)	109.27(18)
C(4)-O(1)-Re	117.4(3)	C(71)-As(2)-C(61)	110.49(18)
N(1)-C(1)-Re	177.1(4)	C(81)-As(2)-C(91)	108.67(19)
N(2)-C(2)-Re	178.5(5)	C(71)-As(2)-C(91)	108.04(18)
N(3)-C(3)-Re	176.9(4)	C(61)-As(2)-C(91)	111.19(18)
O(2)-C(4)-O(1)	126.3(4)	C(66)-C(61)-As(2)	120.0(3)
O(2)-C(4)-C(5)	118.7(4)	C(62)-C(61)-As(2)	118.3(3)
O(1)-C(4)-C(5)	115.0(4)	C(72)-C(71)-As(2)	119.3(3)
N(4)-C(5)-C(4)	117.7(4)	C(76)-C(71)-As(2)	119.6(3)
N(4)-C(5)-C(6)	123.6(4)	C(86)-C(81)-As(2)	118.5(3)
N(4)-C(5)-C(4)	117.7(4)	C(82)-C(81)-As(2)	120.3(3)
C(6)-C(5)-C(4)	118.6(4)	C(96)-C(91)-As(2)	119.0(3)
C(7)-C(6)-C(5)	119.5(5)	C(92)-C(91)-As(2)	119.1(5)
C(7)-C(6)-H(6)	120.2	H(3A)-O(3)-H(3B)	113.3
C(5)-C(6)-H(6)	120.2	H(4A)-O(4)-H(4B)	113.1
C(6)-C(7)-C(8)	119.8(5)		

Table 4.3: Anisotropic displacement parameters ($Å^2 \times 10^3$) for $(AsPh_4)_2[ReN(\eta^2\text{-quin})(CN)_3]\cdot 2H_2O$. The anisotropic displacement factor exponent takes the form: $2\pi^2[h^2a^{*2}U^{11} + \ldots + 2hka^*b^*U^{12}]$.

	U^{11}	U^{22}	U^{33}	U^{23}	U^{13}	U^{12}
Re	27(1)	19(1)	22(1)	-5(1)	0(1)	-6(1)
N(1)	33(2)	30(2)	39(3)	-9(2)	2(2)	-9(2)
N(2)	35(2)	38(2)	53(3)	-17(2)	-7(2)	-5(2)
N(3)	44(2)	27(2)	38(3)	-9(2)	-1(2)	-12(2)
N(4)	27(2)	24(2)	22(2)	-5(2)	2(2)	-7(2)
N(5)	33(2)	30(2)	30(2)	-9(2)	0(2)	-5(2)
O(1)	26(2)	28(2)	-8(1)	6(1)	-10(1)	-
O(2)	46(2)	52(2)	24(2)	-6(2)	4(2)	-21(2)
C(1)	22(2)	22(2)	24(2)	-5(2)	-1(2)	-4(2)
C(2)	31(3)	18(2)	31(3)	-8(2)	-2(2)	-2(2)
C(3)	30(2)	25(2)	25(2)	-8(2)	2(2)	-11(2)
C(4)	32(2)	22(2)	25(3)	-7(2)	7(2)	-9(2)
C(5)	27(2)	27(2)	27(3)	-3(2)	1(2)	-8(2)
C(6)	38(3)	54(3)	24(3)	-5(2)	-7(2)	-20(3)
C(7)	38(3)	58(4)	38(3)	-3(3)	-7(3)	-24(3)
C(8)	30(3)	28(2)	40(3)	-2(2)	1(2)	-10(2)
C(9)	33(3)	35(3)	57(4)	-1(3)	0(3)	-17(2)
C(10)	34(3)	29(3)	64(4)	-8(3)	15(3)	-13(2)
C(11)	53(3)	37(3)	48(3)	-15(3)	22(3)	-22(3)
C(12)	42(3)	32(3)	33(3)	-10(2)	13(2)	-20(2)
C(13)	28(2)	18(2)	32(3)	-2(2)	4(2)	-9(2)
As(1)	19(1)	25(1)	29(1)	-11(1)	5(1)	-8(1)
C(21)	26(2)	29(2)	37(3)	-16(2)	7(2)	-10(2)
C(22)	26(2)	44(3)	33(3)	-7(2)	7(2)	-11(2)
C(23)	25(2)	45(3)	36(3)	-12(2)	-1(2)	-6(2)
C(24)	37(3)	44(3)	39(3)	-17(3)	-6(2)	-10(2)
C(25)	44(4)	103(5)	28(3)	-15(3)	4(3)	-12(4)
C(26)	29(3)	94(5)	36(3)	-22(3)	6(3)	-4(3)
C(31)	21(2)	27(2)	30(3)	-6(2)	6(2)	-10(2)
C(32)	30(3)	39(3)	39(3)	-17(2)	10(2)	-17(2)
C(33)	34(3)	49(3)	42(3)	-15(3)	16(2)	-18(2)
C(34)	27(3)	43(3)	53(4)	-7(3)	11(2)	-19(2)

C(35)	31(3)	34(3)	47(3)	-4(2)	-4(2)	-17(2)
C(36)	28(2)	26(2)	37(3)	-8(2)	5(2)	-13(2)
C(41)	22(2)	27(2)	30(3)	13(2)	8(2)	-13(2)
C(42)	42(3)	22(2)	36(3)	-8(2)	9(2)	-15(2)
C(43)	44(3)	31(3)	41(3)	-18(2)	13(2)	-17(2)
C(44)	30(2)	44(3)	33(3)	-22(2)	8(2)	-17(2)
C(45)	30(3)	44(3)	30(3)	-9(2)	-4(2)	-11(2)
C(46)	28(2)	31(2)	34(3)	-13(2)	-2(2)	-3(2)
C(51)	26(2)	24(2)	29(3)	-9(2)	5(2)	-11(2)
C(52)	27(2)	34(3)	48(3)	-17(2)	12(2)	-14(2)
C(53)	50(3)	49(3)	48(3)	-21(3)	19(3)	-35(3)
C(54)	61(4)	33(3)	46(3)	-17(3)	13(3)	-25(3)
C(55)	42(3)	28(3)	49(3)	-14(2)	8(3)	-6(2)
C(56)	28(2)	26(2)	47(3)	-13(2)	9(2)	-9(2)
As(2)	22(1)	22(1)	23(1)	-7(1)	5(1)	-11(1)
C(61)	19(2)	31(2)	23(2)	-8(2)	7(2)	-11(2)
C(62)	37(3)	28(2)	29(3)	-6(2)	7(2)	-13(2)
C(63)	35(3)	46(3)	32(3)	6(2)	1(2)	-19(2)
C(64)	39(3)	76(4)	26(3)	-14(3)	8(2)	-34(3)
C(65)	35(3)	62(4)	38(3)	-31(3)	14(2)	-25(3)
C(66)	26(2)	32(2)	31(3)	-12(2)	4(2)	-14(2)
C(71)	21(2)	33(2)	26(2)	-13(2)	9(2)	-15(2)
C(72)	31(3)	29(2)	33(3)	-5(2)	2(2)	-12(2)
C(73)	25(2)	42(3)	48(3)	-15(3)	1(2)	-13(2)
C(74)	28(3)	64(4)	49(4)	-19(3)	15(3)	-25(3)
C(75)	49(3)	71(4)	40(3)	-2(3)	12(3)	-40(3)
C(76)	30(3)	46(3)	34(3)	-1(2)	3(2)	-17(2)
C(81)	31(2)	24(2)	26(2)	-7(2)	4(2)	-15(2)
C(82)	43(3)	40(3)	27(3)	-13(2)	10(2)	-23(2)
C(83)	59(4)	48(3)	37(3)	-22(3)	11(3)	-23(3)
C(84)	73(4)	39(3)	35(3)	-12(2)	-4(3)	-30(3)
C(85)	64(4)	49(3)	40(3)	-13(3)	6(3)	-42(3)
C(86)	46(3)	41(3)	40(3)	-15(2)	14(2)	-29(3)
C(91)	21(2)	24(2)	24(2)	-2(2)	3(2)	-7(2)
C(92)	28(2)	37(3)	30(3)	-8(2)	4(2)	-14(2)
C(93)	29(3)	50(3)	32(3)	-3(2)	-5(2)	-12(2)
C(94)	38(3)	33(3)	36(3)	0(2)	1(2)	-2(2)
C(95)	43(3)	23(2)	40(3)	-4(2)	5(2)	-8(2)

C(96)	33(3)	26(2)	31(3)	-8(2)	1(2)	-10(2)
O(3)	47(2)	49(2)	41(2)	2(2)	7(2)	-21(2)
O(4)	78(3)	41(2)	53(3)	-8(2)	2(2)	-17(2)

Table 4.4: Hydrogen coordinates ($\times 10^4$) and isotropic displacement parameters ($Å^2 \times 10^3$) for $(AsPh_4)_2[ReN(\eta^2\text{-quin})(CN)_3]\cdot 2H_2O$.

	x	y	z	U(eq)
H(6)	4956	4378	4499	48
H(7)	6469	4656	3989	55
H(9)	7594	4850	2825	53
H(10)	7866	4893	1483	53
H(11)	6531	4905	610	54
H(12)	4923	4796	1106	41
H(22)	9313	7467	1825	44
H(23)	10620	6256	2970	46
H(24)	10093	6003	4275	50
H(25)	8216	6656	4462	81
H(26)	6876	7841	3321	72
H(32)	5202	9483	2635	41
H(33)	3627	9211	3029	50
H(34)	3011	8197	2426	50
H(35)	3920	7471	1401	46
H(36)	5539	7691	1018	36
H(42)	8322	6479	1298	40
H(43)	8773	5778	166	44
H(44)	8089	7040	-1170	40
H(45)	6996	8997	-1397	45
H(46)	6511	9708	-279	40
H(52)	8228	9965	963	42
H(53)	7909	11895	305	52
H(54)	6133	13381	166	53
H(55)	4681	12948	648	51
H(56)	4964	11024	1235	41
H(62)	9271	2982	1657	39
H(63)	9225	3521	217	50
H(64)	9968	2117	-436	53

H(66)	10786	-419	1772	34
H(72)	7630	2132	2234	39
H(73)	5928	2119	2555	46
H(74)	5841	756	3739	54
H(75)	7448	-629	4590	62
H(76)	9165	-643	4294	47
H(82)	8816	2089	4127	41
H(83)	9046	3410	4662	55
H(84)	10512	3922	4311	56
H(85)	11669	3216	3387	54
H(86)	11407	1932	2824	46
H(92)	11953	-146	4182	38
H(93)	13371	-1992	4838	50
H(94)	13365	-3609	4580	52
H(95)	11947	-3425	3711	47
H(96)	10487	-1604	3079	37
H(3A)	4376	-193	4332	75
H(3B)	3727	826	3679	75
H(4A)	4028	2282	5103	94
H(4B)	4082	1348	4843	94

Table 4.5: Hydrogen bonds for $(AsPh_4)_2[ReN(\eta^2\text{-quin})(CN)_3]\cdot 2H_2O$ [Å and °].

D-H…A	d(D-H)	d(H…A)	d(D…A)	<(DHA)
O(3)-H(3A)…O(4)	0.85	1.97	2.815(6)	173.2
O(3)-H(3B)…N(1)	0.85	2.04	2.867(5)	164.6
O(4)-H(4A)…O(2)	0.85	2.13	2.951(5)	161.6
O(4)-H(4B)…N(3)	0.85	2.04	2.861(6)	162.4

2 SUPPLEMENTARY DATA FOR KINETIC MEASUREMENTS

The tables in this section give the observed first-order rate constants for the reactions described in **Chapter 6**. If the data in the tables were graphically presented in **Chapter 6**, the numbering of the figure is given after the table number. The ligand concentrations (pic, quin and 2,3-dipic) are given in mol dm^{-3} (M); the observed first-order rate constant k_{obs} is given in the unit s^{-1}; temperature is reported in °C.

A5: Kinetic and Spectrophotometric Data for the Reaction between $[ReN(H_2O)(CN)_4]^{2-}$ and Pyridine-2-carboxylate (pic)

Table 5.1: Spectrophotometric data. Absorbance *vs.* $[pic]_T$ at T = 79.81°C, pH = 8.06, λ = 400 nm, μ = 1.0M $NaClO_4$, $[[ReN(H_2O)(CN)_4]^{2-}] = 1.0 \times 10^{-3}$M (Figure 6.2).

[pic] / mol dm^{-3}	Abs.
0.0	0.215
0.1	0.653
0.15	0.721
0.2	0.76
0.3	0.839
0.4	0.915
0.5	0.925
0.6	0.948
0.7	0.979
0.8	1.01
0.9	1.03
1.0	1.037

Table 5.2: **Spectrophotometric data: Absorbance *vs.* pH at T = 80.2°C, λ = 400 nm, μ = 1.0M $NaClO_4$, $[pic]_T$ = 0.1M, $[[ReN(H_2O)(CN)_4]^{2-}]$ =1.0×10^{-3}M** (Figure 6.3).

pH	Abs.	pH	Abs.
8.08	0.723	10.92	0.515
8.21	0.721	11.04	0.509
8.3	0.723	11.14	0.499
8.49	0.721	11.24	0.486
8.61	0.722	11.34	0.458
8.8	0.723	11.41	0.412
8.91	0.724	11.53	0.386
9.08	0.723	11.64	0.363
9.3	0.705	11.74	0.327
9.54	0.697	11.82	0.313
9.64	0.682	11.93	0.306
9.79	0.679	12.04	0.285
9.89	0.672	12.1	0.279
10.1	0.664	12.24	0.275
10.23	0.626	12.32	0.276
10.47	0.608	12.41	0.274
10.64	0.586	12.54	0.275
10.72	0.557	12.61	0.273
10.86	0.544		

Table 5.3: **Kinetic data: k_{obs} *vs.* $[pic]_T$ at different temperatures (fast reactions), pH = 8.05, λ = 400 nm, μ = 1.0M $NaClO_4$, $[[ReN(H_2O)(CN)_4]^{2-}] = 1.0 \times 10^{-2}$M** (Figure 6.4).

[pic] / mol dm^{-3}	Temperature (°C)		
	40.3	30.2	20.4
	(10^3) k_{obs} / s^{-1}		
0.1	83.15(2)	51.54(2)	22.98(1)
0.2	94.37(2)	57.56(2)	25.74(1)
0.3	113.9(3)	61.72(3)	28.17(2)
0.4	133.7(3)	66.98(1)	29.62(3)
0.5	150.7(2)	83.15(2)	30.43(3)
0.6	175.6(2)	88.06(4)	32.93(7)
0.7	198.8(1)	93.18(3)	36.11(6)
0.8	208.3(4)	98.20(6)	37.86(7)
0.9	237.6(2)	122.6(7)	40.46(3)
1.0	246.3(3)	136.0(2)	

Table 5.4: **Kinetic data: k_{obs} *vs.* pH at T = 40.3°C, λ = 400 nm, μ = 1.0M $NaClO_4$, $[pic]_T$ = 0.1M, $[[ReN(H_2O)(CN)_4]^{2-}] = 1.0 \times 10^{-2}$M** (Figure 6.5).

pH	$(10^3)\ k_{obs}\ /\ s^{-1}$	pH	$(10^3)\ k_{obs}\ /\ s^{-1}$
8.01	40.45(2)	11.23	175.4(1)
8.56	42.15(2)	11.33	193.1(4)
8.71	42.43(1)	11.44	206.7(6)
9.01	40.21(1)	11.52	245.4(3)
9.53	51.3(1)	11.64	274.6(3)
9.78	68.12(1)	11.75	285.7(2)
10.15	71.34(2)	11.91	324.2(1)
10.26	83.67(3)	12.01	330.7(1)
10.31	89.02(4)	12.14	342.2(2)
10.43	90.58(3)	12.23	354.5(4)
10.60	104.5(2)	12.33	371.6(3)
10.91	119.1(4)	12.4	372.5(1)
11.04	135.8(2)	12.51	363.7(2)
11.11	160.0(3)		

Table 5.5: **Activation parameters for the kinetic results (fast reaction, k_1)** (Figure 6.6).

T/°C	T/K	1/T	k_1	k_1/T	$\ln(k_1/T)$
40.3	313.45	3.19×10^{-3}	$1.92(5)\times10^{-1}$	6.13×10^{-4}	-7.40
30.2	303.35	3.30×10^{-3}	$8.98(7)\times10^{-2}$	2.96×10^{-4}	-8.13
20.4	293.55	3.41×10^{-3}	$2.10(5)\times10^{-2}$	7.15×10^{-5}	-9.55

Table 5.6: **Activation parameters for the kinetic results (fast reaction, k_{-1})** (Figure 6.7).

T/°C	T/K	1/T	k_{-1}	k_{-1}/T	$\ln(k_{-1}/T)$
40.3	313.45	3.19×10^{-3}	5.90×10^{-2}	1.88×10^{-4}	-8.58
30.2	303.35	3.30×10^{-3}	3.65×10^{-2}	1.20×10^{-4}	-9.03
20.4	293.55	3.41×10^{-3}	2.11×10^{-3}	7.19×10^{-5}	-9.54

Table 5.7: **Kinetic data: k_{obs} *vs.* $[pic]_T$ at different temperatures (slow reactions), pH = 8.06, λ = 400 nm, μ = 1.0M $NaClO_4$, $[[ReN(H_2O)(CN)_4]^{2-}] = 1.0 \times 10^{-3}$M** (Figure 6.8).

[pic] / mol dm^{-3}	Temperature (°C)		
	79.8	70.2	61.1
	$(10^3)\ k_{obs}$ / s^{-1}		
0.1	0.558(1)	0.334(3)	0.191(9)
0.2	0.620(3)	0.440(10)	0.208(6)
0.3	0.767(7)	0.452(3)	0.220(5)
0.4	0.904(3)	0.520(4)	0.241(5)
0.5	1.09(2)	0.620(3)	0.265(5)
0.6	1.14(4)	0.684(1)	0.278(4)
0.7	1.31(1)	0.705(1)	0.295(8)
0.8	1.41(5)	0.773(2)	0.329(7)
0.9	1.50(3)	-	0.349(2)
1.0	1.64(8)	0.917(6)	0.360(3)

Table 5.8: Kinetic data: k_{obs} *vs.* pH at T = 80.2° C, λ = 400 nm, μ = 1.0M $NaClO_4$, $[pic]_T$ = 0.1M, $[[ReN(H_2O)(CN)_4]^{2-}] = 1.0 \times 10^{-3}$M (Figure 6.9).

pH	$10^3 k_{obs} / s^{-1}$	pH	$10^3 k_{obs} / s^{-1}$
8.08	0.565(1)	10.92	4.86(8)
8.21	0.56(8)	11.04	5.16(5)
8.3	0.583(1)	11.14	5.79(9)
8.49	0.702(2)	11.24	6.05(10)
8.61	0.61(2)	11.34	6.15(1)
8.8	0.64(2)	11.41	7.59(2)
8.91	0.684(1)	11.53	8.6(5)
9.08	0.773(2)	11.64	7.80(3)
9.3	0.878(2)	11.74	8.16(5)
9.54	0.904(2)	11.82	8.96(8)
9.64	0.975(2)	11.93	9.54(6)
9.79	1.62(2)	12.04	9.86(4)
9.89	1.93(3)	12.1	10.6(3)
10.1	2.23(3)	12.24	10.7(1)
10.23	2.68(3)	12.32	10.9(6)
10.47	3.52(5)	12.41	11.0(8)
10.64	3.7(4)	12.54	10.9(3)
10.72	3.73(7)	12.61	11.1(3)
10.86	4.66(3)		

Table 5.9: **Kinetic data: k_{obs} *vs.* $[pic]_T$ at different temperatures (slow reactions), pH = 12.61, λ = 400 nm, μ = 1.0M $NaClO_4$, $[[ReN(H_2O)(CN)_4]^{2-}] = 1.0 \times 10^{-3}$M** (Figure 6.10).

[pic] / mol dm^{-3}	Temperature (°C)		
	80.1	70.3	60.0
	(10^3) k_{obs} / s^{-1}		
0.1	10.99(2)	6.58(1)	3.34(5)
0.2	13.2(2)	7.26(1)	3.73(2)
0.3	14.62(2)	7.92(1)	4.56(1)
0.4	15.56(2)	8.56(1)	4.89(1)
0.5	15.88(3)	8.75(1)	5.12(3)
0.6	16.09(4)	9.09(1)	5.26(1)
0.7	16.89(5)	9.28(1)	5.38(1)
0.8	17.3(4)	9.56(2)	5.49(3)
0.9	17.08(1)	9.74(3)	5.60(3)
1.0	17.18(1)	10.06(10)	5.68(3)

Table 5.10: Kinetic data: k_{obs} *vs.* pH at T = 80.3°C, λ = 400 nm, μ = 1.0M $NaClO_4$, $[pic]_T$ = 0.1M, $[[ReN(H_2O)(CN)_4]^{2-}] = 1.0 \times 10^{-3}$M (Figure 6.11).

pH	$(10^3)\ k_{obs}\ /\ s^{-1}$	pH	$(10^3)\ k_{obs}\ /\ s^{-1}$
4.01	0.122(1)	5.93	0.438(10)
4.32	0.131(8)	6.03	0.473(3)
4.41	0.154(4)	6.12	0.588(2)
4.53	0.179(3)	6.23	0.496(1)
4.72	0.178(7)	6.31	0.507(7)
4.82	0.202(9)	6.44	0.514(3)
5.01	0.248(1)	6.62	0.522(4)
5.13	0.265(2)	6.81	0.532(3)
5.21	0.287(9)	7.10	0.601(2)
5.30	0.357(4)	7.26	0.540(1)
5.42	0.367(2)	7.42	0.536(3)
5.51	0.393(8)	7.61	0.544(3)
5.62	0.392(1)	7.83	0.546(2)
5.71	0.420(3)	8.09	0.568(8)
5.80.	0.427(2)		

Table 5.11: Activation parameters for the kinetic results (slow reaction, k_3) (Figure 6.13).

T/°C	T/K	1/T	k_3	k_3/T	$Ln(k_3/T)$
79.81	352.95	2.83×10^{-4}	1.84×10^{-2}	5.2×10^{-5}	-9.862
70.2	343.25	2.91×10^{-4}	1.01×10^{-2}	2.94×10^{-5}	-10.434
61.1	332.75	3.01×10^{-4}	6.04×10^{-3}	1.82×10^{-5}	-10.92

A6: Kinetic and Spectrophotometric Data of the Reaction between $[ReN(H_2O)(CN)_4]^{2-}$ and Quinoline-2-carboxylate (quin).

Table 6.1: **Spectrophotometric data: Absorbance *vs.* $[quin^-]_T$ at T = 80.2° C, pH = 8.08, λ = 450 nm, μ = 1.0M $NaClO_4$ and $[[ReN(CN)_4(H_2O)]^{2-}] = 1.0 \times 10^{-3}$M** (Figure 6.15).

$[quin^-]$ / mol dm^{-3}	Abs.
0.0	0.215
0.1	0.416
0.2	0.534
0.3	0.581
0.4	0.613
0.5	0.647
0.6	0.685
0.7	0.695
0.8	0.710
0.9	0.716
1.0	0.720

Table 6.2: **Spectrophotometric data: Absorbance *vs.* pH at T = 80.4°C, λ = 450 nm, μ = 1.0M $NaClO_4$, $[quin]_T$ = 0.1M, $[[ReN(CN)_4(H_2O)]^{2-}]$ = 1.0×10^{-3}M** (Figure 6.16).

pH	Abs.	pH	Abs.
8.1	0.735	11.25	0.601
8.31	0.741	11.32	0.581
8.7	0.73	11.51	0.537
9.24	0.732	11.6	0.512
9.56	0.73	11.74	0.498
9.91	0.720	11.82	0.473
10.02	0.717	11.90	0.421
10.11	0.702	12.04	0.376
10.15	0.702	12.08	0.351
10.32	0.692	12.15	0.323
10.51	0.681	12.21	0.318
10.61	0.672	12.34	0.312
10.75	0.661	12.38	0.306
10.9	0.631	12.43	0.31
11.01	0.623		

Table 6.3: **Kinetic data: k_{obs} *vs.* $[quin^-]_T$ at different temperatures, pH = 8.02, λ = 400 nm, μ = 1.0M $NaClO_4$, $[[ReN(CN)_4(H_2O)]^{2-}] = 1.0 \times 10^{-2}$M** (Figure 6.17).

$[quin^-]$ / mol dm^{-3}	Temperature (°C)		
	40.2	30.3	20.6
	$10^3 k_{obs} / s^{-1}$		
0.1	76.85(1)	47.44(1)	22.98)4)
0.2	94.50(1)	57.56(2)	25.74(1)
0.3	112.5(1)	61.72(2)	28.17(1)
0.4	133.7(2)	66.69(1)	29.62(2)
0.5	150.7(2)	83.15(3)	30.42(2)
0.6	176.9(1)	88.07(4)	32.43(1)
0.7	198.8(7)	98.10(3)	36.10)1)
0.8	207.9(3)	108.7(1)	37.84(7)
0.9	237.6(1)	122.8(3)	40.46(3)
1.0	246.6(3)	135.9(1)	42.11(1)

Table 6.4: **Kinetic data: k_{obs} *vs.* pH at T = 40.3°C, λ = 400 nm, μ = 1.0M $NaClO_4$, $[quin^-]_T$ = 0.1M, $[[ReN(CN)_4(H_2O)]^{2-}] = 1.0 \times 10^{-2}$M** (Figure 6.18).

pH	$10^3 k_{obs} / s^{-1}$	pH	$10^3 k_{obs} / s^{-1}$
8.03	75.31(2)	10.81	126.51(3)
8.32	75.43(2)	10.93	138.66(3)
8.51	75.26(4)	11.04	151.34(1)
8.73	74.58(3)	11.13	158.70(1)
8.92	76.07(2)	11.31	187.35(2)
9.04	78.12(1)	11.47	187.8(1)
9.51	79.16(1)	11.56	222.80(2)
9.73	80.52(1)	11.71	242.67(4)
9.93	84.38(1)	11.83	256.99(2)
10.10	86.11(2)	11.92	275.4(2)
10.27	85.29(3)	12.03	282.6(1)
10.35	92.68(5)	12.11	290.5(3)
10.46	98.76(2)	12.21	283.6(2)
10.62	110.97(3)	12.31	286.67(2)

Table 6.5: **Activation parameters for the kinetic results (slow reaction, k_1)** (Figure 6.19)

T/°C	T/K	1/T	k_1	k_1/T	$\ln(k_1/T)$
40.2	313.55	0.00319	0.195	6.22×10^{-4}	-7.38
30.3	303.45	0.0033	0.0953	3.14×10^{-4}	-8.066
20.6	293.75	0.00340	0.02172	8.77×10^{-5}	-9.34

Table 6.6: **Activation parameters for the kinetic results (slow reaction, k_{-1})** (Figure 6.20).

T/°C	T/K	1/T	k_{-1}	k_{-1}/T	$\ln(k_{-1}/T)$
40.2	313.55	0.00319	0.056	1.79×10^{-4}	-8.63
30.3	303.45	0.0033	0.0341	1.12×10^{-4}	-9.097
20.6	293.75	0.00340	0.0205	6.97×10^{-5}	-9.57

Table 6.7: **Kinetic data: k_{obs} *vs.* $[quin^-]_T$ at different temperatures (slow reactions), pH = 8.02, λ = 450 nm, μ = 1.0M $NaClO_4$, $[[ReN(CN)_4(H_2O)]^{2-}] = 1.0 \times 10^{-3}$M** (Figure 6.21).

$[quin^-]$ / mol dm^{-3}	Temperature (°C)		
	80.2	71.1	60.4
	$10^3 k_{obs} / s^{-1}$		
0.1	1.321(2)	0.952(3)	0.624(4)
0.2	1.780(4)	1.200(3)	0.690(7)
0.3	2.210(3)	1.380(3)	0.761(4)
0.4	2.570(5)	1.600(1)	0.812(3)
0.5	2.960(3)	1.880(6)	0.886(3)
0.6	3.420(2)	2.140(7)	0.928(2)
0.7	3.890(8)	2.460(3)	1.01(1)
0.8	4.23(2)	2.750(3)	1.18(8)
0.9	4.66(2)	2.990(4)	1.24(4)
1.0	5.12(3)	3.210(1)	1.33(1)

Table 6.8: **Kinetic data: k_{obs} *vs.* pH at T = 80.4° C, λ = 450 nm, μ = 1.0M, $[quin^-]_T$ = 0.1M, $[[ReN(CN)_4(H_2O)]^{2-}] = 1.0 \times 10^{-3}$M** (Figure 6.22).

pH	$10^3\ k_{obs}\ /\ s^{-1}$	pH	$10^3\ k_{obs}\ /\ s^{-1}$
8.1	1.319(3)	11.25	3.76(2)
8.31	1.321(1)	11.32	4.265(3)
8.7	1.348(2)	11.51	4.531(2)
9.24	1.381(3)	11.6	4.985(3)
9.56	1.458(3)	11.74	5.091(1)
9.91	1.498(6)	11.82	5.338(1)
10.02	1.538(3)	11.90	5.499(3)
10.11	1.558(3)	12.04	5.583(3)
10.15	1.667(4)	12.08	5.647(5)
10.32	1.72(1)	12.15	5.749(4)
10.51	1.881(2)	12.21	5.828(2)
10.61	1.93(3)	12.34	5.972(1)
10.75	2.26(4)	12.38	6.01(1)
10.9	3.01(5)	12.43	6.054(2)
11.01	3.38(3)		

Table 6.9: **Kinetic data: k_{obs} *vs.* $[quin^-]_T$ at different temperatures (slow reactions), pH = 12.34, λ = 450 nm, μ = 1.0M $NaClO_4$ and $[[ReN(CN)_4(H_2O)]^{2-}] = 1.0 \times 10^{-3}$M** (Figure 6.23).

$[quin^-]$ / mol dm^{-3}	Temperature (°C)		
	80.2	71.1	60.2
	$10^3 k_{obs} / s^{-1}$		
0.1	6.72(3)	3.248(2)	1.043(4)
0.2	8.81(5)	3.80(3)	1.234(5)
0.3	9.84(3)	4.26(4)	1.412(1)
0.4	10.4(1)	4.51(2)	1.538(2)
0.5	10.5(1)	5.09(3)	1.678(2)
0.6	11.04(2)	5.33(2)	1.768(3)
0.7	11.31(2)	5.53(2)	1.845(4)
0.8	11.52(2)	5.698(1)	1.949(1)
0.9	11.98(3)	5.72(3)	2.025(4)
1.0	12.15(2)	5.96(4)	2.094(2)

Table 6.10: Kinetic data: k_{obs} *vs.* pH at T = 80.6°C, λ = 450 nm, μ = 1.0M $NaClO_4$, $[quin^-]_T$ = 0.1M, $[[ReN(CN)_4(H_2O)]^{2-}] = 1.0 \times 10^{-3}$M (Figure 6.24).

pH	$10^3 k_{obs} / s^{-1}$	pH	$10^3 k_{obs} / s^{-1}$	pH	$10^3 k_{obs} / s^{-1}$
3.55	0.962(4)	4.35	1.150(1)	5.96	1.359(3)
3.61	0.973(1)	4.39	0.16(1)	5.99	1.362(6)
3.67	0.978(1)	4.51	0.191(2)	6.23	1.367(1)
3.75	0.997(2)	4.60	1.214(1)	6.54	1.37(2)
3.79	1.014(3)	4.70	1.237(2)	6.73	1.371(2)
3.82	1.026(1)	5.01	1.292(2)	6.92	1.373(4)
4.02	1.046(1)	5.34	1.326(5)	7.35	1.372(1)
4.08	1.066(5)	5.45	1.335(1)	7.68	1.376(1)
4.11	1.079(7)	5.58	1.345(1)	7.91	1.381(3)
4.13	1.087(3)	5.73	1.354(2)	8.12	1.384(1)
4.16	1.119(4)	5.91	1.355(1)		
4.24	1.147(4)	5.93	1.356(3)		

Table 6.11: Activation parameters for the kinetic results (slow reaction, k_3) (Figure 6.25).

T/°C	T/K	1/T	k_3	k_3/T	$\ln(k_3/T)$
80.2	353.34	0.00283	0.0119	3.38×10^{-5}	-10.295
71.1	344.24	0.00290	0.00551	8.4×10^{-6}	-11.687
60.2	335.55	0.002998	0.00245	7.35×10^{-6}	-11.821

A7: Kinetic and Spectrophotometric Data of the Reaction between $[ReN(H_2O)(CN)_4]^{2-}$ and Pyridine-2,3-dicarboxylate (2,3-dipic).

Table 7.1: **Spectrophotometric data: Absorbance *vs.* $[2,3\text{-dipic}]_T$ at T = 80.5°C, pH = 8.03, λ = 410 nm, μ = 1.0M $NaClO_4$, $[[ReN(H_2O)(CN)_4]^{2-}] = 1.0 \times 10^{-3}$M** (Figure 6.27).

[2,3-dipic] / mol dm^{-3}	Abs.
0.0	0.215
0.1	0.530
0.2	0.719
0.3	0.782
0.4	0.812
0.5	0.878
0.6	0.890
0.7	0.901
0.8	0.918
0.9	0.938
1.0	0.943

Table 7.2: Spectrophotometric data: Absorbance *vs.* pH at T = 80.4° C, λ = 410 nm, μ = 1.0M $NaClO_4$, $[2,3\text{-dipic}]_T$ = 0.1M, $[[ReN(H_2O)(CN)_4]^{2-}]$ = 1.0×10^{-3}M (Figure 6.28).

pH	Abs.	pH	Abs
8.03	0.762	10.82	0.695
8.51	0.758	10.90	0.982
8.72	0.754	11.04	0.662
9.01	0.755	11.10	0.643
9.31	0.756	11.22	0.635
9.42	0.752	11.32	0.612
9.51	0.753	11.48	0.584
9.71	0.751	11.52	0.562
9.83	0.749	11.63	0.534
9.90	0.749	11.74	0.512
10.12	0.748	11.80	0.501
10.25	0.749	11.92	0.473
10.31	0.742	12.01	0.452
10.40	0.737	12.21	0.423
10.51	0.730	12.36	0.418
10.64	0.721	12.41	0.416
10.73	0.710		

Table 7.3: **Kinetic data: k_{obs} *vs.* $[2,3\text{-dipic}]_T$ at different temperatures (slow reactions), pH = 8.03, λ = 410 nm, μ = 1.0M $NaClO_4$, $[[ReN(H_2O)(CN)_4]^{2-}] = 1.0 \times 10^{-3}$M** (Figure 6.29).

[2,3-dipic] / mol dm^{-3}	Temperature (°C)		
	80.5	70.6	61.1
	$10^3 k_{obs} / s^{-1}$		
0.1	1.03(2)	0.721(2)	0.375(4)
0.2	1.47(1)	0.856(2)	0.423(5)
0.3	1.86(3)	0.953(3)	0.487(3)
0.4	2.46(2)	1.35(1)	0.544(3)
0.5	2.85(2)	1.58(3)	0.596(3)
0.6	3.15(1)	1.75(2)	0.672(4)
0.7	3.76(2)	1.94(4)	0.789(4)
0.8	4.35(2)	2.24(3)	0.852(5)
0.9	4.72(2)	2.58(2)	0.925(2)
1.0	5.24(3)	2.76(4)	

Table 7.4: Kinetic data: k_{obs} *vs.* pH at T = 80.4° C, λ = 410 nm, μ = 1.0M $NaClO_4$, $[2,3\text{-dipic}]_T$ = 0.1M, $[[ReN(H_2O)(CN)_4]^{2-}] = 1.0 \times 10^{-3}$M (Figure 6.30).

pH	$10^3\, k_{obs} / s^{-1}$	pH	$10^3\, k_{obs} / s^{-1}$
8.03	1.02(5)	10.82	4.87(1)
8.51	1.015(4)	10.90	5.89(2)
8.72	1.08(4)	11.04	6.98(6)
9.01	1.08(3)	11.10	7.36(6)
9.31	1.12(5)	11.22	7.86(1)
9.42	1.24(3)	11.32	8.12(2)
9.51	1.29(2)	11.48	8.57(2)
9.71	1.37(2)	11.52	8.83(2)
9.83	1.54(2)	11.63	9.01(3)
9.90	1.77(2)	11.74	9.57(1)
10.12	1.92(2)	11.80	9.88(1)
10.25	2.34(1)	11.92	10.3(2)
10.31	2.69(2)	12.01	10.6(2)
10.40	2.98(4)	12.21	11.0(1)
10.51	3.56(3)	12.36	11.1(2)
10.64	3.73(4)	12.41	11.1(1)
10.73	4.32(3)		

Table 7.5: **Kinetic data: k_{obs} *vs.* $[2,3\text{-dipic}]_T$ at different temperatures (slow reactions), pH = 12.41, λ = 410 nm, μ = 1.0M $NaClO_4$, $[[ReN(H_2O)(CN)_4]^{2-}] = 1.0 \times 10^{-3}$M** (Figure 6.31).

[2,3-dipic] / mol dm^{-3}	Temperature (°C)		
	80.1	71.3	61.1
	$10^3 k_{obs} / s^{-1}$		
0.1	11.9(1)	7.58	3.26(1)
0.2	14.8(2)	9.26	4.63(2)
0.3	16.5(3)	11.1	5.43(2)
0.4	17.4(2)	12.2	5.95(2)
0.5	17.9(3)	12.9	6.31(5)
0.6	18.7(3)	13.4	6.44(2)
0.7	19.2(2)	13.8	6.62(1)
0.8	19.5(2)		6.81(2)
0.9	19.8(2)	14.6	6.87(1)
1.0	19.9(1)	14.8	7.13(1)

Table 7.6: **Kinetic data: k_{obs} *vs.* pH at T = 80.6°C, λ = 410 nm, μ = 1.0M ($NaClO_4$), $[2,3\text{-dipic}]_T$ = 0.1M, $[[ReN(H_2O)(CN)_4]^{2-}] = 1.0 \times 10^{-3}$M** (Figure 6.32).

pH	$(10^3) k_{obs} / s^{-1}$	pH	$(10^3) k_{obs} / s^{-1}$
3.92	0.556(4)	5.72	0.965(1)
4.01	0.564(3)	5.93	0.986(2)
4.13	0.567(4)	6.31	1.03(2)
4.26	0.602(1)	6.52	1.04(2)
4.31	0.628(2)	6.78	1.06(2)
4.42	0.639(2)	6.86	1.06(2)
4.55	0.675(2)	7.01	1.06(2)
4.63	0.706(3)	7.45	1.062(1)
4.81	0.756(3)	7.83	1.063(2)
5.23	0.872(2)	8.06	1.063(2)
5.46	0.926(2)		

Table 7.7: Activation parameters for the kinetic results (slow reaction) (Figure 6.33).

T/°C	T/K	1/T	k_3	k_3/T	$\ln(k_3/T)$
80.5	353.64	2.83×10^{-3}	2.09×10^{-2}	5.91×10^{-5}	-9.736
71.1	344.24	2.90×10^{-3}	1.63×10^{-2}	4.73×10^{-5}	-9.959
60.6	333.74	2.996×10^{-3}	7.8×10^{-3}	2.34×10^{-5}	-10.663

APPENDIX B: GENERAL RATE AND EQUILIBRIUM EQUATIONS

B1: GENERAL RATE EQUATIONS

The rate of a reaction can be defined as the change in concentration of a reactant or product per unit time. For a simple reaction such as:

$$A + B \underset{k_{-1}}{\overset{k_1}{\rightleftharpoons}} C \qquad (1)$$

The reaction rate for the above reaction is given by:

$$\text{Rate} = \frac{-d[A]}{dt} = \frac{-d[B]}{dt} = \frac{d[C]}{dt} = k_f[A]^m[B]^n - k_{-f}[C] \qquad (2)$$

with **k** as a proportional constant (the forward rate constant), that relates the rate of change to the reagent concentration (**[ ]** denotes concentration) and the minus sign indicating the disappearance of **A** and **B**. The values **m** and **n** represent the order of the reaction with regard to the concentration of **A** and **B**, with the sum of **m** and **n** equal to the order of the rate law (total reaction). The order is the way in which the rate varies with change in concentration of one or both of the reacting species. These values can be determined experimentally, but this is often difficult. This problem can be circumvented by using pseudo first-order conditions where **[B]** >> **[A]**; **[C]**.

The expression for the observed pseudo first-order rate constant (after integration), is given by **Eq. 3**:

$$k_{obs} = k_f[B]^n + k_{-f} \qquad (3)$$

Appendix B

Pseudo first-order conditions **([B]** at least 10 times in excess of **[A])** resulting in **Eq. 3**, also serve to obtain the rate constant by determining $\mathbf{k_{obs}}$ at different concentration of **B**. It can, furthermore, be used to simplify second order reactions. If the value of **m** = 1, then the reaction is first order in **B** and a graph of $\mathbf{k_{obs}}$ against **[B]** will be a straight line with intercept of $\mathbf{k_{-1}}$ to indicate that there is an equilibrium (reverse reaction) or parallel reaction. In the case of an equilibrium reaction, the equilibrium constant is given by **Eq. 4**:

$$K_{eq} = \frac{k_f}{k_{-f}} \qquad (4)$$

By integrating **Eq. 2** between time = 0 and time = t respectively, the following **Eq. 5** (expressed in terms of **C**) is obtained:

$$\ln \frac{[C]_t}{[C]_0} = k_{obs} t \qquad (5)$$

Beer-Lambert law states that:

$$A = \varepsilon c l \qquad (6)$$

with **A** = absorbance, **ε** = molar extinction coefficient, **c** = concentration and **l** = light path length.

When Beer-Lambert law is incorporated into **Eq. 5** (with $\frac{[C]_t}{[C]_0} = \frac{A_\infty - A_t}{A_\infty - A_0}$) and manipulated, the following **Eq 7** results:

$$A_t = A_\infty - (A_\infty - A_0)e^{k_{obs}\, t} \qquad (7)$$

$\mathbf{A_t}$ and $\mathbf{A_\infty}$ is the absorbance after time **t** and infinite time respectively. The term "infinite time" is defined as the time at which the reaction is complete for all the practical

purposes. The observed rate constant, $\mathbf{k_{obs}}$, can be obtained from a least-square fit of the absorbance *vs.* time data for a first-order reaction using **Eq. 7**.

All the spectrophotometric absorbance *vs.* time data in this study was fitted to **Eq. 7**.

B2: DERIVATION OF THE EQUATION FOR THE EQUILIBRIUM CONSTANT

For the spectrophotometer determination of **K'**.

From the reaction scheme the following reaction between a metal complex and a ligand is given by **Eq. 8**:

$$M\text{-}OH_2 + L \underset{k_{-1};\ +H_2O}{\overset{K_1, k_1;\ -H_2O}{\rightleftharpoons}} M\text{-}L + H_2O \qquad (\mathbf{8})$$

$$K_1 = \frac{[ML]}{[MOH_2][L]} \qquad (\mathbf{9})$$

$$[MOH_2] = \frac{[ML]}{K_1[L]} \qquad (\mathbf{10})$$

$$[ML] = K_1[MOH_2][L] \qquad (\mathbf{11})$$

$$[M]_{tot} = [MOH_2] + [ML] \qquad (\mathbf{12})$$

Substituting **Eq. 11** into **Eq. 12** gives **Eq. 13**:

$$[M]_{tot} = [MOH_2] + K_1[MOH_2][L] \qquad (\mathbf{13})$$

$$[M]_{tot} = [MOH_2](1 + K_1[L]) \qquad (\mathbf{14})$$

$$[MOH_2] = \frac{[M]_{tot}}{(1 + K_1[L])} \quad (\mathbf{15})$$

Substituting **Eq. 10** into **Eq. 12** gives **Eq. 16**:

$$[M]_{tot} = \frac{[ML]}{K_1[L]} + [ML] \quad (\mathbf{16})$$

$$[M]_{tot} = [ML]\left(\frac{1}{K_1[L]} + 1\right) \quad (\mathbf{17})$$

$$[ML] = \frac{[M]_{tot}}{\frac{1}{K_1[L]} + 1} \times \frac{K_1[L]}{K_1[L]} \quad (\mathbf{18})$$

$$A_{obs} = \varepsilon_{MOH_2} A_{MOH_2} + \varepsilon_{ML} A_{ML} \quad (\mathbf{19})$$

$$A_{obs} = \varepsilon_{MOH_2}\left(\frac{[M]_{MOH_2}}{1 + K_1[L]}\right) + \varepsilon_{ML}\left(\frac{[M]_{ML} K_1[L]}{1 + K_1[L]}\right) \quad (\mathbf{20})$$

with $\mathbf{A_{MOH2} = \varepsilon_{MOH2}[M]_{tot}}$ and $\mathbf{A_{ML} = \varepsilon_{ML}[M]_{tot}}$

$$A_{obs} = \left(\frac{[M]_{MOH_2}}{1 + K_1[L]}\right) + \left(\frac{[M]_{ML} K_1[L]}{1 + K_1[L]}\right) \quad (\mathbf{21})$$

$$A_{obs} = \frac{A_{MH_2O} + A_{ML} K_1[L]}{1 + K_1[L]} \quad (\mathbf{22})$$

The **Eq. 22** has the same form as **Eq. 11** and can be used to determine the equilibrium constant, **K'**, from the absorbance *vs.* ligand concentration data.

B3: DERIVATION OF THE ACID DISSOCIATION CONSTANT FOR ONE pK_a VALUE

For an acid/base equilibrium the following **Eq. 23** applies:

$$AH \rightleftharpoons[K_a] H^+ + A^- \qquad (23)$$

At equilibrium, **Eq. 23** gives **Eq. 24**:

$$K_a = \frac{[H^+][A^-]}{[AH]} \qquad (24)$$

Thus,

$$[A^-] = \frac{K_a[AH]}{[H^+]} \qquad (25)$$

and

$$[AH] = \frac{[H^+][A^-]}{K_a} \qquad (26)$$

At any time **t**, the total concentration of **A** is given as:

$$[A]_{tot} = [AH] + [A^-] \qquad (27)$$

Thus, by substituting **Eq. 25** into **Eq. 27** gives **Eq. 28**:

$$[A]_{tot} = [AH] + \frac{K_a[AH]}{[H^+]} \qquad (28)$$

$$[A]_{tot} = [AH]\left(1 + \frac{K_a}{[H^+]}\right)$$

Therefore,

$$[AH] = \frac{[A]_{tot}}{1 + \frac{K_a}{[H^+]}} \qquad (29)$$

Appendix B

By incorporating **Eq. 26** into **Eq. 27** and manipulating gives **Eq. 30**:

$$[A^-] = \frac{[A]_{tot}}{1 + \frac{[H^+]}{K_a}} \quad (30)$$

Multiplying the numerator and denominator in **Eq. 30** by $\frac{K_a}{[H^+]}$ result in **Eq. 31**:

$$[A^-] = \frac{[A]_{tot}\frac{K_a}{[H^+]}}{1 + \frac{K_a}{[H^+]}} \quad (31)$$

From Beer-Lambert law, it is known that the total absorption at any given time **t** is:

$$A_{obs} = \varepsilon_{AH} C_{AH} + \varepsilon_{A^-} C_{A^-} \quad (32)$$

Substituting **Eq. 29** and **Eq. 31** into **Eq. 32** gives **Eq. 33**:

$$A_{obs} = \varepsilon_{AH}\left(\frac{[A]_{tot}}{1 + \frac{K_a}{[H^+]}}\right) + \varepsilon_{A^-}\left(\frac{[A]_{tot}\frac{K_a}{[H^+]}}{1 + \frac{K_a}{[H^+]}}\right) \quad (33)$$

with $\mathbf{A_{AH} = \varepsilon_{AH}[A]_{tot}}$ and $\mathbf{A_{A^-} = \varepsilon_{A^-}[A]_{tot}}$, **Eq. 33** gives **Eq. 34**:

$$A_{obs} = \left(\frac{A_{AH}}{1 + \frac{K_a}{[H^+]}}\right) + \left(\frac{A_{A^-}\frac{K_a}{[H^+]}}{1 + \frac{K_a}{[H^+]}}\right) \quad (34)$$

Multiplying **Eq. 34** by $\frac{[H^+]}{[H^+]}$ result in **Eq. 35**:

$$A_{obs} = \left(\frac{[H^+]A_{AH}}{K_a + [H^+]} \right) + \left(\frac{A_{A^-}K_a}{[H^+] + K_a} \right) \quad (35)$$

By definition $[H^+] = 10^{-pH}$ and $K_a = 10^{-pKa}$, **Eq. 36** is obtained:

$$A_{obs} = \frac{A_{AH}10^{-pH} + A_{A^-}10^{-pK_a}}{10^{-pH} + 10^{-pK_a}} \quad (36)$$

The **Eq. 36** is similar to **Eq. 13** and can be used to determine the acid dissociation constant, pK_a, by fitting spectrophotometric absorbance *vs.* pH data.

B4: DERIVATION OF THE EYRING EQUATION (activation parameters)

The transition state theory states that an activated complex or transition state is in equilibrium ($K_c^{\neq}$ = equilibrium constant) with the reagents before the reaction takes place and that the rate is given by the decomposition rate (**k**) of the activated complex to yield the product:

$$A + B \rightleftharpoons (AB)^{\neq} \xrightarrow{k} \text{product} \quad (37)$$

The second-order rate constant for the above reaction is given by **Eq. 38**:

$$k = \left[\frac{k_b T}{h} \right] K_c^{\neq} \quad (38)$$

with k_b = Boltzmann's constant (1.38066×10^{-23} JK^{-1})

h = Planck's constant (6.62608×10^{-34} Js).

T = temperature in Kelvin

From basic thermodynamics it follows that:

$$\Delta G^{\neq} = -RT \ln K_c^{\neq} = \Delta H^{\neq} - T\Delta S^{\neq} \quad (39)$$

Thus, $$K_c^{\neq} = e^{\frac{-\Delta G^{\neq}}{RT}} \quad (40)$$

with $\Delta G^{\neq}$ = free energy change for activation

R = universal gas constant (8.3145 $JK^{-1}mol^{-1}$)

Substitution in **Eq. 38** gives the Eyring equation (**Eq. 41**):

$$k = T\frac{k_B}{h}e^{\left(\frac{\Delta S^{\neq}}{R}\right)-\left(\frac{\Delta H^{\neq}}{RT}\right)} \quad (41)$$

and its logarithmic form is given by **Eq. 42**:

$$\ln\frac{k}{T} = \ln\frac{k_B}{h} + \frac{\Delta S^{\neq}}{R} - \frac{\Delta H^{\neq}}{RT} \quad (42)$$

Thus, a graph of $\ln\frac{k}{T}$ versus $\frac{1}{T}$ will have a slope of $\frac{-\Delta H^{\neq}}{R}$, with $\Delta H^{\neq}$ = enthalpy change of activation and the Y-intercept yielding $\frac{\Delta S^{\neq}}{R} + \ln\frac{k_B}{h}$, with $\Delta S^{\neq}$ = entropy change of activation.

B5: DERIVATION OF THE RATE EQUATION FOR THE REACTION OF THE AQUA/HYDROXO COMPLEXES WITH MONODENTATE LIGANDS

The following reactions represent the reaction of an aqua or hydroxo complex with a monodentate ligand and the protonation of the aqua complex. These equilibria was used in this study to fit the kinetic data for the fast reactions:

$$M\text{-}OH_2 \rightleftharpoons^{K_{a1}} MOH + H^+ \quad (\mathbf{43})$$

$$M\text{-}OH_2 + L \underset{k_{-1}}{\overset{k_1, K_1}{\rightleftharpoons}} ML + H_2O \quad (\mathbf{44})$$

$$M\text{-}OH + L \underset{k_{-2}}{\overset{k_2, K_2}{\rightleftharpoons}} ML + OH^- \quad (\mathbf{45})$$

The overall rate for reactions (**Eq. 44**) and (**Eq. 45**) is given by the following **Eq. 46**:

$$R = k_1[MOH_2][L] + k_2[MOH][L] - k_{-1}[ML] - k_{-2}[ML][OH] \quad (\mathbf{46})$$

The total concentration of the metal species in the solution is given by the following **Eq. 47.**

$$[M]_T = [MOH_2] + [MOH] \quad (\mathbf{47})$$

The following equation (**Eq. 48**) describes the acid dissociation constant in relation to the concentration of the different species in solution:

$$K_{a1} = \frac{[MOH][H^+]}{[MOH_2]} \quad (\mathbf{48})$$

Eq. 47 and **48** can be written in terms of **[MOH$_2$]**:

$$[M]_T = [MOH_2] + \frac{K_{a1}[MOH_2]}{[H^+]} \quad (\mathbf{49})$$

Eq. 46 and **47** can be written in terms of **[MOH]**:

$$[M]_T = \frac{[MOH][H^+]}{K_{a1}}[MOH] \quad (\mathbf{50})$$

Eq. 49 and **50** can be written as follows:

$$[MOH_2] = \frac{[M]_T}{1 + \frac{K_{a1}}{[H^+]}} \quad (\mathbf{51})$$

$$[MOH] = \frac{[M]_T}{1 + \frac{[H^+]}{K_{a1}}} \quad (\mathbf{52})$$

Substituting **Eqs. 51** and **52** in **Eq. 46**, result in the following **Eq. 53**:

$$R = \frac{k_1[M]_T[L]}{1 + \frac{K_{a1}}{[H^+]}} + \frac{k_2[M]_T[L]}{1 + \frac{[H^+]}{K_{a1}}} - k_{-1}[ML] - k_{-2}[ML][OH^-] \quad (\mathbf{53})$$

Eq. 53 can be written as **Eq. 54**:

$$R = \frac{k_1 + k_2\frac{K_{a1}}{[H^+]}}{1 + \frac{K_{a1}}{[H^+]}}[M]_T[L] - [ML](k_{-1} + k_{-2}[OH^-]) \quad (\mathbf{54})$$

Upon integration and incorporation of the pseudo first-order (**[L] >> [M]$_T$**), **Eq. 55** can be written:

$$k_{obs} = \frac{k_1 + k_2\frac{K_{a1}}{[H^+]}}{1 + \frac{K_{a1}}{[H^+]}}[L] - k_{-1} + k_{-2}[OH^-] \quad (\mathbf{55})$$

Appendix B

Eq. 55 is used to determine with a least-square fit of the $\mathbf{k_{obs}}$ ***vs.*** **[L]** data the different rate constants. The kinetic results (**Chapter 6**) obtained for the first fast reaction for all the ligands studied, were fitted into **Eq. 55**.